



**Proceedings of the Workshop on D-<sup>3</sup>He Based  
Reactor Studies, Held at the Nuclear Fusion  
Institute of the Russian Research Center –  
Kurchatov Institute, Moscow, Russia, 25  
September – 2 October 1991**

June 1993

UWFDM-916

***FUSION TECHNOLOGY INSTITUTE  
UNIVERSITY OF WISCONSIN  
MADISON WISCONSIN***

**Proceedings of the Workshop on D-<sup>3</sup>He Based  
Reactor Studies, Held at the Nuclear Fusion  
Institute of the Russian Research Center –  
Kurchatov Institute, Moscow, Russia, 25  
September – 2 October 1991**

Fusion Technology Institute  
University of Wisconsin  
1500 Engineering Drive  
Madison, WI 53706

<http://fti.neep.wisc.edu>

June 1993

UWFDM-916

# **CONTENTS**

**Introduction to the Soviet - US - Japanese Workshop on D-3He Based Reactor Studies**

**A Statement from the Workshop on D-3He Based Reactor Studies**

**Program of the Workshop**

**Technical Papers**

## INTRODUCTION TO THE OPENING OF THE SOVIET-US-JAPANESE WORKSHOP ON THE D<sup>3</sup>He BASED REACTOR STUDIES

September 25 - October 2, 1991, Moscow, Kurchatov AEI

I welcome our guests who came to turbulent Moscow from the US and Japan and my countrymen and countrywomen gathered here to discuss the problems of energy supply for Earth's inhabitants in the twenty-first century.

We are living at a time when we are forced to be concerned about global conservation suitable for life in the coming centuries. If we exhaust the fuel without accounting for the time of its complete consumption and its detrimental effect of the environment, it may turn out in 15-20 years to be too late to make up for lost time and to recover an equilibrium in the medium of our inhabitation in a form suitable for the continuation of life.

In the twenty-first century only fission, fusion and solar energies can replace that from fossil fuels. Of these three kinds of energy, mankind has mastered only fission energy. However, radioactivity accompanying it worries us and our contemporaries, and will worry our posterity. Undoubtedly, an atomic industry - much less hazardous than today's - will be developed in the coming one or two decades, and will rapidly grow. Progress in mastering solar energy is also not excluded.

However, may one rely on such progress in fusion that it will be able to compete with existing sources in the energy market and play an important role in providing humanity with an environmentally-pure energy source?

This is the main problem to be discussed at our workshop. The competition with other energy sources is very difficult for DT fusion because of its high neutron flux. To compete with fission reactors, which are simple in design and for which operational lifetimes of 30 years have already been demonstrated with promise to be 40 years or longer - is difficult for more complicated DT reactors which have about equal radiation hazards and require the replacement of highly-radioactive first walls and blankets every two to three years because of radiation damage.

The discovery of a million tons of <sup>3</sup>He on the Moon by the scientists at the University of Wisconsin has given birth to a new branch in the fusion program: search for an opportunity to create commercial fusion power production with up to a million times less radioactive hazard than fission power. This branch of fusion has not attracted high financial support yet, but the interest in it rises and we from the fusion community are obliged to completely clarify this problem. It would be a crime to pass by this most favorable opportunity for mankind without paying due attention to it.

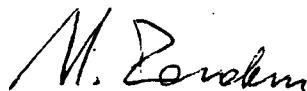


The problem is split into three major parts.

1. Is it possible to solve the plasma and design tasks leading to the construction of  $D^3He$  reactor competitive in the energy market?
2. Is it possible to create on the Moon an economically, environmentally, and socially-acceptable helium-3 mining industry?
3. Do the elements present in Nature allow one to produce low-activation materials which offer a radiation advantage for  $D^3He$  - reactors over fission sufficient to justify the development of a new large and expensive industry? Here one speaks about a new, not yet existing, branch of science of metals and metallurgy - metallurgy requiring many thousand tons of superpure materials.

If the third problem can be solved even only partially in short term program materials would be developed with 10-100 times less activation than those adopted at present in the DT reactor designs, then the  $D^3He$  fuel systems will exclude the need for first wall and blanket replacement. This would make fusion reactors competitive with fission in the energy market because of its reduced attractiveness of the  $D^3He$  fusion, because further improvement in the purity of the components would allow more and more environmentally clean energy sources.

Let us start to work with the hope on successful development of all three problems!



I.N. Golovin

September 24, 1991

A STATEMENT FROM THE  
"WORKSHOP ON D-<sup>3</sup>He BASED REACTOR STUDIES"

Kurchatov IAE, Moscow USSR  
25 September - 2 October 1991

It is our strong feeling, that fusion, as a research field, should always have an appreciable component that aims for its highest potential, and that is dedicated to a search for innovative improvements over what is now perceived as the mainline approach aimed at D-T tokamak reactor. It is our opinion that D-<sup>3</sup>He based systems, in their several embodiments, represent just such a component.

Based on present knowledge, one may expect the following. (1) Fossil fuel utilization will peak and then decline due to its depletion and its negative environmental impact - acid rain and the greenhouse effect. (2) Power generation based on uranium and plutonium fission will continue to develop, but will be hampered by popular opposition related to its well-known radioactive hazards. These factors stimulate the search for an even safer and more ecologically sound energy source. In this regard, fusion and solar energy are ideal sources for power generation.

The fusion community has focused on the D-T fueled tokamak as its mainline approach. Progress on tokamaks has been substantial, and present experiments are on the threshold of D-T ignition. The quadripartite agreement between the USA, Euratom, Japan, and the Soviet Union is working forward the design of ITER, where extended D-T burning and invaluable engineering experience will be achieved.

While D-T reactors are much safer than fission - in that they generate no radioactive fuel ash, the induced radioactivity of today's steel structural components will not differ significantly from fission. Moreover, frequent replacement of the first wall and

blanket are essential, resulting in increased energy cost. Consequently, it is not certain that the present D-T based mainline is the optimal long-term fusion system. We believe that ultimately D-<sup>3</sup>He based systems will be optimal in view of substantially reduced radioactivity and the durability of major systems, components for the full life of the reactor.

The development of D-<sup>3</sup>He fusion should include three major programs. (1) Plasma physics. This can include tokamaks, tandem mirrors, field-reversed configurations, and other innovative high-beta concepts. Such breadth is essential since the optimum confinement geometry for D-<sup>3</sup>He fuel is not yet clear. Also, major D-<sup>3</sup>He burning operations should be considered as an important element in the ITER program. (2) Materials. This includes the technologies of low-activation structural materials and superconductors, and requires comprehensive tests of such materials. (3) <sup>3</sup>He procurement. This includes the development of a permanent manned Lunar settlement and the requisite technologies for <sup>3</sup>He mining. We view <sup>3</sup>He and its byproducts as resources from space that can significantly enhance the earth's environment. This offers the first chance to gain significant economic returns from the exploration of space.

The production of Lunar <sup>3</sup>He relies on the use of solar energy, both in a direct thermal form and to produce electricity on the moon to power mining equipment. Thus the use of <sup>3</sup>He in terrestrial fusion reactors is both synergistic with and complementary to the development of solar energy in space.

Drawing from experience with the quadripartite cooperation on ITER, we consider it to be reasonable to initiate additional multinational D-<sup>3</sup>He fusion programs, including plasma physics, materials, and lunar programs. We recommend that this program should be launched in 1992.

Academician Boris B.Kadomtsev  
Director of Fusion Department of  
Kurchatov Atomic Energy Inst.  
Moscow, USSR

Dr. Gerald L.Kulcinski  
Professor of Fusion Technology  
and Engineering Physics  
Director of Fusion Technology  
Institute. University of  
Wisconsin, USA

Professor Igor N.Golovin  
Kurchatov Atomic Energy Inst.  
Moscow, USSR

Dr. John F.Santarius  
Senior Scientist, Fusion  
Technology Institute  
University of Wisconsin, USA

Professor Vladimir A.Burtsev  
Efremov Scientific Research  
Inst. of Electrophysical  
Apparatus, St.Peterburg, USSR

Dr. Nicolas A.Krall  
President, KRALL Association,  
USA

Professor Vladimir I.Khvesjuk  
Moscow State Technical University  
Moscow, USSR

Dr. Michael E.Mauel  
Associate Professor of Appl.  
Physics, Columbia Univ., USA

Professor Igor V.Barmin  
Design Bureau of General  
Machinery. Splav Technical  
Centre, Moscow, USSR

Dr. Loren C.Steinhauer  
Principal Research Scientist  
STI Optronics, USA

Correspond. Member of USSR  
Academy of Sciences  
Professor Dmitri D.Rjutov.  
Institute of Nuclear Physics  
Novosibirsk, USSR

Dr. Vladislav V. Slavchenko  
Sternberg State Astronomical  
Inst. of Moscow University  
Moscow, USSR

Dr. Eduard J. Rudavsky  
Inst. of Low Temperature  
Physics and Engineering  
Kharkov, USSR

Dr. Vitalii F. Semenov  
Sc. Research Institute of  
Thermal Processes  
Moscow, USSR

Dr. Gerakl M. Baydal  
Leading Engineer  
Scientific-Industrial  
Organization "Energia"  
Moscow, USSR

Professor Hiromu Momota  
National Institute  
for Fusion Science  
Nagoya 464-01  
JAPAN

October 2, 1991

Moscow, USSR

**"Workshop on D-3He Based Reactor Studies"**  
**Kurchatov REI, Moscow, USSR**  
**25 September - 2 October 1991**

**Program**

**Wednesday, 25 September**

9:00 - 9:30                Workshop Opening

**1. PLASMA PHYSICS and CONFINEMENT SYSTEM in D-3He REACTORS**

**A. Tokamaks**

9:30 - 10:50            Kulcinski G.L. (U. Wisconsin) APOLLO; Paper 1A1

11:10 - 12:30          Pistunovich V.I. (Kurchatov Inst.) D-3He Tokamak Reactor  
Parameter Optimization; Paper 1A2

12:30 - 13:50          Santarius J.F. (U. Wisconsin) ARIES-3; Paper 1A3

**Lunch**

**B. Alternate Confinement Concepts**

15:00-16:20            Glagolev V.M. (Kurchatov Inst.) D-3He Reactor DRAKON; Paper  
1B1

16:20-17:40            Khvesjuk V.I. (MSTU) D-3He Tandem Mirror Reactor (power  
balance, ash removal, MHD stability); Paper 1B2

17:40-18:00            Additional discussion

**Thursday, 26 September**

9:00-10:20            Momota H. (NIFS) FRC reactor design, ARTEMIS; Paper 1B3

10:20-11:20            Burtsev V.A (Efremov Inst.) Pulsator Concept: Quasistationary  
Field Reversed Configuration Formation; Paper 1B4

**Coffee Break**

**C. New Ideas**

11:40-12:40            Pastukhov V.P. (Kurchatov Inst.) High-B axisymmetric D-3He  
reactor with internal levitated ring; Paper 1C1

12:40-13:40            Morozov A.I. (Kurchatov Inst.) The problem of traps with  $\beta=1$  and  
the GALATEAS; Paper 1C2

## **Lunch**

- 15:00-16:00      **Mauel M.E.** (Columbia U.) Dipole concept; Paper 1C3
- 16:00-17:00      **Krall N.A.** (D. Krall Assoc.) Spherically convergent ion focus concept; Paper 1C4
- 17:00-17:20      **Ryutov D.D.** (INP) D-3He Mirror Reactor with Fast 3He injection; Paper 1C5 (not submitted)
- 17:20-18:00      Discussion on the advantages and disadvantages of various D-3He reactor concepts.

## **Friday, 27 September**

### **D. Plasma Physics Issue**

- 9:00-10:00      **Medvedev S.Yu.** (Keldysh Inst.) Ideally MHD stable equilibria with high  $\beta$  in a tokamak; Paper 1D1
- 10:00-11:00      **Mauel M.E.** (Columbia U.) High-Poloidal Beta Experiments; Paper 1D2

### **Coffee Break**

- 11:20-12:20      **Kukushkin A.B.** (Kurchatov Inst.) Cuclotron radiation transfer in plasmas with strong magnetic field: effect of quasi-linear diffusion; Paper 1D3
- 12:20-13:20      **Kostenko V.V.** (MSTU) ECR electron heating in an open trap with creation of high anisotropic electron population; Paper 1D4 (not submitted)
- 13:20-14:20      **Steinhauer L.C.** (STI Optronics) FRC stability and transport physics; Paper 1D5

## **Lunch**

- 15:20-16:00      Discussion on plasma physics issues.

## **2. ENGINEERING and RESOURCE PROBLEM**

### **A. Engineering Issues Unique to D-3He Fusion Systems**

- 16:00-17:00      **Momota H.** (NIFS) 15 MeV proton direct conversion scheme; Paper 2A1
- 17:00-18:00      **Santarius J.F.** (U. Wisconsin) State of the art of rectennas; Paper 2A2

## **Saturday and Sunday (28 and 29 September) - Free Time**

### **Monday, 30 September**

#### **B. Low-Activation Materials**

- 9:00-10:00            **Ivanov L.I.** (Bajkov Inst.) The problem of low-activation materials; Paper 2B1 (not submitted)
- 10:00-10:50        **Per'kova G.N.** (Giredment) Vanadium alloys and their properties; Paper 2B2

#### **Coffee Break**

- 11:10-12:00        **Votinov S.N.** (Bajkov Inst.) Radiation resistance of the vanadium alloys; Paper 2B3
- 12:00-13:00        **Kulcinski G.L.** (U. of Wisconsin) Reduced activation stainless steels for fusion reactors; Paper 2B4
- 13:00-14:00        **Dergunova E.A.** (Bochvar Inst., Kurchatov Inst.) The possibility of manufacturing low-activation superconductors; Paper 2B5
- 15:00-17:00        Excursion to the installations T-15, T-10, PR-8, IREC and Ogra-4

### **Tuesday, 1 October**

#### **C. Lunar Helium-3 Mining**

- 9:00-10:20        **Barmin I.V.** (DBGMB) Permanent lunar base construction and development; Paper 2C1
- 10:20-11:40        **Kulcinski G.L.** (U. Wisconsin) A resource assessment and extraction of lunar He3; Paper 2C2
- 12:00-13:00        **Borisov A.S.** (DBGMB) Lunar robots; Paper 2C3
- 13:00-14:00        **Mikheev V.A.** (FTLTI) Cryogenic technology for lunar helium-3 extraction; Paper 2C4

#### **Lunch**

- 15:00-16:20        Four Short motion pictures (DBGMB): Permanent lunar base construction; Lunar machinery; Taking the lunar soil; Remote analysis of Venus soil
- 16:20-17:00        Discussion of low-activation materials and lunar mining issues

### **Wednesday, 20 October**

- 9:00-10:20        **Santarius J.F.** (U. Wisconsin) Space propulsion based on D-3He fusion; Paper 2C5



10:20-11:40      **Pavshuk V.A.** (Kurchatov Inst.) Fission reactors for the power supply of permanent lunar bases; Paper 2C6

**Coffee Break**

**3. Summary**

12:00-12:30      Summary statements on D-3He fusion

12:40-14:00      Discussion of the full problem: "ENERGY TO EARTH FROM SPACE"

**Lunch**

15:00-17:00      Conclusion; approval and signing of a joint memorandum

# The Case For D<sup>3</sup>He Fusion Power Plants\*

by

G. L. Kulcinski, J. P. Blanchard, G. A. Emmert, L. A. El-Guebaly, H. Khater, C. W. Maynard, E. A. Mogahed, J. F. Santarius, M. E. Sawan, I. N. Sviatoslavsky, L. J. Wittenberg

Fusion Technology Institute  
University of Wisconsin  
Madison, WI

## I. Introduction

The use of thermonuclear fusion to generate electricity has been studied since 1951. While there have been a multitude of confinement concepts proposed to produce that electricity, one thing that has stayed essentially constant is the fuel cycle. The use of deuterium (D) and tritium (T), either in magnetically or inertially confined plasmas, has been the subject of over 50 major reactor designs published since 1970<sup>(1)</sup>. However, there has been a growing disenchantment with this fuel cycle over the past decade because of the problems associated with handling the 14 MeV neutrons which carry 80% of the thermonuclear energy<sup>(2,3)</sup>. Scientists all over the world have been searching for a better way to provide society with a clean, economical, and safe supply of energy for centuries to come<sup>(4-7)</sup>. The purpose of this paper is to present a more attractive alternative to our present DT fusion path and that is, to eventually use the D<sup>3</sup>He fusion cycle.

## II. Why Would We Want to Change?

There is a simple logic sequence that one can follow in analyzing whether one should stay with the DT or move, in the long run, to the D<sup>3</sup>He fuel cycle (see figure 1). The first question, and the theme of this paper, to ask is:

***"Will the D<sup>3</sup>He fuel cycle produce electricity significantly cleaner and safer than the DT cycle?"***

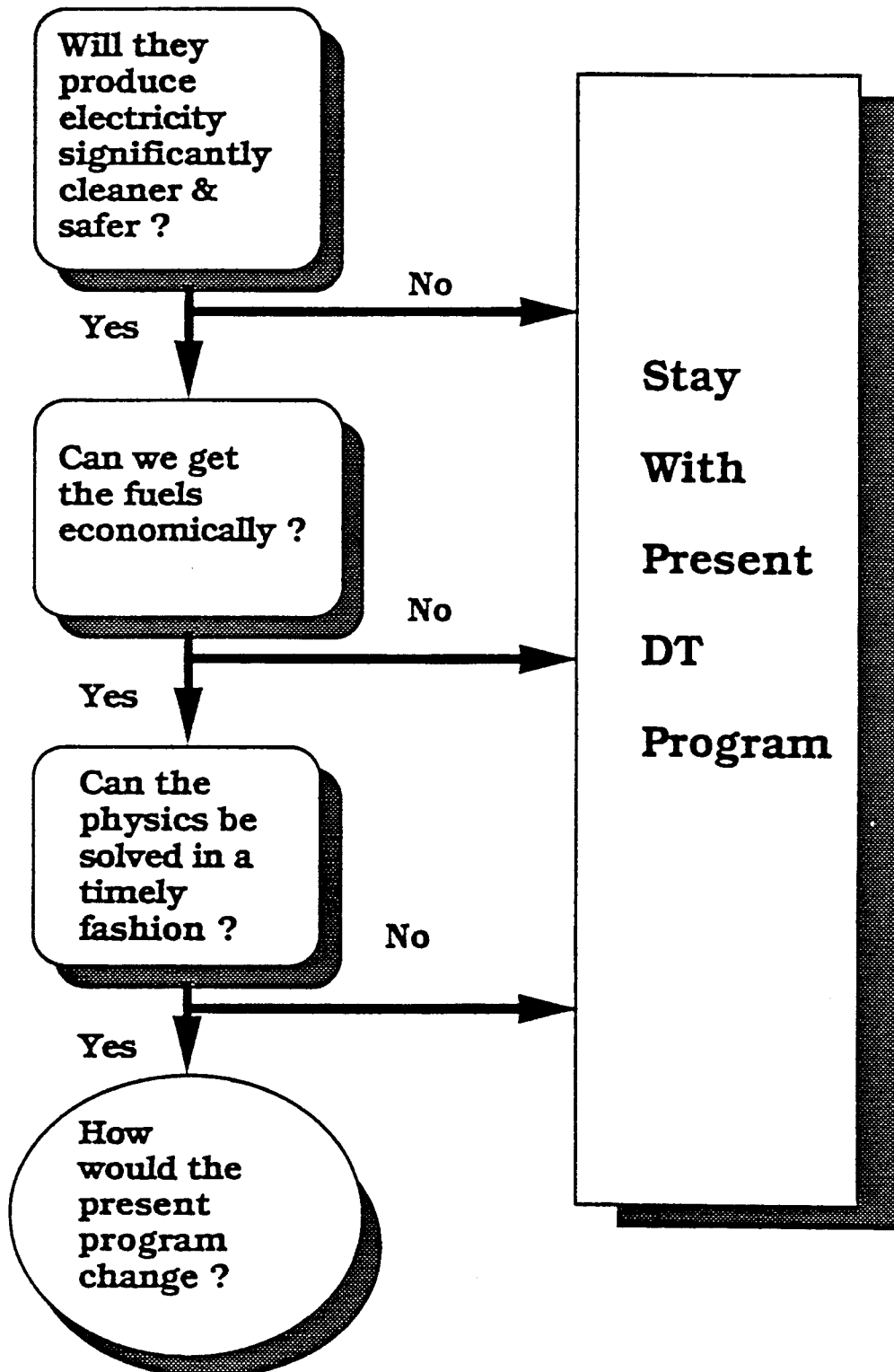
If the answer to that question is no, then because of the well known problems of <sup>3</sup>He fuel resources or the increased difficulty in the D<sup>3</sup>He plasma physics, one should stay with the DT fuel. If one can show that there are significant safety and environmental advantages to the D<sup>3</sup>He cycle, then one must face the next question.

---

\*A version of this paper has been submitted to Fusion Technology

Figure 1

## Logical Questions About the Use of Advanced Fuels Versus DT



***"Can we get the  $^3\text{He}$  fuel economically?"***

If the answer to that question is no, then regardless of its attractive safety and environmental features, one would stay with the DT cycle. On the other hand, if one could obtain the  $^3\text{He}$  economically, then we would have to consider the next question.

***"Can the physics problems be solved in a timely fashion?"***

Having an attractive fuel cycle and plenty of fuel is no good if it would take 50 years or more, beyond that required for the DT cycle, to solve the plasma physics problems. On the other hand, if the plasma physics solutions can be obtained in no more than, say 10 years, after the similar solution are obtained in the DT case, then we must ask ourselves:

***"How would the present fusion program change?"***

The main objective of this paper is to concentrate on the first question and try to answer it by comparing two recent fusion power plants, each based on a different fuel cycle. The question of the fuel cycle has been addressed elsewhere<sup>(8)</sup> and the question of the development time for the fuel cycles can logically follow this paper.

### **III. Framework for Comparisons**

Because there have been no convincing studies to show that one could burn the  $\text{D}^3\text{He}$  fuel economically in inertially confined systems, this study will concentrate on magnetic confinement only. The choice of the magnetic systems to compare is a bit more complicated. A Tokamak confinement approach would be the most relevant in the current climate of research around the world but that choice does bias the results against the  $\text{D}^3\text{He}$  fuel cycle. A high beta (ratio of the plasma pressure to the magnetic pressure) system, e.g., a FRC, Tandem Mirror, Electrostatic, Multipole, or RFP confinement approach, would be much better for the  $^3\text{He}$  cycle. Unfortunately, most of the research on the above concepts has been curtailed in the U. S. due to budgetary considerations and the effort outside the U. S. is at a relatively low level. Therefore, the Tokamak was chosen for this study even though it must be recognized at the outset that if the  $\text{D}^3\text{He}$  cycle can compete with the DT cycle in Tokamaks, it can be even much more favorable in the other high beta systems.

The choice of specific DT designs to compare against was between the STARFIRE<sup>(9)</sup> and the ARIES-I<sup>(10)</sup> conceptual studies. The STARFIRE design is a much more conservative system, both from the standpoint of physics and technology, than the ARIES-I study. However, the ARIES-I project was completed in 1991

( vs 1980 for STARFIRE) and therefore felt to be more representative of the current physics data base. The choice of the D<sup>3</sup>He design was relatively easy as there has been only one detailed, first plasma stability regime, tokamak in the literature; namely the Apollo series<sup>(11-14)</sup>.

It is only possible, in this short paper, to list a few of the more important parameters of each design (see Table 1) and the rest of this paper will concentrate on the environmental and safety factors.

<p style="text-align: center;">Table 1. A Comparison of the Key Features of 1000 MWe Tokamaks -the DT Based ARIES-I and the D<sup>3</sup>He Based APOLLO</p>			
Parameter	Units	APOLLO <sup>(14)</sup>	ARIES-I <sup>(10)</sup>
Fuel Cycle		D <sup>3</sup> He	DT
Aspect Ratio		3.15	4.5
Major Radius	m	7.89	6.75
B <sub>max</sub>	T	19.3	21.3
<T <sub>i</sub> >	keV	57	20
nτ <sub>E</sub>	10 <sup>14</sup> s/cm <sup>-3</sup>	29	3.7
Current	MA	53.3	10.2
Average Neutron Wall Loading	MW/m <sup>2</sup>	0.1	2.21
Structural Material		Low Activation Steel	SiC
Heat Transport Fluid		Organic @ 2 MPa	He @ 10 MPa
Power Conversion		Rectenna + Rankine	Rankine
Max First Wall Temp.	°C	550	1000
Total Thermal Power	MWth	2144	2543
Cost of Electricity	1991 mills/kWh	77	80

Aside from being slightly bigger in size, the maximum magnetic field is smaller in Apollo. The average ion temperature, the required nτ<sub>E</sub>, and the plasma current are all larger in Apollo than the values in ARIES-I. The extremely small neutron wall loading (by a factor of over 20) allows the use of an organic coolant in the Apollo reactor and, as shown later, this feature will have a major impact on the environmental and safety features of the D<sup>3</sup>He

reactors. The high fraction of power in synchrotron radiation also allows direct conversion of thermonuclear energy to electricity in Apollo. This higher efficiency is achieved at relatively modest temperatures compared to the DT system and the final cost of electricity is in fact slightly lower in the advanced fuel system.

#### IV. Radiation Effects

One of the major differences between DT and D<sup>3</sup>He reactors is the level of neutron irradiation to the reactor structural materials. Key parameters of the neutron exposure are given in Table 2.

<b>Table 2. Summary of the Radiation Damage Parameters in the ARIES-I<sup>(10)</sup> and APOLLO-L3<sup>(14)</sup> Reactors</b>			
<b>Parameter</b>	<b>Units</b>	<b>Apollo (D<sup>3</sup>He)</b>	<b>Aries-I(DT)</b>
First Wall Structural Material		Low Activation Stainless Steel	SiC
Neutron Wall Loading			
	MW/m <sup>2</sup> Ave.	0.1	2.21
	MW/m <sup>2</sup> Peak	0.14	3.34
Displacement Damage			
	dpa per MWy/m <sup>2</sup>	22.2	≈10
	Peak dpa/FPY	3.11	≈33
	Peak dpa @ End of Life	93 @ 30 FPY's	≈200 @ 6 FPY's
Transmutation Rates			
	appm He per MWy/m <sup>2</sup>	115	1156
	appm H per MWy/m <sup>2</sup>	381	618
	Peak appm He/FPY	16.1	3861
	Peak appm H/FPY	53.3	2064
	Peak appm He @ End of Life	483 @ 30 FPY's	23,120 @ 6 FPY's
	Peak Burn Up @ End of Life %	Transmutation not Burn Up	1.7 % C 0.08% Si

It is clear that the low neutron flux associated with the  $D^3He$  reaction greatly reduces the dpa rate as well as the production of helium and hydrogen gas atoms in the first wall materials. The maximum reactor damage level of  $\approx 90$  dpa in stainless steels at  $\approx 550^\circ C$ , while containing  $\approx 500$  appm He, have already been shown to perform satisfactorily<sup>(15)</sup>. It is also worth noting that if the SiC reaches its hoped for life of 20 MWy's/m<sup>2</sup>, almost 2% of the carbon atoms will literally be turned to gas and every atom will have been displaced on the order of 200 times! There is no data at these conditions from which to make predictions of the ability of SiC to maintain its strength and vacuum sealing properties at temperatures of  $1000^\circ C$ . From this it is easy to see why a major materials development program is required before DT fusion power plants made from SiC could even be considered.

## V. Radioactivity

In order to calculate the level of radioactivity induced in the structures, one must use the appropriate neutron spectra and the actual blanket and shield structure. Previous studies<sup>(16,17)</sup> have discussed the details of such analyses and only the results will be listed here.

The normal indicator of the long term level of radioactivity in a nuclear system is the manner in which the waste can be stored. The crude differentiations of "near surface" and "deep geological" disposal have been supplemented with Class A,B,C, ..., defined in more detail elsewhere<sup>(16)</sup>. For the purposes of this paper, the near surface category of Class A waste is the most desirable because it requires only minimal packaging and it only has to be monitored for 100 years. Class C, while still acceptable, requires more substantial packaging and a 500 year monitoring time. Obviously, any near surface burial scheme is preferable to a deep geological facility.

The categorization of the long term waste from the DT(Aries-I) and  $D^3He$  (Apollo) reactors is summarized in Table 3. It is shown that the modified HT-9 and SiC structural materials, qualify for Class A, near surface burial waste, as does the isotopically tailored W on the divertors of both reactors. However, the  $Li_2ZrO_3$  only qualifies for Class C waste even if one could isotopically tailor approximately 150 tonnes of Zr over the life of the reactor to the following composition.

Isotope	Natural	Tailored
$^{90}Zr$	51.46	0.06
$^{91}Zr$	11.23	0.01
$^{92}Zr$	17.11	99.91

Similarly, the tungsten isotope  $^{186}\text{W}$  must be significantly reduced by isotopical tailoring to the composition below in order to achieve near surface waste burial status.

<b>Isotope</b>	<b>Natural</b>	<b>Tailored</b>
$^{180}\text{W}$	0.00135	0.02
$^{182}\text{W}$	11.23	4.44
$^{183}\text{W}$	14.4	90.0
$^{184}\text{W}$	30.6	5.18
$^{186}\text{W}$	28.4	0.36

The technology required to isotopically tailor 100's of tonnes of W and Zr per year still has to be developed for DT reactors. Thus, it possible that this technology research alone could require a decade of development after the announced physics breakeven point is first reached. Such a long R & D time is the reason that many think that  $\text{D}^3\text{He}$  will in fact result in a lower cost of electricity in the long run..

<b>Table 3</b> <b>The Categorization of Long Term Waste From Fusion Reactors</b>		
	<b>Apollo (<math>\text{D}^3\text{He}</math>)</b>	<b>Aries-I (DT)</b>
Structural Material	Low Activation Ferritic Steel	SiC
WDR* Class A Rating	0.88	-----
WDR* Class C Rating	-----	0.1
Neutron Multiplier	None Needed	Be
WDR* Class A Rating	None Needed	$\ll 0.1$
Breeder Material	None Needed	$\text{Li}_2\text{ZrO}_3$ (99.9% $^{92}\text{Zr}$ )
WDR* Class C Rating	None Needed	0.05
Divertor Coating	W(90 % $^{183}\text{W}$ )	W(90 % $^{183}\text{W}$ )
WDR* Class A Rating	0.1	-----
WDR* Class C Rating	-----	0.1

\* If the WDR rating is  $< 1.0$ , then the material qualifies for burial in that category

## **VI. Safety**

A common method of assessing the overall safety of a nuclear power plant is to calculate its Level of Safety(LSA) rating as outlined in previous papers (18,19). There are 4 levels to consider ranging



from the worst, (LSA-4), where active measures must be used to prevent fatalities. The most favorable LSA rating is the #1 level, which basically says, there is no conceivable way that energy in the reactor could mobilize enough radioactivity to cause any civilian casualties.

A measure of the radioactive inventories, potential sources of radioisotope mobilization and estimated offsite effects of the worst conceivable accidents is given in Table 4.

<b>Table 4.</b> <b>A Comparison of the Key Safety Features For DT &amp; D<sup>3</sup>He Fusion Reactors</b>		
	<b>Apollo (D<sup>3</sup>He)</b>	<b>Aries-I(DT)</b>
Decay Heat From In Vessel Components At Shutdown	5.62 MW	Not Given
T <sub>max</sub> in LOCA	600 °C	1000 °C
Offsite MEI* Dose Due to LOCA	4.4 Rem	130 Rem (Assumes Only 2% of Modules Fail)
T <sub>max</sub> in LOCA With Organic Fire	1200 °C	NA
Offsite MEI* Dose Due to LOCA and Organic Fire	126 Rem	NA
LSA Rating	1	2 **

\* MEI≡ Maximum Exposed Individual

\*\* On the basis that more than 2% of the Aries-I Modules Can Fail

It is important to note that the entire W divertor plate (of the new isotopic ratio) is assumed to be released along with the alloying elements in equilibrium with the temperatures listed above. Even under those circumstances, the offsite dose from an Apollo reactor to the Maximum Exposed Individual (MEI) is less than 200 Rem, the dose required for evacuation. This logic allows the D<sup>3</sup>He reactor to be given the LSA rating of 1. The less favorable LSA 2 rating was given to the Aries-I on the basis of more than 2% of the SiC modules that hold the Li<sub>2</sub>ZrO<sub>3</sub> could fail.

## VII. Conclusions

The technology and safety advantages of the D<sup>3</sup>He cycle have been examined and it is concluded that "Yes, the D<sup>3</sup>He fuel cycle will produce electricity cleaner and safer than the DT fusion reaction". The main reason for this statement is the greatly

reduced number of neutrons which need to be handled. Most attention has been focused on the reduction in radioactivity in  $^3\text{He}$  fuel system. However, the reduction in radiation damage is perhaps even more important. Such a reduction allows:

- A "permanent" first wall to be constructed
- Less radioactive waste to handle
- A more reliable reactor performance to be anticipated
- A wider choice of structural materials

There are also the benefits of Class A waste and the low afterheat which is intimately tied with the safety of the nuclear core. It is felt that these technological benefits outweigh the disadvantages associated with the higher  $\langle T_i \rangle$ ,  $n\tau_E$ , and plasma currents that are characteristic of  $\text{D}^3\text{He}$  operation in Tokamaks.

## VII. Acknowledgement

The authors would like to acknowledge partial support for this work from the Grainger Foundation, the Bechtel Corporation, and the Wisconsin Electric Utility Research Foundation.

## X. References

- 1.) G.L. Kulcinski, "What Have Fusion Reactor Studies Done For You Today?," J. Fusion Energy, **4**, 171 (1985)
- 2.) N.M. Ghoniem and G.L. Kulcinski, "A Critical Assessment of the Effects of Pulsed Irradiation on Materials," Nuclear Technology/Fusion, **2**(2), April (1982)
- 3.) G.L. Kulcinski, "Fusion Reactors: Their Challenge to Materials Scientists," Contemporary Physics, **20**, 417-47 (1979).
- 4.) W. Kernbichler, G. H. Miley, and M. Heindler, "Comparison of the Physics Performance of  $\text{D}^3\text{He}$  Fusion in High and Low Beta Toroidal Devices," to be published, 1992
- 5.) H. Momota, et. al., "Conceptual Design of  $\text{D}^3\text{He}$  FRC Reactor ARTEMIS", to be published, Proc. Us-USSR Workshop on Advanced Fuel Fusion, Moscow, Oct., 1991
- 6.) I. N. Golovin, " $\text{D}^3\text{He}$  Tandem Mirror Reactor," to be published, Proc. Us-USSR Workshop on Advanced Fuel Fusion, Moscow, Oct., 1991

- 7.) A. Hasegawa, L. Chen, and M. Mauel, "A  $D^3He$  Fusion Reactor Based on a Dipole Reactor," Nuclear Fusion, 30, No. 11, 2405(1990)
- 8.) L.J. Wittenberg, J.F. Santarius and G.L. Kulcinski, "Lunar Source of He-3 for Commercial Fusion Power," Nuclear Technology/Fusion, 10, 167(1986)
- 9.) "Starfire- A Commercial Tokamak Fusion Power Plant Study," ANL/FPP-80-1, Argonne National Laboratory, September, 1980.
- 10.) "ARIES-1, A Tokamak reactor Study," to be Published, UCLA, 1992
- 11.) G.L. Kulcinski, G.A. Emmert, L.A. El-Guebaly, H.Y. Khater, J.F. Santarius, M.E. Sawan, I.N. Sviatoslavsky, W.F. Vogelsang, and L.J. Wittenberg, "Apollo - An Advanced Fuel Fusion Power Reactor for the 21st Century," Fusion Technology, 15, 1233 (1989)
- 12.) G.A. Emmert, G.L. Kulcinski, J.P. Blanchard, L.A. El-Guebaly, H.Y. Khater, J.F. Santarius, M.E. Sawan, I.N. Sviatoslavsky, L.J. Wittenberg, R.J. Witt, "Apollo-L2, An Advanced Fuel Tokamak Reactor Utilizing Direct Conversion," Proc. of 13th Symp. Fusion Engineering, Knoxville, TN, IEEE, 1043(1990)
- 13.) G.L. Kulcinski, J.P. Blanchard, J.P. Castro, L.A. El-Guebaly, G.A. Emmert, H.Y. Khater, E.A. Mogahed, J.F. Santarius, M.E. Sawan, I.N. Sviatoslavsky, R.J. Witt, L.J. Wittenberg, "Apollo-L3, An Advanced Fuel Fusion Power Reactor Utilizing Direct and Thermal Energy Conversion," Fusion Technology, 19, 791(1991)
- 14.) G. A. Emmert, G.L. Kulcinski, J.P. Blanchard, L.A. El-Guebaly, H.Y. Khater, C. W. Maynard, E.A. Mogahed, J.F. Santarius, M.E. Sawan, I.N. Sviatoslavsky, L.J. Wittenberg, "An Improved First Stability Advanced Fuel Tokamak, Apollo-L3", Fusion Technology, to be published
- 15.) R. L. Klueh, K. Ehrlich, and F. Abe, "Ferritic/Martensitic Steels for Fusion Reactor Applications", to be published, Fusion Technology
- 16.) H. Y. Khater, and M. E. Sawan, "Safety and Environmental Aspects of Apollo-L2  $^3He$  Reactor", 14th IEEE/NPSS Symp. Fusion Engr., Sept. 30, 1991 San Diego, CA, To Be Published

- 17.) H. Attaya, M. E. Sawan, and G. L. Kulcinski, "Waste Disposal of Candidate Structural Materials in Fusion reactors Utilizing Different Fuel Cycles", to be Published Fusion Technology
18. ) S. J. Piet, E. T. Cheng, L. J. Porter, " Accident Safety Comparison of Elements to Define Low Activation Materials" EGG-FSP-8552, Idaho national Laboratory, July 1989.
- 19.) J. P. Holdren, D. H. Berwald, R. J. Budnitz, J. G. Crocker, J. G. Delene, R. D. Endicott, M. S. Kazimi, R. A. Krakowski, G. C. Logan and K. R. Schultz, " Report of the Senior Committee on Environmental, Safety, and Economic Aspects of Magnetic Fusion Energy," UCRL-53766 (Sept. 25, 1989) p. 69.

# D<sup>3</sup>He TOKAMAK-REACTOR PARAMETER OPTIMIZATION

S.G.Bespoludennov, V.I.Khripunov, V.I.Pistunovich  
I.V.Kurchatov Institute of Atomic Energy, Moscow

To obtain the optimal parameters of the D<sup>3</sup>He tokamak-reactor the stationary 1D-power balance model was used. The model is based on real equilibrium magnetic field configuration, consistent with the plasma parameters. Power balance equation has the next form:

$$P_{aux} + P_F = P_\tau + P_B + P_{\gamma}, \quad P_{aux} \approx P_{cd} \quad (1)$$

where  $P_{cd} = \frac{1}{2} n_{e20} I_F R / \gamma \tau_c$  - current drive power,  $P_{\tau} = \frac{3}{2} \langle nT \rangle / \tau_c$  - power of conductive losses, defined by the energy confinement time,  $P_B$  and  $P_{\gamma}$  - bremsstrahlung and synchrotron radiation power losses.  $I_B = I - I_{ps}$ , the bootstrap current  $I_{ps}$  and current drive efficiency  $\gamma_{cd}$  for neutral beam are defined from [1].

In determining of fusion power density three base reaction and the reaction of neutral beam with plasma ions are taken into account:

$$P_F = P_{DHe} + P_{DD} + P_{DT} + P_{fb},$$

where:

$$P_{DHe} (\text{MW/m}^3) = A n_D n_{He} \langle \sigma v \rangle_{DHe} 18.35,$$

$$P_{DD} (\text{MW/m}^3) = A (n_D^2 / 2) \langle \sigma v \rangle_{DD} (0.82 + 4.03) / 2, \quad (2)$$

$$P_{DT} (\text{MW/m}^3) = A n_D n_T \langle \sigma v \rangle_{DT} 3.52.$$

Reaction rates in  $10^{-16} \text{cm}^3/\text{s}$  are determined by approximate formulas [2],  $A = 1.602 \cdot 10^{-3}$ , for DD-reaction the sum on two channel was used. DHe-reaction power density of deuteron beam with energy  $E_0 = 1.2 \text{ MeV}$  and plasma is determined by:

$$P_{fb} = f P_{cd} (18.35 / 1.2) / V.$$

Reaction probability  $f$  is defined in [3],  $V$  - plasma volume.

Plasma density and temperature profiles are:

$$n(r) = n_0 (1 - (r/a)^2)^{\alpha_n} \quad \text{and} \quad T(r) = T_0 (1 - (r/a)^2)^{\alpha_T}$$

Plasma components density is determined by total plasma density with the help of relative concentration [4]:

$$\xi = n_{He} / n_D, \quad \zeta = n_T / n_D, \quad n = n_D + n_{He} + n_T + n_e$$

$$n_D = n / (2 + 3\xi + 2\zeta), \quad n_{He} = \xi n / (2 + 3\xi + 2\zeta), \quad n_T = \zeta n / (2 + 3\xi + 2\zeta),$$

$$n_e = n_D + n_T + 2n_{He} = (1 + 2\xi + \zeta) n / (2 + 3\xi + 2\zeta)$$

The temperature of all plasma components is assumed to be equal.

Bremsstrahlung radiation power loss was calculated by next formula:

$$P_B (\text{MW/m}^3) = 5.35 \cdot 10^{-3} Z_{eff} T_{kev}^{1/2} n_{e20}^2 K, \quad (3)$$

$$\text{here } K = \left(1 + \frac{2T}{T_0}\right) \left\{1 + \frac{2}{Z_{eff}} \left(1 - \frac{1}{(1+T/T_0)}\right)\right\} - \text{relativistic}$$

$$\text{coefficient, } T_0 = m_e c^2 = 511 \text{ keV, } Z_{eff} = \frac{\sum n_i Z_i^2}{n_e} = \frac{1 + 4\xi + \zeta}{1 + 2\xi + \zeta},$$

$n_{20}$  - density in  $10^{20} \text{m}^{-3}$ .

Resulting synchrotron radiation power loss  $P_c = Q_0 \Phi$ .

$$Q_0 (\text{MW/m}) = 6.25 \cdot 10^{-3} n_{e20} T_{\text{kev}} (1 + T/204) B_T^2 \quad (4)$$

Transparency factor [5]:  $\Phi = \Phi_0 \left[ \xi_H + (1-R_W)^{0.56} (1-\xi_H) \right]$ ,

$$\Phi_0 = 7.7 \cdot 10^{-3} T_{\text{kev}}^{3/2} / L_0^{0.56}, \quad L_0 = 6.03 \cdot 10^3 n_{e20} a_{\text{eff}} (\text{m}) / B_{\text{OT}}$$

where  $\xi_H$  - part of holes in reflect wall surface,  $R_W = 0.9$  - wall reflection coefficient,  $a_{\text{eff}} = a k^{1/2}$  - "effective" plasma radius,  $B$  - toroidal magnetic field (T). Transparency factor is calculated at average value of plasma density and temperature and with vacuum magnetic field on axes  $B_0$ . This expression for transparency factor is differ from Trubnikov's formula [6]:

$$\Phi_T = 5.2 \cdot 10^{-3} T_{\text{kev}}^{3/2} \sqrt{\frac{(1+\chi)(1-R_W)}{L_0}}$$

The correction factor for the field inhomogeneity  $\chi = \frac{18a}{R \sqrt{T}}$

and more weak dependence from  $L_0$  may result in 50% and more increase of  $\Phi_T$  relative to  $\Phi$ .

Energy confinement time is determined by ITER-89 power law scaling for H-mode with enhancement factor multiplied on 1.8 respective to recent DIII-D experiments:

$$\tau_E^{\text{ITER89-P}} = 0.048 M^{0.5} I_p^{0.85} R^{1.2} a^{0.3} k^{0.5} n^{0.1} B^{0.2} P^{-0.5}, \quad \tau_E = 1.8 H \tau_E^{\text{ITER89-P}}, \quad H = 2.2,$$

This is in good consistency with the next scaling [7]:

$$\tau_E = 0.191 P_{\text{MW}}^{-0.46} I_{\text{PMA}}^{1.03} R_m^{1.48},$$

where  $P = (P_F + P_{\text{cd}} - P_B) V$  - total plasma heating power.

To determine the average power densities in balance equation (1) the integration of expressions (2)-(4) on plasma volume was made.

Calculations shows, that optimal for maximal fusion power density is the value of  $\xi=0.7$  (corresponding to mixture of 60% D and 40%  $^3\text{He}$ ). The tritium concentration  $\zeta$  in calculations is equal to zero. At the first phase of investigation the range of optimal parameters at anyone energy confinement scaling is determined. The value of  $M = (P_F + P_B) / P_F$  is chosen as a figure of merit. The dependence of  $M$  from  $\beta^c$  for different value of aspect ratio  $A=R/a$  is obtained. The acceptable region of  $\text{D}^3\text{He}$  reactor parameters are aspect ratio near 2 and  $\beta \sim 15\text{-}20\%$ . The increase of  $B$  at  $\beta=\text{const}$  results in  $M$  decrease.

At the second phase of investigation the reactor parameters optimization with account of conductive heat losses is done. The value of  $Q=P_F/P_{\text{aux}}$  is chosen as a figure of merit, where

$P_{\text{aux}} = -P_F + P_T + P_B + P_C$  - the power to obtain the balance. In Fig.1 the  $Q$  and power dependence from plasma temperature is shown for next parameters:  $R=7\text{m}$ ,  $a=2.8\text{m}$ ,  $A=2.5$ ,  $B=5\text{T}$ ,  $\beta=15\%$ ,  $k=2.5$  (plasma elongation),  $q_\psi=3$  (safety factor on the plasma edge),  $I_p=50\text{MA}$ ,  $I_{\text{ps}}/I_p=0.29$ ,  $\xi_H=0$ ,  $R_W=0.9$ ,  $\alpha_n=0.5$ ,  $\alpha_t=1$ . The optimal temperature for reaching maximum  $Q$  is 40 keV.

In virtue of obtained data we made next conclusions:

1. The aspect ratio decrease is profitable to increase Q-value and to reduction of  $P_{aux}$ . However in this case the plasma current  $I_p$  increase, the bootstrap current part  $I_{bs}/I_p$  decrease and the current drive power  $P_{cd}$  increase. In Fig.2 the results of optimization by aspect ratio with  $R=7m$ ,  $\beta=15\%$  and  $B=5T$  are shown. Optimal value of aspect ratio, when current drive power is sufficient for power balance, is  $A=2.5$ .

2. To increase Q-value is possible by  $\beta$  growth. The Q and total power dependence from  $\beta$  is shown in Fig.3. It should be noted, that  $P_{cd}$  and  $P_{aux}$  have insignificant increment with  $\beta$  increase.

3. The major radius R increase results in increase of Q-value. The results of optimization by R are shown in Fig.4. From the condition  $P_{cd}=P_{aux}$  the value  $R=7m$  is selected. The optimal Q dependence on (A,R)-plane is shown in Fig.5.

4. The plasma elongation increase permit to enlarge the Q-value. The results of optimization by k are shown in Fig.8. The increase of Q is due to  $P_f$  growth and  $P_{aux}$  fall down.

5. In Fig.7 the Q and power variation with B increase is shown. At constant plasma current the B growth practically give not a gain of Q, however  $P_{aux}$  significantly increase in this case. At constant q on plasma edge the B growth permit to sharply increase Q-value, however in this case current drive power P increase to unreal high value. From this consideration and due to magnetic field restriction on toroidal coil we choose  $B=5T$ .

6. Q gain may be possible at more peaking profiles of plasma density and temperature. The profiles influence is shown in Fig.8. More peaked n and T profiles results in  $P_{cd}$  increase and  $P_{aux}$  decrease, that mean the transition from steady state reactor with  $P_{cd}=P_{aux}$  ( $\alpha_n=0.5$ ;  $\alpha_T=1$ ) to pulse reactor in which the significant part of current is supported inductively.

As a conclusion from the optimization calculations it may be recommended the next set of plasma parameters for experimental fusion reactor, that may be a prototype for energetic reactor:  $R=7m$ ,  $A=2.5$ ,  $B=5T$ ,  $I_p=50MA$ ,  $I_{bs}=0.29I_p$ . For different plasma profiles the fusion power and Q may change in the range:

$P_f = 1.1 \text{ GW} - 1.5 \text{ GW}$ ;  $Q = 3.3 - 14$ . Maximal magnetic field on toroidal coil  $B_m < 11T$ . Inductive plasma current changes from  $I_{ind}=0$  (steady state regime) to 27 MA (pulse regime). Auxiliary heating power  $P_{aux}$  with peaked profiles decreased from 340 MW to 100 MW.

For base variant the stationary tritium density  $n_T \approx 10^{11} \text{ cm}^{-3}$  and respectively the relative concentration  $\zeta \approx 0.2\%$ . This results in neutron power about 20 MW of 2.45 MeV neutrons and about 30 MW of 14.1 MeV neutrons.

~~D<sup>3</sup>He-reactor design parameters.~~ In the following the some estimates for the ~1GW-reactor design parameters are listed which are obtained for the reference parameter sets. The fusion reactor is taken to be characterized energetically by set of energy flow and conversion efficiency parameters, by fuel recycling efficiency limits, and the amount of net electrical power output that eventually becomes available to external

consumers. At the same time safety potential or radioactive health hazards of a fusion plant will be a consequence of neutron activation of structural material and tritium in fuel systems.

No neutrons and tritium are produced directly from the  $D^3He$  fusion. When the suppression of unavoidable DD and DT side reaction is not perfect, neutrons produced in plasma activate the first wall and shield materials.

Calculations shows the that neutron production can actually be reduced in  $D^3He$  plasma. So it is expected to largely reduce the neutron load and engineering problems associated with the neutron damage of the first wall and with the blanket. But even under low neutron wall loading conditions ( $0.03MW/m^2$  in our case (see Table) conventional stainless steel is not suitable for hands-on maintenance.

Since radiation damage effects will greatly be reduced in  $D^3He$  reactor the first wall-shield will last for the full life of the reactor. The projected lifetime of structure surrounding the plasma equals the reactor lifetime( $\sim 30yr$ ). The use of only one blanket shield assembly for the full reactor life has the additional advantage of reducing the total amount of material to be stored and may result economy penalty. But now in terms of activation and waste disposal hazards the operational safety advantages are less clear and appear to be strongly material dependent. A first wall and shield structure of water cooled SiC and B<sub>4</sub>C for thermal neutron absorption are attractive for the case.

The  $D^3He$  fuel cycle have a clear advantage over DT fuel cycle in terms of tritium hazards. There is no tritium breeding requirement in the blanket associated with  $D^3He$ -fuels. Tritium is generated as reaction product from the proton branch of the DD reaction. The tritium produced in plasma, which does not burn during its residents in the torus. Thus some tritium will be present in the plasma exhaust in the plasma fuel cycle. Clearly the tritium handling is reduced by two orders of magnitude for  $^3He$  rich mixes. On the other hand it is obvious that tritium represents a potential hazard also in the  $D^3He$  case.

The principal parameters for the designs are indicated in table. Stationary regime and pulsed mode for driven case are assumed. The relative importance of synchrotron losses in our case is not a significant contribution to the power balance. 40-50% of the power is associated with the leakage plasma. The leakage plasma could be candidate for high efficiency direct conversion. However a significant fraction of charged particle energy is lost via radiation. Respectively low thermal, direct conversion and injection efficiencies of 35, 65, and 50% assumed for near term construction time. The 10% on-site electrical power consumption for auxiliary equipment including coils and fuel cycle was proposed. The total power in neutrons is reduced to 4-5% in the case of 0.7:1  $^3He/D$ -density ratio. Blanket power multiplication factor of 1.3 and 4. for 14.1 MeV and 2.45 MeV neutrons was estimated.

These results demonstrates that a  $D^3He$  tokamak reactors of modest size (1 GWth) and operating in the  $Q>10$  mode is potentially feasible.

Since breeding is not required, a high temperature blanket and a helium cooling system can be utilized to achieve higher



cooling cycle efficiency 45%. The freedom of design afforded by the non-breeding blanket can provide a longer life and it is possible to approach the maximum plasma density without restricting the blanket life as occurs with DT.

If total direct conversion efficiency of 0% is obtained, in comparison to 45% efficient thermal cycle, then a gain of 300 and 800 MW would result for the steady state and pulsed cases.

Thus direct energy conversion is an essential element of  $D^3He$ . Possible approaches include electrostatic particle collection, synchrotron radiation conversion and others [8]. However, a number of design problems arise and the ability to incorporate these techniques into a tokamak configuration requires more study.

#### References

1. ITER Physics Design Guidelines:1989, IAEA, Vienna, 1990.
2. S.V.Putvinskij, Preprint KIAE-4532//6, M.,1987.
3. V.I.Pistunovich, Plasma Physics, vol.2, p.3, 1987.
4. I.N.Golovin, Preprint KIAE-4885/8, Moscow, 1989.
5. S.Atzeni,G.Vlad,4-th Int.Workshop on ECI,Roma,March 1984,p.35.
6. B.A.Trubnikov, Plasma Theory Questions, vol.7, p.274, 1973.
7. T.C.Simenon, ITER Phys./Design Work Session. San Diego, Cal., July 10-18, 1991.
8. J.F.Santarius, et al. UCLA-PPG-1274,Oct.1989.

Table

#### Design parameters for ignited $D^3He$ tokamak

$$\begin{aligned}
 R &= 7m, & A &= 2.5, & (a &= 2.8m), \\
 B_0 &= 5T, & B_{max} &< 11T, \\
 I_p &= 50 \text{ MA}, & I_{bs} &= 0.29 I_p = 15 \text{ MA}, \\
 \text{Plasma volume} &- 3900 \text{ m}^3, & \text{Chamber surface} &- 1500 \text{ m}^2, \\
 && D/^3He\text{-density ratio} &0.7.
 \end{aligned}$$

	Steady State	Pulsed Mode (3000s/200s)
$Q = P_{fusion} / P_{aux}$	3.3	14
Fusion power, GW	1.1	1.5
Neutron power, MW: 2.45 Mev	20	26
14.1 Mev	26	52
Total power, MW	1210	1670
Radiation power, MW	500 -	780
Drive power (1.2MeV-neutral beam), MW	340	100
Neutron wall load, MW/m <sup>2</sup>	~ 0.03	~ 0.05
Radiation wall load, MW/m <sup>2</sup>	0.3	0.5
Direct conversion efficiency, %	65 (70)	65 (70)
Thermal cycle efficiency, %	35 (45)	35 (45)
Injector efficiency, %	50 (50)	50 (50)
Gross power, MW.	600 (800)	800 (1100)
Net electric power, MW.	-140 (+90)	500 (800)
Overall net plant efficiency, %	-13 (+8)	35 (53)

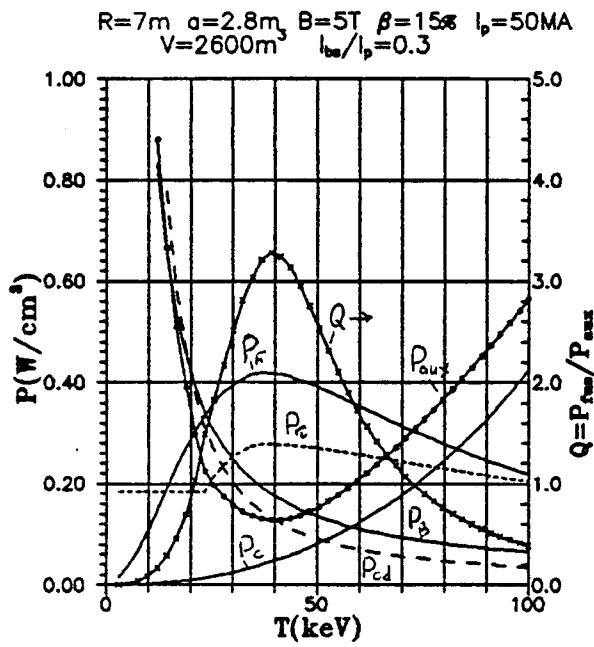


Fig. 1

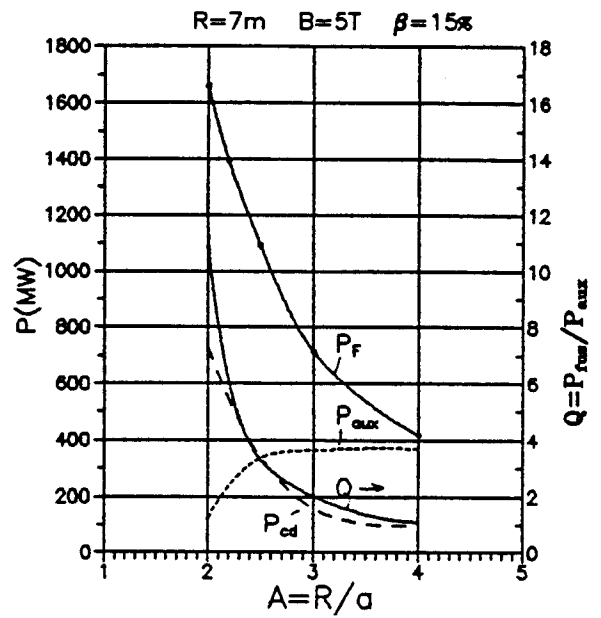


Fig. 2

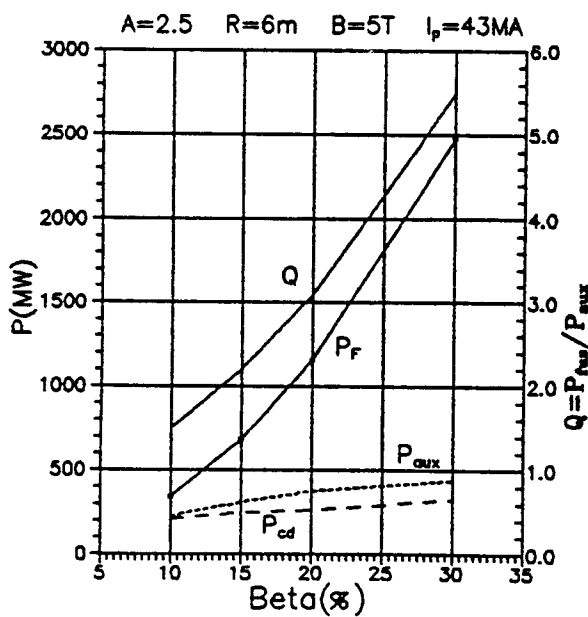


Fig. 3

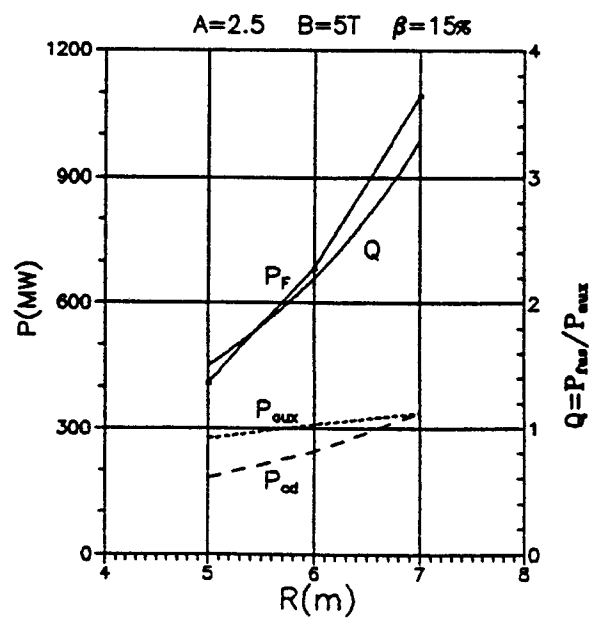


Fig. 4

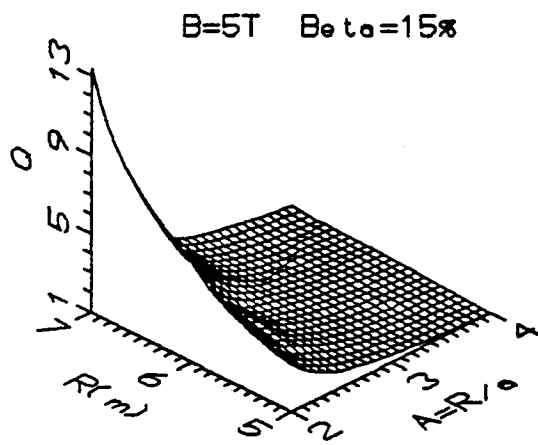


Fig. 5

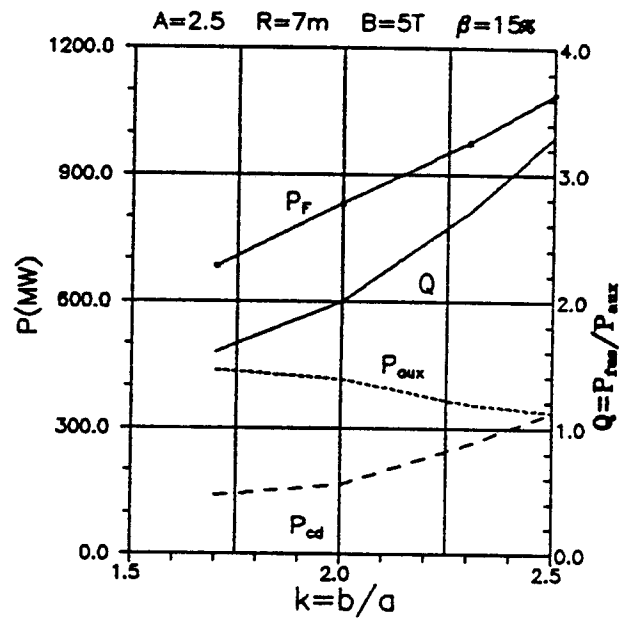


Fig. 6

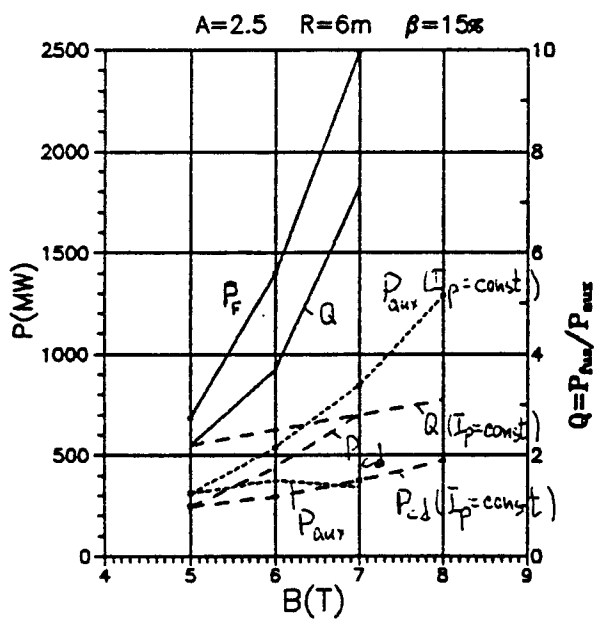


Fig. 7

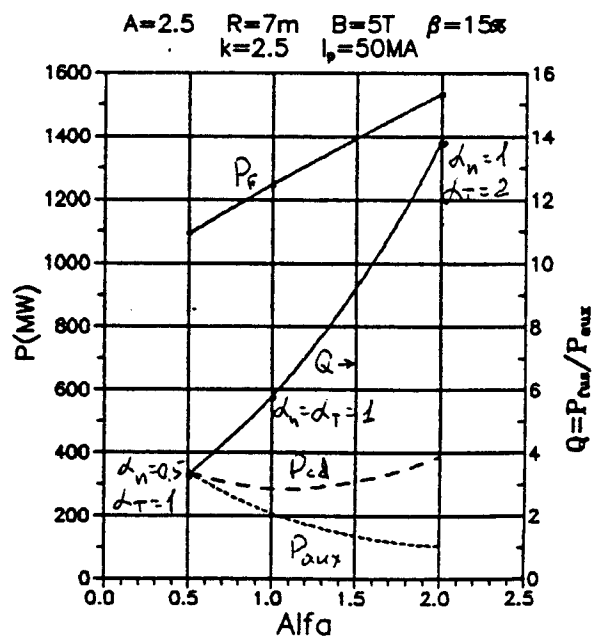


Fig. 8



# The ARIES-III D-<sup>3</sup>He Tokamak Reactor Study

John F. Santarius

University of Wisconsin, Madison, WI 53706

and the ARIES Team

## Abstract

*This paper briefly summarizes the key features of and issues for a preliminary version of the ARIES-III commercial tokamak reactor conceptual design. The ARIES project is a national study by the U.S. fusion community of various visions of a commercial tokamak reactor. ARIES-III has been designed to produce 1000 MWe from a tokamak utilizing the D-<sup>3</sup>He fuel cycle and operating in the second-stability MHD regime. Features of the device include the use of an organic coolant in the thermal power conversion cycle, a low releasable radioactive inventory during credible accidents, a first wall and shield that could survive a loss-of-coolant accident without structural damage, and a 'conventional,' high-recycle divertor. The final report [1] for the ARIES-III study is in progress, so the present information should be regarded as subject to change. The ARIES-III final report should be consulted for official reference parameters and detailed design descriptions.*

## 1 Overview

The ARIES, *Advanced Reactor Innovation and Evaluation Study*, project is designing several variants of commercial tokamak fusion reactors, with broad participation, primarily by the U.S. fusion community [1, 2]. The principal groups participating in the ARIES project are shown in Fig. 1.

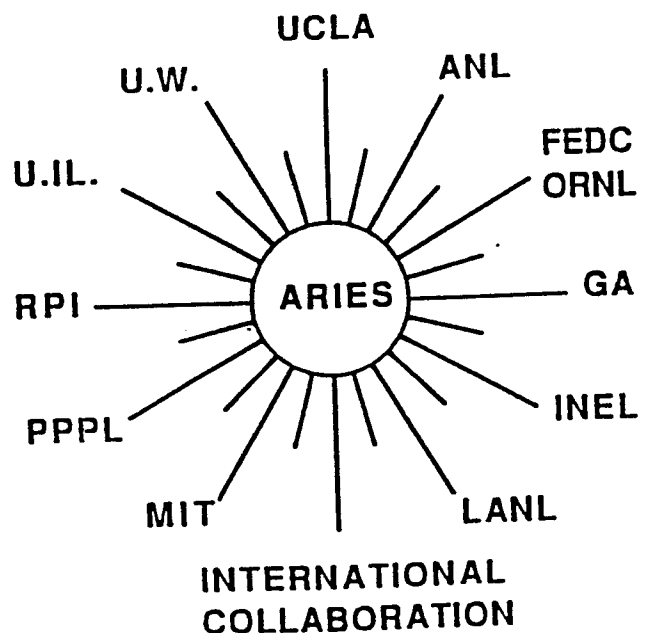


Figure 1: Principal ARIES project participants.

ARIES-III is one of three tokamak reactor *visions* being designed in detail within the ARIES project. The three visions are:

1. ARIES-I: A D-T, first-stability regime tokamak extrapolated from the ITER physics data base;
2. ARIES-II: A D-T, second-stability regime tokamak; and
3. ARIES-III: A D- $^3\text{He}$ , second-stability regime tokamak.

The ARIES-I final report is in press, the ARIES-III report in final edit, and the ARIES-II study is scheduled to be completed in March, 1992. Other options considered for ARIES-III were operation in the first-stability regime and utilization of the spherical torus configuration—that is, a very low aspect ratio tokamak.

The primary objectives for the ARIES-III study were to:

- Develop self-consistent design approaches for D- $^3\text{He}$  tokamak reactors.
- Determine potential economic, safety, and environmental features of this class of tokamak reactors.
- Identify critical physics and technology issues for D- $^3\text{He}$  tokamak reactors.
- Identify key issues that are specific to D- $^3\text{He}$  tokamak reactors.
- Identify key areas where use of D- $^3\text{He}$  fuel has resulted in improvements in reactor performance.

A viable, D- $^3\text{He}$  tokamak reactor—in comparison to a D-T tokamak reactor—must

overcome the relatively low fusion power density in the plasma. Figure 2 shows that, at the ion temperature corresponding to the peak power density for the respective fuel cycle, D-T fuel has about an 80 times higher power density than a 1:1 mixture of  $^3\text{He}$  and D. For a 1:2  $^3\text{He}$ :D mixture, the power density can be increased somewhat, but with an increased neutron production due to D-D reactions. The neutron production from these fuel cycles is shown in Fig. 3. In order to compete in the market-

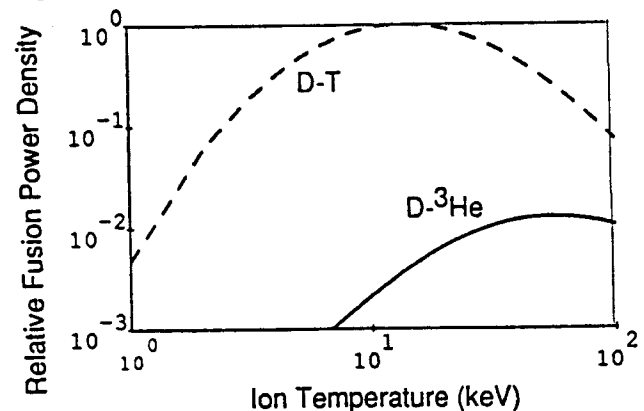


Figure 2: *Local fusion power density in the plasma for D-T and D- $^3\text{He}$  fusion fuels.*

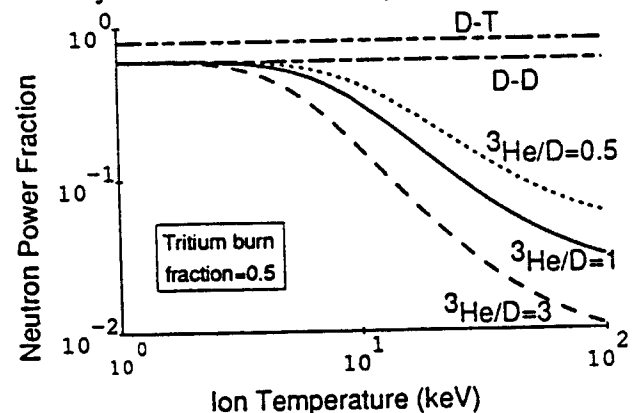


Figure 3: *Ratio of neutron power to fusion power for the D- $^3\text{He}$ , D-T, and D-D fusion fuel cycles. Several values of the ratio of  $^3\text{He}$  to D density are given for D- $^3\text{He}$ .*

place with a D-T reactor, a D- $^3\text{He}$  reactor must demonstrate that the engineering advantages derived from the reduced neutron flux and increased charged-particle power

fraction can compensate for the physics difficulties caused by the reduced plasma power density.

The key parameters of ARIES-III are listed in Table 1.

Table 1: *Key parameters for the ARIES-III D-<sup>3</sup>He commercial tokamak reactor design (preliminary).*

Plasma major radius	7.5 m
Plasma minor radius	2.5 m
Toroidal B-field on axis	7.6 T
Toroidal beta	24 %
Plasma current	30 MA
Electron temperature	53 keV
Electron density	$3.3 \times 10^{20} \text{ m}^{-3}$
Ion density	$2.1 \times 10^{20} \text{ m}^{-3}$
$Z_{eff}$	2.0
Total fusion power	2682 MW
Net electric power	1000 MWe
Recirc. power fraction	24 %
Ave. neutron wall load	$0.079 \text{ MW/m}^2$

## 2 ARIES-III Physics

Because of the relatively low fusion power density for a D-<sup>3</sup>He plasma, the operating-space design window is limited. Coupled

with the high plasma temperature and high magnetic field, this leads to the constraint that the first wall must be highly reflective to synchrotron radiation, so that most of the synchrotron radiation produced is reabsorbed in the plasma. This limits the choice of coating materials for the first wall to copper, beryllium, or tungsten; for ARIES-III, beryllium has been chosen. The required energy confinement time is  $\sim 7$  times the ITER-89P multiplier, or about twice that of the recently discovered VH-mode [3]. The small design window and the large energy confinement time required also lead to a design point with a fusion-ash particle confinement time to energy confinement time ratio of  $\tau_p^{ash}/\tau_E^{bulk} = 2$ . The assumption of a smaller  $\tau_p^{ash}/\tau_E^{bulk}$  ratio would allow a somewhat lower confinement multiplier. The relation of these values for ARIES-I, ARIES-III, and a D-<sup>3</sup>He first-stability tokamak to the present data base is shown in Fig. 4.

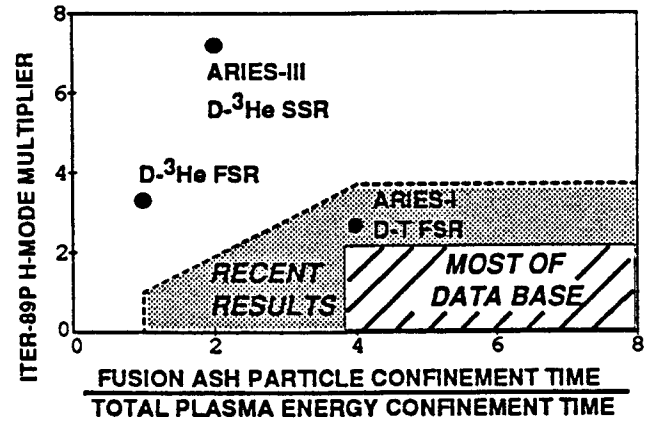


Figure 4: *Comparison of the ARIES first and second stability tokamak reactor cases with regard to energy confinement and to the ratio of fusion-ash to fuel-particle confinement.*

The MHD equilibrium and stability properties of ARIES-III have been investigated in considerable detail—leading to a second-stability design point at  $\beta = 24\%$ . Precise profile control is necessary to ensure

ballooning stability, as is feedback control of kink modes. An unanticipated difficulty of operation in the second-stability regime is that the bootstrap current constitutes a large overdrive beyond the plasma current necessary for equilibrium. This leads to a large external power for current drive. Neutral beams were chosen over fast waves, primarily because neutral beams provide about twice the efficiency in driving the current for ARIES-III parameters.

A D-T startup phase is used in ARIES-III, leading to  $\sim 1000$  MW of neutron power lasting for  $\sim 140$  s. The increased neutron heating can be handled by the magnets, but  $\sim 100$  MW of additional ICRF power beyond that absorbed from the neutral beams is required during startup.

A 'conventional,' high-recycle divertor appears to be viable, assuming L-mode plasma scaling at the edge, but design margins are small. The divertor plates are coated with a 4-mm layer of tungsten to reduce erosion during disruptions. During a disruption, the thermal energy dissipated is about 10 GJ, and the magnetic energy dissipated is about 5 GJ. Assuming a thermal quench time of 0.1–1 ms and a pessimistic vapor shielding factor of two, the resulting vaporization is about 0.2 mm Be for the first wall, and 3.9 mm W for the divertor. Higher vapor-shielding factors will reduce the erosion proportionately, but the plates will require re-coating after a few disruptions. Assuming a current quench time of 5–100 ms, initial analyses indicate that the electromagnetic forces give rise to only a few tenths of a MPa of pressure on the steel shield structure, so that the ARIES-III shield should be robust against a current quench.

### 3 ARIES-III Engineering

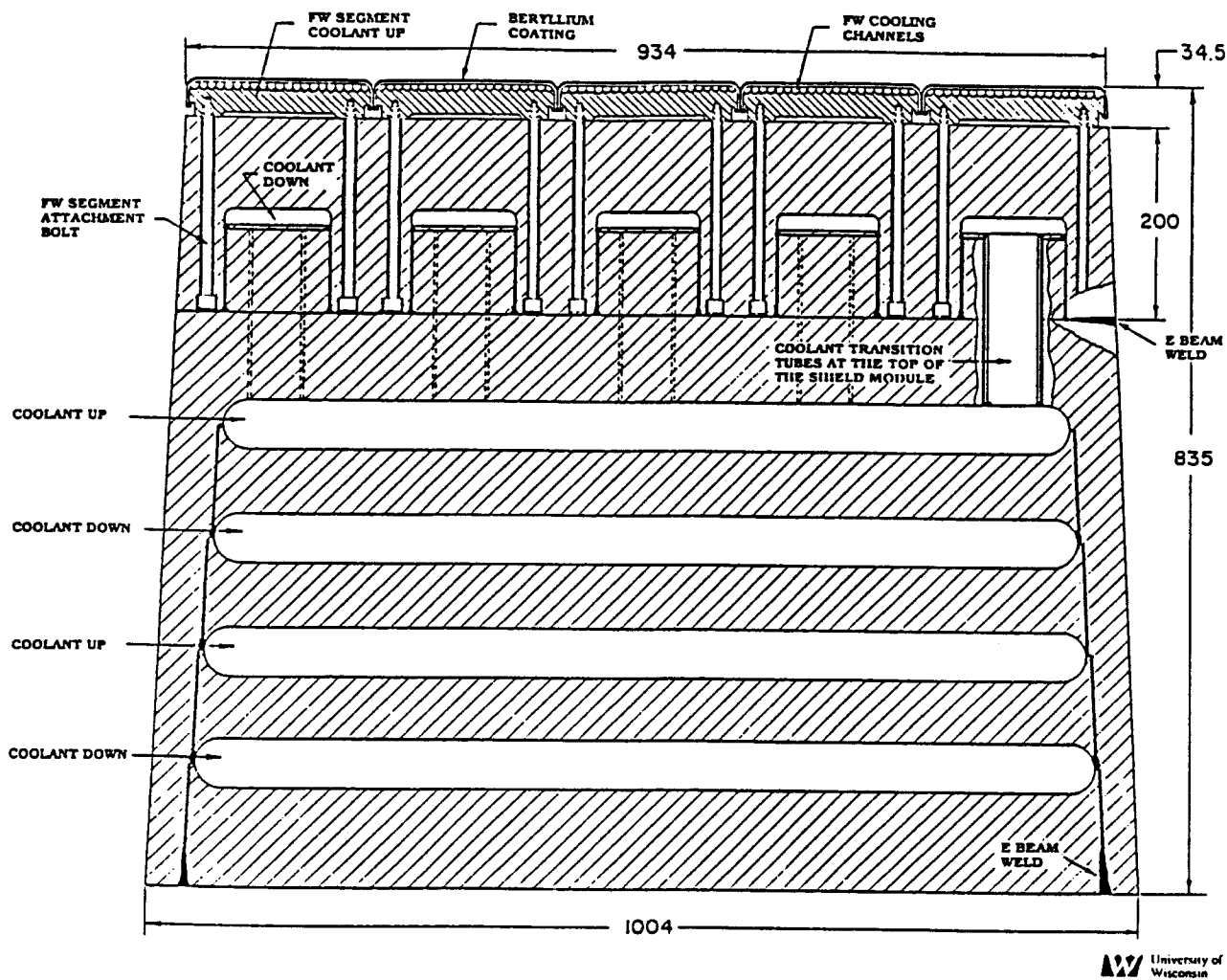
The ARIES-III shield will be constructed of a modified HT-9 alloy, with greatly reduced concentrations of niobium, molybdenum, and nickel. This leads to a substantial reduction of the neutron-induced, long-lived radioactivity and to a permanent shield. In contrast, the first wall and blanket of a typical D-T fusion reactor must be replaced five to ten times during the reactor's lifetime. The ARIES-III shield will qualify as Class A, low-level waste.

A key element of the ARIES-III design is that the afterheat is so low that a loss-of-coolant accident (LOCA) will neither melt the structure nor degrade the properties of the materials—so that protection of the economic investment is assured. The releasable radioactive inventory during credible accidents is also calculated to be low.

The outboard shield module is shown in Fig. 5. The 0.6 mm steel first wall is coated with a 1.5 mm thick layer of beryllium to efficiently reflect the synchrotron radiation produced by the plasma and to protect the steel first wall against disruptions. A 100  $\mu$ m layer of tungsten is located between the beryllium and the steel structure to prevent their interaction. The tritium production rate in the Be layer, the first wall, and the shield is  $<90$  Ci/d, and the induced radioactivity in the coolant is very low.

The reduced neutron flux of the D-<sup>3</sup>He fuel cycle allows the use of an organic coolant for the thermal power conversion cycle, because there is much less radiolytic decomposition than there would be in a D-T fusion reactor. Organic coolants operate at low pressure, allow high temperature, possess





University of Wisconsin

Figure 5: Schematic view of the ARIES-III outboard shield module in mid-plane cross section.

good heat-transfer characteristics, and generate very little corrosion. They do, however, decompose by both radiolysis and pyrolysis, thus requiring some coolant replacement, fast flow to avoid choking, and chemical waste disposal. The organic coolant HB-40 has been chosen for the reference case, and the power cycle efficiency is 44%.

## 4 Comparison of Key Issues for First and Second Stability Regime Operation

In the process of selecting the second-stability regime for the reference ARIES-III design, the ARIES team also examined the first-stability regime. A comparison of the key issues for these regimes is given in Table 2.

Table 2: *Key issues for first and second stability, D-<sup>3</sup>He, tokamak reactors.*

First Stability Regime	Second Stability Regime
$\tau_p^{ash} \leq 1.5\tau_E^{bulk}$	$\tau_p^{ash} \leq 3\tau_E^{bulk}$
H-mode confinement factor $\sim 3.5$	H-mode confinement factor $\sim 7$
Plasma current $> 50$ MA	Plasma current $> 30$ MA
Bootstrap current fraction $\sim 40\%$	Bootstrap current overdrive
Synchrotron current drive	Careful tailoring of plasma profiles
Rectenna synchrotron radiation conversion	Second stability regime experimental verification

Although the first-stability case is closer to the present energy-confinement data base, the particle-confinement limit for the fusion ash is more stringent than that of the second-stability case—possibly necessitating active pumping of the fusion ash. There is substantial overdrive of the plasma current in the second-stability case, but the bootstrap current in the first-stability case is only  $\sim 40\%$  of the plasma current, so that the use of synchrotron radiation current drive to limit the total external current-drive power is required. The predicted cost of electricity in the second-stability case is somewhat lower than that of the first-stability case, which invoked high-efficiency rectenna conversion of synchrotron radiation—an interesting technology that requires some extrapolation from the present data base.

There were various viewpoints within the ARIES team regarding the technical feasibility and attractiveness of these options, and the majority of the ARIES team favored the second-stability regime for the reference

ARIES-III design.

## 5 Conclusions

A detailed, integrated design of a second-stability, D-<sup>3</sup>He, commercial tokamak reactor, ARIES-III, has been performed. Several physics requirements are a significant extrapolation beyond the present data base and require verification. These include: second-stability regime operation, a high energy confinement factor, a relatively small design window, strict profile control, and an active kink stability control system. A D-T startup phase appears necessary, requiring  $\sim 100$  MW of additional ICRF power.

The engineering requirements are modest for the shield, and are generally not more difficult than those of a D-T reactor, except for the first-wall design, where a beryllium coating is necessary to reflect synchrotron radiation efficiently. Advantages include: elim-

ination of a tritium breeding blanket, use of organic coolant in a 44% efficient power cycle, a first wall and shield design that can survive a loss-of-coolant accident without structural damage or significant radiation release, and a low releasable radioactive inventory during credible accidents. The cost of electricity is comparable to that of the first-stability, D-T reactor, ARIES-I.

## Acknowledgement

This research was funded by the U.S. Department of Energy.

## References

- [1] F. Najmabadi, R.W. Conn, et al., "The ARIES-III Tokamak Reactor Study—Final Report," UCLA Report UCLA-PPG-1384 (1992).
- [2] F. Najmabadi, R.W. Conn, et al., "The ARIES-III D-<sup>3</sup>He Tokamak-Reactor Study," *Proc. 14th IEEE Symposium on Fusion Engineering* (IEEE, NY, 1992).
- [3] T.C. Simonen, "Recent Results from DIII-D," *Proc. 14th IEEE Symposium on Fusion Engineering* (IEEE, NY, 1992).

A  $D^3He$ -FUSION DRAKON TRAP - BASED REACTOR

Glagolev V.M. (reporter), Barinov M.A., Dobryakov A.V., Kuvshinov B.N., Leneva A.E., Petrov V.S., Proshin M.A., Timofeev A.V., Khripunov V.I., Sherstnev K.B.

## Abstract

Theory of equilibrium and stability, plasma transport coefficients in the dracon-trap are given in the paper. The method for direct conversion of fusion energy from charged particles to the electric one is considered. The technical proposal of a  $D^3He$  - fusion reactor has been developed, and calculations of its main characteristics (magnetic configuration, plasma parameters, shielding against neutron radiation) have been done.

## I. Introduction

The magnetic dracon-trap includes two long straight pieces with the magnetic field, (mirror type), the ends of which are closed with special curvilinear equilibrium elements (CRELs). The specific feature of a dracon is in that the CRELs at low  $\beta \sim 6-8\%$  in them ( $\beta$  is the ratio of a plasma pressure to the magnetic one) provide  $\beta \sim 60-80\%$  in the mirrors practically independently of their length [1]. At large plasma volume in straight pieces the main energy release is realized in them, and, as a result, the dracon is a closed trap with high  $\beta$ .

Another feature of the trap related with the toroidal drift compensation in CRELs is a low plasma heat conduction exceeding the classical one, calculated from the magnetic field of straight pieces, not higher than by the order of magnitude. The losses in this case are related to the toroidal drift of resonance particles, trapped in the CRELs, similar to the drift of superbananas in stellarators. The mentioned features of dracon have allowed us to consider the opportunity to use it for realization of a fusion reactor with the mixture  $D^3He$  [3]. For this purpose we have made a number of theoretical studies and have developed the trap modification which seems to be optimal at present with respect to its main parameters: equilibrium, stability, plasma transport coefficients. Note that the plasma parameters in the  $D^3He$  - reactor should be rather high -  $\beta \geq 30-40\%$  at the plasma temperature  $T=50-70$  keV and the confinement time  $\sim 10-20$  sec [4] - in connection with a strong cyclotron radiation. As shown in [3], it will be possible to realize ignition in the dracon trap due to a low value of  $\beta$  in CRELs, if the plasma volume in straight pieces two-three-times exceeds its volume in CRELs, mirror ratio being equal 2.5-3. The results of approximate calculations for the parameters of a commercial  $D^3He$  - dracon reactor, its thermal power is about 1000 MW, are given in this paper, and the possible technique of direct fusion energy conversion into electricity is considered.

## 2. The main reactor parameters

Calculations of parameters for a commercial reactor, at the thermal power of 1000 MW, are based on [3]. The reactor (top view) is depicted in Fig.1. The CREL includes some pieces of solenoid with helical magnetic axis. The hydromagnetic stability is realized with a stabilizer having a straight magnetic axis due to a local triangular - elliptic deformation of round magnetic surfaces [5]. The main reactor parameters are given in Table I.

Table I  
The main parameters of a dracon reactor

Parameter	Unit	Magnitude
Plasma radius in straight pieces	m	1.4
Chamber radius in straight pieces	m	1.6
Plasma radius in CREL	m	0.8
Chamber radius in CREL	m	1.0
Length of a straight piece	m	40.
Stabilizer length	m	14.
Radius of magnetic axis curvature in the central helical solenoids	m	3.2
Radius of magnetic axis curvature in the helical solenoids at the edges	m	3.5
Reactor chamber volume	m <sup>3</sup>	700.
Reactor chamber surface area	m <sup>2</sup>	1000.
Maximal magnetic field in CREL	Tl	15.
Magnetic field in straight piece	Tl	5.
Deuterium ( $n_d$ ) and helium-3 ( $n_{He}$ )		
plasma density at $n_d = n_{He}$	m <sup>-3</sup>	$10^{20}$

## 3. Assessment of neutron parameters for the reactor, dracon-type

The parametric calculation for a volumetric source of the fusion neutrons produced in the plasma of the fusion reactor, dracon-type, using the fuel mixture of D<sup>3</sup>He, is made for the ion temperature  $T_i$  50 keV, at two ratios of densities for the reacting mixture components,  $n_d = n_{He} = 10^{14} \text{ cm}^{-3}$  and  $n_d = 1/2 n_{He} = 0.7 \cdot 10^{14} \text{ cm}^{-3}$ . The density and temperature profiles are assumed to be flat. The necessary reaction rates in D<sup>3</sup>He - plasmas are taken from [6].

Assuming  $n_d \tau \sim 10^{15} \text{ cm}^{-3} \text{ s}$  ( $\tau$  is the tritium confinement time), one obtains the reactor parameters for a modification having the temperature equal 50 keV (Table 2). They show that the neutron loading upon the first wall, in the main rectilinear piece, is less than that characteristic for a D-T tokamak-reactor by more than two orders of magnitude. In the curvilinear piece (CREL-Zone) it is additionally twice lower.

Table 2  
Power parameters of the facility

Fuel composition, $n_d/n_{He}$		1/1	1/2
Piece of the chamber:	rectilin, curvilin	rectilin, curvilin	
Neutron current upon the chamber wall, $10^{10} \text{ cm}^{-2} \text{ s}^{-1}$ , with the energies 2.45 MeV and 14.1 MeV	$n_{2.45}$	7.3	3.6
	$n_{14.1}$	3.3	1.5
Neutron loading, $\text{MW/m}^2$	$n_{2.45}$	0.028	0.014
	$n_{14.1}$	0.075	0.036
Fusion power, MW		730	630
Power of a neutron component, MW	$n_{2.45}$	25	13
	$n_{14.1}$	65	31
Total power, MW		900	780

Such a change in the neutron loading essentially increases the service life of the first wall. It becomes comparable with the service life of the reactor itself, 30 years.

As for the counter-radiation shield thickness for superconducting magnets, the specific energy release in the materials (usually at the level  $\sim 1 \text{ mW/cm}^3$ ) and the corresponding power consumption for sustaining a superconducting state, as well as the permissible condition on the surface under "manual" servicing ( $\sim 2.5 \text{ mber/hour}$ ) are the most important parameters.

Proceeding from these data, one should assume the typical shield thickness, made of steel and borated water, to be equal 70 cm [8].

#### 4. Direct conversion of a fusion energy into electricity

We have chosen the circuit diagram [9] for direct conversion. In this case the direct conversion starts to be realized in the magnetic field of a dracon, it makes a natural transition into the magnetic field of a converter (Fig.2). We consider, as mentioned above, that the main contribution into a diffusive plasma flux is done by resonance particles. At the plasma periphery one should locate the "end electrodes" to realize the circuit diagram [9] at the CREL-field maximum (at the CREL centres). The potential distribution shown in Fig.3 is produced due to an effect of coupling with the ends. The opportunity to produce the electric field equal  $20 \text{ kV/cm}$ , perpendicular to the magnetic one, in the plasma at the density  $\sim 10^{12} \text{ cm}^{-3}$  was experimentally proved [10]. Resonance particles do not reach the electrodes. Therefore the plasma flux has an electric (not thermal) contact with them. The arrival of passing particles at the electrodes is eliminated with the divertor located at the CREL-centre. The magnetic field inhomogeneity in dracon and in the converter, in the presence of an electric field, results in the drift of resonance particles, depicted in Fig.3. In the process of drift motion the kinetic energy of particles is

transformed into the electric one. According to [9], the particles lose the longitudinal energy faster than the transversal one. This results in the trapping of particles in the converter. The current to the external circuit passes through the electrodes (2), (3) in Fig.2.

The direct conversion circuit modification is shown in Fig.4. Here the converter is separated from the main plasma confinement region with a separatrix zone. This allows one to reduce the magnetic field distortion in the plasma confinement region the increased size of the conversion zone. An undesirable effect of adiabatic invariant loss by the particles during the motion near a separatrix can be eliminated with the electric field perpendicular to the magnetic one. The dynamics of particles in the vicinity to the separatrix is computed and shown in Fig.5 to illustrate the above said. From Fig.5 it follows that the particles rapidly pass from the separatrix zone to the adiabatic one in the converter in the presence of the electric field, the drift in which is comparable with the toroidal magnetic drift.

#### Reference

1. Glagolev V.M., Kadomtsev B.B., Shafranov V.D., Trubnikov B.A. Nucl. Fusion, Plasma Physics, 1981, v.1, Rep E-8.
2. Galeev A.A., Sagdeev R.Z. Voprosy teorii plazmy, 1973, v.1, p.205.
3. Glagolev V.M. Meeting on D<sup>3</sup>He. Moscow IAE 1990 p.81
4. Golovin I.N. Preprint IAE N 4885/8 M 1989
5. Glagolev V.M., Leneva A.E. Fizika Plasmy, 1990, v.16(5), p.636
6. J.R.NcNally, Jr., K.E.Rothe, R.D.Sharp. "Fusion Reactivity Graph & Tables for charged Particles Reactions". ORNL-TM-6914, 1970.
7. M.E.Sawan and P.L.Walstrom, "Superconducting Magnet Radiation Effects in Fusion Reaction Technology, vol.10, nov.1986. pp.741-746.
8. W.F.Vogelsing and H.Y.Khater, "The Impact of D-<sup>3</sup>He Fusion Reactors on Waste Disposal". Fusion Engineering and Design, vol.5 (1988), pp.367-377.
9. Timofeev A.B. Fizika Plasmy, v.4(4), p.826, 1978.
10. G.F.Abarashidov, V.I.Volosov et al. Meeting on mirror traps, Moscow. 1989, p.109.

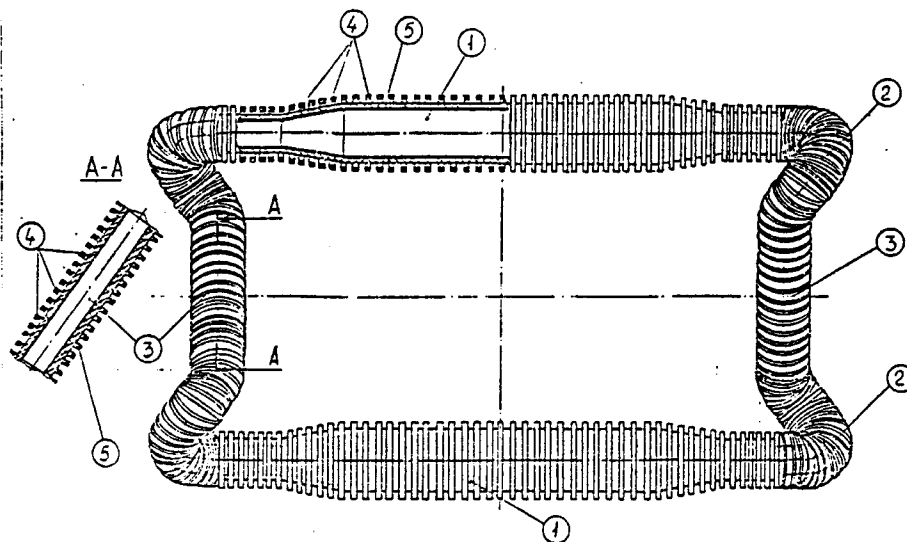


Fig. 1.

$D^3He$ - dracon reactor diagram  
 1. Straight piece (mirror). 2. Helical solenoids. 3. Stabilizer.  
 4. Coils. 5. Shield against a neutron flux.

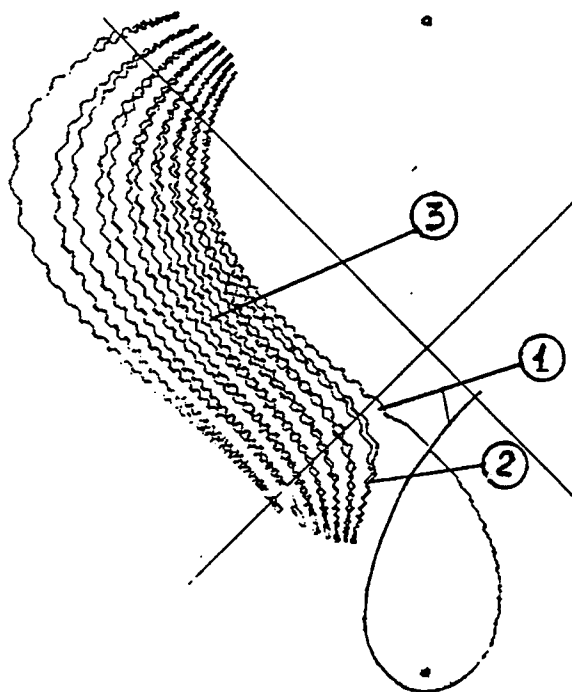


Fig. 5.

Ion motion in the converter,  
 in the vicinity to the separatrix  
 1. Separatrix.  
 2. Ion trajectory in the  
 vicinity to the separatrix.  
 3. Ion trajectory in the converter.



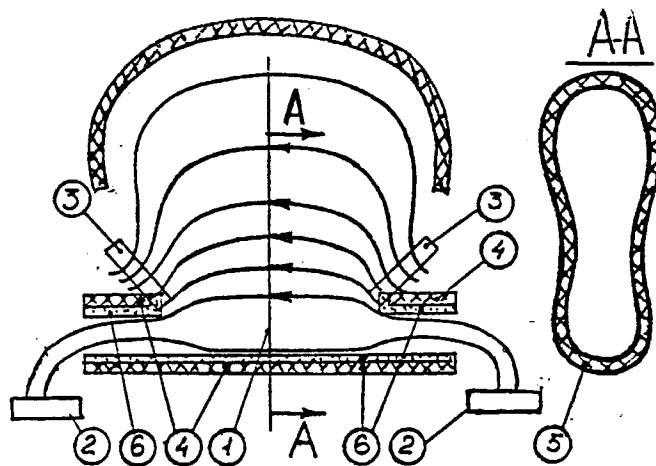


Fig. 2.  
Dracon with a built-in  
converter

1. Mirror.
2. End electrodes in CREL.
3. End electrodes in the  
converter.
4. Mirror coils.
5. Converter coil  
(AA-cut in the cross-section)
6. Shield against a  
neutron flux.

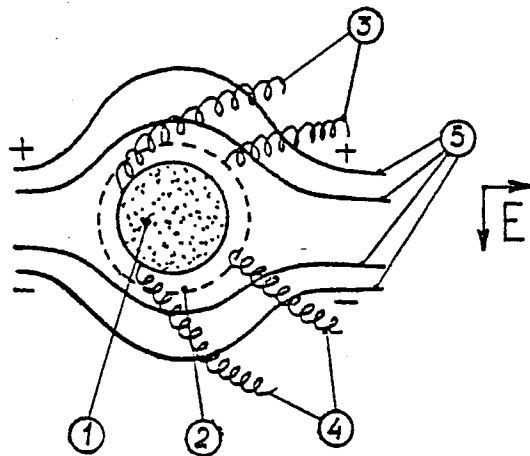


Fig. 3.  
Motion of particles and the  
potential distribution in  
the AA-cross-section Fig. 2

1. Plasma.
2. Divertor layer of passing  
particles.
3. Trajectory of ions.
4. Trajectory of electrons.
5. Equipotential surfaces in  
the field of CREL-end  
electrodes.

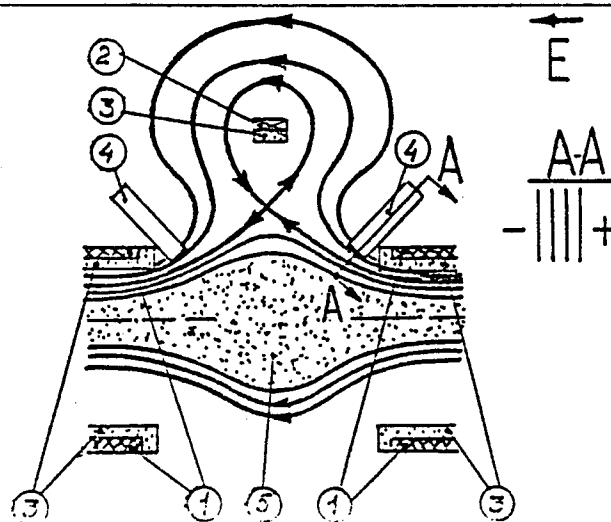


Fig. 4.  
Converter with a separatrix

1. Mirror coils.
2. Converter coil.
3. Shield against neutron  
flux.
4. End electrodes of the  
converter.
5. Plasma of passing  
particles.

$D^3He$  TANDEM MIRROR REACTOR

Golovin I.N.  
Kurchatov Atomic Energy Institute,

Khvesyuk V.I., Poletaev D.L., Shabrov N.V.  
Moscow State Technical University

Numerical calculations results of  $D^3He$  tandem mirror reactor (TMR) are presented. Such magnetic system type was chosen by following reasons:

1. For the positive plasma power balance maintenance (total fusion power exceeds the loss power) and effective reactor operation high plasma beta is necessary [1]. From the other hand, it provides fusion output more then 2 MW/m<sup>3</sup>, required for commercial power device.

2. Both in TMR and in closed systems ash accumulation problem will be one of the most difficult in  $D^3He$  fuel cycle case. But mirrors have a natural means for plasma cleaning. Ash and impurities quantity in TMR can be controlled.

These advantages together with other ones [1] make TMR the prime candidate for the future  $D^3He$  fusion reactor.

Now the most important problem is investigation of the power efficiency of such reactor. In ref. [2-4] several estimates of  $D^3He$  TMR power efficiency were carried out. Notice, that these works used plasma model based on the power and particles balance equations. Ash accumulation and fusion power redistribution in plasma were not calculate correctly. But these processes are very important ones for the  $D^3He$  reactor. Therefore we studied the ash kinetics in detail. First of all, numerical simulation of central cell plasma was made, because central cell is the fusion generation zone and TMR parameters are directly related to central cell plasma processes. Such approach permits us to investigate the central cell power balance and determine the basic parameters of plasma (power multiplication factor Q, partial  $\beta$ , etc.).

Then the general consideration of the plasma processes in  $D^3He$  TMR was carried out. On the base of this analysis the main requirements to different TMR parts (plugs, thermal barriers) were determined.

The methods and results of calculations are discussed below.

## KINETICS OF CENTRAL CELL PLASMA

In this section a profound analysis of plasma power balance, ash accumulation and neutron production in central cell was treated. Both Coulomb and nuclear elastic scattering must be considered in such study. So central cell plasma model was based on the coupled nonlinear kinetics equations set with both Fokker - Planck and Boltzmann collisional operators for all ash species ( $p$ ,  $\alpha$  and  $T$ ) and balance equations set for maxwellian particles species ( $D$ ,  $^3\text{He}$  and electrons). Total central cell plasma  $\beta$  and fuel ions temperature  $T_i$  were taken to be the main variable parameters in our study. Calculations were done for  $\beta=0.7$ ,  $T_i=50...100$  keV,  $n_D=n_{He}$ , ion confining potential  $\Phi_i/T_i=3...4$ , central cell magnetic field  $B_c=5T$ , vacuum mirror ratio  $R=2...5$ , plasma radius  $R_{pl}=1m$ , first wall reflection coefficient  $c_r=0.9$ .

Modeling results show that ash accumulation problem will be one of the most difficult ones for  $D^3\text{He}$  fueled reactor. Ash densities and partial betas increase rapidly when  $\Phi_i$  became sufficiently large (fig. 1). So assuming total beta constant we have partial fuel beta and fusion power output decreasing. It has a great influence on plasma power balance (fig.2). Central cell plasma power multiplication factor  $Q$  obtained in our calculations doesn't exceed 2 (fig.3).

Comparison of our results with early  $D^3\text{He}$  TMR plasma calculations (ref. [2-4]) shows that exact account of thermalized ash accumulation and ash - fuel power exchange leads to significant modification of all reactor plasma parameters.

Besides, tritium density and neutrons power level estimates have been done. Neutrons take away about 2% of the total reactor fusion power and 14 MeV neutrons part is less than 1% only (fig. 4). This is  $D^3\text{He}$  reactor adventure that stimulate the search of reactor power efficiency increasing methods.

The possible one is central cell plasma cleaning by means of ash resonant pumping. Estimates have been done for ash pumping influence investigation. We assumed that particles having a resonant energy  $E^*$  are removing from plasma volume

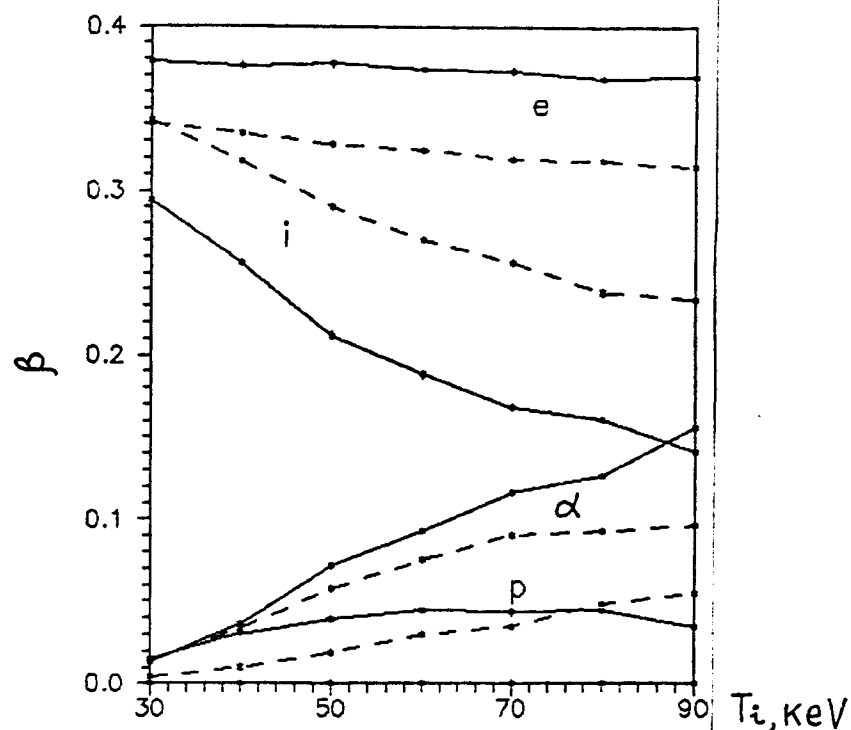


Fig.1. Partial betas for central cell plasma species.  
( $T_i=60\text{keV}$ ,  $R=5$ , solid -  $\Phi_i/T_i=4$ , dashed -  $\Phi_i/T_i=3$ ).

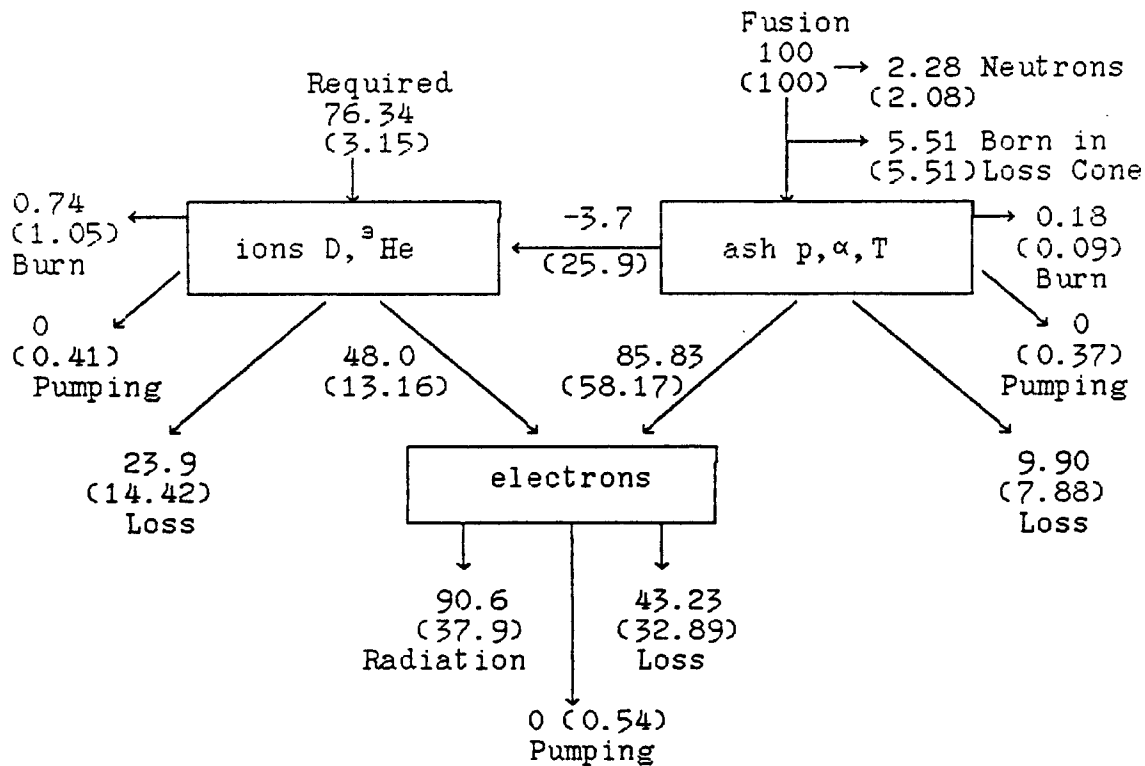


Fig.2. Central cell plasma power balance. ( $T_i=60\text{keV}$ ,  $\Phi_i/T_i=4$ ,  $R=5$ ) In brackets -with ash pumping ( $E^*=T_i$ ,  $\tau^*=10^{-2}\text{sec}$ ).

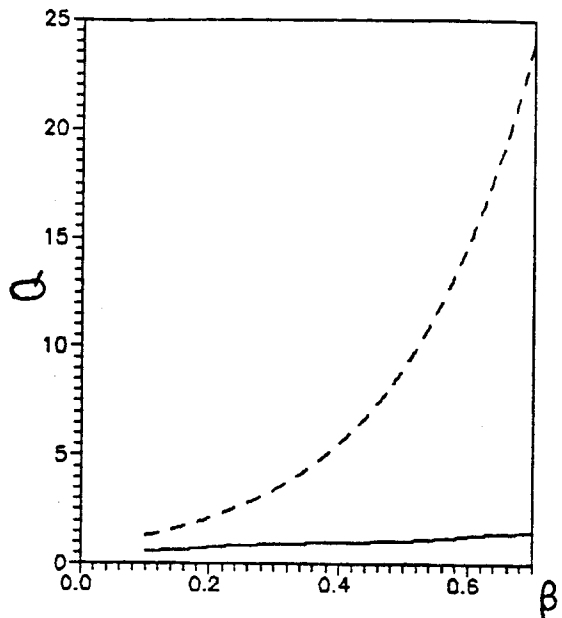


Fig. 3. Power multiplication factor  $Q$  vs. total plasma  $\beta$  ( $T_i = 60 \text{ keV}$ ,  $\Phi_i / T_i = 4$ ,  $R = 5$ )  
Dashed - with ash pumping  
( $E^* = 90 \text{ keV}$ ,  $\tau^* = 10^{-2} \text{ sec}$ )

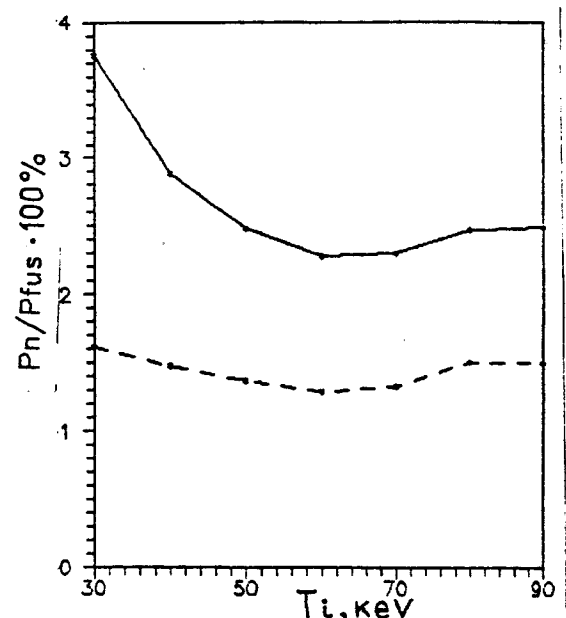


Fig. 4. Neutrons part in fusion power (in percents). Dashed - 14 Mev neutrons part  
( $T_i = 60 \text{ keV}$ ,  $\Phi_i / T_i = 4$ ,  $R = 5$ ).

during pumping time  $\tau^*$  and magnetic field perturbation takes place in the barrier region, so pumping acts on passing particles only. Ions removal was accompanied by equal electron loss that have been taken into account in ambipolarity and power balance equations.

Calculations were made for resonant energies and pumping times varied in following range  $\tau^* = 10^{-1} \dots 10^{-3} \text{ s}$ ,  $E^* = (0.5, 1, 2, 3, \dots, 6) \times T_i$  for  $T_i = 60 \text{ keV}$  and  $\Phi_i / T_i = 4$ . Results are presented on fig. 2, 3 show that "cold" ash removal really leads to significant reactor power efficiency increasing ( $Q \geq 20-30$ ).

Certainly, our pumping modeling is very rough, because of resonant pumping possibilities have not been studied extensively yet. In particular, possible resonant interval width, pumping intensities range and its power price (required power input) are vague now.

Notice, that we have not model precisely radial transport influence in our work. However, it can be a more relevant issue in a case of large ions confining potential and plasma simulation results depend significantly from this process proper account.

## GENERAL PLASMA BALANCE ANALYSIS

For different conceptual design problems consideration the total TMR plasma model was developed. It includes all parts of the reactor and interactions between them. The model is based on the system of energy and particle balance equations. Its characteristic property is fact of using kinetic calculations for ash species.

The model was applied for investigation of the high ion-confining potential forming conditions. This problem is especially important for  $D^3He$  reactor in which  $T_i$  and  $\phi_i/T_i$  must be large. Creation of the potential barrier about or more than 4 ions temperature have the practical interest. We obtained that there is the optimum value of the plug  $\beta_p$  (finally, the plug injection current), for maximum  $\phi_i/T_i$  forming if plasma parameters in central cell and input plug power are fixed (fig.5). Deviation from the optimal  $\beta_p$  decreases the  $\phi_i/T_i$  ratio. Such type of dependence is

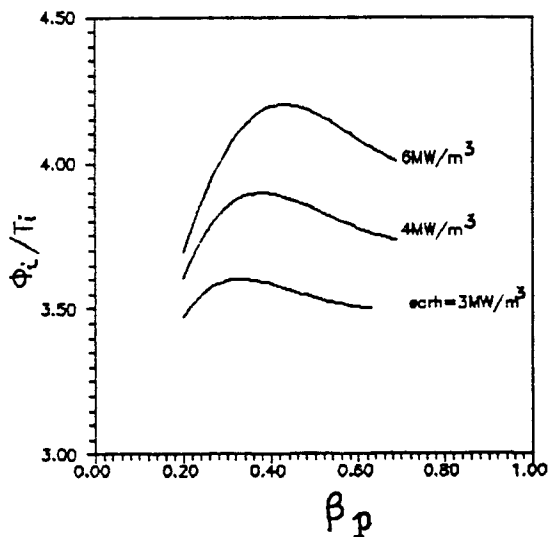


Fig.5.  $\phi_i/T_i$  ratio for different  $\beta_p$  ( ECRH in plug-var.)

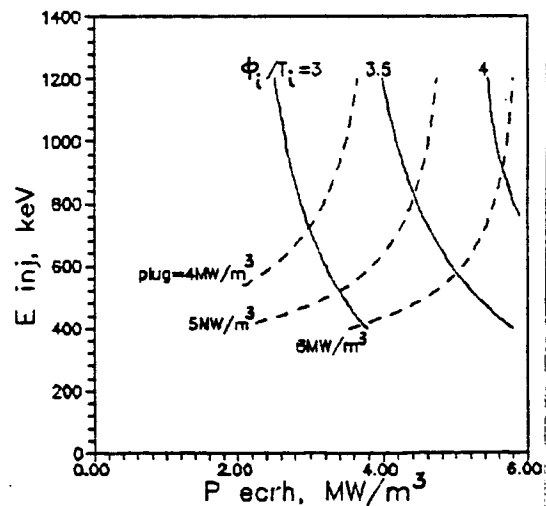


Fig.6. Plug injection and ECRH parameters influence on  $\phi_i/T_i$ .

determined by common influence of two factors: plug density increasing and plug electrons temperature decreasing.  $\phi_i/T_i$  maximum magnitude and location depend from the heating parameters in the plug, plasma parameters in the central cell and thermal barrier.

Fig.6 displays the results, which allow us to determine requirements to the injection and ECRH parameters in the plug. Let's note high ECRH level necessity for  $D^3He$  TMR plugs. The neutral beams input power in plug is limited by  $\beta_p$ -allowable injection current and achievable injection energy. The results were calculated with pre-assigned parameters, which are presented in table. This table includes obtained main  $D^3He$  TMR plasma parameters either.

TABLE.  $D^3He$  TMR PLASMA PARAMETERS

* central cell magnetic field	5 T
* choke magnetic field	25 T
* maximum ion-plug field	10 T
* minimum magnetic field	5 T
central cell floating potential	367 keV
* ion-confining potential	200 keV ( $\phi_i/T_i=4$ )
* thermal barrier potential	260 keV
<u>central cell</u>	
* average $\beta$	0.7
fuel $\beta$	0.25
electrons $\beta$	0.344
ash $\beta$ ( $\beta_p, \beta_\alpha$ )	0.106 (0.092, 0.014)
* fuel ion <sup>p</sup> temperature	50 keV
electrons temperature	46 keV
deuterium $\tau$	10 sec
helium-3 $\tau$	334 sec
ash density	$6.4 \times 10^{18} \text{ m}^{-3}$
( $n_p, n_\alpha, n_\tau$ )	( $2.6 \times 10^{18} \text{ m}^{-3}, 3.6 \times 10^{18} \text{ m}^{-3}, 1.9 \times 10^{17} \text{ m}^{-3}$ )
* $^3He$ to D density ratio	1
<u>plug</u>	
* average plug $\beta$	0.5
average ion energy	836 keV
electron temperature	189 keV
* injection energy	700 keV
* plug to central cell volume ratio	0.01
<u>specific powers in plasma</u>	
fusion power	$3.8 \text{ MW/m}^3$
neutron power	$0.12 \text{ MW/m}^3$
plasma power multiplication factor Q	19
plug neutral beam power	$0.6 \text{ MW/m}^3$
plug ECRH power	$6.0 \text{ MW/m}^3$
power required for thermal barrier	not calculated
pumping power loss	not calculated

\*) pre-assigned values

## SUMMARY

Our calculations data confirm the possibility of high efficiency  $D^3He$  TMR plasma regimes ( $Q \geq 20$ ) realization. So further work is required for more profound  $D^3He$  plasma investigation and TMR conceptual design. First of all it is necessary to concentrate attention on the following problems:

a) ash pumping from  $D^3He$  reactor theory and methods development;

b) high TMR plug and barrier potentials creation study (more then 200 keV is necessary for plug and more then 250 keV for thermal barrier potential);

c) investigation of instability of the high  $\beta$  plasma.

It is clear that correspondent numerical models and methods for all these problems consideration must be developed.

## REFERENCES

1. Hershkowitz N., Miyoshi S., Ryutov D.D., Nucl. Fusion 27 (1990) 1761.
2. Shuy G.W., Dabiri A.E., Gurol H., Fus.Technol. 9 (1986) 459.
3. Santarius J.F., Nucl. Fusion 27 (1987) 167.
4. I.N.Golovin, V.I.Khvesyuk, et al. Proc. Intern. School of Plasma Phys. Workshop. - Varenna (1989) 673.



# CONCEPTUAL DESIGN OF D-<sup>3</sup>He FRC REACTOR "ARTEMIS"

H.Momota,  
National Institute for Fusion Science, Nagoya 464-01, Japan  
co-authored with  
A.Ishida, Niigata University, Niigata 950-21, Japan  
Y.Kohzaki, Institute for Future Technology, Tokyo 102, Japan  
G.H.Miley, University of Illinois, Urbana, IL 61801  
S.Ohi, Osaka University, Suita 565, Japan  
M.Ohnishi, Kyoto University, Uji 611, Japan  
K.Sato, Himeji Institute of Technology, Himeji 671-22, Japan  
L.C.Steinhauer, STI Optronics Inc., Bellevue, WA 98004  
Y.Tomita, National Institute for Fusion Science, Nagoya, Japan  
M.Tuszewski, Los Alamos National Laboratory, Los Alamos, NM 87545

## 1. Introduction

Progress in fusion research has been achieved mainly on tokamak experiments, and a scientific feasibility experiment will be performed before long on this concept. Nevertheless, a number of engineering problems have to be resolved before D-T fueled tokamaks become accepted as commercial fusion reactors. Development of a reasonable tritium breeding blanket is one such example. Among those, certain engineering problems for a commercial D-T fusion reactor are attributed to 14MeV neutrons, which seem very hard to resolve.

Deuterium and helium-3 fusion fuels are considered to mitigate these engineering problems associated with 14MeV neutrons. With those fuels, the fraction of 14MeV neutrons in the total fusion power decreases to a few percent<sup>1,2)</sup> and more than 70% of fusion power is carried by 14.7MeV fusion protons and the diffused thermal fuel component.. If these charged particles can be conducted<sup>1)</sup> to direct energy converters, we are able to achieve a highly efficient fusion plant by employing D-<sup>3</sup>He fuels. Physics requirements such as the confinement parameter  $n\tau$  and the operation temperature  $T$  needed to sustain D-<sup>3</sup>He fusion reactions are as high as  $10^{21}$ sec/m<sup>3</sup> and around 100keV, respectively. In order to reduce a synchrotron radiation loss and to obtain consequently a higher plant efficiency, a large plasma beta-value (>30%) is also recommended. Accessibility of high-power direct energy converters is necessary to utilize the power carried by charged particles.

By its intrinsic characteristics a field-reversed configuration (FRC) seems to meet the above requisites. The plasma is confined by closed lines of force for good confinement and surrounded by open lines of force for charged particles extraction. Since an FRC has no toroidal magnetic field for plasma stability, a stably confined FRC plasma so far obtained in experiments<sup>3,4)</sup> has an extremely high beta value (>50%).

A conceptual design study of this D-<sup>3</sup>He FRC fusion reactor "ARTEMIS" has been carried out for the purpose of examining its attractive characteristics and clarifying the critical issues for commercial fusion reactors.

## 2. "ARTEMIS" Reactor Concept

The  $D-^3He$  fueled FRC fusion reactor "ARTEMIS" consists of a formation chamber, a burning chamber, and a pair of direct energy converters all of which are connected by the magnetic lines of force (Fig.1). An FRC plasma is produced at the start by the

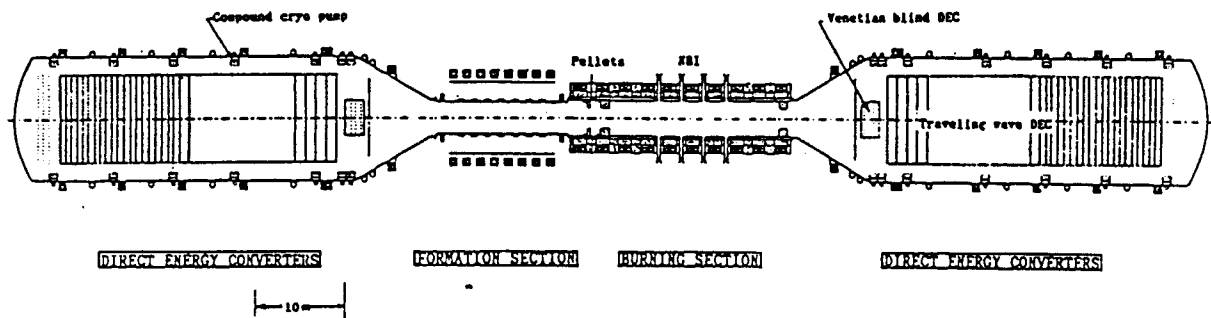


Fig.1: A whole view of the  $D-^3He$  FRC reactor "ARTEMIS" composed of formation chamber, burning chamber, and direct energy converters

conventional reverse-biased fast theta pinch method in the formation chamber and then translated to the burning chamber. A combination of neutral deuterium beam injection (NBI), fueling, and a slow magnetic compression in the burning chamber brings the volume, the temperature, and the number density of the plasma up to those for the  $D-^3He$  burning state. The bulk of the  $D-^3He$  fusion energy is carried by charged particles along the lines of force, which connect to a pair of direct energy converters. A smaller fraction of the fusion energy is carried by neutrons and photons to the first wall of the burning chamber. This energy is converted to electricity by turbine-generators.

### [Fusion Plasma]

The formation chamber is arranged symmetrically so as to reduce error fields to a level as low as possible. Therefore only a small port for gas puffing is installed in a symmetric coils and vacuum chamber system. Then, reliable FRC plasma formations can be achieved even for a very low feeding gas pressure. A fast rising theta-pinch discharge with a one turn voltage of 400kV in a filling gas pressure of 0.05Pa and bias field of 0.035T produces an initial FRC plasma whose parameters are listed in Table 1-a. The plasma is then translated to the burning chamber due to an unbalanced cusp magnetic field. During the translation, the FRC seems to conserve particle numbers of respective species, the total energy, the trapped flux, and its "Intelligence". Plasma parameters obtained in this way at the burning chamber are listed in Table 1-b.

Phase	a	b	c
Plasma Radius (m)	0.7	1.0	1.12
Plasma Length (m)	4.8	14.8	17.0
Plasma Temperature (keV)	1.0	1.0	87.5
Electron Density ( $\cdot 10^{20}/m^3$ )	4.1	0.62	6.6
Trapped Flux (Wb)	0.086	0.086	3.66
External Magnetic Field (T)	0.56	0.22	6.7
s-Value	5.9	2.7	9.2
Plasma Beta-Value	0.92	0.83	0.90

Table 1: Plasma parameters at the phases  
a: after the formation of the FRC  
b: after the translation of the FRC  
c: steady burning state

In the burning chamber, the FRC plasma is heated by means of energetic neutral deuterium beam injection, whose maximum power is 100MW. A slow magnetic compression is also applied. The injected particles form an ion beam current which plays a roll of the seed current needed to sustain or increase the trapped magnetic flux of an FRC. The plasma evolves in its volume, the density, and the temperature for a burning plasma. During the evolution, the ratio of the current carried by the energetic beam

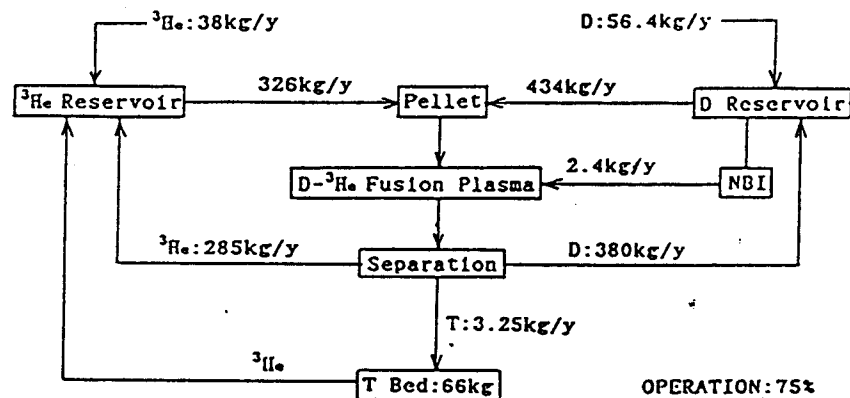


Fig.2: A chart of particles flows in "ARTEMIS": A certain part of fusion particles are lost directly and others are diffused out of plasma.

particles to the total plasma current is high enough to stabilize an FRC against macroscopic modes. A set of plasma parameters obtained in this way are tabulated in Table 1-c.

In a D-<sup>3</sup>He burning FRC plasma, a current drive due to the preferential trapping of fusion protons assisted by a small amount of external beam injections is sufficient to sustain an equilibrium in a steady burning state<sup>5)</sup>. The particle flows in this steady burning D-<sup>3</sup>He FRC plasma are exhibited in Fig.2, where the unknown particle transport is tentatively

assumed to be 206 times the classical rate<sup>6)</sup>.

[Reactor System]

A fairly low feeding gas pressure of 0.05Pa and a high one-turn voltage of pinch coils are needed to obtain an FRC with a low s-value. Insulation for this high voltage is achieved by applying a 4-stage tandem structure of the pinch coils.

Pulse SC coils of 1.87MAT/coils at the formation chamber raises the magnetic field up to 1.26T in a period of 50msec. Fast coils for this compression (25T/sec, max.1.26T) are ready to perform with the present technology, since a fast rising superconducting coil which gives a rising rate of 200T/sec and a maximum field of 4T has been examined<sup>7)</sup> with a 3-staged strand cable. A large radius, 5m, is chosen for the compression coils in order to reduce the coupling with the coaxial pinch coils, 2.1m radius, with an assist of a magnetic shielding plates.

The development of pellet acceleration is one of the most important engineering problems in fusion research: a representative speed of a pellet needed to inject a pellet deeply into a plasma center is several times  $10^4\text{m/sec}$ , which may be compared with a presently available speed:  $10^3\text{m/sec}$ . In "ARTEMIS" design, however, a pellet of  $1.8\text{mm}^3$  volume consists of a cylindrical ice deuterium vessel and inner liquid helium-3 is dropped every 0.9 seconds. Fabrication of the pellet is rather simple. When a pellet locates near the center of the chamber, FRC plasma moves towards the pellet at a high speed more than  $10^4\text{m/sec}$  with the aid of an applied cusp field and consequently engulfs it deeply inside the plasma.

A set of 10 superconducting coils of 14.2MAT/coils and radius of 3.5m is installed at the burning chamber and supplies a magnetic field of 6.7T. The required averaged current density of  $30\text{A/mm}^2$  is conventional and the stress of 300MPa is easily held by a reinforced structure of strand cable.

For the purpose of heating the plasma as well as driving plasma current which is needed to sustain the plasma in a steady equilibrium, injections of 1MeV deuterium neutral beam particles are employed. The maximum power of 100MW is required for the start up and 5MW to sustain the plasma in the steady burning state. The development of this neutral beam is presently within the scope in R&D programs for ITER.

One of the most important technologies to be developed for a D-<sup>3</sup>H<sub>e</sub> FRC reactor is the direct conversion of fusion power carried by charged particles. For the thermal component of a plasma, a "Venetian blind type" generator<sup>8)</sup> (VBDEC) might be applicable. For 14.7MeV fusion protons, however, the energy is too high to maintain the necessary electrical insulation. The concept of a "traveling wave direct energy converter"<sup>9)</sup> (TWDEC) is developed based on the principle of a "Linac"<sup>10)</sup>.

### 3. Characteristics of ARTEMIS

A conceptual design of D-<sup>3</sup>He FRC power reactor "ARTEMIS" has been carried out, whose power flow chart is exhibited in Fig.3. All of the technological bases employed for this

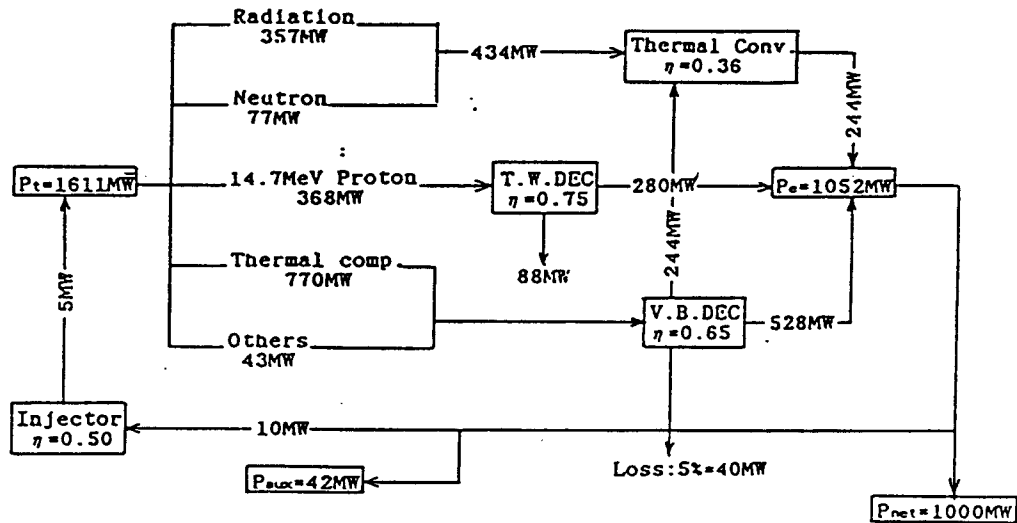


Fig.3: A power flow diagram of D-<sup>3</sup>He FRC power plant "ARTEMIS": On the bases of high efficiency of the direct energy converters, an overall plant efficiency is as high as 62%.

design are conventional. A conversion efficiency of heat energy to electricity is assumed to be 36%. Owing to the high efficiencies of direct energy converters, the overall plant efficiency is estimated as high as 62%. The principal parameters of the plant are shown in Table 2. The device consists of straight tubes forming a linear geometry and is consequently easy to disjoint for maintenance.

On the bases of the ESECOM study<sup>11)</sup>, costs of electricity have been estimated. Table 3 summarizes the costs of electricity (COE) for the D-<sup>3</sup>He FRC reactor "ARTEMIS". An average load factor of 75% is assumed. It must be noted that the fuel cost (assumed cost of helium-3 obtained from the Lunar soil<sup>12)</sup> of 0.2M\$/kg) contributes only 4%. Since the total weight of the reactor, excluding NBI, is approximately 3,300tons which is 1/3 of a corresponding light water reactor and the geometry is very simple, the estimated COE is as cheap as 28.7mills/kWh from "ARTEMIS", which is cheaper than the estimated COE from a presentday light-water reactor.

Fusion Plasma	
Volume:	( $r_s=1.12m$ , $l_s=17m$ ) $67 m^3$
Fuels:	$D_2^3He$ : $n_{D_2}:n_{He} = 1:2$
Averaged Electron Density:	$6.6 \cdot 10^{20}/m^3$
Temperature ( $T_i = T_e$ )	$87.5keV$
Beta-Value	90 %
Chamber	
Formation Chamber:	$r=1.8m$ , $L=15m$ , $t=0.15$ Alumina Tube
Burning Chamber:	$r=2.0m$ , $L=25m$ , $t=0.05m$ Ferritic Steel
Heat Load on the First Wall:	$1.70 MW/m^2$
14MeV Neutron Load on the First Wall:	$0.26 MW/m^2$
Energy Conversion Chamber:	$r=10m$ , $L=50m$ SS Vessel
Magnetic Coils	
Pinch Coils:	$r=2m$ , $L=10m$ 4-stage tandem, Cu, $L_c=1.6\mu H$
Pulse Coils:	$r=5m$ , NbTi/Cu/CuNi, Max 200T/sec 4T, $1.87MAT \cdot 8$
Slow Coils:	$r=3m$ , NbTi/Cu/CuNi, Max 7T, $14.2MAT \cdot 10$
Heating and Current Drive: NBI	
Start Up:	Max 1400 keV, 100 MW, $D^0$ Injection
Steady Burning:	1000 keV, 5 MW, $D^0$ Injection
Fueling: Packman Method, Liq. $^3H_2$ in Iced D Vessel	
Deuterium:	56.4 kg/year
Helium-3:	38.0 kg/year

Table 2: Principal parameters of the  $D-^3He$  FRC fusion reactor "ARTEMIS"

Capital Cost	146.0 M\$/y	0.0644* (99)
Operation and Maintenance	34.6 M\$/y	0.020* (99)
Fuel Cost	8.0 M\$/y	0.20M\$/kg=40kg/y
Total Cost(TAC)	188.6 M\$/y	
Cost of Electricity (Average Load Factor:75%)		
28.7 mills/kWh		

Table 3: Cost of electricity from "ARTEMIS" design

#### [REFERENCES]

- 1) H.Momota, et al.; Nuclear Inst./Meth. in Physics Research vol.A271 (1988) 7
- 2) W.Kernbichler and M.Heindler; Nuclear Inst./Meth. in Physics Research vol.A271 (1988) 65
- 3) R.E.Siemon, et al.; Fusion Technology vol.9 (1986) 13
- 4) M.Tuszewski; Nuclear Fusion vol.28 (1988) 2033
- 5) H.L.Berk, H.Momota, and T.Tajima; Physics of Fluids vol.30 (1988) 3024
- 6) S.P.Auerbach and W.C.Condit; Nuclear Fusion vol.21 (1981) 927
- 7) H.Momota et al.; Proc. 13 Symposium on Fusion Technology vol.2 (Pergamon,1984) 1463
- 8) R.W.Moir and W.I.Barr; Nuclear Fusion vol.13 (1973) 35
- 9) H.Momota; LA-11808-C (Los Alamos, May 1990) 8; Details will be published
- 10) D.W.Fry, R.B.R.S.Harvie, L.B.Mullett, and W.Walkinshaw; Nature vol.160 (1947) 351
- 11) B.G.Logan et al.; IAEA CN-50/G-I-5 (Held at Nice, 1988)
- 12) L.J.Wittenberg, J.F.Santarius, and G.L.Kulcinski; Fusion Technology vol.10 (1986) 167

# PULSATOR CONCEPT. QUASISTATIONARY FIELD REVERSED CONFIGURATION FORMATION

V.A.Burtsev, V.M.Kozhevin, V.N.Litunovsky

D.V.Efremov Scientific Research Institute  
of Electrophysical Apparatus,  
189631, St.Peterburg, USSR

## ABSTRACT

Concept for formation of quasistationary magneto-plasma configuration of FRC-type by means of toroids cyclic injection and merging in the confinement chamber (PULSATOR) is analyzed in the paper.

Possible use of quasistationary plasma accelerators for formation of high  $\langle \beta \rangle$  toroids is considered. The requirements to formation of FRC's with fusion parameters are evaluated and given. Possibility of equilibrium FRC configurations existence with the finite toroidal field value is shown.

Also an experimental installation SAPEIR for FRC formation investigations is briefly described and the results of preliminary experiments performed on it are given.

## INTRODUCTION

It's known that D-3He-fuelled fusion reactor with magnetic confinement should meet more strict requirements in comparison with D-T-fuelled one. It can be attributed firstly to the necessary high plasma temperature ( $T \approx 50$  keV) and Lawson's parameter ( $n\tau \approx 10^{15} \text{ cm}^{-3} \cdot \text{s}$ ). The analysis shows that fusion systems based on the FRC are rather promising from the view point of possible creation of aneutronic fusion reactors. In this case the important potential advantages of such systems (high  $\langle \beta \rangle$ , possibility of translation, cylindrical magnet system of confinement chamber) can be realized, apparently with the highest efficiency. Evaluating prospects of using similar configurations for aneutronic fusion reactor creation we should bear in mind that to achieve appropriate technical and economical factors of reactor with quasi-stationary mode of operation, the lower bound  $\eta_{in} \approx 0.3$  is set on the efficiency of the toroid formation system (in the general case it is the efficiency of energy coupling into the burning toroid) /1/.

Taking into account all abovesaid, one of the most important problems, while developing the concept of aneutronic fusion reactor based on the FRC, seems to be need of highly effective means for formation of FRC with technology appropriate for the reactor-relevant machines.

In this paper the concept of formation of the quasistationary magnetoplasma configuration of FRC-type by means of the toroids cyclic injection and merging in the burning chamber (PULSATOR) is analyzed. Possibilities to use magnetized quasistationary plasma accelerators as means for high  $\langle \beta \rangle$  toroids formation are considered and also the experimental device "SAPFIR" for simulation of such method is briefly described and preliminary experimental results are given.

# 1. FORMATION OF QUASISTATIONARY CONFIGURATION OF FRC-TYPE IN A D-3He FUELED REACTOR

As it has been noted, the required plasma temperature in D-3He reactor is very high what appreciably complicat creation of the system for formation of configuration with the reactor-relevant parameters. Therefore we think that the most feasible approach for solution of this problem is one based on very close interrelation of the plasma configuration formation and plasma burning. In this case under the appropriate conditions the FRC plasma heating up to necessary high temperatures will be possible due to energy utilization of fusion reaction products. It's natural that to provide the conditions for the plasma selfheating, (quasi) stationary maintaining of the magneto-plasma configuration is necessary, as the typical time for energy transport from high energy particles to the working mixture ions must be less than the lifetime of this configuration. Applied to FRC, such a problem is complicated due to the circumstance that the dominating mechanism, upon which the lifetime depend, in such type of configurations is an anomalous transport of particles and the lifetime of a single toroid with the reactorrelevant parameters appears to be less than the time for energy transport of high-energy particles to plasma.

The most attractive seems the way (quasi) stationary maintaining of FRC configuration based upon the toroids periodic injection and merging in the confinement chamber, as it naturally uses experimentally demonstrated properties of the compact toroids-possibility for their translation and merging (Fig.1). PULSATOR-concept is based on use of the above properties

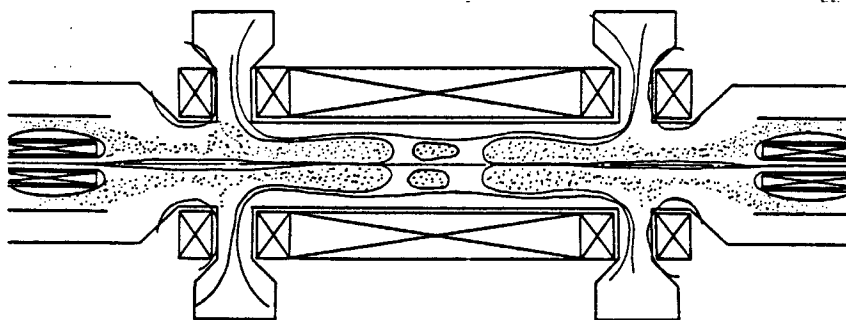


Fig.1.

applying them to the toroids with programmed parameters /2, 3/. In this case the transition to quasistationary burning of D-3He-mixture should be realized at reactor startup replacement of tritium in the injected toroids for 3He. Necessary

condition for such process is (and it has been said earlier) sustaining of D, T, 3He-mixture burning during each cycle, In paper (3) the conditions necessary for self-sustained fusion reaction in D-T-3He plasma mixture are evaluated at constant bremsstrahlung load to the first wall. The criterion, of the plasma partial composition and the toroid temperature relations is obtained. The dependencies of concentration of the plasma different components upon the temperature are given in Fig.2, for example. Constant specific radiation loading is provided due to



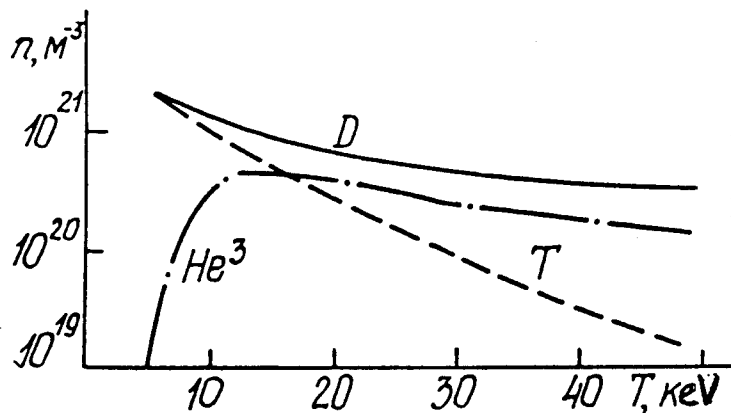


Fig. 2.

are significantly reduced, as the fluence at this time will be negligible.

In more details, the plasma self-heating dynamis was considered using non-stationary model taking into account toroid's dynamics, heating and cooling down of the plasma components, energy and particle losses due to anomalous diffusion, annihilation and restoration of the toroid magnetic flux processes in the confinement chamber. Different versions of the plasma self-heating from  $T \approx 7-10$  keV up to  $T \sim 60-80$  keV have been calculated, one of them is shown in Fig. 3. Plasma energy content and

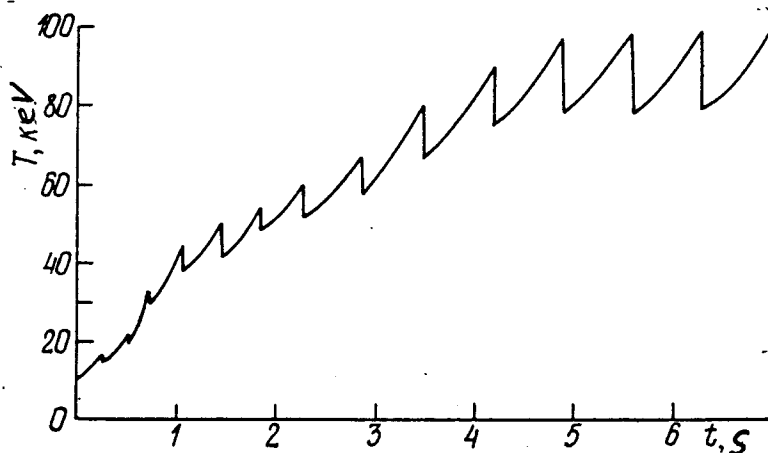


Fig. 3.

programmed change of the injected toroid plasma composition and magnitude of the poloidal magnetic flux what indicates, in particular, the necessity to develop the method for toroids formation when the toroid plasma heating and its magnetic configuration formation are separated. We should notice that in the start up phase the limitations on the specific neutron load to the first wall

also the toroid length varied insignificantly (5-10%) in the confinement chamber during the cycle even at  $\nu \approx \nu_0 \approx \tau_N^{-1}$ .

It should be emphasized that in the stationary phase of the reactor operation it is sufficient according to calculations to inject "cold" toroids ( $T \approx 1$  keV) to sustain the plasma burning process. It gives possibilities for significant reduction of requirements to the toroid injectors

in the stationary phase.

In paper /4/ was experimentally demonstrated possibility of spheromaks merging. In /3/ some results of more exact calculations of merging of non-symmetrical toroids with different closed magnetic fluxes are given.

Let's consider, in brief, possible use of the fusion reaction products energy to sustain the thermonuclear burning in FRC-plasma.

$\alpha$  - particles and protons confinement in FRC-configuration also depends upon such processes as particles drift in non-uniform magnetic field, Coulomb collisions with electron and also collec-

tive effects. It's important that these particles should leave the toroid, giving the most part of their energy. We may suppose that lack of their energy utilization may be attributed to collision less character of their escape. In paper /5/ were found so-called critical surface inside which the region of absolute  $\alpha$ -particles confinement for two analytical models of the magnetic field in toroid. The volume of these regions was shown to depend upon  $\varepsilon = r_a/r_s$  parameter, where  $r_a$  - is the Larmor radius of  $\alpha$ -particle with energy calculated by the magnetic field on the separatrix. The volume of absolute confinement is decreased and critical surface is contracted around the magnetic axis with higher  $\varepsilon$ . However, taking into account that the fusion reactions proceed most intensively in the magnetic axis region (at constant temperature over the toroid cross-section), we obtain that most part of high-energy particles appear in the zone of absolute confinement. In paper /3/ it is shown that  $\varepsilon$ -parameter for each type of high-energy particles is unambiguously determined by the product  $B_w \cdot r_s$ , where  $B_w$  is the magnetic field near the first wall the flux conserver. The most part of  $\alpha$ -particles and protons will exist in the region of absolute confinement at  $B_w \cdot r_s \approx 20$  T.m, typical for reactor relevant conditions.

To our mind, the method for the compact toroid formation by means of magnetized plasma accelerators is of great interest. Applied to the high- $\langle\beta\rangle$  toroid formation this method needs further studying in aspect of minimizing the ejected magnetic flux of the accelerator. Considering possible formation of toroids with the fusion parameters, the significant point upon which (alongside with other factors) depend the future of such a technology is control of an electrode erosion being the source of high-Z impurities. We think that quasistationary plasma accelerators (QPA) offer definite potential advantages from the above viewpoints. The results of theoretical study of the plasma stationary flows in similar accelerators are given for example in paper /6/.

Below we emphasize the specific features of such accelerators:

- two-stage acceleration with preliminary ionization and acceleration of plasma in the special input block;
- shaping of an accelerating channel (more often of inner electrode-cathode) aiming at optimization of the accelerating process;
- possibility of transition to ion-current transfer in an interelectrode gap of the accelerator.

We suppose these specific features to be significant interest from the viewpoint of the FRC-formation technology realization by means of coaxial plasma accelerators.

As the analytical consideration show, the minimization of the ejected toroidal magnetic flux of the plasma accelerator is possible in principle. It is possible due to shaping of the radial density profile of the plasma flow in the acceleration channel, appropriate conditions for ion current-transfer in the inter-electrode gap and choice of the modes with the "replacement factor" permitting separation of ion and electron flows outside the accelerator muzzle.

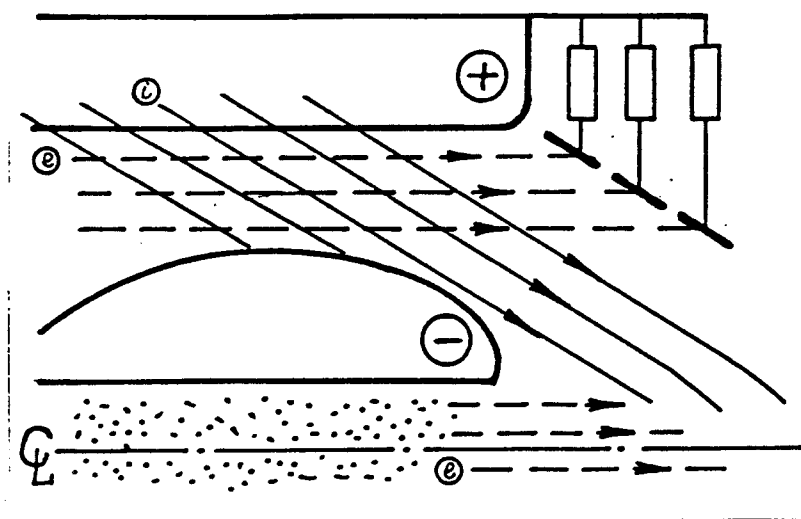


Fig.4.

To realize this possibility the sectionalized anode with varying potential aimed to receive an electron flow should be placed outside the accelerator muzzle (Fig.4). Ion flow in this case is directed to the near axis compression zone. To compensate the charge, resulted from the flows separation, it's necessary to form a dense plasma column in the cavity of the central electrode. This cylindrical cavity is also used to locate

the solenoid of the "poloidal" magnetic flux ( $\Phi_s$ ) and to divert the impurity ions out of the compression zone. An electric field resulted from separation of the plasma jet charges leads to the current shortcircuiting through the divertor plasma column.

The evaluation of requirements to the characteristics of the plasma accelerator for formation of the FRC with fusion parameters show, that the required voltage is of the following view:

$$eU_p \approx 12 (T_e + T_i).$$

Thus, for a facility with the reactor-relevant parameters ( $T_e \approx T_i \approx 8$  keV) the discharge voltage at the accelerator electrodes  $U_p \approx 150-200$  kV is needed.

In paper /3/ the parameters evaluations of a D-3He fueled hypothetical fusion reactor made using "pessimistic" low-hybrid scaling for the particles confinement time and limited bremsstrahlung load to the the first wall  $q_R \approx 5$  MW/m<sup>2</sup> are given. Necessary level of energy content of a burning plasma toroid should be  $W_p = 10$  GJ. In this case, the energy content of injected toroid in the start-up phase should be  $W_p \approx 0.5$  GJ ( $f \sim 1$  Hz - the injection frequency) and in stationary phase  $W_p \sim 0.1$  GJ. Performed optimization calculations of a fusion reactor parameters have shown possibility of such reactor power reduction to the level  $P_2 \sim 1$  GW and, respectively the less stringent requirements to the power of the toroid injector supply system.

The evaluations of possible minimization of the toroidal field carried out of the QPA show, that although its magnitude may be small, however it will have apparently a finite value in the formed toroid. In this connection, study of this field effect upon the toroid parameters is of great interest. Performed calculations based on solution of Grad-Shafranov's equation, taking into account the toroidal magnetic field  $H_\theta$  show that equilibrium configurations exist at any values of  $H_{\theta max}/H_{z sep}$  although this parameter have a strong effect both upon geometrical ( $r_s, Z_s$ ) and physical parameters ( $\langle \beta \rangle, \Phi_{max}$  - poloidal flux,  $p_{max}$  - plasma pressure) of the toroid.

Thus in the frameworks of calculational models it is shown that there exist equilibrium configuration of the plasma toroids at any  $H_0/H_z$  parameters.

## 2. EXPERIMENTAL INSTALLATION "SAPFIR" FOR STUDY OF THE FRC FORMATION USING THE PLASMA ACCELERATOR

Designing the plasma accelerators the following parameters were taken as the reference:  $W_p \approx 100$  kJ - is the maximum energy content of the plasma flow,  $\mathcal{E}_i \approx 1.0$  keV - is the ions energy,  $\tau_p = 0.1-0.3$  ms is the pulse duration. To attain these parameters the acceleration scheme with the working gas (hydrogen, deuterium) preionization in a special input block and shaped acceleration channel cross-section was realized.

In the modes with the discharge current  $I_p = 250-300$  kA, high speed ( $v_m \approx 2.5 \cdot 10^7$  cm/s at  $U_0 = 4.5$  kV) well formed plasma flows were observed. Preliminary experiments were performed at the value of the gun flux  $\Phi_G \approx 10$  mWb. The toroidal induced currents in the rods of flux conserver have been register.

## CONCLUSIONS

Performed evaluations of possible use of the toroid injection and merging for quasistationary maintaining of the FRC-type configuration have shown that its future use depends upon solution of two main problems:

1. Attainment of high efficiency of separate high  $\langle \beta \rangle$  toroid formation;
2. Development of the FRC-formation technique suitable for a fusion-reactor.

Analysis of possible quasistationary plasma accelerators application for similar technique indicates that this direction is promising.

## REFERENCES

1. V.A.Burtsev, V.M.Kozhevin, M.V.Krivosheev et al., Aneutronic fusion power plant based on pulsatory FRC, 5th All-Union Conference on Engineering Problems of Fusion Reactors (10-12.10.1990), Leningrad) Theses, M., 1990, p.p.18-20.
2. V.A.Burtsev, V.D.Djattov, V.M.Kozhevin, V.N.Litunovsky, Pulsatory compact tor, Reports of 3th All-Union Conference on Engineering Problems of Fusion Reactors (20-22.06.1984, Leningrad), M., 1984, v.I. p.p.45-52.
3. V.A.Burtsev, S.V.Bozhokin, G.I.Dudnikova et al., D-3He fueled quasistationary fusion system based on FRC, Voprosy atomnoi nauki i tekhnikiy Ser. Thermonuclear Fusion, M., 1989, N 1, p.p.46-52.
4. K.Watanke, K.Ikegami, N.Nagata et al., Merging experiment and simulation of compact toroid, Plasma Phys. and Contr. Nucl. Fus. Res., 9th IAEA Cofer.Proc, 1983, v.3, p.p.311-319.
5. S.V.Bozhokin, On  $\alpha$ -particles confinement in the devices on CT type, Fizika plasmy, M., 1986, v.12, N 1, p.p.1292-1297.
6. A.I.Morozov, L.S.Solov'jev, Stationary plasma flows in the magnetic field, In the book: Voprosi teorii plasmy, M., Atomizdat, 1974, p.p.3-87.

HIGH  $\beta$  AXISYMMETRIC D-<sup>3</sup>HE REACTOR WITH INTERNAL LEVITATED COIL

A.I.Morozov, V.P.Pastukhov, A.Yu.Sokolov

I.V.Kurchatov Institute of Atomic Energy, Moscow, USSR

## ABSTRACT

Physical concept of an innovative fusion reactor suitable for D -<sup>3</sup>He fuel is discussed. The discussion includes the following problems: equilibrium and stability, internal coil structure, parameters estimations, neutron and radiation fluxes on the coil surface. Main attention is focused on the relevant mechanism of the plasma thermal flux to the coil.

Physical concept of D-<sup>3</sup>He reactor based on the spherator-like toroidal field free magnetic system with internal levitated coil (ring) is discussed. The similar concepts of reactor with internal levitated coils (reactors of GALATEAS class) were discussed recently in [1-3].

Axisymmetric magnetic configuration shown at fig.1a is formed by the superposition of vertical mirror field produced by external coils and internal ring field. Ring current is opposite to external coil currents. Separatrix location depends on ratio of these fields. The internal ring (fig.1b) consists of the super conducting core with radius  $r_{sc}=0.3$  m, thermal shield layer with thickness of 0.1 m, neutron shield layer with thickness of 0.4 m and high temperature sheath. The total ring current  $I_R=23$  MA approximately corresponds to the maximum permissible current density for a multi-filamentary Nb<sub>3</sub>Sn conductor. For minor ring radius  $a=0.8$  m and major ring radius  $R_R=4$  m, the total ring mass is estimated as  $3.5 \cdot 10^5$  kg.

The  $R_R$  value is chosen on the base of transport processes estimations which are discussed below. Mirror and complete vacuum midplane fields at the axis are 0.8 T and 2.9 T correspondly. The ring weight is balanced by Ampere force corresponding to the radial magnetic mirror field component  $B_r=60$  gauss. As a result the equilibrium ring position is found to be just 5 cm below the mirror field midplane. We don't discuss the problem of the ring position stability maintenance, because the such problem was successfully solved at the LSP and FM-1 spherators [4]. It should be mentioned that the ring stability would be provided by the slow feed-back system.

The axisymmetric plasma equilibrium is described by Grad-Shafranov equation:

$$\Delta\psi - \frac{2}{r} \frac{\partial\psi}{\partial r} + 4\pi r^2 \frac{dp(\psi)}{d\psi} = 0 \quad (1)$$

where  $\psi$  is poloidal magnetic flux,  $p(\psi)$  - plasma pressure. To perform detailed calculations of a finite  $\beta$  equilibrium configuration one must know explicit form of  $p(\psi)$ , which is to be determined by an analysis of MHD-stability and transport processes. Nevertheless some important qualitative features of equilibrium are available to be discussed immediately. The equilibrium configuration is topologically similar to the compact torus one but the reverse field configuration is generated mainly by the ring current, thus plasma current plays auxiliary role. The plasma pressure has maximum at some closed magnetic surface  $\psi=\psi_{\max}$  situated between the separatrix and the ring surface (fig.1). The pressure decreases both to the ring surface and to the separatrix which plays role of a natural divertor. With plasma pressure increase the magnetic flux is forced out from high pressure volume to the separatrix mainly, where the magnetic field is less than one is near the ring. This process conserves the magnetic field topology but causes the appearance of the significant hot plasma volume with weak magnetic field.

With respect to a global mode plasma stability the magnetic system considered has a number of advantages in comparison with the conventional compact torus because the internal ring plays the role of rigid stabilizing tire. In particular the configuration must be stable with respect to the tilt mode and the rotational mode  $m=2$ . The pressure and magnetic field in the external region between surface  $\psi_{\max}$  and the separatrix decrease to the periphery. This circumstance can lead to interchange instability. However as it was shown in paper [3] for the compact torus there is the self consistent pressure profile with  $p=0$  at the separatrix being marginally-stable with respect to the interchanges. Function  $p(\psi)$  is determined by the equation:

$$pU^\gamma = \text{const}; \quad U(\psi) = \oint dl/B, \quad (2)$$

$\gamma$  - adiabatic exponent.

The transport processes are the least determined element for all reactor projects. However we shall try to make reasonable estimates. According to papers [6,7] where the transport processes to the internal ring surface were investigated the plasma layer with falling temperature profile has to be formed between the hot nuclear reactions region and the ring. There are no drives for MHD-instabilities (in particular for the interchange mode) in this internal layer. Neoclassical transport through the system is eliminated due to axisymmetry and the absence of the toroidal field. Therefore the transport due to drift instabilities only can occur in the internal layer in addition to the pure classical one.

The principle circumstance for the transport processes in the layer is the strong recycling, because all charged particles getting the ring surface return to the plasma after neutralization. This process causes the essential plasma cooling and density increase near the ring surface. Estimations for the reactor parameters show that the total internal layer thickness is much greater than the thickness of recycling zone where neutral particles are ionized. Thus the particle flux in the main volume of the layer has to vanish. The particle flux vanishing in the case of pure classical transport leads to the condition  $nT^{1/4} = \text{const}$  [6].

According to [7] corresponding  $n$  and  $T$  profiles are unstable with respect to the drift-cyclotron instability (DCI) or it's high frequency limit - low hybrid drift instability (LHDI). Moreover the particle flux generated by these instabilities has the direction from the ring surface to the hot plasma. The instability modifies  $n$  and  $T$  profiles up to achievement of a balance between classical and anomalous particle fluxes. DCI-amplitude is restricted at the significantly low level under this condition and the classical ion thermal conductivity remains to be dominant transport

mechanism but with modified  $n$  and  $T$  profiles.

Fig.2 from [7] demonstrates the results of self consistent internal layer thermal flux calculations which are performed taking into account the influences of DCI and bremsstrahlung radiation under reactor conditions:  $n=4 \cdot 10^{14} \text{ cm}^{-3}$ ,  $T=50 \text{ kev}$ . The difference between  $q_o$  and  $q_L$  (fig.2) is caused by energy losses from layer due to bremsstrahlung radiation. If  $\xi > 1.14$  thermal flux transforms to bremsstrahlung radiation completely. Thermal flux obtained is approximately ten times less than the flux which is maximum acceptable one from the point of view of the ring surface thermal loading.

The thermal flux in the external region (from the hot region to the separatrix)  $q_{\text{ext}}$  may exceed essentially the thermal flux in the internal layer  $q_{\text{int}}$  due to smaller magnetic field and possibility of excitation of some MHD-fluctuations and higher level of drift-fluctuations in the external region. In addition to the absolute value of  $q_{\text{ext}}$  it is very important to know equilibrium location of ignited hot zone in the case of essentially different heat conductivities  $\chi_{\text{ext}}$  and  $\chi_{\text{int}}$  in the external region and in the internal layer. The simple analysis of the steady thermal flux distribution provides us by relation:

$$\frac{q_{\text{ext}}}{q_{\text{int}}} \approx \frac{l_{\text{ext}}}{l_{\text{int}}} \approx \left( \frac{\chi_{\text{ext}}}{\chi_{\text{int}}} \right)^{1/2}, \quad (3)$$

where  $l_{\text{ext}} = |\nabla T/T|_{\text{ext}}^{-1}$ ,  $l_{\text{int}} = |\nabla T/T|_{\text{int}}^{-1}$ . Assuming for the estimations the typical thermonuclear reactor value  $q_{\text{ext}} \approx 300 \text{ W/cm}^2$  and taking  $q_{\text{int}} \approx 20 \text{ W/cm}^2$ ,  $l_{\text{int}} \approx 0.1 \text{ m}$  we find  $l_{\text{ext}} \approx 1.5 \text{ m}$ ,  $\chi_{\text{ext}}/\chi_{\text{int}} \approx 225$ . The above estimations appear to be quite reasonable, although the real ratio  $\chi_{\text{ext}}/\chi_{\text{int}}$  can get another value.

The estimations obtained allow us to verify  $R_R$  value mentioned above and evaluate the total reactor power. We choose the internal layer thickness to be equal to double 14.6 Mev proton gyroradius. In this case the nuclear reaction products will transmit their energy to the bulk of plasma before they get the ring surface. Thus  $L \approx 3l_{\text{int}}$ ,  $l_{\text{ext}}/L \approx 5$ . Taking into



account the real field strength ratio the last relation leads to the condition  $\psi_{\max}/(\psi_R - \psi_{\max}) \approx 3$ , where  $\psi_R$  is the magnetic flux corresponding to the ring surface. This relation for magnetic fluxes for the given value of  $(\psi_R - \psi_{\max})$  corresponds to  $R_R = 4\text{m}$  in our case.

Finally we presents estimations of the main energetic parameters. Hot ignited zone volume is evaluated as  $200 \text{ m}^3$ . Supposing that  $\text{D-}^3\text{He}$  reaction power density is  $5 \text{ MW/m}^3$  one can get the total reactor power about 1 GW. The total bremsstrahlung radiation power is about 200 MW. The total cyclotron radiation power is about 40 MW because the volume average hot zone beta  $\langle \beta \rangle_h \approx 5$  due to strong plasma diamagnetism. The over-all energy flux density to the ring is about  $80 \text{ W/cm}^2$  and is provided mainly by bremsstrahlung radiation. Assuming the radiation from the ring surface as a black body radiation we find the equilibrium temperature has to be  $1940^\circ \text{K}$ . The necessary thermal flux density at the external boundary of the hot zone estimated from the energy balance is about  $300\text{--}350 \text{ W/cm}^2$  and coincides with the above assumption.

#### R E F E R E N C E S

- [1] - Morozov A.I., Pis'ma v ZhTF (Sov.Phys. JTP Lett.), 16 (1990) 86.
- [2] - Hasegava A, Chen L, Mauel M.E., Nuclear Fusion 30 (1990) 2405.
- [3] - Morozov A.I., Workshop on low radioactive  $\text{D-}^3\text{He}$  nuclear fusion (Report issue), Institute of Atomic Energy, Moscow (1991) 133.
- [4] - Yoshikawa S, Nuclear Fusion, 13 (1973) 433.
- [5] - Vabishevich P.N., Degtyarev L.M., Drozdov V.V, Poshehonov Yu.Yu., Shafranov V.D., Fizika Plazmy (Soviet Journal of Plasma Physics) 7 (1981) 981.
- [6] - Morozov A.I., Pastukhov V.P., Fizika Plazmy (Soviet Journal of Plasma Physics) 17 (1991) 1220.
- [7] - Pastukhov V.P., Sokolov A.Yu., Nuclear Fusion, 32 (1992)

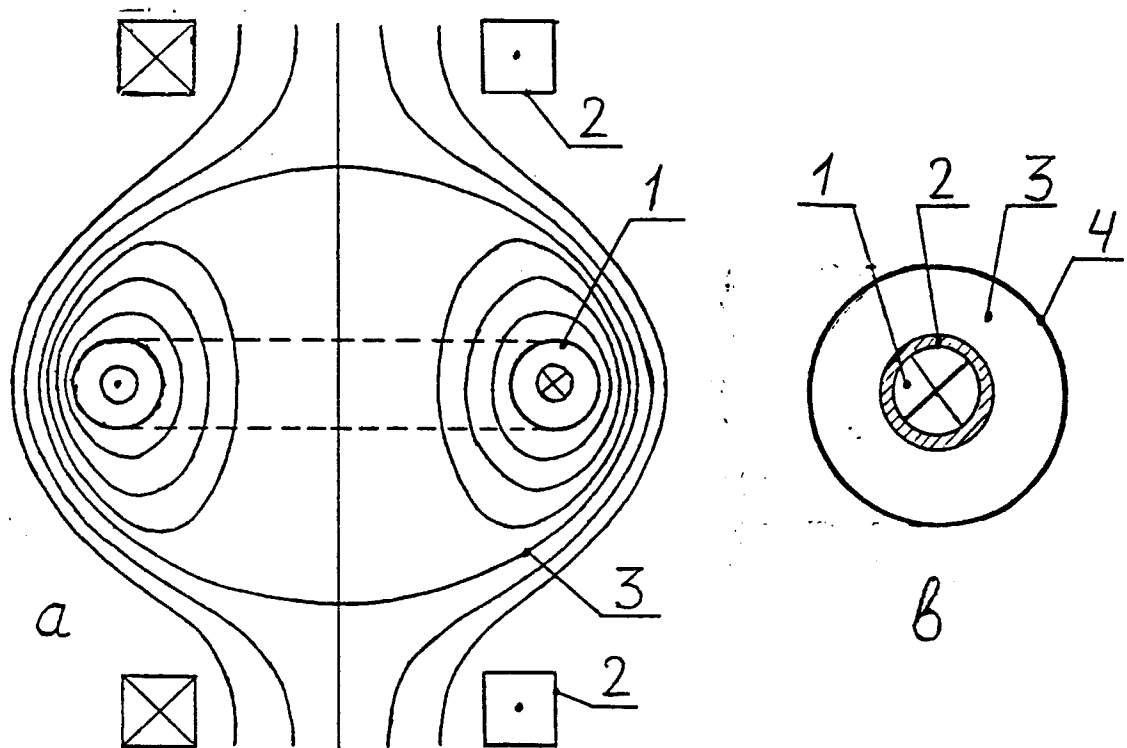


Fig.1 a) - Vacuum configuration of magnetic field. 1 - internal levitated ring, 2 - external mirror field coils, 3 - magnetic separatrix. b) - Internal ring cross section. 1 - super conducting core, 2 - thermal shield layer, 3 - neutron shield layer, 4 - external high temperature sheath.

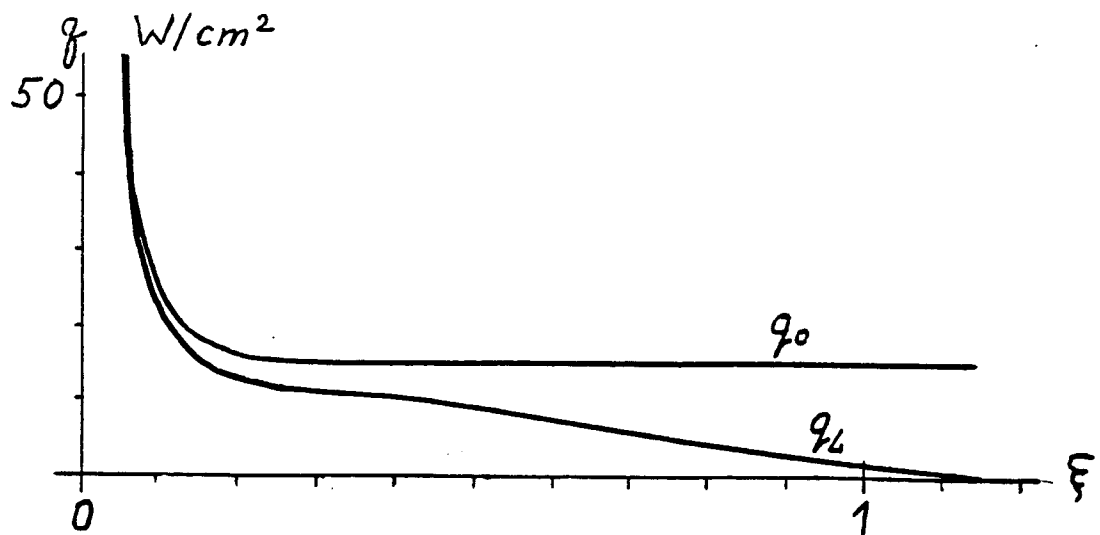


Fig.2 Thermal flux density coming from hot zone ( $q_0$ ) and thermal flux density achieving the ring ( $q_L$ ) vs the layer thickness  $L$ ;  $\xi = L/\rho_d(m_d/m_e)^{1/2}$ ,  $\rho_d$  - hot deuteron's gyroradius.

A problem of traps with  $\beta=1$  and Galateas

A.I.Morozov

*Abstract.* The urgency of studying and utilizing Galateas-magnetic traps with plasma-submerged conductors - is emphasized. In the traps of such a type the values of  $\beta=1$  are easily attained. An attention is paid to electrically-discharged traps, where new levers for controlling plasma processes emerge and, even more, a hot plasma can be automatically prepared. Some approaches to calculations of equilibrium axisymmetric Galatea configurations with  $\beta=1$  are formulated within the frameworks of hybrid and hydrodynamic approximation.

1 *Necessity in the traps with  $\beta=1$ .* One can have two approaches to the problem of hyperteemperature systems. One of them is to "pull" the existing diagrams of high temperature DT-reactor to a hyperlever. Another is to start the search for and to make an analysis of new and well-forgotten previously-developed diagrams which could provide an effective solution to problems arising here. A given paper, being a continuation of [3], is referred to the second approach.

Magnetic traps, including points, lines or volumes, where a magnetic field turns out to be zero, are called plasma traps with  $\beta=1$ , according to tradition. In other words, these traps include the zones, where local  $\beta_{loc} = \infty$ . The importance of such traps has been discussed in [1,2,3]. Let us reproduce the main statement from these papers.

The traps with  $\beta=1$  are of great practical importance for various purposes. Such traps can be used as technological plasma baths for treatment of details, as gas discharged chambers in ion injectors, as plasma guides etc. The traps with  $\beta=1$  are, in principle, the most desirable ones for the controlled fusion. It is explained by a number of reasons. First of all, they allow one to restrict oneself by low magnetic field limits, thus realizing the transition to the traps with new structural parameters. One can judge about this from the following parameters. At the field strength  $H_0 = 100$  Oe the trap can confine the plasma at

$$n_0 = 10^{12} \text{ cm}^{-3} \quad T_i + T_e = 300 \text{ eV} \quad (1a)$$

and at  $H_0 = 1000 \text{ Oe}$ , respectively

$$n_0 = 10^{13} \text{ cm}^{-3} \quad T_i + T_e = 3 \text{ keV} \quad (1b)$$

It means that the search studies can be performed with cheap facilities.

Then, the traps with  $\beta=1$  can play a great role as hypertemperature reactors, i.e. the reactors with  $T_e \geq 50 \text{ keV}$ , where synchrotron radiation is of principal importance. DD and  $D^3\text{He}$  - reactors are referred to them. It is important to emphasize the fact that the traps with  $\beta=1$  allow one not only to reach new ranges of parameters. They are based in many aspects on another physical ideology than that on which the traps with  $\beta \ll 1$ , popular at present, are based. Indeed, the very idea of plasma confinement by a magnetic field is illogical in a certain sense, since the magnetized plasma behaves itself as a quasi-diamagnetic substance and tends to leave the trap by all possible means. Fortunately, plasma electrons and ions are not diamagnetic balls, therefore the plasma is a quasi-diamagnetic, and the modern traps are based on this "quasi". It is evident that the magnetic field should be used not as medium of plasma "dwelling", but a "fence" surrounding the region occupied by plasma [1,2,3]. It means the transition to the traps with  $\beta=1$ .

2 *"Galateas" and "mixinas"* Classical traps with  $\beta=1$  are various spindle cusp modifications with large axial and radial slits. These slits are too great for fusion reactors, and they cannot be closed by traditional techniques. However, if one uses a non-traditional approach, the slits can be easily closed. For this purpose, it is sufficient to introduce some properly-chosen levitating conductors with currents into the magnetic system, along with the ground-resting coils. The well-known traps, tornado-type [4], multipoles [5] etc, are produced in such a way. A solid body analogue of ASTRON with  $\beta=1$ , called "Galatea-A", where the radial slit is closed (fig 1) and the diffusive traps proposed by the author (Gabi is a chain of Galateas-A and Hega is a heliocoidal pipe with diffusively-scattering walls [2]) are referred to this approach.

All the traps with the conductors, around which the plasma flows, independently of fact that these conductors are closed (as

in multipoles) or rest upon the leads-in at their ends (similar to tornados), were proposed in [1] to be called "Galateas", meanwhile the floating conductors to be called "mixinas". The Galateas emerged at the dawn of controlled fusion studies were displaced from the main way of development by the general enthusiasm related with tokamaks, on one side; on the other one, by the general opinion of enormous engineering difficulties related with the production of mixinas operating under reactor conditions. However, as shown in our papers [1,3] in the general form and in a number of studies abroad [5,6] in some fragments, this opinion is erroneous. At the same time, the realized experiments have shown some prospects for Galateas as plasma systems. So, the parameters comparable with the assessment (1) were attained on a tornado. Some scaling estimations for experimental facilities having the parameters of T-10 and for those of full-scaled reactors with DT and  $D^3He$ , based on the Gabi-trap, are given in [3].

3 *Electrically discharged traps (EDT)* The use of electrostatic fields (E-fields) in the traps, as known, is multilateral. It gives not only some additional means for arranging the confinement process but allows one to effectively produce hot plasma in the traps in many cases, and, sometimes, to partly-recuperate the energy of escaping plasma. In this connection, it is useful to pay attention to our previously published paper [7], where an electrostatic plasma trap (ESPT) was proposed and partly studied. In the ESPT the ion Larmor radius  $\rho_i$ , is greater than the characteristic size of a plasma volume,  $L$

$$\rho_i > L \quad (2)$$

Therefore ions were confined by the E-field here. The field itself, in its turn, was sustained by magnetized electrons. Moreover, the continuously applied E-field heated electrons, which, in their turn, ionized neutrals. The produced ions, being accelerated in the E-field towards the ESPT axis, produced a hot ( $\sim 1$  keV) ion component there. At the same time, moving away from the axis ions returned their energy to the electric circuit.

In traps with  $\beta=1$  the condition (2) is also performed the same functions as those in ESPT. Note, that an electric field is also used in tornados for obtaining hot plasma.

The class of electrically discharged traps (fig 2), which "IXION" belongs to, O.A.Lavrentiev's and M.S.Ioffe's [8]

magnetoelectric traps, ESPT, tornado at the stage of "warming" and others will undoubtedly play an essential role in future too. In particular it would be useful to study multipoles in the EDT-mode.

It is easy to see that the role of the negative electrode submerged into a plasma within the hot-plasma EDT can be played by a neutral or a negatively charged ion beam, piercing the trap. Loosing electrons, it will sustain the potential of the irradiated zone.

4 *On equilibrium configurations in a Galatea-A* In [8] it has been shown that the nature of particle confinement in axisymmetric traps with  $\beta=1$  qualitatively depends on the sign of product

$$\mu = D \Psi_{r \rightarrow 0},$$

where  $D \equiv m r V_\theta + e/c \Psi$  is the generalized momentum,  $\Psi_{r \rightarrow 0}$  is the magnitude of a magnetic field function in a plug at  $r \rightarrow 0$ . The sign of  $\mu$  in both plugs for a Galatea-A is the same. Therefore all the particles in the trap can be divided into two groups: those with  $\mu < 0$  and those  $\mu > 0$ . The first particles were called co-particles and second, counter-ones in [9]. There it was also mentioned that effective cross-sections of an axial slit for co- and counter-particles would be different

$$S_{\text{eff}}^{(\text{co})} \sim \pi \rho_{in}^2 \quad S_{\text{eff}}^{(\text{counter})} \sim 2 \pi R \rho_{in} \quad (3)$$

If one takes a single Galatea-A and fills with plasma, the counter-particles will leave the trap for a short time and plasma begins to rotate. The plasma in such a regime can live for a long time. So, if the volume of Galatea-A  $V = 30 \text{ m}^3$ , thermal velocity  $v_T = 10^8 \text{ cm/s}$ , magnetic field  $H_{axis} = 10^5 \text{ Oe}$ , one finds

$$\tau^{(\text{co})} = \frac{4 V \langle n \rangle}{2 S_{\text{eff}}^{(\text{co})} v_{T1} n_{ax}} \approx \left[ 5 \frac{\langle n \rangle}{n_{ax}} \right] \text{ sec}$$

Thus one has a hope on obtaining a positive yield with one trap. The above-said requires the detailed study of a transitional plasma-field layer. In a given paper we shall consider the statement of a problem for calculating a collisionless equilibrium configuration of the layer produced at the contact of plasma with a magnetic "coat" (see fig 1). Such a statement is true when particles diffusing beyond the transitional layer can freely escape along magnetic field lines.

At the same time, the plasma shell of a mixina should be calculated with due regard for diffusion, since the sink of

captured particles is absent. The corresponding calculations for classical and anomalous transports were done in [10].

In consideration of an equilibrium layer configuration it is sufficient to use a hybrid approximations representing ions by their kinetics and electrons by hydrodynamics. In this case the thermalized potential [11]

$$\Phi_* \equiv \Phi - 1/e \int \frac{dp_*}{n} = \Phi_*(\Psi) \quad (4)$$

is retained along magnetic field lines  $\Psi = \text{const.}$

Under real conditions  $\Phi_*(\Psi)$  can be fixed by the set of electrodes located at the trap ends, similar to their location in ESPT [11]. The azimuthal electron velocity is related with  $\Phi_*(\Psi)$  through the relationship

$$V_\theta = -c \frac{d\Phi_*}{d\Psi} \quad (5)$$

The ion component dynamics, under given assumptions, unambiguously defined, when the ion distribution in the zone without magnetic field, depending on energy  $\varepsilon$  and generalized momentum  $D$ , is preset

$$f = f_0(\varepsilon, D) = f(M V^2/2 + e\Phi, m r V_\theta + e/c \Psi) \quad (6)$$

Taking account of fact that the plasma in the trap is quasineutral, one obtains from (4) and (6)

$$n_0(\Phi_* - \Phi) = \int f dV = n_1(\Phi, \Psi, r)$$

Hence, the explicit form of the dependences are the following

$$\Phi = \Phi(r, \Psi), \quad n = n(r, \Psi) \quad (7)$$

Using Maxwell equations and the relationships found above, one obtains the equation for  $\Psi$

$$\Delta^* \Psi = \frac{4\pi}{c} \text{re} [\int V_\theta f dV - V_\theta n_0] = -\frac{4\pi}{c} r j_\theta(r, \Psi) \quad (8)$$

which defines the configurations at given currents through the coils. Knowing the configuration, one can make the precise statement of a problem on its stability.

The confinement of a fast rotating plasma ( $\Omega R \gg v_i$ ), early or late, will result in the spread of a transitional layer due to transversal diffusion. As a result, the configuration becomes a hydrodynamic one, and one may use, at a good conductivity, the formalism developed in [11].

However, if  $\rho = \rho(\Psi)$  and angular velocity  $\Omega$  does not depend on  $r$  and on  $z$ , the calculation of a configuration will be simplified

and reduced, it is easy to be sure of that, to the solution of the generalized Grad-Shafranov equation

$$-\Delta^* \Psi = 4\pi r^2 \rho \Lambda' + \left(\frac{4\pi}{c}\right)^2 I I' \quad (9)$$

Here

$$\Lambda(\Psi) \equiv \int \frac{dp}{\rho} + \frac{\Omega^2}{2} r^2 \quad I(\Psi) = \frac{c}{4\pi} r H_\theta$$

*Conclusion* At present the Galatea diagram with  $\beta=1$  cannot be responsibly called the most promising one, as well as parameters of the reactor based on it cannot be reliably estimated. It is explained, first of all, by the absence of experimental data and well-analyzed theories. Therefore intense experimental studies of a tornado, multipoles, organisation of test experiments with Galateas-A, with multipoles in the electrically discharged modes etc are the most urgent tasks in a given field. The test experiments are cheap and can be related with practical problems of the present day plasma technology. It is natural that the multilateral development of the theory for Galateas is necessary.

#### Referencies

- 1 Морозов А.И., Письма ЖТФ, 1990, т.16, в.15, с 86-89
- 2 Морозов А.И. Там же с 89-93
- 3 Морозов А.И. Сборник докладов на Совещании по малорадиактивному термоядерному синтезу. 1991 Москва Институт атомной энергии им.И.В.Курчатова, с 133-149.
- 4 Перегуд Б.П. и др ВАНТ, серия т.я. синтез, в. 3, 1984, с.46-51.
- 5 Yoshikawa S, Chen L, Mauel M. Nucl. Fus., 1973, v 13, n 3, p 433- 449.
- 6 Hasegawa A., Chen L., Mauel M., Nucl., Fus., 1990, v 30, n 11, p 2405-2412.
- 7 Морозов А.И., Жуков В.В., Письма в ЖЭТФ, 1973, т 18, в 6, с 373-375.
- 8 Иоффе М.С., Канаев Б.И., Пастухов В.П. и др Итоги науки и техники, серия Физика плазмы, т 9, М. 1989, с 5-54.
- 9 Морозов А.И. Физика плазмы, 1991, т 17, № 3, с 402-403
- 10 Морозов А.И., Пастухов В.П., Соколов А.Ю. Настоящий сборник.
- 11 Вопросы теории плазмы, в 8, М. Атомиздат, 1974.



# D-3He dipole fusion reactor

M. E. Mauel

*Department of Applied Physics, Columbia University, New York, New York 10027 U.S.A.*

(November, 1991)

A new fusion device has been recently suggested by Hasegawa and co-workers [*Nuclear Fusion* 30 (1990) 2405] based on a relatively small, levitated superconducting ring. This dipole magnetic field appears suitable for D-<sup>3</sup>He fusion, since dipole-confined plasma is predicted to be stable at high beta while the confinement of high-energy charged fusion products can be controlled using resonant and/or non-resonant static magnetic perturbations. Direct conversion as well as removal of fusion ash seems possible. In a dipole magnetic field, even an equilibrium plasma having a "flat" phase-space density satisfying  $\partial f_0(\mu, J, \psi)/\partial \psi = 0$ , where  $\psi$  is the flux function, has a steep enough pressure profile for high fusion reactivity within the core yet is stable to low frequency instabilities for local beta exceeding unity. To a good approximation, the dipole fusion concept is the first fusion device to have both "macroscopic" (or MHD stable) equilibrium and a "microscopic" equilibrium (since a plasma having  $\partial f_0/\partial \psi = 0$  is immune to low-frequency-driven anomalous transport). This report summarizes and motivates the dipole fusion concept. In addition, the parameters of a new, mechanically-supported dipole experiment are presented.

## 1. INTRODUCTION

In 1987, Hasegawa introduced the concept of a dipole fusion reactor<sup>1</sup>. Hasegawa recognized that, in usual magnetic confinement devices, low frequency fluctuations lead to anomalous radial diffusion of particles and heat to the outer wall. On the other hand, in the dipole magnetic field, low-frequency fluctuations can lead to an *inward radial diffusion* even in the presence of a relatively steep inward pressure gradient,  $\partial \ln P / \partial r > -20/3$ . In the dipole magnetic field, radial diffusion results from low-frequency azimuthal drift resonances,  $\omega_d(\mu, J, \psi) = \omega_{lf}$ , where the drift frequency is dependent on the magnetic moment,  $\mu$ , the parallel adiabatic invariant,  $J = \oint v_{\parallel} dl$ , and the flux or third adiabatic invariant,  $\psi$ . Significant heating (cooling) and compression (decompression) of the plasma occurs because the LF oscillations break the third adiabatic invariant while  $\mu$  and  $J$  are conserved because  $\omega_{lf} \ll \omega_b \ll \omega_c$ , with  $\omega_b$  representing the bounce frequency and  $\omega_c$  representing the cyclotron frequency. For a collisionless plasma, all induced radial transport will cease when  $\partial f_0(\mu, J, \psi)/\partial \psi = 0$ , where  $f_0$  is the particle distribution function expressed in terms of the actions,  $\mu, J, \psi$ . This process has fundamental importance both for understanding collisionless confinement in dipole fusion devices but also for the understanding of collisionless particle transport in planetary magnetospheres. When strong drift-resonant fluctuations are present, the final  $\partial f_0/\partial \psi = 0$  profile will result whether the source of plasma particles is located at the high-field region near the ring or located at the plasma edge. For the dipole reactor, energetic neutrals are injected into the reactor

core region, the plasma is initially unstable with respect to interchange instabilities. These instabilities naturally induce low-frequency oscillations,  $\omega_{lf}$ , diffusing plasma radially outward until the marginally stable equilibrium  $\partial f_0 / \partial \psi = 0$  (or  $\partial \ln P / \partial r = -20/3$ ) is achieved. In planetary magnetospheres, cool plasma is injected at the plasma edge (for example, from the solar wind) and transported and heated inward to higher fields.

In this report, the D-<sup>3</sup>He dipole reactor concept first presented by Hasegawa and co-workers<sup>2,3</sup> is summarized. Section 2 presents an example of a dipole fusion reactor using a relatively small levitated superconducting magnet. Section 3 discusses the important issue of MHD equilibrium and stability. Section 4 discusses the control of energetic fusion products. Section 5 discusses a new laboratory experiment which will be used to investigate collisionless particle transport in a dipole magnetic field. Section 6 provides a brief summary along with a discussion of areas requiring more study.

## 2. DESCRIPTION OF A CONCEPTUAL DIPOLE FUSION REACTOR

Figure 1 shows a schematic diagram of a dipole D-<sup>3</sup>He fusion reactor configuration first presented in Refs. 2 and 3. The dipole magnetic field is produced by a properly shielded and insulated superconducting coil. Much weaker magnetic mirror coils magnetically levitate and stabilize the superconducting magnet. A very large vacuum vessel contains the dipole coil, and, although the overall size of the reactor is large (about 50 m), the "high-technology" superconducting magnet is only 4 m in outside diameter. The large vacuum region is important to the dipole concept since it allows the field strength to decay by nearly four orders of magnitude from the coil to outer wall.

This large variation of the magnetic flux function,  $\psi$ , distinguishes this reactor concept from earlier concepts such as the spherator (with purely poloidal magnetic field)<sup>4</sup> and the levitron (with combined poloidal and toroidal fields)<sup>5</sup>. These earlier devices were initially limited by transport to mechanical coil supports that were not magnetically-shielded<sup>6</sup>, but later experiments with levitated superconducting dipoles indicated that "fluctuations or convective cells" reduced confinement by at least a factor of four compared with classical expectations (as described in Ref. 5). Unlike the dipole reactor, the plasma equilibrium in a spherator required  $\partial f_0 / \partial \psi - (rB)^{-1} \partial f_0 / \partial r$  to be very large, and this fact may explain the presence of low-frequency

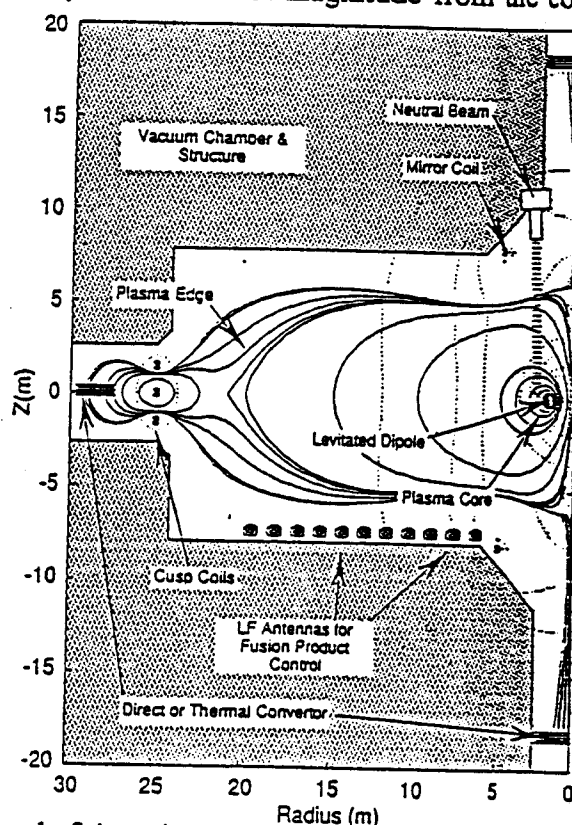


Figure 1. Schematic cross-sectional diagram of one possible configuration of a D-<sup>3</sup>He dipole fusion reactor.

fluctuations or convection cells which were observed together with degraded confinement. In the dipole reactor design, low-frequency fluctuations and convective cells can not lead to enhanced losses since  $\partial \hat{f}_0 / \partial \psi = 0$ .

The plasma within a dipole fusion reactor could be produced with neutral beam injection into the high-field core region. A target plasma would be produced with, for example, electron cyclotron resonance heating, and good neutral beam penetration is possible by aiming the beams along the axis of the dipole as indicated in Fig. 1. As the plasma pressure builds in the core region, the plasma becomes initially unstable with respect to interchange instabilities. As the plasma diffuses outward, the magnetic moment,  $\mu$ , the parallel adiabatic invariant,  $J = \oint v_{\parallel} dl$

would remain approximately constant because  $\omega_{lf} \ll \omega_b \ll \omega_c$ . The outward diffusion adiabatically cools the plasma until the marginally stable equilibrium  $\partial \hat{f}_0 / \partial \psi = 0$  is "naturally" achieved. On the longer "collisional" time scale, pitch-angle scattering would alter the distribution so that it takes the form  $\hat{f}_0(E, \psi)$ , although pitch-angle scattering will not significantly change the total pressure profile,  $P(r)$ .

Figure 2 illustrates an expanded view of the dipole coil and hot core plasma shown in Figure 1. The coil consists of three superconducting subcoils each near the maximum permissible current density for multi-filamentary Nb<sub>3</sub>Sn conductor. (This coil design strategy is the same as that used in the high field, D-<sup>3</sup>He tokamak reactor design presented in the ESECOM study [7].) For this dipole reactor example, the inner conductor operated with 5 kA/cm<sup>2</sup> at 20 T; the middle conductor operated at 15 kA/cm<sup>2</sup> at 16 T; and the outer conductor at 40 kA/cm<sup>2</sup> at 12 T. The coil shield and dewar are designed to follow the inner most field line, and this places most of the shield on the outside of the conductors—the direction of most of the residual neutron flux.

In order to illustrate the scaling of the dipole fusion reactor to larger fusion power, we have considered (in Ref. 3) how the dipole reactor would change if an "advanced" superconductor technology could be developed that would allow the current density and magnetic field strength within the conductor to double. If the reactor was maintained at the same size, the inner subcoil must operate with 10 kA/cm<sup>2</sup> at 40 T; the middle subcoil operated at 30 kA/cm<sup>2</sup> at 32 T; and the outer subcoil at 80 kA/cm<sup>2</sup> at 24 T. The total coil current would increase from 20 MA to 40 MA, and the total stored energy of the coil would increase to 3.2 GJ. Indeed, if a

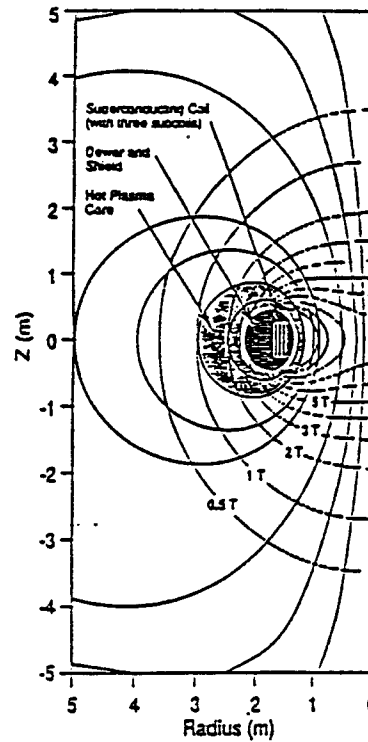


Figure 2. A close-up cross-sectional view of the high-field dipole magnet used in the configuration shown in Figure 1.

superconducting magnet of this type could be built, it would also greatly simplify other magnetic fusion configurations. The coil shield is designed to follow the inner most field line, and this has the added advantage that most of the shielding is located on the outside of the conductors, and this is the direction of most of the residual neutron flux.

As the magnetic field is increased in a dipole fusion reactor, it is advantageous to maintain constant the plasma beta,  $\beta = P/(B^2/2\mu_0)$ , by increasing the plasma density. By operating at the maximum plasma beta, the fusion power is maximum. By operating at the same temperature, the optimal operating point, maximizing the D-<sup>3</sup>He cross-section and minimizing radiation, can be maintained. The higher-field dipole reactor would have a burning core located near the 4 T surface less than 0.5 m from the outer shield of the levitated coil. Within the core, the plasma temperature would be 75 keV, the electron density would be  $9.6 \times 10^{20} \text{ m}^{-3}$ , and the plasma beta would be 3. The reactor's power output due to the primary D-<sup>3</sup>He reaction would increase by a factor of 16, up to 1.1 GW. The total stored plasma energy must be 700 MJ, giving a self-sustained burn for a confinement time of only 0.6 seconds. We note that for fixed temperature and  $\beta \sim 1$ ,  $\omega_{pe}/\omega_{ce} > 2$  is constant as  $B$  increases, so the ratio of the electromagnetic skin-depth ( $c\omega_c/\omega_{pe}^2$ ) to the machine size is constant and the fraction of power lost due to synchrotron radiation should not increase significantly<sup>8</sup>. Furthermore, if inward heat conduction to the superconducting ring is determined by the classical formula of collisional thermal conductivity,  $\kappa_i$  (which scales as  $B^2$  under these conditions), then the characteristic time of plasma heat conduction would increase to the very long time of  $\tau = 4 \Delta r^2/\kappa_i \sim 120$  seconds.

A critical aspect of this higher-field dipole reactor is the warm-up time for the superconductor. This is determined by the surface temperature of the outer shield and the ability to insulate windings from the shield. Previous studies of a levitated-coil D-He<sup>3</sup> fusion reactors<sup>9,10</sup> indicate that pulse-lengths of one to ten days are possible provided that the equilibrium shield temperature can be maintained below 1400 °C. Assuming that the radiation power to the shield increases as the square of the density, the 16-fold increase in shield heating would raise the outer shield temperature from 800 °C (in the low-field case) to 1800 °C (in the high-field case). As suggested in Ref. 3, it is conceivable to install a compact cooling system inside the shield which is driven by an external source of microwave or laser power and which enables the reactor to operate continuously.

Generation of electricity involves either a thermal or direct conversion of the energetic fusion products at specific locations at the outer wall. At reactor start-up, the fusion products would be confined by maintaining axisymmetry and preserving the angular momentum. After ignition, a fraction of the energetic protons and alphas can be directed to conversion sites by means of a superposition of an axial field or by breaking axisymmetry.

### 3. PLASMA EQUILIBRIUM AND STABILITY

The unique feature of the dipole magnetic field is the rapid increase with radius of the volume of "tubes" containing equal magnetic flux. This feature produces a steep radial gradient of the plasma pressure, density, and temperature, even when  $\partial \hat{f}_0 / \partial \psi = 0$ . On a time scale that is short compared with the collisional pitch-angle scattering time but long compared with the particle bounce time,  $\mu$  and  $J$  are constant, and fluctuations can not lead to net transport of particles or energy with this class of distribution functions. For an ideal dipole field, the density and pressure scales with radius as  $n \sim r^4$ ,  $P_{\perp} \sim r^7$ , and  $P_{\parallel} \sim r^6$ .

Collisions or microinstabilities would isotropize the pressure and lead to a distribution function which can be expressed in the form  $\hat{f}_0(E, \psi)$ , where  $E$  is the total particle energy. In this case, the scaling of the plasma density does not change although the isotropic plasma pressure would scale as  $P \sim r^{-20/3}$  which is a marginally stable pressure profile with respect to ideal MHD<sup>11</sup>. In Refs. 2 and 3 a kinetic ballooning theory is presented showing that a pressure profile having  $P \sim r^{-20/3}$  remains stable even as  $\beta$  approaches 300 %. On still a longer time scale, collisions would also lead to radial particle and heat transport. However, as described in the previous section, the time scale for this process is much longer than the energy confinement time required for sustained D-<sup>3</sup>He burning.

Finally, it should also be noted that as the plasma beta increases, the shape of the flux surfaces in a dipole will change dramatically. The plasma diamagnetic currents, stretch the equatorial field lines and slow the radial decrease of the magnetic field strength. This type of equilibrium has been observed in the Jovian magnetosphere<sup>12</sup> where a steady-state plasma equilibrium "maintained" by the solar wind has  $\beta > 1$  and a plasma pressure concentrated near the equatorial plane.

#### 4. FUSION PRODUCT CONTROL

In order to achieve ignition in a D-<sup>3</sup>He fusion reactor, the energetic protons and alpha particles must be confined. On the other hand, in order to prevent the dilution of the fuel by ash accumulation and to provide a means for reactor burn control, the reactor should have a means to reduce energetic particle confinement and divert the charged particles either to a direct or thermal convertor.

This control can be facilitated in the dipole fusion reactor, for example, by breaking axisymmetry. Since the ratio of energies between the thermal plasma and the fusion products is large ( $T_e \sim T_i \approx 75$  keV whereas  $E_\alpha = 3.6$  MeV and  $E_p = 14.7$  MeV), the field strength of the dipole can be made large enough to maintain adiabaticity of the thermal plasma but (for a reasonably sized reactor) the fusion products will be non-adiabatic. Charged particles lose adiabaticity when  $v/\omega_c L > 0.12 \sin \theta_v$ , where  $v$  is the velocity of the particle,  $L$  is the equatorial radius of the particle's flux-surface, and  $\theta_v$  is the particle's pitch angle at the equatorial plane with respect to the magnetic field. Adiabaticity is relatively easy to maintain for the thermal plasma but difficult for the energetic fusion products.

However, since the dipole is axisymmetric, canonical angular momentum is conserved, and charged particles are radially localized provided that  $v/\omega_c L < 1/4$ <sup>13</sup>. For the reactor design shown in Figure 1, both the protons ( $v/\omega_c L = 0.11$ ) and the alpha particles ( $v/\omega_c L = 0.054$ ) are non-adiabatic but still radially-localized. Since the orbits of the charged fusion products are already chaotic, by applying either non-resonant or drift-resonant non-axisymmetric magnetic perturbations. For example, recent numerical calculations have shown that when the azimuthal mode number,  $m$ , of an applied static magnetic perturbation is chosen to produce a drift-bounce resonance, strong radial diffusion can develop. However, those lower energy particles satisfying only higher-order resonances remain adiabatic, producing negligible diffusion. Since only energetic particle can resonant with low  $m$  numbers, the radial confinement of fusion products can be selectively enhanced to cause their outward motion to the direct convertors or process sites located at the reactor wall. The high energy particles can also be extracted without breaking axial symmetry, and this possibility has been discussed in Ref. 2.

## 5. AN EXPERIMENT WITH A MECHANICALLY-SUSPENDED DIPOLE

A Collisionless Terrella Experiment (CTX) has been recently assembled at Columbia University. The purpose of this experiment is to understand collisionless particle transport in planetary magnetospheres induced by low-frequency fluctuations. The experiment will test our fundamental understanding of chaos, transport, and stability of energetic particles confined within a dipole magnetic field. This will be accomplished by carefully observing the threshold, onset, and effects of the hot electron interchange (HEI) and related instabilities. In this experiment, the HEI instability serves as an easily-observed and easily-controlled "model instability." It will be used to demonstrate the general stability and transport principles applicable to low-frequency, drift-resonant fluctuations found in the space environment.

The experiment will begin by generating a population of energetic electrons trapped within the dipole magnetic field. These electrons are formed *in situ* by cyclotron resonance heating. As seen previously (in other magnetic topologies), these electrons become unstable to a spectrum of low-frequency interchange (HEI) instabilities and induce rapid, collisionless radial transport. The onset of the instability can be controlled by controlling the background neutral pressure. The amplitude, frequency, and wavelength of the unstable modes will be measured by magnetic and electrostatic probes. By comparing the onset of radial transport with the time-evolution of each unstable mode, we will be able to observe the conditions for  $(\psi, \phi)$ -chaos in a dipole magnetic field. As the hot electron profile evolves, we will also for the first time observe marginally-stable pressure profiles and test theories of adiabatic transport under conditions preserving  $(\mu, J)$  conservation.

These experiments will be guided and interpreted by numerical and theoretical analyses. By making correlations between laboratory and numerical simulations, we will be able to apply directly the principles learned from our observations to analogous processes occurring in planetary magnetospheres. Figure 3 shows a cross-sectional diagram of the CTX experiment.

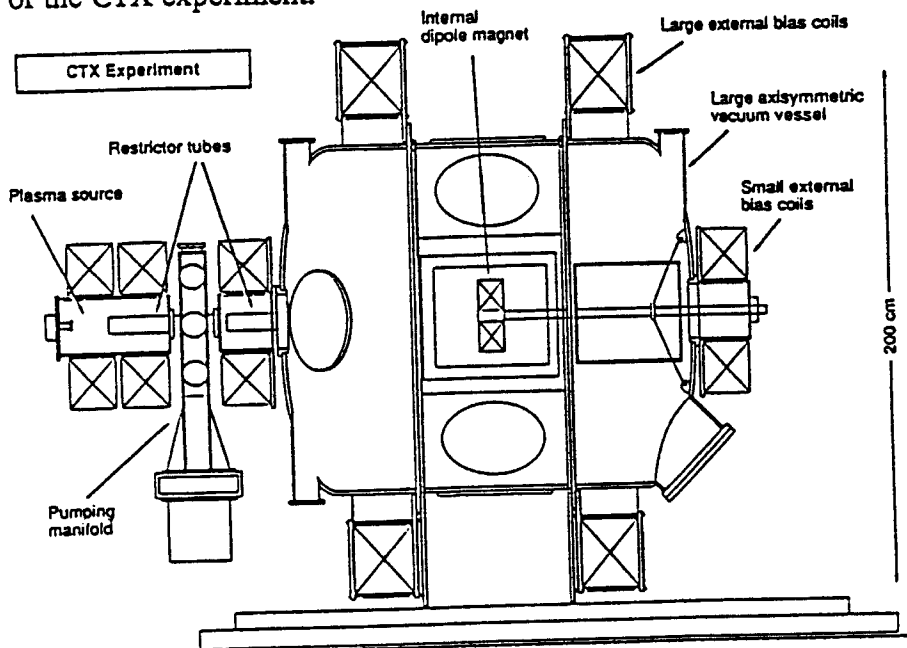


Figure 3. A schematic drawing showing the cross-section of the Columbia CTX experiment. The mechanically-supported dipole is encased in a stainless steel vacuum case, and it enters the vacuum chamber from the right side of the drawing.

## 6. DISCUSSION

The D-<sup>3</sup>He dipole fusion reactor is an innovative concept that originated from consideration of the simplest possible magnet geometry and the modern understanding of collisionless transport induced from low-frequency fluctuations. Although the basic reactor concept present here appears very attractive, considerable experimental and theoretical study is still required. These include: (1) an experimental verification of the stability and confinement properties of the  $\partial \hat{f}_0 / \partial \psi = 0$  equilibrium, (2) a detailed study of the fraction of cyclotron radiation emitted from the high field regions within the inner bore of the ring, and (3) a detailed study of the transport to the inner ring. It is very gratifying to learn of the theoretical derivations of Pastukhov and Sokolov presented at this conference<sup>14</sup>.

## REFERENCES

1. A. Hasegawa, Comments on Plasma Phys. Contr. Fusion, 11, 147 (1987).
2. A. Hasegawa, L. Chen, M. Mauel, *Nuclear Fusion*, 31, 125 (1991).
3. A. Hasegawa, *et al.*, to appear in *Fusion Technology* (1992).
4. See for example, R. Freeman, *et al.*, "Confinement of Plasmas in the Spherator", *Plasma Physics and Controlled Nuclear Fusion 1971*, IAEA-CN-28/A-3, Vol. 1, p. 27, and references cited within.
5. See for example, A. F. Kuckes and R. B. Turner, "Plasma Confinement and Potential Fluctuations in a Small Aspect Ratio Levitron", *Plasma Physics and Controlled Nuclear Fusion 1968*, IAEA-CN-24/C-8, Vol. 1, p. 427, and references cited within.
6. B. Lehnert, *et al.*, "Plasma Confinement and Heating in the Internal Ring Device F IV", *Plasma Physics and Controlled Nuclear Fusion 1971*, IAEA-CN-28/A-4, Vol. 1, p. 59.
7. *Report of the Senior Committee on Environmental, Safety, and Economic Aspects of Magnetic Fusion Energy*, J. P. Holdren, *et al.* (Sept., 1989), University of California Report UCRL-53766. Available from the National Technical Information Service, U.S. Department of Commerce, Springfield, VA, U.S.A.
8. D. J. Rose and M. Clark, Jr., *Plasmas and Controlled Fusion*, (Wiley, New York, 1961).
9. R. W. Conn, *et al.*, *Plasma Physics and Controlled Nuclear Fusion 1980*, IAEA-CN-38/V-5 (1980).
10. G. W. Shuy, Y. C. Lee, F. Kantrowitz, *Comments Plasma Phys.* 6, 155 (1981).
11. B. B. Kadomtsev, *Review of Plasma Physics*, Ed. by M. A. Leontovich, Consultant Bureau, New York, 1966, p. 170.
12. N. F. Ness, *et al.*, *Science*, 206, 966 (1979) also S. M. Krimigis, *et al.*, *Science*, 206, 977 (1979).
13. A. J. Dragt and J. M. Finn, *J. Geophysical Res.*, 81, 2327 (1976).
14. V. P. Pastukhov and A. Yu. Sokolov, "On Anomalous Transport Processes near a Levitated Coil Immersed into the Plasma", submitted to *Nuclear Fusion*.

## THE POLYWELL™, A SPHERICALLY CONVERGENT ION FOCUS CONCEPT

Nicholas A. Krall

Krall Associates  
1070 America Way  
Del Mar, CA 92014

### 1. INTRODUCTION

The Polywell™/SCIF concept for controlled thermonuclear fusion is a novel attempt to achieve fusion by the use of highly non-Maxwellian electron and ion distributions. The device magnetically confines electrons by a quasi-spherical-cusp magnetic field, forming a potential well. Ions are electrostatically confined by this well, converging to a dense focus in the center of the spherical potential, where the fusion rate is large because of the high local density of transient energetic ions.

This concept, a magnetic version of a Spherically Convergent Ion Focus (SCIF) device, was invented and proposed by R. W. Bussard<sup>1-2</sup> as a significant variation of earlier studies on electrostatic confinement.<sup>3-5</sup> High energy electrons are injected into a quasi-spherical-cusp magnetic field, thus creating a potential well of sufficient depth to accelerate ions from low energy at the periphery to fusion energies within a focus at the center of the sphere. This magnetic geometry is MHD stable, by the nature of the cusp fields. Injection of electrons keeps the system electrically nonneutral, so that the potential well which accelerates the ions is maintained at a constant value sufficient to confine the ions within the device, returning them again and again at high velocity to the central focus. Essential to the success of the scheme is that the cusp field confine the electrons sufficiently long that the power required to maintain the cloud of energetic electrons is less than the fusion power produced by the convergent ion beams. Equally essential is that the ions maintain their nonthermal velocity distribution, with primarily radial flow, long enough to produce fusion in the dense focus at the center of the sphere. A schematic of the concept is shown in Figure 1.



Fusion schemes which use electrostatic fields to accelerate and project ions onto a reacting region have a natural advantage for use with advanced fuels such as  $D-^3He$  compared to systems which confine a thermal plasma, because the need to heat the plasma to the increasingly high temperatures required for burning advanced fuels is replaced by a simple increase in the electrostatic accelerating voltage. The potential of the device for  $D-^3He$  operation is enhanced by the ability to tailor the ion energy distribution function to be maximum at the energy at which the cross section for fusion is also a maximum. The scaling guides in Table I indicate the path to that application. Since even the fuel ions have orbits the size of the device, the orbits of fusion products will clearly not be confined in the device. This makes ideas such as direct conversion of charged particle energy to electricity an appealing possibility.

## 2. ION CONVERGENCE

The non-Maxwellian nature of the ion distribution is in strong contrast with the requirements of more typical magnetic confinement fusion schemes, which rely on magnetic fields to confine thermal plasmas of the energy and density required for fusion, with these parameters relatively constant over the device. In contrast, the Polywell<sup>™</sup> produces fusion in the dense core, where ions are not in fact confined, but are passing through on orbits which intersect the core on each of a large number of passes. The magnetic confinement in the system is of a much lower density cloud of electrons.

A possible problem is effect of collisions, which drive ions toward equilibrium, destroying convergence. We have calculated this effect, and find that the deflection from radial flow due to collisions is extremely small on a single pass. In contrast, the collision frequency near the turning points, where the ions were born and have low energy, is comparable to the transit time across the device. Thus rapid collisions at the edge have the effect of "healing" the ion distribution from alterations which occurred during a transit, maintaining it isotropic at the edge, and thus by conservation of angular momentum highly non-Maxwellian in the interior.

Equally essential to ion convergence is the requirement that the ions not be substantially deflected by the magnetic field during their orbit. This means

that the ion must be born at location where  $B$  is not too large. This will place considerable constraint on the ion source design.

The radial density profile can be calculated from the Liouville theorem (conservation of phase space). If we assume that at birth the ion distribution function is uniform in energy up to some small energy  $E_0$ , and uniform in angular momentum up to some small azimuthal velocity  $v_\perp$ , the distribution is subsequently described in terms of the constants of the motion ( $E = (1/2)M(v_r^2 + v_\perp^2) - e\phi$ ,  $rv_\perp$ ). The Vlasov equation for steady state is  $F(E, rv_\perp) = \text{constant}$ , so the density everywhere is determined by the potential and the value of  $F$  at the ion birth point. Integrating  $F$  over velocity determines the density. There are three regions. For a very small distance from the birth point, the potential is negligible, and the density is given by  $n = n_{\text{edge}}$ . Since the maximum well depth is in the keV range, compared with ion birth energies in the few eV range, a little way toward the center it will be true that  $E_0 \ll 2e\phi$ , and  $Mv_{\perp 0}^2(R/r)^2 < 2e\phi$ . In that range, which includes most of the profile, the density is given by  $n \propto (R/r)^2$ . Moving inward, the  $(R/r)^2$  factor eventually becomes substantial, so that the density becomes much larger than  $n_0$ . Eventually, the radius is so small that  $Mv_{\perp 0}^2(R/r)^2 > 2e\phi_{\text{max}}$ . Inside that radius the density is nearly constant, with

$$n_c = (R^2/r_c^2) n_0 \quad , \quad (1)$$

$$r_c = (Mv_{\perp 0}^2/2e\phi_{\text{max}})^{1/2} R \quad . \quad (2)$$

Thus the ion orbits are of the size of the device, the ion density increases as  $1/r^2$  to a large density at the center, and size of the core and the central density are determined by the angular momentum at the outer turning points of the ion motion. This leads to the overall view of the Polywell™/SCIF shown in Figure 1.

### 3. ELECTRON CONFINEMENT

The basic magnetic geometry which confines electrons in the Polywell<sup>™</sup> is shown in Figure 2, which shows the magnetic field lines in a plane through the center of the device. In the third dimension, the magnetic field continues to be a set of point cusps arranged in an alternating pattern in a generally spherical geometry. This field arrangement is the basis of the Polywell<sup>™</sup> concept, and can correspond to various orders of polyhedra. The lines shown correspond to an  $m = 3$  configuration, called a truncated cube, with  $B = B_0 (r/R)^m$  fairly far out from the center of the configuration.

Electrons are injected into this geometry from electron guns at high energy, since the maximum potential well that can be obtained will be approximately equal to the incoming electron energy. The current from the gun must be chosen so as to at least balance the electron losses. Losses directly through the cusp may be expected to be inversely proportional to the strength of the magnetic field. The "standard" expression for the point-cusp confinement time is

$$t_c = t_{\text{transit}} R^2/a_0^2, \quad (3)$$

where  $a_0$  is the gyroradius and  $R$  the radius of the device. This confinement behavior has been widely postulated, but never proven. Demonstrating that this is the actual loss rate in a cusp is an important part of our program.

### 4. POWER BALANCE IN THE POLYWELL<sup>™</sup>

It is instructive to combine the classical estimates of power loss and gain into a sample of the parameters that a successful proof-of-principle experiment or energy breakeven experiment might have. This is done in Table I, which gives a set of parameters appropriate to reactor conditions, and for parameters appropriate to an experiment which provides a significant test of the concept. Table I includes the scaling with electron confinement and other parameters, so it is straightforward to calculate degradation of performance with degraded values of electron confinement, as well as enhanced performance by

increasing the size, field strength, or density in the device. Although the fuel in the example of Table I is DT, extension to D-<sup>3</sup>He is straightforward from the scaling guidelines indicated in the last column. Note that an experiment with a 1 meter radius has volume of order 3 cubic meters, in contrast with a toroidal device of 1 meter minor radius and 3 meter major radius which has a volume of order 50 meters. This difference in size, combined with the high  $\beta$  nature of the device, makes for an economical experimental study program and commercial development path, if nature should prove to be not too harsh when the inevitable physics anomalies which plague all plasma devices begin to be uncovered and understood.

## 5. CONCLUSIONS

The potential advantages of this approach to fusion are many:

- The electrons are magnetically trapped in a high  $\beta$ , MHD stable configuration.
- The magnetic fields are relatively small, because the plasma density is low at the  $\beta = 1$  point, due to the  $1/r^2$  density decrease away from the core. This allows the use of a low technology magnet system.
- There is no heating system as such. The electron guns provide the energy used to accelerate the ions to fusion velocities. These guns are external to the system, and so do not depend on interaction of a remote heating system with the plasma interior, as in current drive or ECRH and similar wave heating systems which are an integral part of magnetically confined equilibrium fusion schemes.
- The fusion products are not confined. Thus there will be no "ash" buildup, and the escaping particles can be used in direct conversion schemes.
- Application to D-<sup>3</sup>He and other advanced fuels can be achieved by increasing the energy of the electron guns.

In summary, the advantage of the Polywell<sup>™</sup>/SCIF approach is that it offers a high  $\beta$  geometry with no complex auxiliary heating or confinement systems; in

practice this means that the scheme can be tested with fairly modest budgets, with a fairly short development path. The tradeoff of course is that the physics of the device is not simple at all, encompassing as it does a highly nonequilibrium system with widely varying parameters at different radial points in the device.

#### REFERENCES

1. R. W. Bussard, "Method and Apparatus for Controlling Charged Particles," U.S. Patent Number 4,826,626 (May 2, 1989).
2. R. W. Bussard, "Some Physics Considerations of Magnetic Inertial-Electrostatic Confinement: A New Concept for Spherical Converging-Flow Fusion," Nuclear Technology/Fusion (1991, in press).
3. P. T. Farnsworth, "Electric Discharge Device for Producing Interactions Between Nuclei," U.S. Patent Number 3,258,402 (June 28, 1966).
4. R. L. Hirsch, "Inertial-Electrostatic Confinement of Ionized Fusion Gases," J. Appl. Phys. 38, 4522 (1967).
5. O. A. Lavrent'ev, "Electrostatic and Electromagnetic High-Temperature Plasma Traps," Ann. New York Acad. Sci., 251, 152 (1975).

Table I. Polywell<sup>tm</sup>/SCIF parameters for DT fusion with classical loss rates.

	Fusion Reactor	Concept Test Experiment	Performance Scaling
Device Radius R	2 m	1 m	---
Ion Source Radius	1 m	0.5 m	---
Magnetic Field B <sub>0</sub>	1 T	0.2 T	---
Electron Gun Energy E <sub>e</sub>	50 keV	20 keV	---
Ion Source Energy E <sub>0</sub>	5 eV	5 eV	---
Bulk Density n <sub>0</sub>	$2 \times 10^{20} \text{ m}^{-3}$	$10^{16} \text{ m}^{-3}$	---
Core Density n <sub>c</sub>	$2 \times 10^{24} \text{ m}^{-3}$	$4 \times 10^{19} \text{ m}^{-3}$	$n_0(E_e/E_0)$
Core Radius r <sub>c</sub>	$10^{-2} \text{ m}$	$0.8 \times 10^{-2} \text{ m}$	$(E_0/E_e)^{1/2} R$
Electron Confinement Time $\tau_e$	120 ms	2 ms	Classical $\sim R^3 B_0^2 / E_e^{3/2}$
Electron Injection Current	5 kA	50A	$n_0 R^3 / \tau \sim n_0 E_e^{3/2} / B_0^2$
Fusion Power (MW)	800 MW	---	$n_0^2 R^3 E_F (E_e/E_0)^{1/2} \sigma_F$
Electron Loss (MW)	40 MW	---	$n_0 R^3 E_e / \tau_e (\text{cusp}) \rightarrow n_0 E_e^{5/2} / B_0^2$
Radiation Loss (MW)	4 MW	---	$n_0^2 R^3 T_{e,c}^{1/2} (E_e/E_0)^{1/2}$
E <sub>Fusion</sub> = 15 MeV	---	---	
Gain $\equiv$ Fusion Power/ Electron Loss	20	---	$n_0 E_F B_0^2 R^3 \sigma_F / E_e^2 E_0^{1/2}$

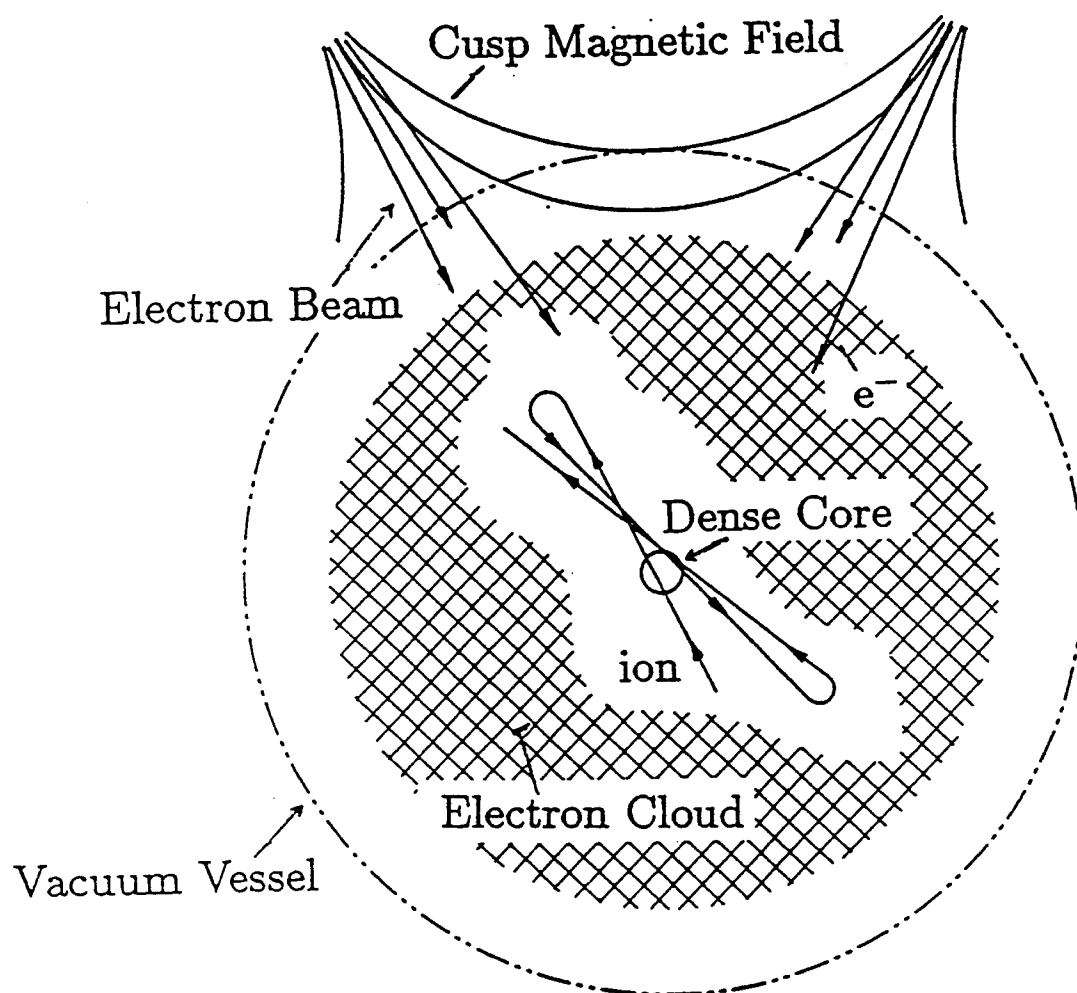
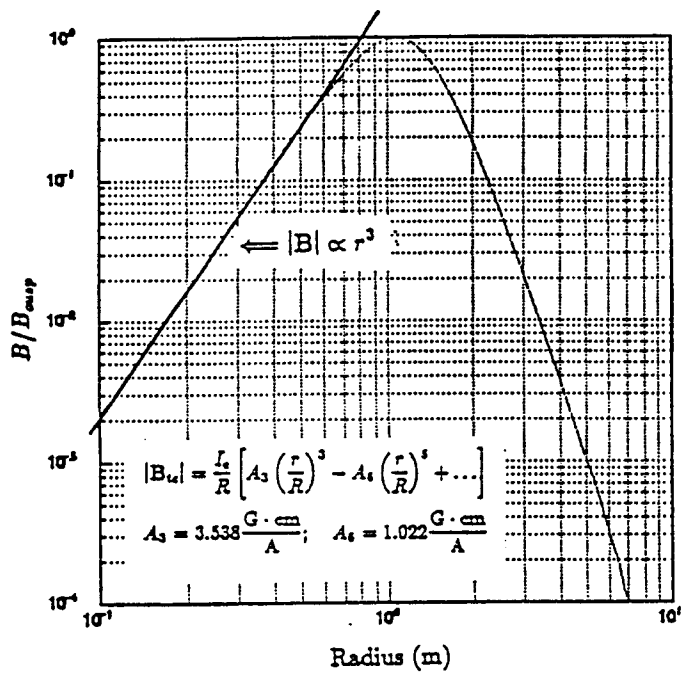
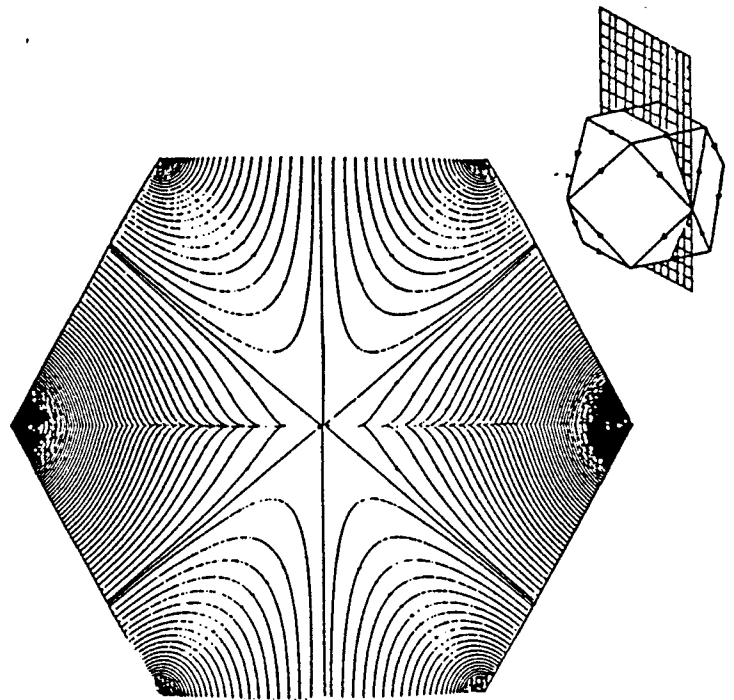


Figure 1. Polywell™/SCIF schematic.



Magnitude of B



Lines of Force

Figure 2. The Polywell<sup>™</sup> magnetic geometry.



**Paper 1C5**

**D-<sup>3</sup>He Mirror Reactor with Fast <sup>3</sup>He Injection**

**D.D. Ryutov**

**(paper not submitted)**



# Ideally MHD Stable Equilibria with High $\beta$ in Tokamak

Degtyarev L.M., Medvedev S.Yu.

Keldysh Institute of Applied Mathematics  
USSR Academy of Sciences, Moscow, USSR

## Abstract

The calculations of ideal  $\beta$  limits are reported for tokamak plasma under wide change of geometry and profiles. The stability of internal and external modes is considered both in the first and the second stability regions for ballooning modes.

## 1. First region of tokamak stability

Ideal MHD instabilities impose the limitations on the values of  $\beta$  in stable toroidal plasma equilibrium configurations. High- $n$  ( $n$  - toroidal wave number) ballooning modes and low- $n$  external kink modes are well-known instabilities to avoid in order to reach high  $\beta$  values in tokamak. External kink  $\beta$  limit is well described by Troyon scaling:

$$\beta(\%) = g I_N \quad I_N = I(MA)/a(m)B_0(T), \quad (1)$$

$$g = 2.5 - 3.0,$$

when wall stabilization is not taken into account [1]-[2]. The same scaling with  $g=4$  can be applied to equilibria in the first region of ballooning mode stability. Second stability region of ballooning modes is an attractive way to overcome Troyon limit. However conducting wall or feedback stabilization should be used to stabilize external kink modes.

### 1.1 Troyon scaling

Troyon scaling (1) shows the way to increase  $\beta$  in tokamak by increasing normalized current  $I_N$ . The following expression estimates  $I_N$ :

$$I_N = \frac{5}{2} \frac{1 + \kappa^2}{q_s(A-1)}, \quad (2)$$

where  $A=R_0/a$  is aspect ratio,  $\kappa$  - plasma cross-section elongation,  $q_s$  - safety factor at plasma boundary [3]. The necessary condition for stability of force-free ( $\beta=0$ ) plasma equilibrium against external kink mode:  $q_s > 2$  - gives maximum value of  $I_N$  (corresponding  $q_s=2$ ). At fixed  $q_s$  the value of  $I_N$  increases with higher elongations and lower aspect ratios which results in higher  $\beta$  limit (Troyon scaling).

The scaling (1) is only a guideline through numerous equilibrium configurations which differ in current, pressure and safety factor profiles. Typical dependence  $\beta(I_N)$  is shown in Fig.1 [2]. The curve  $\beta(I_N)$  has some spikes for  $2 < q_s < 4$ . The ravines for  $q_s$  slightly lower than 3 and 4 correspond to "instability gaps" for external kink modes. They disappear with increasing boundary shear. Toroidal current density profile effects kink mode  $\beta$  limit weaker in the case of higher boundary

shear [4]. So due to high boundary shear the scaling (1) is valid under toroidal current density variations. However higher boundary shear gives rise to low shear region near the axis at fixed global shear and ballooning mode instability forces pressure gradient to be low there (flat pressure profiles).

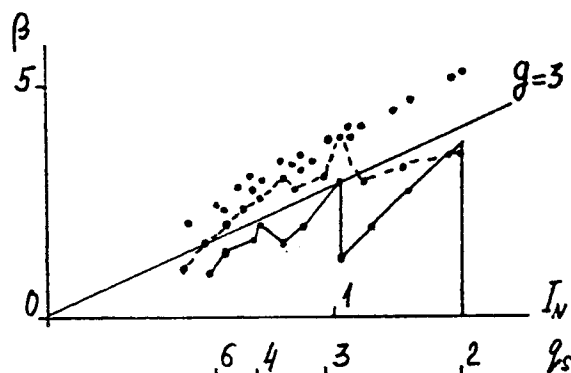


Fig.1 Ballooning  $\beta_{\infty}$  and external  $n=1$  kink  $\beta_{n=1}$  beta limits vs normalized current for  $A=4$ ,  $\kappa=1.6$ , triangularity  $\delta=0.3$ . Solid line denotes  $\beta_{n=1}$  for lower edge shear ( $j_2=1$ ), broken line for higher shear ( $j_2=2$ ).

### 1.2 Low aspect ratios and high elongations

The scaling (1) for  $A < 2$  and  $\kappa > 2$  has to be supplied with some restrictions. Instead of  $q_s > 2$  the limit  $q_s > q_s^* > 2$  is set by kink instability due to coupling of surface waves and internal modes even at  $\beta=0$ . Typical dependencies of  $\beta(I_N)$  is given in Fig.2 for  $A=1.6$  [3] and in Fig.3 for  $\kappa=2.5$ . Increasing  $\kappa$  does not enhance essentially limiting  $\beta$  values in comparison with  $\kappa=1.6$  (Fig.1).

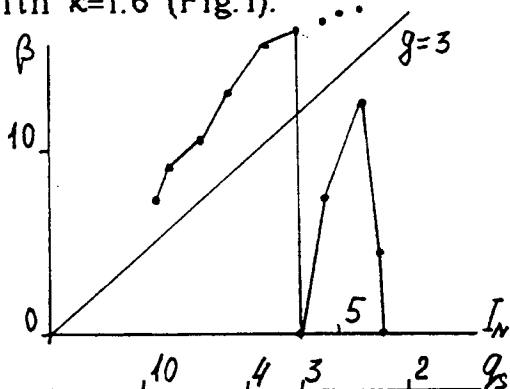


Fig.2 Beta limits for  $A=1.6$ ,  $\kappa=1.6$ ,  $\delta=0.3$

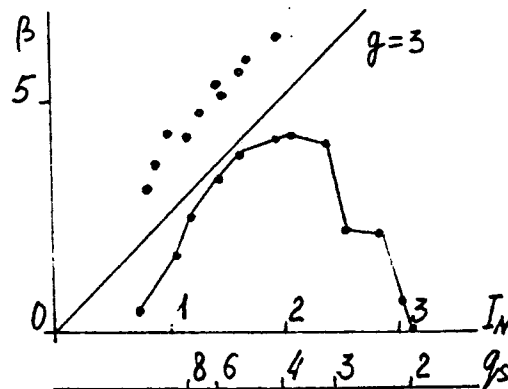


Fig.3 Beta limits for  $A=4$ ,  $\kappa=2.5$ ,  $\delta=0.3$

For low  $A$  limiting  $\beta$  is restricted by ballooning mode instability almost for all  $q_s > q_s^*$  giving  $g=4$  in scaling (1). The dependence of  $q_s^*$  on aspect ratio for  $\beta=0$  is given in Table 1[3].

Table 1 Limiting values of  $q_s$  and  $I_N$  against external  $n=1$  mode vs aspect ratio;  $\kappa=1.6$ ,  $\delta=0.3$ ,  $q_0=1.1$ ,  $j_2=1$

$A$	1.6	1.5	1.4	1.2
$q_s^*$	2.2	2.6	3.0	5.0
$I_N$	5.6	6.4	6.4	8.6

The growth of limiting normalized current with aspect ratio is much slower than that defined by  $q_s=2$ . In general the value of  $q_s^*$  depends on plasma profiles: higher boundary shear (lower shear near the axis) corresponds to higher values of  $q_s^*$ .

As a conclusion,  $\beta$  limits for low aspect ratio configurations is in accordance with scaling (1) ( $g=4$ ) with limiting current  $I_N < I_N^*$  at least for high boundary shear and flat pressure profile.

### 1.3 Peaked pressure profiles

The stability of equilibria with peaked pressure profiles favorable for tokamak-reactor needs special attention. For such equilibria ballooning (Mercier) modes are unstable near the axis for typical high edge - low axis shear configurations when safety factor at the axis  $q_0 \approx 1$  (internal inductance  $l_1 = 2 \int B_p^2 dV / \mu_0^2 I^2 R_0 \approx 0.7$  for ITER parameters). External and internal mode coupling due to high values of pressure gradients near magnetic axis results in lower  $\beta$  limit against kink modes. There are two ways to stabilize ballooning modes in the region near the axis: to increase shear there or to increase the value of  $q_0$ . Both ways lead to lower values of internal inductance  $l_1$  and lower edge shear. However even if the shear is sufficient to remove ravines from  $\beta(l_N)$ -dependence and to make  $\beta$  limit insensitive to edge current density profile variations, the values of limiting  $g_{n=1} = \beta / I_N$  against external  $n=1$  kink mode are lower than that for flat pressure profiles  $g \approx 4$ . The values of  $g_{n=1}$  for high  $q_0$ , high  $q_s$  case are given in Table 2 [5].

Table 2. Limiting values of  $\beta$  and  $g$  against external  $n=1$  mode for  $p=p_0(1-\psi)^\alpha$ ;  $A=2.79$ ,  $\kappa=2.0$ ,  $\delta=0.4$ ,  $q_0=1.6$ ,  $q_s=5.6$ ,  $j_2=3$

$\alpha$	$\beta_{n=1}$	$g_{n=1}$
1.1	4.6	3.0
1.5	4.2	2.7
2.0	3.8	2.5

Note that the values of  $g_{n=1}$  decreases with increasing pressure peaking.

### 2. Second stability region

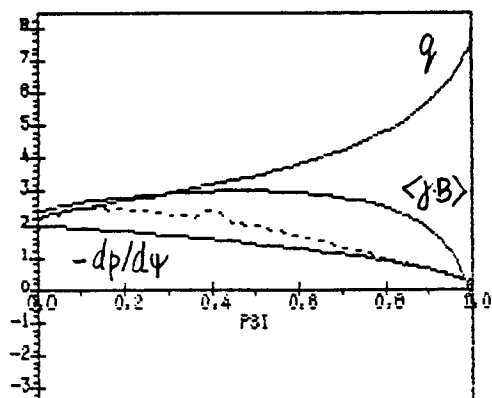
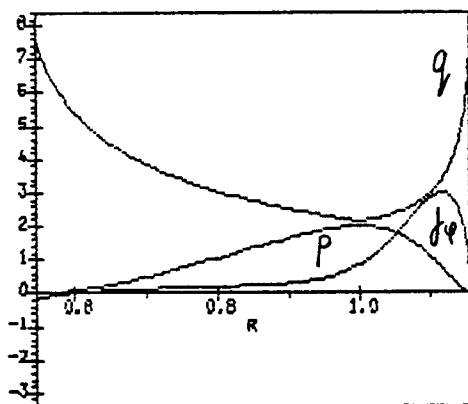
The transition to the second region of ballooning mode stability is possible because of local shear reversal due to magnetic surfaces shift at high beta. When the points of vanishing local shear are close to the region of favorable magnetic field line normal curvature  $k_n = (\mathbf{B}/|\mathbf{B}|) \nabla(\mathbf{B}/|\mathbf{B}|) \cdot \nabla\psi / |\nabla\psi|$  ballooning modes can be stable at any value of pressure gradient [6], [7]. The local shear reversal is enhanced if global shear is low or plasma cross-section shape is bean-shaped [8], [9]. External kink modes can hardly be stable at high values of  $\beta$  in the second stability region without outer conducting wall.

Another point of concern is low- $n$  infernal mode [10] becoming unstable when the region of low shear and high pressure gradient exists in high- $n$  ballooning mode stable plasma. Shear requirements are contradictory from the points of view of second stability region access and stability of infernal modes. Pressure profile also is important role for stable second stability access [9].

To investigate the access in ITER geometry we choose high shear equilibrium with safety factor defined by the following toroidal current density profile at  $\beta=0$

$$R j_\phi = (1 - \psi^{j_1})^{j_2}, \quad j_1=0.5, \quad j_2=0.5, \quad q_0=2.17, \quad q_s=7.6,$$

$\psi$  - normalized poloidal flux. The  $q$  profile is quite close to that of [7], where low aspect ratio and high  $q$  equilibria were found favorable "to allow the connection between first and second stability regimes". Unfortunately used pressure profile  $p=p_0(1-\psi)^{1.5}$  is not very suitable to reach unlimited high  $\beta$  in the second region. When  $\beta \approx 5\%$  ( $g \approx 4.5$ ) Mercier criterion is violated near the axis. At higher values of  $\beta > 10\%$  ( $g > 7.5$ ) the region near the edge goes unstable (Fig.4). The reason for that is insufficient shear reversal on the outer magnetic surfaces due to low pressure gradient there. The instability region grows with  $\beta$  which means that plasma edge does not transfer to second stability region. At lower values of edge shear ( $q_0=4$ ,  $q_s=7.6$ ,  $j_2=0.2$ ) the instability region shifts to the boundary and shrinks but emerges at approximately the same  $\beta$  value.



BETA= 10.27  
G= 7.76  
BETAP= 2.62  
PO/PA= 2.55  
PZA/PAZ= 1.60  
LI(1)= 0.38  
LI(3)= 0.39  
Q0= 2.17  
QS= 7.61

AS= 2.79  
EL= 2.00  
N= 61 M= 66



Fig.4 Equilibrium and profiles for ITER geometry plasma  $A=2.79$ ,  $\kappa=2.0$ ,  $\delta=0.4$ . Abscissae:  $R$  - major radius normalized to magnetic axis value,  $\psi$  - normalized poloidal flux; ordinate scale is for  $q$  values only, arbitrary units for others. Broken line shows limiting pressure gradient against ballooning modes;  $p=p_0(1-\psi)^{1.5}$

Higher pressure gradients near the edge and lower near the axis are needed to make the stable transition possible. Pressure profile  $p=p_0(1-\psi^{1.5})$  is suitable for it. However corresponding toroidal current density profile reaches maximal value at the edge (Fig.5).

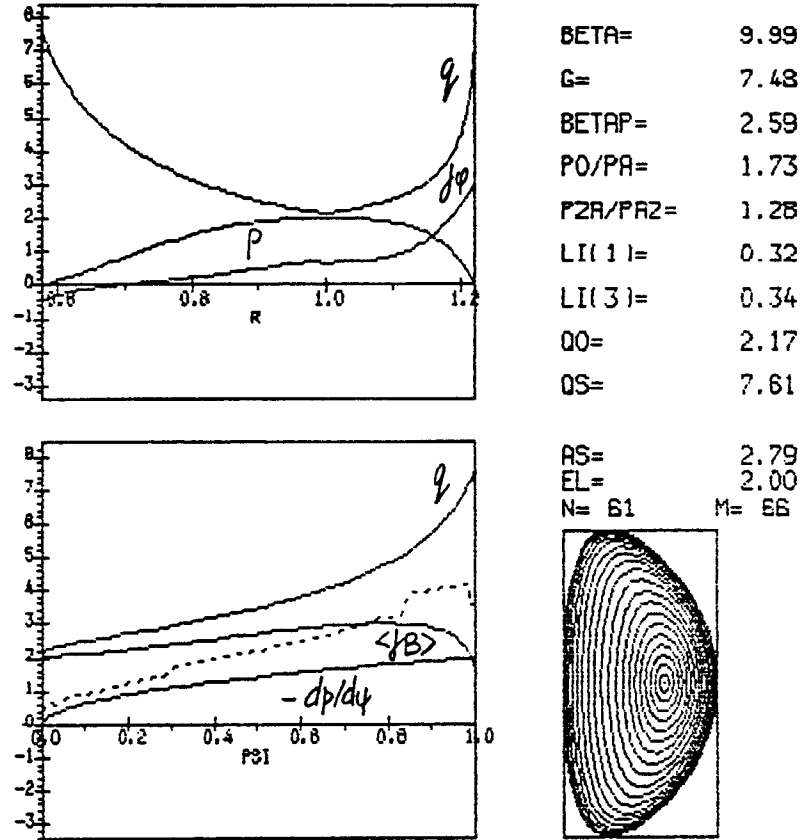


Fig.5 Equilibrium and profiles for ITER geometry plasma in second stability region for each magnetic surface;  $p=p_0(1-\psi^{1.5})$

Global mode stability of the plasma in second stability region was studied in [7], [9]. Close to plasma conducting wall (wall radius  $a_w=1.2a$ ) and sufficient shear to stabilize infernal mode was found to provide low- $n$  mode stability in the second stability region for any value of  $\beta$ .

2D ideal MHD stability code TORUS [11] was used for low- $n$  mode computations with number of magnetic surfaces  $N_\psi=121$  and number of poloidal harmonics  $L_\theta=33$  for equilibria of the type of Fig.5 and Fig.4. Kink mode stability ( $n=1,2$ ) was obtained for very high values of  $\beta$  and  $p=p_0(1-\psi^{1.5})$ , but needed for stability values of  $a_w$  are lower than that for the case of  $p=p_0(1-\psi)^{1.5}$  (Fig.6). The difference is due to higher edge current density for the case of Fig.5.

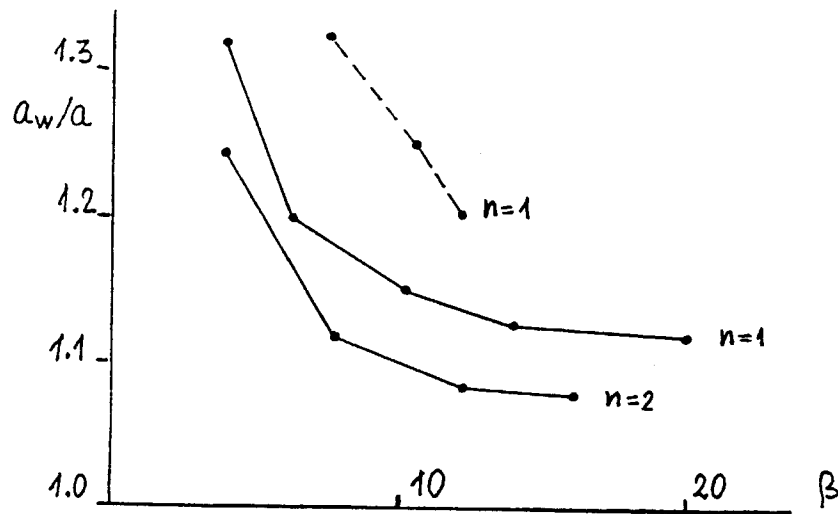


Fig.6 Wall location required for marginal stability against  $n=1,2$  modes for  $p=p_0(1-\psi^{1.5})$  (solid) and  $p=p_0(1-\psi)^{1.5}$  (broken)

### Conclusions

Troyon scaling can be used as a guideline to define  $\beta$  limits for plasma with high boundary shear, flat pressure profiles and  $q_0 > 1$ . Lower aspect ratio seems to be the most robust way to reach high- $\beta$  values due to higher plasma current. The external kink current limit  $q_s > q_s^* > 2$  should be taken into account.

Pressure profiles with low gradient near magnetic axis and high gradient near plasma edge are favorable for second stability region access. However for corresponding skin type current density profiles conducting wall has to be closer to plasma to stabilize external kink modes.

### References

1. Troyon F., Gruber R., Saurenmann H., Semenzato S., Succi S., Plasma Phys. Controlled Fusion 26(1983)209
2. Degtyarev L.M., Drozdov V.V., Martynov A.A., Medvedev S.Yu., Sov. J. Plasma Phys. 11(1985)
3. Bespoludennov S.G., Degtyarev L.M., Medvedev S.Yu., Sov. J. Plasma Phys. 12(1986)
4. Degtyarev L.M., Medvedev S.Yu., Shear and current density effect on tokamak kink mode instability, Proc. Europ. Conf. Plasma Phys. Controlled Fusion, Venice, 1989
5. Degtyarev L.M., Medvedev S.Yu., MHD beta limits at high  $q_0$ , ITER, August 1991
6. Greene J.M., Chance M.S., Nucl. Fusion 21(1981)453
7. Gerver M.J., Kesner J., Ramos J.J., Phys. Fluids 31(1988)2674
8. Chance M.S., Jardin S.C., Stix T.H., Phys. Rev. Lett. 51(1983)1963
9. Manickam J., J. Comput. Phys. 66(1986)324
10. Manickam J., Pomphrey N., Todd A.M.M., Nucl. Fusion 27(1987)1461
11. Degtyarev L.M., Medvedev S.Yu., Comput. Phys. Commun. 43(1986)29



# Recent high poloidal beta experiments and their implications for high beta D-<sup>3</sup>He tokamak fusion

M. E. Mauel

*Department of Applied Physics, Columbia University, New York, New York 10027 U.S.A.*

(November, 1991)

Recent high  $\epsilon\beta_p$  experiments using the Tokamak Fusion Test Reactor (TFTR) have demonstrated two important results relevant to the possible development of D-<sup>3</sup>He tokamak fusion. First, these experiments demonstrated sustained operation at the equilibrium poloidal beta limit for several energy confinement times. Discharges at  $\epsilon\beta_p > 1.25$  were observed to have a natural, inboard divertor, and reconstructions of these equilibrium illustrated the "Maximak" tokamak configuration first discussed by Mukhovatov and Shafranov [*Nuclear Fusion* 11 (1971)]. Secondly, during the course of these experiments, a rapid toroidal current "ramp-down" technique was used to study the effects of transient current profile modification. By rapidly decreasing the plasma current just prior to the start of neutral beam injection, high  $\epsilon\beta_p$  discharges were produced having a Troyon normalized toroidal beta nearly twice as large as previously obtained in TFTR. All of these discharges were computed to be within the first stability regime, and high  $\epsilon\beta_p$  discharges produced using the current ramp-down technique had global energy confinement times as long as 3.5 times the L-mode predictions. These results illustrate that advanced tokamaks using current profile control may significantly exceed previously observed operational beta limits.

## 1. INTRODUCTION

During the 1989-1990 experimental run of TFTR, high  $\epsilon\beta_p$  experiments were conducted by a collaboration of scientists from Columbia University, the Princeton Plasma Physics Laboratory, and the Massachusetts Institute of Technology. These experiments demonstrated that transient current profile modification generated by a rapid decrease of the toroidal current significantly increased the operational Troyon-normalized beta limit and increased the global energy confinement time<sup>1</sup>. In addition, these experiments were the first to maintain high  $\epsilon\beta_p$  discharges with a natural inboard divertor for several energy confinement times<sup>2</sup>. Since the curvature of the applied vertical field is constant as  $\beta_p$  increases in TFTR, the appearance of the poloidal field null corresponds to operation at the equilibrium poloidal beta limit. This configuration was originally referred to as the "Maximak" by Mukhovatov and Shafranov<sup>3</sup> since it corresponds to the maximum allowable plasma pressure for a given plasma current and plasma cross-section.

High poloidal beta operation has long been known to offer advantages to fusion reactor design<sup>4</sup>. When a tokamak operates with high  $\beta_p$ , high fusion reactivity is maintained at reduced current. Low current operation reduces the power required for steady-state current drive and the adverse consequences of disruptions. In addition,

as  $\beta_p$  exceeds approximately  $\varepsilon^{-1/2}$ , a large fraction of neoclassical bootstrap current can further reduce current drive requirements.

In this report, the results from the TFTR high  $\varepsilon\beta_p$  experiments are summarized. The expansion of TFTR's operational beta limits is emphasized. Section 2 presents two representative low-current, high  $\varepsilon\beta_p$  discharges. Section 3 illustrates the "Maximak" equilibrium first observed transiently with the pulsed HBT tokamak<sup>5</sup> and then for several energy confinement times with the TFTR. Section 4 discusses the importance of current profile control in achieving high Troyon-normalized beta. In this section, the current profiles from high  $\varepsilon\beta_p$  discharges prepared with a rapid current ramp-down are compared with "supershot" profiles. Section 5 re-emphasizes the importance of high poloidal beta and current profile control in order to achieve higher fusion reactivity at lower plasma current.

## 2. DESCRIPTION OF THE TFTR HIGH POLOIDAL BETA DISCHARGES

The first high  $\varepsilon\beta_p$  discharges with a natural divertor were obtained in TFTR with equal co- and counter-tangential injection of high-power neutral beams into low current discharges with  $I_p = 0.3$  MA. This current level was chosen since  $\varepsilon\beta_p$  would exceed unity in TFTR with L-mode confinement when  $I_p < 0.5 \text{ MA} \times (P_{aux}/10 \text{ MW})^{1/2}$  and since kink and ballooning instabilities can usually be avoided by operating with  $\langle \beta \rangle < 10^{-8} C_T I_p / aB$  where  $C_T$  is  $\sim 2.7$  for supershots<sup>6</sup>. However, because of the onset of MHD activity, earlier attempts to reach high  $\beta_p$  with TFTR supershots failed to exceed  $\varepsilon\beta_{p,dia} \sim 0.7$  even with  $I_p$  as low as 0.6 MA. To circumvent this limit, gas puffing was used to produce target plasmas with higher density and broader density profiles than found in the earlier TFTR attempts to reach high  $\varepsilon\beta_p$ .

Figure 1 illustrates the time histories of two discharges that reach high  $\varepsilon\beta_p$  and form a natural divertor with a separatrix passing through an inboard poloidal field null. Figure 1a shows the time evolution of a constant current, 0.3 MA discharge, and Figure 1b shows the time evolution of a discharge with neutral-beam injection occurring when  $I_p \approx 0.4$  MA and immediately after a rapid current ramp-down from 0.85 MA.

For both examples, the injected neutral beam power was switched on gradually to 18 MW so that the TFTR feedback control system could hold constant the plasma radial position and toroidal current. The signals from a collimated  $D_\alpha$  detector and a vertical field monitor are shown suggesting the formation of the natural divertor. The  $D_\alpha$  signal shown in Figure 1 detects light

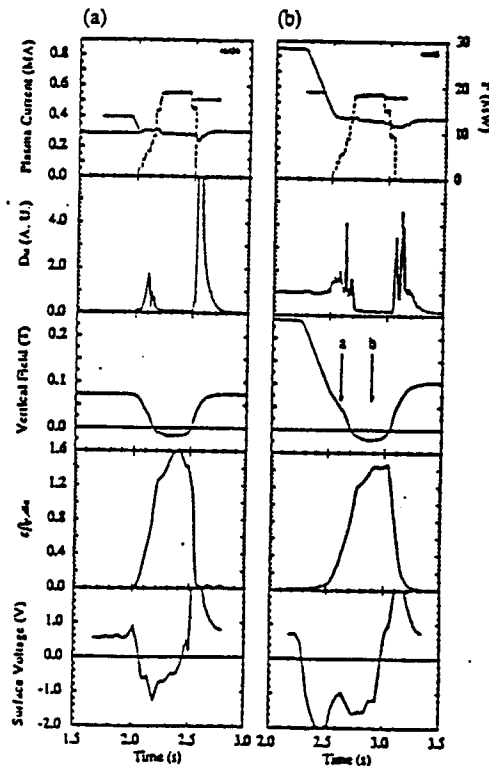


Figure 1. Example TFTR high  $\varepsilon\beta_p$  discharges with (a) constant  $I_p$  and (b) a rapid  $I_p$  ramp-down.

emitted from the midplane of the inside limiter. The vertical field monitor measures the poloidal field at a position 0.11 m behind the inside limiter surface. Five other  $D_\alpha$  and fourteen other poloidal field monitors measure the  $D_\alpha$  emission and poloidal field at other poloidal locations around the vacuum chamber. As the neutral beams are switched on, the  $D_\alpha$  light initially increases due to the added beam fueling, rising density, and increased particle recycling typical of beam-heated discharges. After 180 msec of NBI, the midplane  $D_\alpha$  signal nearly vanishes indicating the disappearance of particle recycling at this location. At approximately the same time, the inside vertical field changes sign, indicating that a poloidal field null has moved within the vacuum chamber.

The evolution of  $\epsilon\beta_{p,dia} \equiv 4\epsilon \int dV p_\perp / \mu_0 R^* I_p^2$  and the plasma's surface voltage are also shown Figure 1. As shown in the figure, the reduction in the  $D_\alpha$  signal and the reversal of the inboard vertical field occur when  $\epsilon\beta_{p,dia}$  exceeds 1.2. The large negative surface voltage represents the removal of poloidal flux by the ohmic heating feedback system. This prevents the plasma current from increasing as a result of the presence of neutral beam current drive, the generation of bootstrap current, and the reduction of the plasma's internal inductance as the magnetic axis shifts outward.

As we increased  $I_p$ ,  $\epsilon\beta_p$  decreased since for these discharges  $\tau_E$  scaled approximately as  $I_p$ . For reasons still not fully understood, confinement improved as we rapidly decreased the plasma current just prior to the start of neutral beam injection. High  $\epsilon\beta_p$  discharges with  $I_p \geq 0.4$  MA were only produced using this technique, and Figure 1b illustrates the time evolution of this type of discharge. Since the plasma pressure increases in proportion to  $I_p^2$  for discharges with equal poloidal beta, these higher current discharges have significantly higher electron and ion temperatures. As explained in Ref. 1, high  $\epsilon\beta_p$  discharges have been produced with final plasma currents up to 1 MA by using the current ramp-down technique, and these plasmas exhibit high fusion reactivity.

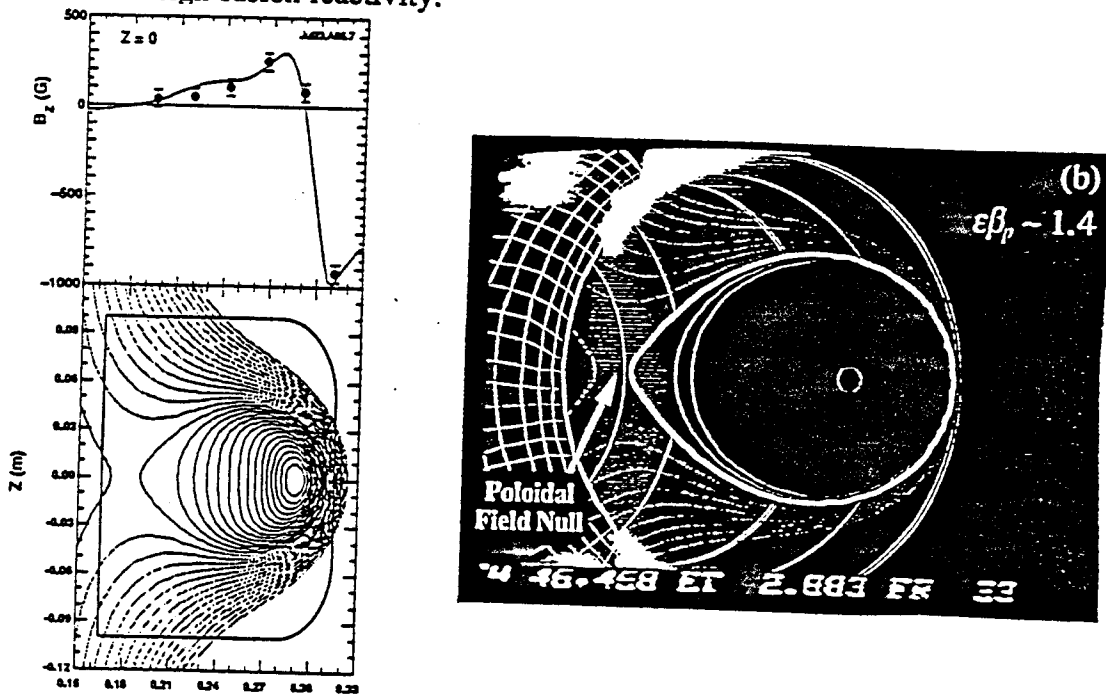


Figure 2. The equilibrium reconstructed from experimental measurements from (a) HBT and (b) TFTR. In (b) the equilibrium is superimposed on a visible light photo of the deuterium recycling light.

### 3. EXPERIMENTAL OBSERVATIONS OF THE "MAXIMAK"

Other tokamaks have produced plasmas with  $\epsilon\beta_p > 1$ , but these experiments have either been unable to produce the "Maximak" configuration (i.e. with a natural divertor) or they have been unable to sustain one. ECRH was used in TOSCA to produce discharges with  $\epsilon\beta_p \sim 1$ , but no divertor was observed<sup>7</sup>. The DIII-D<sup>8</sup> and Versator-II<sup>9</sup> tokamaks also produced low current discharges with  $\epsilon\beta_p > 1$  without producing a natural divertor or reaching the equilibrium limit. Finally, short-lived, high  $\epsilon\beta_p$  discharges have also been produced in the HBT tokamak either by ramping down the plasma current<sup>10</sup> or by a rapid reversal of the toroidal field<sup>11</sup>. In the latter case, both a natural divertor and the equilibrium poloidal beta limit<sup>12</sup> were observed although only for 5–20  $\mu\text{sec}$ . Figure 2a shows the "Maximak" equilibrium reconstructed from HBT experimental measurements.

The most convincing measurement of the TFTR natural divertor was a sequence of visible light pictures taken every 16 msec with a tangentially viewing video camera

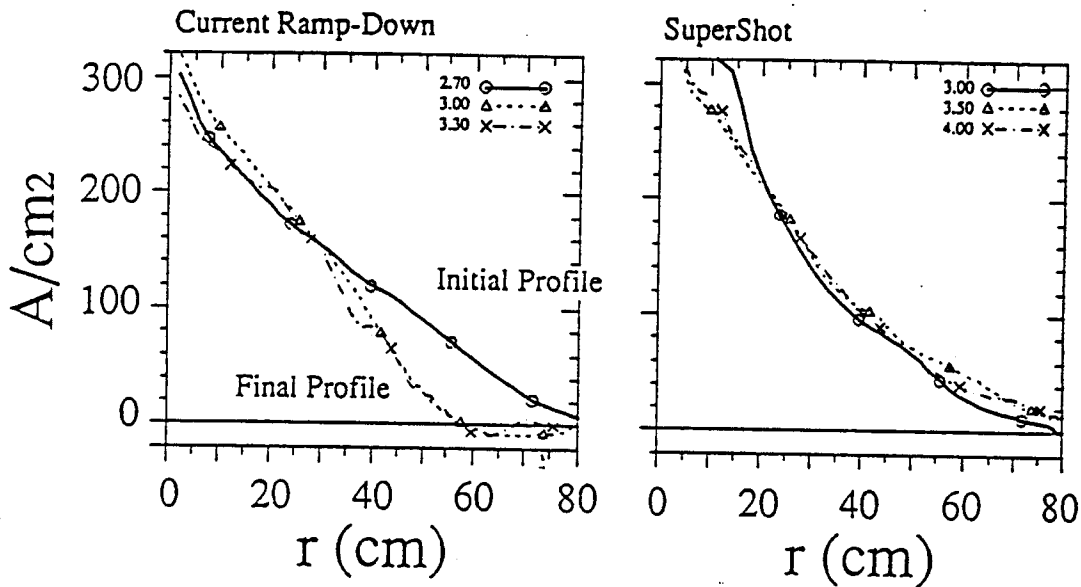


Figure 3. The toroidal current profiles from (a) a 1.6 MA to 1.0 MA ramp-down shot, and (b) a 1.6 MA supershot.

showing the evolution of a high  $\beta_p$  discharge prepared as shown in Figure 1b. Figure 2b shows one of these frames, taken when  $\epsilon\beta_p \sim 1.4$ . This video frame shows the penetration of the separatrix deep into the vacuum vessel as  $\epsilon\beta_p$  increases to its peak value. The bright recycling light now occurs only at the top and bottom parts of the limiter. An elliptically-shaped region with much reduced emission occurs within the divertor volume. Superimposed onto the video is a reconstruction of the equilibrium from experimental measurements.

The equilibrium poloidal beta limit was reached in these example discharges without observing any MHD activity resulting from macroscopic instabilities and without leaving the first stability regime of ideal ballooning mode theory. (Although under some circumstances, we did observe fast disruptions and coherent MHD oscillations.) This is noteworthy because high  $\epsilon\beta_p$  has usually been associated with the second stability regime<sup>13,14</sup>.

#### 4. CURRENT PROFILE MODIFICATION

Rapidly decreasing the plasma current prior to neutral beam injection has proven to be an important tool to investigate the effects of current profile on plasma stability and confinement. Figure 3 compares the current profile from a 1.6 MA to 1.0 MA high  $\epsilon\beta_p$  discharge and a 1.6 MA TFTR supershot computed using the TRANSP code<sup>15</sup>. As can be seen, the rapid current ramp-down removes and slightly reverses the current density at the edge of the plasma without significantly changing the current profile in the core. The plasma internal inductance,  $l_i$ , the edge  $q$ , and the edge shear increase. Additionally, the density profile of the high  $\epsilon\beta_p$  discharge is somewhat broader than the supershot profile. The current profile modification has extended by nearly a factor of two the operational limit of the Troyon-normalized beta. Figure 4 summarizes the operational space of the TFTR supershots and the high  $\epsilon\beta_p$  discharges. As the cylindrical  $q^*$  decreases, a Troyon beta limit,  $\beta_N \leq 4.5$ , is approached.

#### 5. DISCUSSION

Achieving tokamak operation at the maximum possible  $\beta_p$  has long been of interest, since high  $\beta_p$  operation allows the toroidal current to be reduced without reducing the thermonuclear fusion power. Low current minimizes the adverse effects of plasma disruptions and the power required to maintain the current in steady-state. The recent TFTR high  $\epsilon\beta_p$  experiments have shown that the maximum  $\beta_p$  allowed by equilibrium considerations can be sustained in a tokamak. At

low current, this equilibrium poloidal beta limit can be reached while remaining within the first region of ballooning stability. Furthermore, by using a transient current profile modification technique, these TFTR experiments have shown that a significant expansion of the Troyon-normalized beta limit results for discharges having a low edge current and a high edge shear. Since an advanced tokamak must operate at higher pressure than a D-T device in order to burn D-<sup>3</sup>He fuel, the ability of a tokamak to operate at high  $\beta_p$  and high  $\beta_N$  are particularly crucial to D-<sup>3</sup>He operation. Additional experiments are needed to investigate the stabilizing effects of current profile control and to demonstrate the means to maintain these currents continuously.

#### ACKNOWLEDGEMENT

This work represents a summary of results obtained from the Columbia University, P.P.P.L., and M.I.T. high  $\epsilon\beta_p$  collaboration. The author would like gratefully acknowledge the contributions of his colleagues listed in Refs. 1, 2, and 5. This research is sponsored by the U.S. Department of Energy under contracts

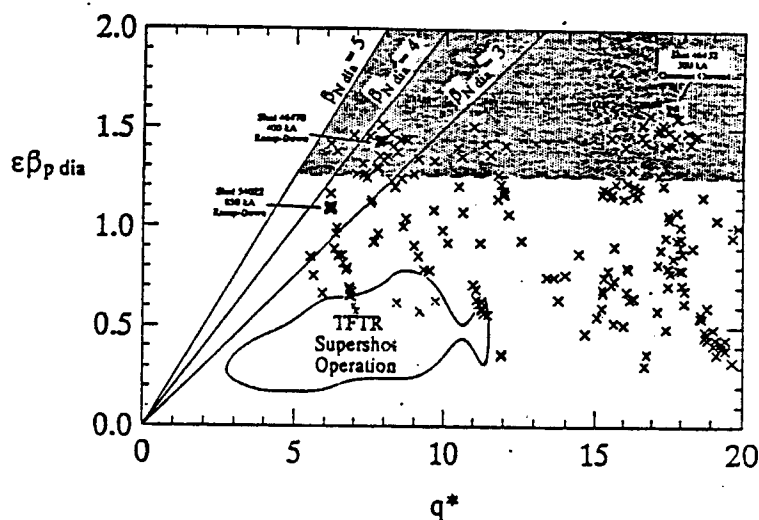


Figure 4. A summary of the operational limits for TFTR including the recently achieved high  $\epsilon\beta_p$  shots.

numbered DE-FG02-89ER53297, DE-AC02-76-CHO-3073, and DOE grant DE-FG02-90ER54084.

## REFERENCES

1. G. A. Navratil, *et al.*, *Plasma Physics and Controlled Fusion Research 1990* (IAEA, Vienna, 1991).
2. S. Sabbagh, *et al.*, *Physics of Fluids B* 3 (1991) 2277.
3. V. S. Mukhovatov and V. D. Shafranov, *Nuclear Fusion* 11 (1971) 605.
4. V. D. Shafranov, *Fusion Reactor Design Problems*, (IAEA, Vienna, 1974) 249.
5. T. H. Ivers, *et al.*, *Plasma Physics and Controlled Fusion Research 1990* (IAEA, Vienna, 1991).
6. K. McGuire, *et al.*, *Plasma Physics and Controlled Fusion* 30 (1988) 1391.
7. M. W. Alcock, *et al.*, *Plasma Physics and Controlled Fusion Research 1982* (IAEA, Vienna, 1983), Vol. 2, p. 51.
8. T. C. Simonen, *et al.*, *Physical Review Letters* 61 (1988) 1720.
9. S. C. Luckhardt, *et al.*, *Physical Review Letters* 62 (1989) 1508.
10. A. V. Deniz, *et al.*, *Physics of Fluids* 29 (1986) 4119.
11. A. V. Deniz, X. Li, and T. C. Marshall, *Physics of Fluids* 30 (1987) 2527.
12. T. H. Ivers, *et al.*, *Plasma Physics and Controlled Fusion Research 1990* (IAEA, Vienna, 1991).
13. J. M. Greene and M. S. Chance, *Nuclear Fusion* 21 (1981) 453.
14. M. Gerver, J. Kesner, and J. J. Ramos, *Physics of Fluids* 31 (1988) 2674.
15. R. J. Goldston, *et al.*, *Journal of Computational Physics* 43 (1981) 61.

# Cyclotron Radiation Transfer in Plasmas with Strong Magnetic Field : Effects of Quasi-Linear Diffusion

A.B.Kukushkin

I.V.Kurchatov Institute of Atomic Energy  
123182 Moscow, USSR

## Abstract

An effect of the deviation of the electron plasma from Maxwellian velocity distribution due to quasi-linear diffusion produced by the transfer of intense cyclotron radiation is investigated. Its role for the local energy balance and total cyclotron radiation losses of an inhomogeneous plasma in a system with strong magnetic field and highly reflecting walls is estimated.

## 1. Introduction

The increasing interest to advanced thermonuclear fuel D-He<sup>3</sup> (see, e.g., [1]) makes reasonable a more detailed analysis of electron cyclotron radiation (ECR) losses because of their significant role for both total and local energy balance of plasma. Contrary to D-T reactor where spontaneous emission of the ECR is of importance as a diagnostic tool only, and apart of the problems of auxillary heating and current drive by locally injected intense ECR waves, spontaneous ECR in a hot D-He<sup>3</sup> plasma confined by a strong magnetic field is likely to make a dominant contribution to the total energy balance. Thus, the estimates [1] show that in order to make a reliable prediction for D-He<sup>3</sup> reactor prospects we ought to know ECR losses to an accuracy not worse than ~ 10%. Therefore it is worthwhile not only to improve existing numerical methods of calculating within (conventional to D-T reactor) schemes but to analyze a new factor, not ever considered, as well. The present paper deals with a qualitative analysis of the effect of quasi-linear (QL) diffusion, produced by the transfer of intense ECR, on the value of ECR losses in a system with strong magnetic field. Such an approach requires self-consistent treatment of radiative transfer and electron QL diffusion. (It should be noted that corresponding treatments of the problems of auxillary heating and current drive by ECR waves face the necessity of radiative transfer calculation only in allowing for the absorption of injected ECR wave moving along its ray).

Detailed description of the total ECR losses of maxwellian electron plasmas has been developed for the first time by Trubnikov in [2,3] (homogeneous slab) and modified in [4] (homogeneous plasma, scaling laws allowing for inhomogeneous toroidal magnetic field and reflecting walls). Further treatments within the same framework are fully reflected in survey [5] (for the results allowing for the inhomogeneity of electron density and temperature see [6]). However, the descriptions of spatial profile of ECR losses available in literature are achieved as a rule through ad hoc procedure of a proper reduction of the total

losses that leads, in particular, to incorrect results for energy balance in peripheral plasma even in sign. Consistent treatment of spatial profiles of ECR energy balance, which includes separate calculation of local emission and absorption, has been achieved by Tamor both numerically (see [7-9]) (by Monte-Carlo technique) and "semi-analytically" [10] (with good accuracy, by a simple fast routine for computation), in the latter version, under justifiable assumptions indicated below (Sec.3).

In present paper we derive a general result for the effect of QL diffusion in radiative transfer of intense waves in plasmas on the local energy balance (Sec.2) and discuss the influence of QL-effects on the ECR transfer in an inhomogeneous plasma in a system with strong magnetic field and highly reflecting walls (Sec.3).

## 2. Effect of QL diffusion in radiative transfer by intense waves

Space-time evolution of radiation intensity  $J(\phi, \vec{r}, t)$ , differential with respect to electromagnetic wave (photon) parameters  $\phi$ ,  
 $\phi = \{ \omega, \vec{n}, \zeta \}$

where  $\omega$  and  $\vec{n} = \vec{k}/k$  are the wave (i.e., photon or plasmon) frequency and direction of propagation, respectively,  $k$  is the wave vector, parameter  $\zeta$  describes polarization state of the wave, is determined by the equation of the well-known form (see, e.g., [11]):

$$\left( \frac{1}{v_g} \frac{\partial}{\partial t} + \vec{n} \frac{\partial}{\partial r} \right) \left\{ \frac{J(\phi, \vec{r}, t)}{N_r^2} \right\} = -\kappa(\phi, \vec{r}, t) \left\{ \frac{J(\phi, \vec{r}, t)}{N_r^2} \right\} + Q, \quad (1)$$

where  $\kappa$  is absorption coefficient (probability of absorption per path's unit length),  $Q(\phi, \vec{r}, t)$  is the distribution of energy, spontaneously emitted per unit volume and per unit time, in wave parameters  $\phi$  (i.e., the corresponding source function),  $N_r$  is ray refractive index,  $v_g$  is group velocity. Equation (1) should be solved with account of boundary conditions for the intensity including possible reflection of waves.

Equation (1) has solution in the form of the integral over ray path. In case of multiple reflection at the media boundary (e.g., tokamak wall) the path's total length may be formally infinite, therefore integration should be carried out by successive account of closest parts of the path. Alternatively, the process described by eq.(1) can be simulated by Monte-Carlo modeling of photon (plasmon) history.

In the medium with dispersion (plasmas) the dispersion relation connecting the frequency  $\omega$  and wave vector  $k$  must be added to equation (1). For this reason the substitution of the dependence  $k=k(\omega, \zeta)$  from the dispersion relation  $\epsilon(\omega, k, \zeta)=0$  is implied, where  $\epsilon$  is the dielectric permittivity.

In case of radiative transfer by emission and absorption of electromagnetic waves by plasma electrons, the quantities  $Q$  and  $\kappa$  are expressed in terms of the electron distribution function (EDF)  $f(\vec{r}, \vec{p}, t)$ . Thus,

$$Q(\phi, \vec{r}, t) = \int q_1(\vec{r}, \vec{p}, \phi, t) f(\vec{r}, \vec{p}, t) d\vec{p} \quad (2)$$

where the function  $q$  is the corresponding emission rate by an



individual electron. Absorption coefficient, which allows for "true" absorption and stimulated emission, can be expressed generally in the form

$$\kappa(\phi, \vec{r}, t) = \int \kappa_1(\vec{r}, \vec{p}, \phi, t) f(\vec{r}, \vec{p}, t) d\vec{p} \quad (3)$$

where the quantity  $\kappa$  can be reduced in long-wave limit to a differential, in momentum  $p$ , operator.

In case when source function  $Q(\phi, \vec{r}, t)$  doesn't depend (of course, implicitly, via corresponding distortions of the EDF) on the intensity  $J(\phi, \vec{r}, t)$ , direct solving of equation (1) practically exhausts the problem of radiative transfer. It is this framework within which the problem of radiative transfer has been considered in [2-11].

The evolution of the EDF,  $f(\vec{r}, \vec{p}, t)$ , can be described by the Fokker-Planck equation which allows for distant Coulomb collisions (operator  $C$  in the non-relativistic, Landau, or fully relativistic, Belyaev-Budker, form, see [12]), spontaneous emission of waves (term  $E_j$ ) and their absorption (term  $A_j$  which allows for QL diffusion). In long-wave limit, emission and absorption terms can be expressed in a divergence form. Thus, equation for the EDF has the form

$$\frac{d}{dt} f(\vec{p}, \vec{r}, t) = \frac{\partial}{\partial p_j} [E_j f - A_j f] + \hat{C}[f] \quad (4)$$

where

$$\frac{d}{dt} = \left( \frac{\partial}{\partial t} + \vec{v} \frac{\partial}{\partial \vec{r}} + \vec{F} \frac{\partial}{\partial \vec{p}} \right), \quad (5)$$

$\vec{F}$  is external force (e.g., macroscopic magnetic field and electrostatic potential).

In what follows we restrict ourselves to the case when the interaction of plasma electrons with electromagnetic waves distorts only the derivatives of the EDF (i.e., absorption processes,  $\kappa$  and  $A$ ) at rather high electron energies whereas the EDF as itself (and, consequently, emission processes) approximately conserve their equilibrium (Maxwellian) form,  $f=f_0(p)$ . In this case the Coulomb collision term transforms to

$$\hat{C}[f] = - \frac{\partial}{\partial p_j} [A_j^c (f - f_0)] \quad (6)$$

where operator  $A_j^c$  describes absorption of plasma electric microfield by an individual electron in distant collisions (treated either as purely Coulomb or with appropriate account of a screening due to dynamical polarization as in Balescu-Lenard collision term).

According to general laws of conservation there should be interrelation between operators  $\kappa$  and  $A$  and between quantities  $q$  and  $E$ , namely:

$$\int d\phi \left\{ \frac{J(\phi, \vec{r}, t)}{N^2} \right\} \kappa_1(\vec{r}, \vec{p}, \phi, t) = v_j \hat{A}_j = \hat{Q}_{abs} \quad (7)$$

$$\int d\phi q_1(\vec{r}, \vec{p}, \phi, t) = v_j E_j = Q_{em} \quad (8)$$

$$d\phi = d\omega d\Omega_n \sum_{\zeta} \quad (9)$$

where operators  $Q_{abs}$  (and  $Q_{em}$ ) gives the values of energy

absorbed (and emitted) by an individual electron of momentum  $\vec{p}$ .

We also assume that Coulomb (electron-ion) collisions assure isotropic, in pitch-angles, form of the EDF, thus depending on electron energy  $\varepsilon$  only,  $f = f(\varepsilon)$  (this is true to a large extent even for auxiliary heating by ECR waves). Isotropic form may be additionally maintained by isotropic form of radiation intensity  $J$  (cf. Sec.3). In this case we have

$$\dot{Q}_{abs} = \int d\phi \left\{ \frac{J(\phi, \vec{r}, t)}{N^2} \right\} \sigma_{abs}(\vec{r}, \vec{p}, \phi) n\omega \frac{\partial f}{\partial \varepsilon} \quad (10)$$

where  $\sigma_{abs}(\vec{r}, \vec{p}, \phi)$  is the cross-section of absorption of the wave quantum of parameter  $\phi$  (and, in particular, of energy  $n\omega$ ).

In case of magnetized plasmas the action of the term with Lorentz force in left side of eq.(4) is incorporated into the quantity  $\sigma_{abs}$  (it therefore appears to be the cross-section of absorption by an elementary Larmor circle), so that operator  $\partial/\partial \vec{p}$  in eq.(4) and, consequently, eqs.(7) and (8) should be properly modified. However, for the case of isotropic EDF implications of this modification can be sometimes unnoticeable, e.g., the quantities

$$s(\omega - \vec{k}\vec{v}) \vec{k} \partial f / \partial \vec{p} \quad \text{and} \quad k_{||} \partial f / \partial p_{||} + [(\omega - k_{||} v_{||}) / v_{||}] \partial f / \partial p_{\perp}$$

are both reduced to  $\omega \partial f / \partial \varepsilon$ .

Neglecting effects of inhomogeneity described by operator  $\vec{v} \partial / \partial \vec{r}$  and solving eq.(4) in stationary case, we arrive at the result

$$\frac{\partial f}{\partial \varepsilon} = \left( \frac{\partial f}{\partial \varepsilon} \right)_0 \left[ 1 + Q_{em} / Q_{abs}^c \right] \left[ 1 + Q_{abs} / Q_{abs}^c \right]^{-1} \quad (11)$$

where all the quantities  $Q$  are eigenvalues of corresponding operators for equilibrium EDF, and operator  $Q_{abs}^c$  is defined in terms of operator  $A_j^c$  similarly to the definition of  $Q_{abs}$ .

Substituting eq.(11) into eq.(10) and assuming the smallness of deviation from equilibrium, we obtain that in case considered, the effect of QL diffusion leads to a simple modification of absorption coefficient which allows for a finite ratio  $R$  of the rate of energy loss (income) by an electron due to its interaction with waves to the rate of permanent energy exchange of an electron with plasma due to Coulomb collisions (i.e., to the rate of relaxation of the EDF to equilibrium):

$$\kappa_1 f(\vec{r}, \vec{p}, \phi, t) = [\kappa_1 f_0] / [1 + R(\vec{r}, \vec{p})] \quad (12)$$

$$R(\vec{r}, \vec{p}) = (Q_{abs} - Q_{em}) / Q_{abs}^c \quad (13)$$

And finally the total rate of energy gain per unit volume takes the form ( $N_r \approx 1$ ):

$$Q^\Sigma(\vec{r}) = \frac{d\varepsilon}{dVdt} = \int \left[ \frac{J(\phi, \vec{r}) \kappa_1(\vec{r}, \vec{p}, \phi) f_0}{1 + R(\vec{r}, \vec{p})} - q_1(\vec{r}, \vec{p}, \phi) f_0 \right] d\vec{p} d\phi \quad (14)$$

where numerator in eq.(13) is equal to

$$(Q_{abs} - Q_{em}) = \int \left[ J(\phi', \vec{r}) \kappa_1(\vec{r}, \vec{p}, \phi') f_0 - q_1(\vec{r}, \vec{p}, \phi') f_0 \right] d\phi' / f_0 \quad (15)$$

It should be noted that within the framework of our assumptions, the QL-effects influence total radiation rate  $Q$ ,

eq.(14), explicitly by changing effective absorption coefficient and implicitly by changing intensity  $J$  which should be found by solving eq.(1) with modified absorption coefficient.

The quantity  $Q_{abs}^C$  for electron velocities  $v \gg v_T$  ( $v_T$  is thermal velocity) can be estimated as ( $L$  is Coulomb logarithm)

$$Q_{abs}^C \sim 2\pi n_e e^4 L / m_e v \sim \left( \frac{n_e}{10^{15} \text{ cm}^{-3}} \right) \left( \frac{10^9 \text{ cm/s}}{v} \right) L \cdot 4 \cdot 10^{-11} \text{ W} \quad (16)$$

An analysis of eq.(14) shows that the effective value of the quantity  $R$  has the following estimate :

$$[R(\vec{r}, \vec{p})]_{eff} = (Q^\Sigma)_0 / [Q_{abs}^C (\delta N/N)]_{v=v_{eff}} \quad (17)$$

where  $v_{eff}$  is effective value of velocity which contributes dominantly to total rate in equilibrium case (integral (14) for  $R=1$ );  $\delta N/N$  denotes the relative number of electrons which are lying in this domain in momentum space;  $(Q^\Sigma)_0$  is the local value of power income per unit volume computed for the case of equilibrium EDF.

### 3. Effects of QL diffusion in transfer of cyclotron radiation in magnetically confined plasmas

For the case of the transfer of cyclotron radiation in magnetically confined plasmas we can estimate the role of QL diffusion effects with the help of a proper modification of Tamor's approach [10]. This approach is based on two assumptions: a) radiation field is isotropic and b) most of energy is carried by frequencies for which plasma is optically thin although it become s thick due it multiple reflection from the walls.

An analysis of QL diffusion effect on the local energy balance (14), carried out within the framework of Tamor's approach [10], shows that the deviation of total (integral over plasma volume) losses of plasma appears to be determined by the value of local distortion of the absorption in peripheral plasma. This plasma, together with reflecting walls, plays the role of an effective attenuator of the radiation emitted by hot central plasma. In particular, for the case of dense plasma (e.g.,  $n_e \geq 10^{14}$ , for  $B \sim 5T$ ,  $T_e^0 \sim 50 \text{ keV}$ ,  $(1-R) \sim 0.01$ ) peripheral plasma has positive energy balance (i.e., absorbs more energy than emits). Since a) effective spectral width of energy loss rate appears to be smaller than one for the intensity itself and b) electron-wave interaction has resonance character, the value of  $R_{eff}$  may not be negligible. In this case one has a rise of the profile of energy losses that results in the increase of total radiation losses.

The estimates of  $R_{eff}$  show that for sets of parameters which are of interest for future D-He<sup>3</sup> based thermonuclear reactor, there can be fulfilled conditions for which one should take into account the effect of QL diffusion in radiative transfer of intense waves in plasmas.

It should be noted that the results of Sec.2 are also applicable to the description of QL-effects in case of energy transfer by longitudinal waves (i.e., by plasmons). This type of transfer was considered in [13]. It was shown that even for

maxwellian plasmas there exist a possibility of substantial acceleration of heat transport due to non-local correlation of plasma temperature and, correspondingly, non-diffusional law of heat propagation ( $r(t) \propto t^\nu$ , where  $\nu > 1/2$  contrary to  $\nu = 1/2$  in case of diffusion). For instance, heat transfer by Bernstein waves across a strong homogeneous magnetic field (here  $\nu > 1$ ) can compete with corresponding conventional collisional thermoconductivity (see [13]). It can be shown that the QL-effects may appreciably increase the role of thermoconductivity by plasma waves so that this mechanism may be considered as one of possible mechanisms of anomalous electron thermoconductivity.

Thus we arrive at the conclusion that in case of strong magnetic field the energy balance studies require description of global heat transport (by transverse and longitudinal waves) within the framework of kinetic description of plasma electrons. The corresponding numerical simulations should investigate following physical effects: "enlightment" of medium due to saturation of absorption process and non-diffusional law of heat propagation.

### References

1. Proc. of Workshop on the D-He<sup>3</sup> Based Low-Radioactivity Thermonuclear Fusion, Moscow, Kurchatov IAE, April 1991, (Ed. I.N.Golovin) (in Russian).
2. Trubnikov B.A., in Plasma Physics and the Problems of Thermonuclear Reactions, Ed. Leontovich M.A., Vol.3, Pergamon Press, London (1959) 122.
3. Trubnikov B.A., Bazhanova A.E., Ibid., p.141.
4. Trubnikov B.A. in Reviews of Plasma Physics, Ed. Leontovich M.A., Vol.7 (Consultants Bureau, New-York, 1979) 345.
5. Bornatici M., Cano R., De Barbieri O., Engelmann F., Nucl.Fusion, 23(9) (1983) 1153.
6. Atzeni S., Vlad G., Proc. 4th Int. Workshop on ECI, Roma, March 1984, p.35.
7. Tamor S., Studies of Emission and Transport of Synchrotron Radiation in Tokamaks, Science Applications Inc., La Jolla, Report LAPS-72, SAI- 023-81-110 LJ (March 1981).
8. Tamor S., Nucl.Fusion, 18(2) (1978) 229.
9. Tamor S., Nucl.Instr. and Meth.Phys.Res., A271 (1988) 37.
10. Tamor S., Simple Fast Routine for Computation Energy Transport by Synchrotron Radiation in Tokamaks and Similar Geometries, Science Applications Inc., La Jolla, Report LAPS-72, SAI- 023-81-189 LJ (May 1981).
11. Bekefi G., Radiation Processes in Plasmas, John Wiley and Sons, Inc., New-York (1966).
12. Lifshitz E.M. and Pitaevskii L.P., Physical Kinetics, Vol.10 of Theor. Phys. Course, Pergamon Press, L., 1981.
13. Kukushkin A.B., Lisitsa V.S., Savel'ev Yu.A., JETP Lett., 46 (1987) 448.

**Paper 1D4**

**ECR Electron Heating in an Open Trap with  
Creation of High Anisotropic Electron  
Population**

**V.V. Kostenko**

**(paper not submitted)**

## FRC Stability and Transport Physics

Loren C. Steinhauer  
STI Optronics  
Bellevue, WA 98004, USA

### I. Introduction

As early as the late 1950's, theta pinches operated with a reversed-bias magnetic field, produced field-reversed configuration (FRC) like entities. These plasmas survived only for times comparable to the end-flow time as in normal theta pinches. FRCs were first taken seriously as a magnetic confinement concept in the late 1970's. This came about because of favorable results from experimental programs begun in the Soviet Union (1971) and the US (1976), and reported some time later.<sup>1,2</sup> In these experiments the rapid internal flux annihilation and tearing instabilities characterizing the early theta-pinch experiments were overcome by improved purity, avoidance of "overcompression" by the magnetic field, care with magnetic field uniformity and a variety techniques to control the formation process. Control of the only obvious disruptive instability, the rotational mode, was demonstrated in Japan in 1982.<sup>3</sup> This advance led to FRC lifetimes limited only by the resistive decay of the magnetic configuration.

Since that time, the research has focussed largely on the lingering question of an FRC's vulnerability to an ideal MHD mode, the internal tilt, which has the potential to disrupt the magnetic configuration. The non-observance of this mode was ascribed to 1) the difficulty of making a non-intrusive measurement of an internal mode, and 2) operation only in conditions where ion kinetic effects stabilize the tilt. These factors led to the decision in the US to construct the "Large-s Experiment" (LSX) at STI Optronics, the principal purpose of which was to explore the limits of kinetic stabilization. The "s" parameter measures the number of local ion gyroradii across the minor radius of the FRC. Increasing s should produce a transition from kinetically-dominated to MHD-like behavior. A secondary purpose of LSX was to determine the confinement behavior of more MHD-like FRCs. LSX began operations in late 1990.

This paper describes recent advances in understanding FRC equilibrium (Sec. II), the tilt instability (Sec. III), and FRC confinement (Sec. IV). Included in these discussions will be preliminary reference to results from the LSX experiment.

### II. Equilibrium

Typical FRC equilibria have a somewhat elongated separatrix, and thus lend themselves to simple descriptions such as 1) radial force balance,  $p + B^2/2\mu = B_e^2/2\mu$  (p and B are the local pressure and magnetic field;  $B_e$  is the external magnetic field), and 2) the average- $\beta$  condition<sup>2</sup>  $\langle\beta\rangle = 1 - x_s^2/2$  [ $\langle\beta\rangle$  is the average  $\beta$  (based on  $B_e$ ) over the

midplane inside the separatrix;  $x_s \equiv r_s/r_c$  where  $r_s$  and  $r_c$  are the separatrix and coil radii]. The internal flux line structure may be either "elliptical" or "race-track" shape depending on the shape of the separatrix. A new class of analytic FRC equilibria have been found which are consistent in an approximate sense with the external (vacuum) magnetic field structure produced by a straight coil.<sup>4</sup> For separatrix elongations,  $E > 2$  these equilibria have race-track like internal flux lines;  $E \approx 3 - 10$  is typical of FRC experiments.

Another feature of FRC equilibria recently discovered is related to the internal current density structure. A current profile parameter can be defined as follows

$$h \equiv (j_\theta/r)_{O\text{-point}} / \langle j_\theta/r \rangle. \quad (1)$$

Examples of equilibria with "flat" current profile ( $h=1$ ) are the familiar Hill's vortex and the analytic equilibrium described earlier.<sup>4</sup> "Peaked" and "hollow" current profiles correspond to  $h > 1$  and  $h < 1$ , respectively. A recent study found that experimental FRCs consistently exhibit a hollow current profile,<sup>5</sup> as shown in Fig. 1. Here  $h$  was inferred in two ways: 1) measurement of the density profile using multichord interferometry (closed symbols); and 2) global transport modelling which matches observed particle and flux loss times (open symbols). The behavior shown in Fig. 1 exhibits a kind of "profile consistency." This has tentatively been ascribed to the interplay between local instabilities (perhaps ballooning) and normal diffusive transport.

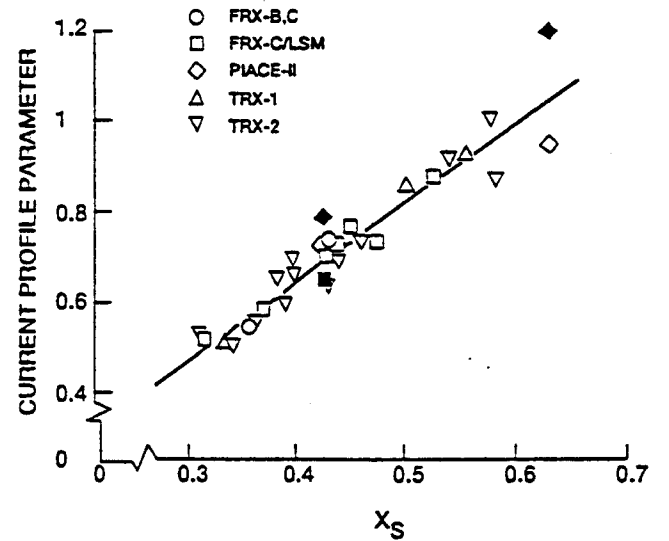


Fig. 1 Current profile parameter inferred for several experiments

### III. Tilt Stability

The most comprehensive theory thus far applied to describe kinetic effects on the tilt mode is the Vlasov-fluid (VF) model, which assumes fully kinetic, collisionless ions and a cold electron fluid. This study reported that the growth rate was substantially reduced when  $s$  is comparable to unity.<sup>6</sup> Because the scale of the associated computation is so massive, the study employed a trial function approach based on the eigenfunction found by an ideal MHD computation. More recent VF model treatments have addressed the variational problem using a limited basis set; these results have not yet been reported.

In view of the cumbersomeness of VF computations, an alternative approach was developed based on the gyroviscous model,<sup>7</sup> which is a fluid-based representation of transverse kinetic effects. This model avoids the inherent singularity, at the O-point, of the standard "finite larmor radius" expansion approach. Transverse kinetics is only one of several effects described by the more comprehensive VF model, which also includes parallel kinetics, resonant particle effects, and the Hall effect. Thus the gyroviscous model, in effect, isolates the effect of transverse kinetics. The principal result of this study was the verification of a scaling for the regime of gyro-stable tilt:

$$S^* < \text{Const } E, \quad (2)$$

where  $S^* \equiv r_s/(c/\omega_{pi})$  ( $r_s$  is the separatrix radius,  $c/\omega_{pi}$  is the collisionless skin depth), and  $E$  is the separatrix elongation.

A more recent study of gyroviscous stability employed realistic equilibria<sup>8</sup> indicated that the proportionality constant in eq. 2 is  $C \approx 3.5$ . It was also verified that gyroviscous theory compares well with the more comprehensive VF model: Including simple modifications reflecting the Hall effect and parallel kinetics, the gyroviscous model is within 30 percent of predictions by the VF model.

The gyroviscous result is compared with experimental examples of long-lived FRCs in Fig. 2. The solid line is the predicted marginal stability boundary for a gyrofluid plasma. The dashed line also includes the estimated effects of parallel kinetics and the Hall effect.. Essentially all of the examples fall within the predicted stable regime.

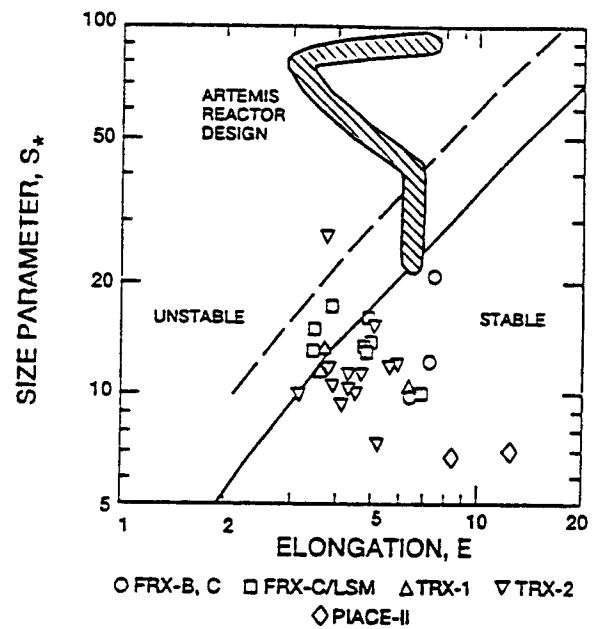


Fig. 2 Comparison of gyro-stability theory with long-lived FRC experiments

The only exception in Fig. 2 are for operation on a modified version of the TRX-2 facility.<sup>9</sup> Not shown are recent results from LSX where long-lived plasmas fall along or slightly above the dashed line and have elongations in the range of 4 to 10. Also shown in Fig. 2 are conditions, from formation to ignition, in the ARTEMIS reactor design.<sup>10</sup>

The first detailed measurements of the tilt mode were performed on the FRX-C/LSM device using a Mirnov probe array on the outer surface of the vacuum chamber.<sup>11</sup> The signals were Fourier analyzed to isolate the tilt component. This technique is in fact an indirect measurement of the tilt since the primary disturbance is believed to be inside the separatrix. Nevertheless, 3D-MHD simulations showed that weak though measurable



signals can be expected near the wall. These observations are consistent with theoretical predictions in several respects: 1) observed signal growth rates compare well with MHD predictions; 2) the spatial structure of the observed signals resemble that in 3D-MHD simulations; 3) degraded confinement was consistently observed for tilt signals above a certain level; and 4) FRCs where *stable* disturbances were observed consistently fell within the stable regime shown in Fig. 2. Experiment and theory, however, differed in several important respects: 1) the peak amplitudes of observed tilt signals are 3-5 times smaller than predicted by nonlinear MHD simulations; and 2) although tilt simulations led, without exception, to total disruption of the configuration, long-lived, FRC-like entities were generally observed to survive the instability event. Moreover, in recent LSX examples, tilt disturbances generated during the formation phase were observed to decay; according to gyroviscous theory these examples lie within the unstable regime.

A tentative explanation for the cited discrepancies is as follows. The instability event may actually be a multi-mode phenomenon involving a number of modes with higher azimuthal mode number ( $n > 1$ ) in addition to the tilt ( $n = 1$ ). (Indeed higher- $n$  modes were generally observed to have amplitudes comparable to that of the tilt.) The instability event may simply rearrange the FRC into a stable configuration rather than cause its disruption. In the course of producing a stable equilibrium (with, perhaps, hollow current profile), The restructuring would dissipate some of the internal flux. If stable FRCs must have hollow profiles, this would partly explain why FRC formation in larger devices is more difficult for larger devices: the formation process in a theta pinch tends to produce a more peaked (higher  $h$ ) current profile in a larger device. This trend can be overcome to some extent by improved controls on the formation process.

#### IV. Confinement

Profile consistency has profound consequences on the confinement since the internal structure is controlled (presumably) by an instability rather than transport in the usual sense. It determines, e.g. the ratio of the density at the separatrix to the average density. Of course, transport still plays an important role; since it governs how fast particles are depleted near the edge (by diffusion across the separatrix) it therefore sets the rate of the restructuring process. Attention is limited here to particle confinement, although the internal flux and energy confinement will be similarly influenced by the restructuring.

Particle confinement in a "profile consistent" FRC is calculated as follows. The decay rate of the particle inventory,  $\langle n \rangle \pi r_s^2 l_s / \tau_N$ , is balanced by the flow across the separatrix,  $2\pi r_s l_s n_s v_{ds}$ , where  $n_s$  and  $v_{ds}$  are the density and diffusion velocity at the edge. Thus

$$\tau_N = (\langle n \rangle / n_s) r_s / 2v_{ds} . \quad (3)$$

The edge layer flow is found by solving the quasisteady continuity equation (slab model):

$$d(nv_d)/dr = n/\tau_{||} ; \quad (4)$$

here, the endloss in the edge layer is represented as a particle sink with timescale  $\tau_{\parallel}$ . Once the transport mechanism is identified, solving eq. (4) is straightforward. Suppose, as is common for drift instabilities, the diffusion rate is proportional to the square of the drift parameter,  $D = D_0(\rho_i/L_n)^2$ , where  $\rho_i$  is the ion gyroradius and  $L_n$  is the local density gradient scale length. Then the particle confinement time is

$$\tau_N = (\langle n \rangle / n_s) (r_s / \rho_i)^{1/2} (r_s^2 / D_0)^{1/4} \tau_{\parallel}^{3/4}. \quad (5)$$

The particle confinement is then a hybrid of the internal, diffusive time scale, represented by  $r_s^2/D_0$ , and the axial confinement time in the edge layer,  $\tau_{\parallel}$ . Comparison of this prediction with experiment awaits the application of the transport rate caused by the acting turbulence mechanism, e.g. low-frequency drift modes.<sup>12</sup> Equation 5 emphasizes the important role played by axial confinement in the edge layer. Indeed in a reactor plasma it will likely be necessary to enhance edge layer confinement by applying mirrors: this would significantly increase  $\tau_{\parallel}$ , especially for high-temperature plasmas.

In conclusion, recent experimental and theoretical FRC studies show the following: 1) FRC equilibria exhibit "profile consistency" with typically hollow current profile; 2) the tilt stability of nearly all experiments can be explained by gyroviscous fluid theory; and 3) profile consistency has a profound influence on particle confinement and increases the importance of confinement in the edge layer. This defines clear objectives for future study: 1) what is the local instability mechanism responsible for the profile consistency; 2) can sufficiently hollow current profile lead to stabilization of the tilt and related higher-n modes; and 3) what is the transport rate for the dominant turbulence mechanism and its effect on confinement in a "profile-consistent" FRC.

## References

1. A.G. Es'kov, et al., in Plasma Physics and Controlled Nuclear Fusion Research (Proc. 7th Int. Conf, Innsbruck, 1978), Vol. 2, IAEA, Vienna (1979) 187.
2. W.T. Armstrong, et al., Phys. Fluids 24, 2068 (1981).
3. S. Ohi, et al, Phys. Rev. Lett. 51, 1042 (1983).
4. L.C. Steinhauer, Phys. Fluids B, 3081 (1990).
5. L.C. Steinhauer, and A. Ishida, "Profile Consistency in Equilibria of Field-Reversed Configurations", submitted to Phys. Fluids B (1991).
6. D.C. Barnes, et al., Phys. Fluids 29, 2616 (1986).
7. L.C. Steinhauer and A. Ishida, Phys. Fluids B, 2422 (1990).
8. A. Ishida, et al., "Tilt Stability of a Gyroviscous Field-Reversed Configuration with Realistic Equilibria", submitted to Phys. Fluids B (1991).
9. J.T. Slough and A.L. Hoffman, Nucl. Fusion 28, 1121 (1988).
10. H. Momota, et al., "Conceptual Design of D-<sup>3</sup>He FRC Reactor "ARTEMIS", accepted for publication in Fusion Technology (1992).
11. M. Tuszewski, Phys. Fluids B 3, 2856 (1991).
12. N.A. Krall, Phys. Fluids 30, 878 (1987); Phys. Fluids B 1, 1811 (1989).

## 15MeV PROTON DIRECT ENERGY CONVERSION

Hiromu Momota  
National Institute for Fusion Science, Nagoya 464-01, Japan

## 1. Physical Background

Since a large amount of fusion power is carried by charged particles in a D-<sup>3</sup>He burning FRC reactor, a use of highly efficient direct conversion of the energy into electricity is recommended to achieve an attractive fusion power plant. The application of direct energy converters in a plasma device is often a serious problem, since a fairly large area of ion collector plate might be required to decrease the input power density and to remove the heat reasonably. Fortunately an FRC plasma is surrounded by open lines of force and thus is suitable for the application of direct energy converters.

The fusion power carried by charged particles consists of 810MW of thermal ions and 368MW of 14.7MeV protons in the "ARTEMIS" design. In order to recover the energy carried by thermal ions, Venetian blind type direct energy converters<sup>1)</sup> (VBDEC) with 5-stage fin arrays with a higher conversion efficiency, the size, and the applied voltage of the ion collector. A pair of traveling-wave direct energy converters<sup>2)</sup> (TWDEC) are installed at both downstream ends of the VBDECs, for the purpose of converting the kinetic energy of 14.7MeV protons whose energy is much higher than an applicable electrostatic potential. After the proton beam is modulated at the modulator to form a bunched proton beam, bunched protons are trapped into a traveling electrostatic wave whose phase velocity is decreasing. The principle of this converter is a reciprocal of a Linac<sup>3)</sup>. A schematic drawing of components is given in Fig.1.

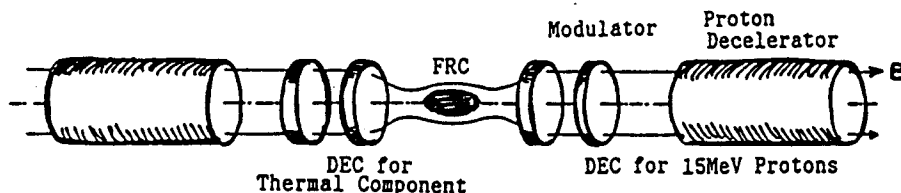


Fig.1 A schematic drawing of the components

The energy spectrum of energetic fusion protons spreads due to the Doppler effect of fuel particles by 0.9MeV around the mean value of 14.7MeV. The radius of the proton beams are expanded along the expanding lines of force to be 5m and the energy perpendicular to the lines of force is converted to the parallel one. The density of the beam protons is as low as  $2 \times 10^{10}/\text{m}^2$ .

Since the space potential produced by the protons in a typical length of 30m is 400kV which is much lower than the proton energy of 14.7MeV, the collective effects of charged protons are ignored and the motion of the protons can be described as a single particle.

## 2. Modulation of Proton Beam

At the modulator, an propagating electrostatic wave potential, whose phase velocity  $U$  is identical to the mean velocity of fusion protons, i.e.,  $5.3 \times 10^7$  m/s:

$$V(z,t) = V_m \left\{ \frac{(z-Ut)}{d} - 2 \left[ \frac{(z-Ut)}{2d} - 1 \right]^2 - \right. \\ \left. - V_m \left\{ \frac{Ut}{d} + 2 \left[ -\frac{Ut}{2d} + 1 \right]^2 \right\} \right.$$

is applied with a set of grids array at an interval  $z=(0,d)$ . The function  $[x]$  represents the maximum integer that is smaller than the value  $x$ . Let's a proton is  $z=0$  at the time  $t=t_0$  and whose velocity is  $v$ , then the velocity suffer a change by the applied electrostatic field by an amount:

$$\delta v = (2eV_m/M) * (t_0/d)$$

at downstream of the modulator. The position  $z(t)$  of the proton at time  $t$  is

$$z(t) = vt - \{1 - (Ut)/(vt_f)\} * vt_0$$

Here we have defined the time  $t_f = (MUd)/(2eV_m)$ . It should be noted that if all protons have a common velocity  $U$  then the value  $z(t_f) = Ut_f$  is independent of initial condition:  $z=0$  at  $t=t_0$  and protons are focused to the point  $z_f = d * (MU^2)/(2eV_m)$ . The applied potential and trajectories of protons whose velocity is  $U$  are illustrated in Fig.2.

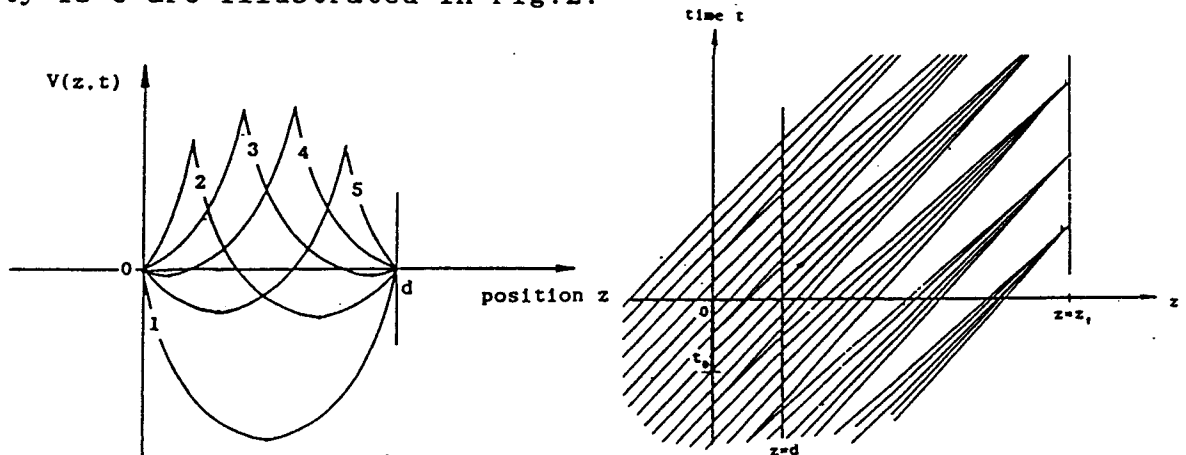


Fig.2 Applied Electrostatic potential and resultant change in trajectories of protons

As is explained previously, the velocity spectrum of fusion protons is spreading by  $\Delta v$  and it prevents proton beam from ideal focusing. The spread of focus point  $\Delta z$  is given by

$$\Delta v = (MU^2/2eV_m) \cdot d(\Delta v/U)$$

### 3. Deceleration of Bunched Beams

At the focus point, bunched beams are trapped into a traveling electrostatic wave  $V_d(z, t)$ , which is also produced with a set of grid array:

$$V_d(z, t) = V_d \sin \Psi(z, t)$$

$$\Psi(z, t) = \int_{z_f}^z k(\xi) d\xi - \omega t + \phi$$

Let's a proton is

$$z = z_f \quad \frac{dz}{dt} = U \quad \text{at} \quad t = t_f$$

the equation of motion:

$$M \frac{d^2 z}{dt^2}(t) = -ek(z)V_d \cos \Psi(z, t)$$

can be solved by introducing the condition:

$$\Psi(z=z_f, t=t_f) = -\omega t_f + \phi = \Psi_f$$

which states that the phase where the proton is trapped conserves its value during the process. The equation of motion is then:

$$\frac{d^2 z}{dt^2}(t) = -\frac{e}{M} k(z)V_d \cos \Psi_f$$

and solutions can be expressed in terms of  $z$ :

$$k(z) = \frac{\omega}{U} \left\{ 1 - \frac{3}{2} \varepsilon \frac{\omega(z-z_f)}{U} \right\}^{-1/3}$$

and

$$\frac{dz}{dt}(z) = U \left\{ 1 - \frac{3}{2} \varepsilon \frac{\omega(z-z_f)}{U} \right\}^{1/3}$$

where we have introduced the small quantity

$$\varepsilon = \frac{2eV_d}{MU^2} \cos \Psi_f$$

For a positive value of  $\cos \Psi_f$ , the wave number of the applied traveling wave increases and inversely the velocity of the proton decreases.

We will consider motion of a particle whose initial position suffers a perturbation:  $z=z_0+\xi$ . The equation of motion is then

$$\frac{d^2}{dt^2}(z+\xi) = -\frac{e}{M} k(z)V_d \cos(\Psi_f+k\xi)$$

or

$$d^2\xi/dt^2 = (e/M)kV_d \sin\Psi_f + k\xi$$

Thus a proton is decreasing if

$$\cos\Psi_f > 0$$

and

its trapping is auto-phasing if

$$\sin\Psi_f < 0$$

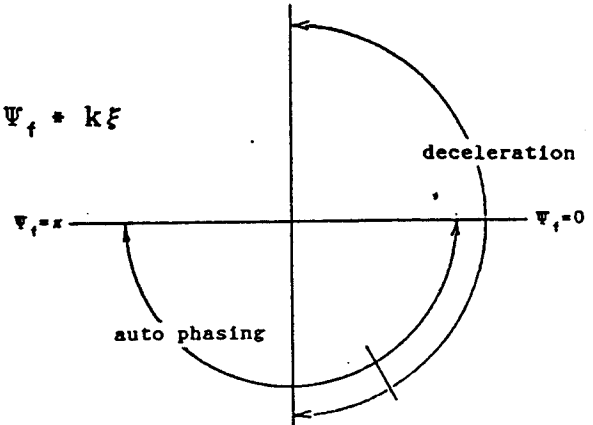


Fig.3 Condition for Decelerating and Auto-Phasing

In order to examine the above discussions, numerical calculations of particle trajectories have been carried out, obtaining the consistent results.

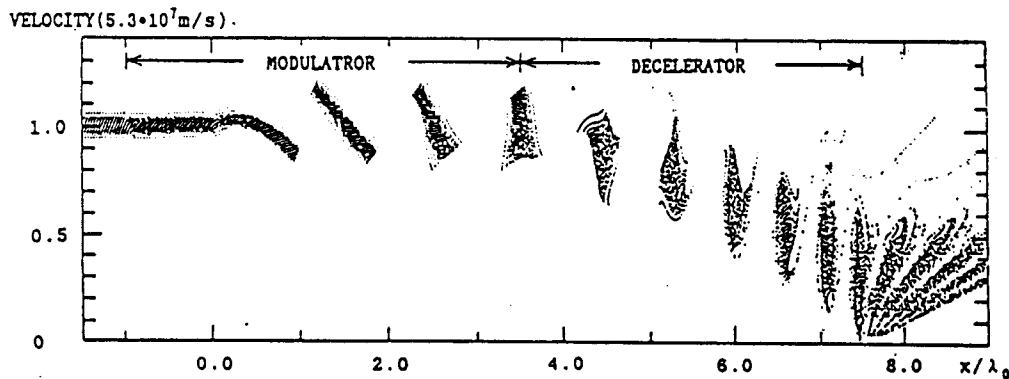


Fig.4 Phase space plots of fusion protons: Applied maximum voltage at the modulator and the decelerator is respectively 0.82MV and 0.42MV. 95% of protons are trapped and decelerated.

#### 4. Assembly of the traveling Wave Direct Energy Converter

The assembly of the traveling wave direct energy converter consists of 24 mesh grids, i.e., 5 for the modulator and 19 for the decelerator, and located as is shown in Fig.5. Each mesh grid is made of water cooled pipes of 17mm diameter and 1mm

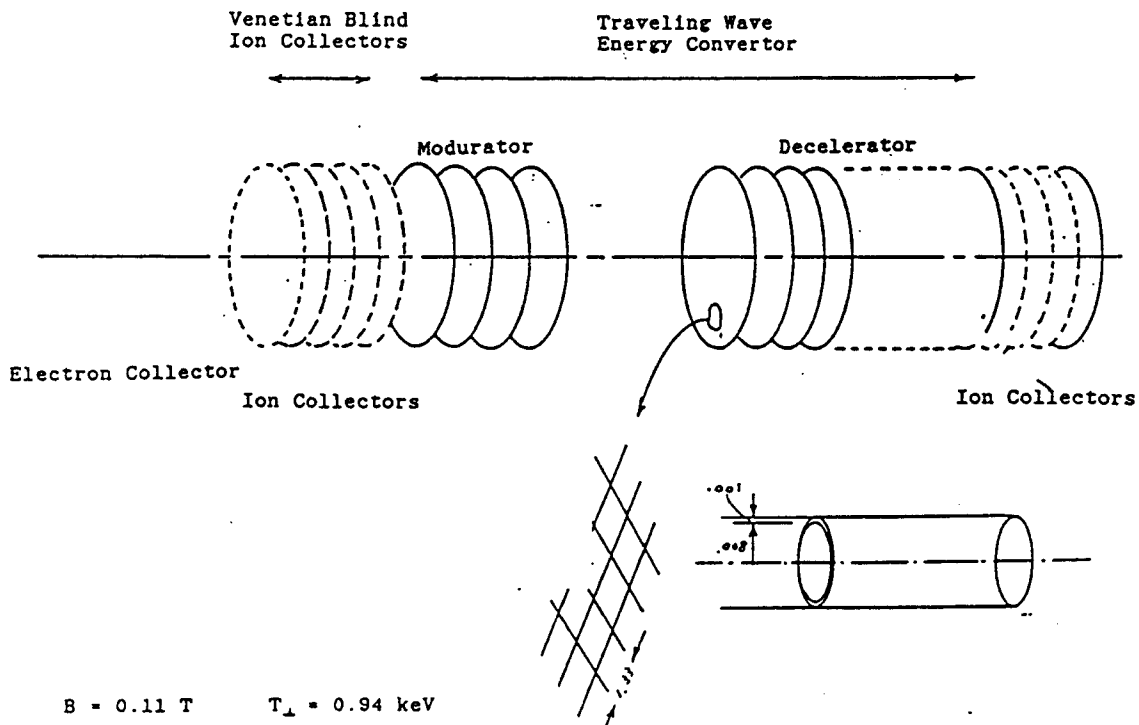


Fig.5 Assembly of a Traveling Wave Direct Energy Converter

thickness and arranged with a distance of 1.3m. A pressure difference of 5MPa is applied to cool the pipes and the stress due to pressurized water is 40MPa, which is much smaller than the allowable limit for this pipe. The total power needed to cool the grid is estimated as 140kW. The energy flow in the traveling wave direct energy converter of this structure is exhibited in Fig.16. The total flux of 14.7MeV protons is  $183\text{MW}$  or  $7.8 \cdot 10^{19}/\text{s}$  into a traveling wave direct energy converter. The total power flow in this converter is shown in Fig.6.  $2.81 \cdot 10^{19}$  protons/s among  $7.8 \cdot 10^{19}$  protons/s loose

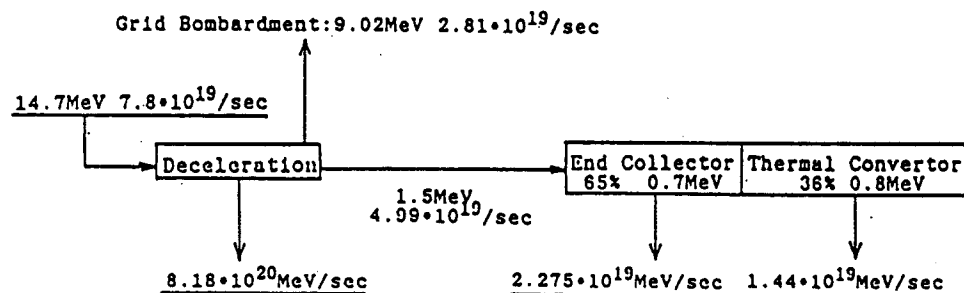


Fig.6 An Energy Flow Chart of the Traveling Wave Direct Energy Converter

their energy by the bombardment onto the grid structure and

power of 131MW is extracted with a set of mesh grids and a power of 12MW is carried to the end collectors where 5.9MW is collected as electricity. The overall efficiency obtained from this converter can be estimated as high as 75%.

At the decelerator, bunched protons convert their energy by inducing electrostatic potential into grids which are connected by a transmission line with load resistances which are adjusted so as the grid potential to be the value  $V_d$ .

Thus the total efficiency of TWDEC for fusion protons is approximately 75%.

#### [REFERENCES]

- 1) R.W.Moir and W.I.Barr; Nuclear Fusion vol.13 (1973) 35
- 2) H.Momota; LA-11808-C (Los Alamos, May 1990) 8
- 3) D.W.Fry, R.B.R.S.Harvie, L.B.Mullett, and W.Walkinshaw;  
Nature vol.160 (1947) 351



# Rectennas for Synchrotron Radiation Energy Conversion in D-<sup>3</sup>He Tokamaks

John F. Santarius

*University of Wisconsin, Madison, WI 53706*

## Abstract

*Rectennas, or rectifying antennas, provide the potential for highly efficient conversion of synchrotron radiation to electricity in a D-<sup>3</sup>He tokamak fusion reactor. This paper will give an overview of energy conversion using rectennas in a tokamak and describe the key issues for rectenna development and operation.*

## 1 Overview

Rectennas (rectifying antennas) were developed in the 1970's, partly in support of research on Solar Power Satellites. The present state of the art is that thin-film rectennas have been demonstrated at 2.45 GHz with 85% RF-to-DC conversion efficiency [1]. The circuit can be simple, consisting of an antenna, one or a few diodes, and a few resistors and capacitors. For space power transmission, the system of generator, transmitter, and receiver is large at 2.45 GHz, so an incentive exists for developing higher frequency systems. Much of the information in this paper results from

research programs at NASA Lewis Research Center and elsewhere aimed at such systems.

The concept of directly converting synchrotron radiation to electricity at an efficiency of approximately 80% using rectennas was originated by Grant Logan [2]. The idea is to channel synchrotron radiation out of the tokamak using overmoded waveguides and convert it in a separate chamber. In D-<sup>3</sup>He tokamak reactors, it may be possible to transform as much as 50% of the fusion power into synchrotron radiation. Although 2.45 GHz technology exists, the technology remains to be demonstrated at frequencies of interest for fusion—about three orders of magnitude higher. Nevertheless, the rectenna option appears feasible, as it requires integrated circuit technology well within the state of the art, and high frequency diodes are developing at a rapid pace. Rectenna costs are uncertain, but appear reasonable based on extrapolation from costs for large production runs of large-scale integrated circuits.

The remainder of this paper will discuss the critical questions for the use of rectenna energy conversion. These are:

- Can a large fraction of the fusion power be generated as synchrotron radiation with reasonable physics assumptions?
- Is rectenna conversion of synchrotron radiation compatible with synchrotron current drive?
- What will the synchrotron radiation spectrum be?
- Can synchrotron radiation be wave-guided from the plasma chamber to a conversion cavity with acceptable losses?
- What efficiency can rectennas achieve in the frequency range of interest?
- What will be the cost of a rectenna conversion system?

## 2 Plasma Power Balance and Current Drive Considerations

To use rectenna conversion most effectively in a power plant, a high fraction of the fusion power should be generated as synchrotron radiation. This places more stringent requirements on energy confinement, since the synchrotron radiation is an added energy loss channel. Because the total synchrotron power loss is proportional to  $(BT)^{2.5}$ , high synchrotron radiation fractions push parameters toward high magnetic fields and temperatures higher than optimum from a power density point of view. Also, it may be necessary, rather than simply desirable, in this conversion mode to enhance transport of the ash above that of the fuel ions to avoid choking of the fusion burn. Nevertheless, it appears to be a smaller physics step to go

to high synchrotron radiation fractions from minimum synchrotron radiation than it is to go from D-T to D-<sup>3</sup>He.

The spectrum of synchrotron radiation will be spread from  $\sim 1.5$ –30 THz, peaked at  $\sim 5$ –10 THz, based on calculations for ARIES-III [3, 4]. Reflections from the tokamak chamber walls will tend to depolarize the spectrum, and the calculations discussed below assume a random polarization. Assuming that the chamber walls are highly reflecting and that the waveguide is a total absorber, most of the synchrotron radiation produced will be lost out the waveguide, rather than absorbed in the first wall.

The question of whether synchrotron radiation conversion by rectennas is compatible with synchrotron current drive has been raised. The original synchrotron radiation current drive concept used a "scallop" first wall, with one side of the scallop highly reflective and the other very absorptive. The essential physics is to have differential momentum absorption. By properly recessing and angling the synchrotron waveguide in a D-<sup>3</sup>He tokamak, the same preferential absorption would occur. In either method, only the absorbed synchrotron radiation power would be a net loss to the plasma.

## 3 Design Issues

### 3.1 Waveguide Design

A highly overmoded, circular waveguide can be used for transporting the synchrotron radiation from the plasma core to a separate conversion chamber lined with rectennas [5]. The waveguide losses will be less than 5% of the total power entering the waveguide for a

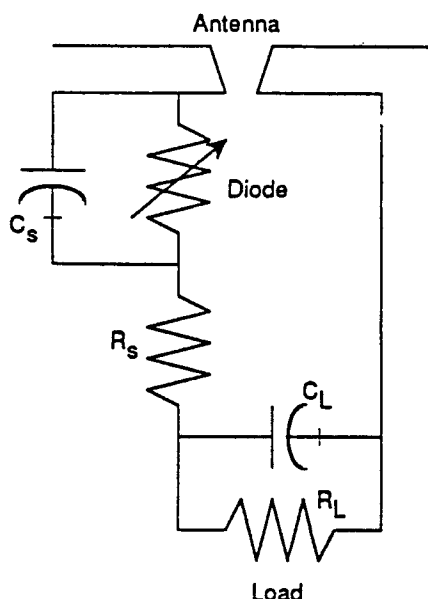


Figure 1: *One potential rectenna circuit [2].*

ratio of waveguide length to diameter of 30. Depending on shield design considerations, the waveguide diameter would be 10–20 cm for 3–6 m of length and then it would widen to reduce losses until the conversion cavity was reached. Because heat absorbed in the waveguide wall will probably be rejected, a design goal of 2–3% loss seems reasonable.

The waveguide would be evacuated to approximately the tokamak chamber pressure (and might even be the vacuum pumping port), so no microwave transmission window is required.

### 3.2 Rectenna Design

The state of the art in integrated circuit technology design is 100 times smaller than the approximately 0.1-mm range required for the synchrotron radiation conversion antennas. A possible circuit option is shown in Fig. 1 [2]. The key circuit component that is not presently available at the high frequencies of interest is the diode. However, the field of vacuum microelectronics (for field-

effect diodes) has been progressing rapidly in frequency. Monolithic microwave integrated circuits have been constructed which have achieved a cutoff frequency of 1.25 THz [6]. In the relevant time frame, the availability of suitable diodes appears likely.

The efficiency of full-wave rectifying circuits has been calculated to approach 100% with log-spiral antenna geometries that give a frequency range of 2–10 times the nominal resonant frequency [5]. If such geometries are compatible with the integrated circuit design, broad-band coverage of this amount would suffice to keep the number of differently tuned rectennas small. The cavity could then be covered with a variety of differently resonant rectennas, since the reflectance off of a non-resonant rectenna should also approach 100% efficiency.

Present thinking about rectenna design is that the basic geometry would be a dielectric slab with the antennas facing the synchrotron radiation, with coolant channels through the dielectric, and with the remaining circuit components on the opposite side of the slab, as shown in Fig. 2. Connecting the antennas to the other components appears to be feasible using stripline techniques. The key difficulty in designing circuits at the very high frequencies of interest is capacitive coupling. The design goal of 1 MW/m<sup>2</sup> heat dissipated appears to be feasible, although detailed thermal hydraulics calculations remain to be done.

Experimental programs exist in two regimes that bracket the range of interest for D-<sup>3</sup>He tokamak reactors [7]. Currently, these are all relatively small programs at modest funding levels.

Present rectenna costing is based on the assumption that the costs will be comparable

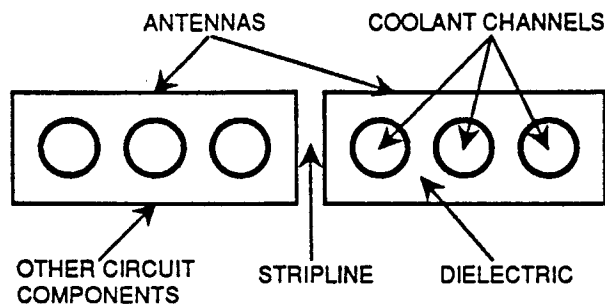


Figure 2: *One potential rectenna geometry.*

to large production runs of similarly sized integrated circuits. A preliminary estimate, based on Turner, et al. [8], is that \$0.375/We is reasonable.

## 4 Conclusions

Synchrotron radiation conversion by rectennas is intrinsically a  $D-^3\text{He}$  mode of operation because of the leverage gained by a high ratio of synchrotron radiation power to fusion power. The presumed benefits in power plant simplicity, reliability, and cost must be balanced against the more difficult physics requirements and the need to demonstrate rectenna technology at the high frequencies of interest. Because the extension of plasma parameters is less than that required to go from  $D-T$  to  $D-^3\text{He}$ , and because the technology extrapolation appears to be straightforward, rectenna conversion of synchrotron radiation is an attractive option for  $D-^3\text{He}$  tokamak reactors.

## Acknowledgement

This research was funded by the Grainger Foundation, the University of Wisconsin, and the U.S. Department of Energy.

## References

- [1] W.C. Brown, "Rectenna Technology Program: Ultra Light 2.45 GHz Rectenna and 20 GHz Rectenna," Report prepared for NASA Lewis Research Center under contract NAS3-22764 (1987).
- [2] B.G. Logan, "Economical  $D-^3\text{He}$  Fusion Using Direct Conversion of Microwave Synchrotron Radiation," Fusion Power Associates Annual Meeting, April 24, Washington, DC (1986).
- [3] W. Kernbichler, private communication (1989).
- [4] R.W. Conn, et al., "ARIES-III Final Report," to be published as a UCLA report (1992).
- [5] M.J. Schaffer, private communication (1989).
- [6] W-J. Ho, et al., "Monolithic Integration of HEMTs and Schottky Diodes for Millimeter Wave Circuits," IEEE GaAs IC Symposium, p. 301 (1988).
- [7] J.L. Christian, Jr. and R.J. Acosta, "Candidate Technologies for Beamed Space Power Application," NASA Lewis Report draft (1989).
- [8] E. Turner et al. "Application Specific MMIC: A Unique and Affordable Approach to MMIC Development," IEEE 1988 Microwave and Millimeter-Wave Monolithic Circuits Symposium (1988).

**Paper 2B1**

**The Problem of Low-Activation Materials**

**L.I. Ivanov**

**(paper not submitted)**

## VANADIUM ALLOYS AND THEIR PROPERTIES

Authors: I.P.DRUZHININA, A.V.YELUTIN,  
G.N.PERKOVA, N.A.ZENTSOVA,  
M.S.LALAYAN, A.G.ARAKELOV,  
A.F.GEKOV, L.P.ONISENKO,  
A.N.SOLOMAKHIN

## ALLOYS COMPOSITION

The Giredmet scientists developed vanadium-based alloys of two, three, four and five components. According to the functional application the developed vanadium alloys may be conventionally subdivided into two groups of structural and high-temperature alloys. The binary structural alloys contain following components in fractions expressed as percentage: nearest to 70% of Titanium, 1.5% of Zirconium, 60% of Niobium, 30% of Tantalum, 20 % of Chromium, 25% of Molibdenum, 20% of Tungsten and 2% of Rhenium. The group covers three-component alloys, as well of such systems as: Vanadium-Niobium-Titanium, Vanadium-Niobium-Zirconium, Vanadium- Chromium-Titanium.

The above alloys, but for those alloyed with Titanium, contain the following amount of impurities (interstitial im.) expressed as percentage (according to a mass): 0.01-0.03 Oxygen; 0.005-0.015 Nitrogen; 0.01- 0.03 Carbon; 0.001-0.002 Hydrogen.

Due to an excessive content of Oxygen in Titanium, Vanadium alloys, alloyed with Titanium contain nearest to 0.09% of Oxygen. The content of the rest controllable impurities (Silicon, Aluminium, Ferrum) does not exceed 1% in total.

The composition of three-, four-, five-component high-temperature alloys includes Titanium, Chromium, Molibdenum, Niobium, 1-3% of Zirconium and 0.1-0.4% of Carbon (2,3,4) as an alloying component.

The amount of interstitial and substitutional impurities in the above alloys is at a lower level.

## ASSORTMENT OF ALLOYS

The Vanadium alloys are released in the form of ingots having the diameter close to 160 mm, the weight of about 80 kg; blanks of the dimentions of 30 x 110 x 600mm, rods of the diameter of 5 - 80mm; sheets having dimentions 1 x 450 x 800 mm, strips of the thickness and width of 0.1 - 5 x 230 mm, of length of about 3 m; tubes with the diameter from 6.9 x 0.4 upto 130 x 1 mm; foil of the thickness of about 50 mcm.

Semifinished products are supplied in bulk after annealing. Production of semifinished may achieve dozens of tonnes a.a.

## PROPERTIES OF ALLOYS

Sheets with the thickness of 1 and 2 mm have been produced by the methods of high- and low-temperature plastic deformation from ingots for the subsequent study of mechanical properties in the range of temperatures with -196 to 1200°C for high-temperature resistance at 700-1100°C and weldability.

Before testing the sheet specimens have been subjected to annealing at the temperatures of 900-1300°C capable to obtain the size of grains of 20-30 mcm. The process of annealing has been conducted in vacuum of at least 10E-4 torr during 1 hour.

The specimens intended for testing in tension, impact viscosity and for the bending angle were in conformity with GOSTs 1497-84, 9454-78, 3728-78.

Mechanical properties of certain alloys among those developed determined at temperatures of testing -196, 20, 800°C are given in the Tables 1,(1,2).

Mechanical properties of annealed sheet specimens of Vanadium alloys at temperatures of tests: -196, 20, 800°C

Composition of alloy, expressed as percentage by fractions	Testing temperature, °C							
	-196			20			800	
	$\sigma_b$	$\delta_{10}$	$a_n$	$\sigma_b$	$\delta_{10}$	$a_n$	$\sigma_b$	$\delta_{10}$
V-(5-15)Ti	820-1010	21-18	1.0-0.9	520-560	23-24	1.8-1.2	350-390	22-17
V-8 Cr	650(*)	25	1.5(*)	500	27	2.0	260	25
V-8 Cr-15 Ti	-	-	0.5	660	26	0.8	400	24
V-8 Cr-1Zr-0.1C	750	26	0.4	450	22	1.2	190	30
V-8Cr-(5-15)Ti-1Zr-0.1C	1000-1240	27-16	0.6-0.5	580-790	26-23	1.1-0.9	230-330	39-40
V-1Zr	530	31	1.4	260	30	1.4	190	7
V-3Zr-0.2C	-	-	0.5	340	26	0.7	120	35
V-10Nb-1Zr-0.2C	930	20	0.7	600	20	1.1	380	20
V-10Mo-2.5Zr-0.3C	660(*)	21(*)	0.4(*)	560	20	0.6	170	40

$\sigma_b$  - MPa;  $\delta_{10}$  %;  $a_n$  - J/sq.m

(\*) Testing temperature -70°C

High strength, plasticity and impact viscosity are characteristics of those alloys at the above temperatures.

Weldability of those alloys was originally estimated by a tendency to formation of "Shrinkage cracks"(\*). If such a tendency was not available with the alloys, impact viscosity and bending angle of welded joints were determined.

Welding of annealed sheet material was conducted in the electron-beam plant.

The data of Table 2 prove the high values of weldability characteristics. Impact viscosity of welded joints (welds) may be increased 2-3 times by heat treatment.

Bending angle and impact viscosity  
of welded joints in specimens of  
vanadium alloys at the temperature of  
testing 200°C.

Composition of alloy expressed as percentage by fractions	Bending angle, in $\alpha$ degrees	Impact viscosity $a_n$ -MJ/m <sup>2</sup>
V-8Cr	180	1.8
V-8Cr-1Zr-0.1C	120	0.3
V-8Cr-15Ti-1Zr-0.1C	90	0.2
V-3Zr-0.2C	180	0.4
V-10Nb-1Zr-0.2C	160	0.3
V-10Mo-2.5Zr-0.3C	140	0.1

High-temperature resistance was determined with standard annealed sheet specimens having thickness of 1mm and total length of 110 mm at length of the working portion of 50mm.

The studies were conducted according to the method of programmable variable deformation rates of 0.12 - 6000%/hour-1 at temperatures of 700, 800, 900 and 1000°C.

The results of determination of creep resistance of two alloys at the temperature of 800-1000°C are given as an example on Fig.1,2.

The obtained results prove an appropriate high-temperature resistance of vanadium alloys.



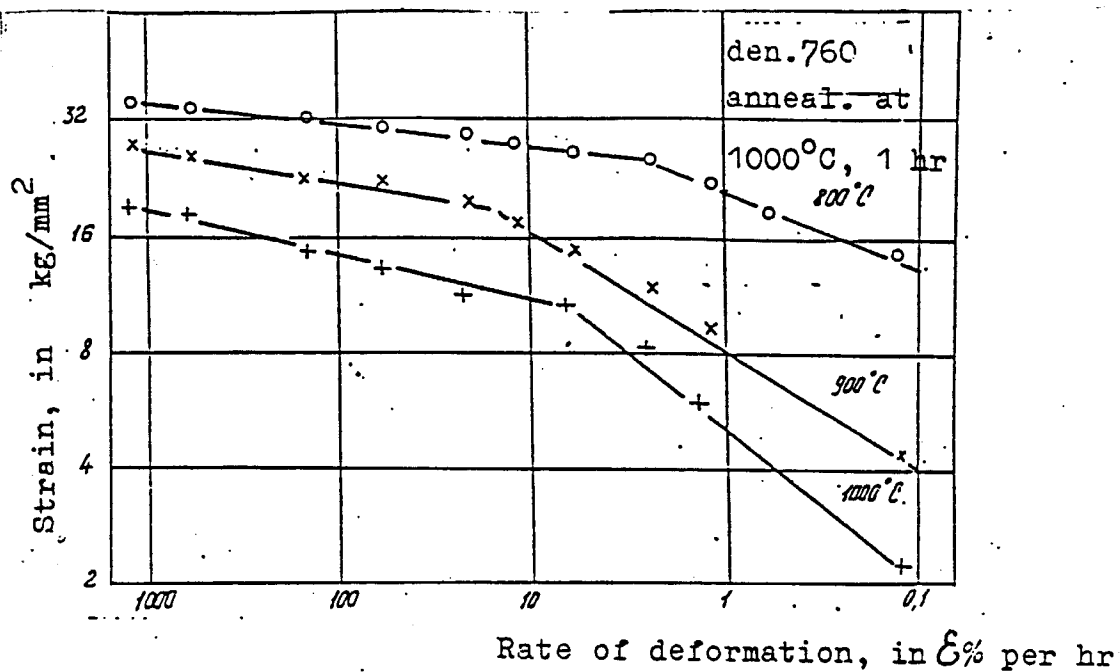


Fig.1. High-temperature capacity of VCTZC  
vanadium alloy, V-8Cr-5Ti-1Zr-0,1C

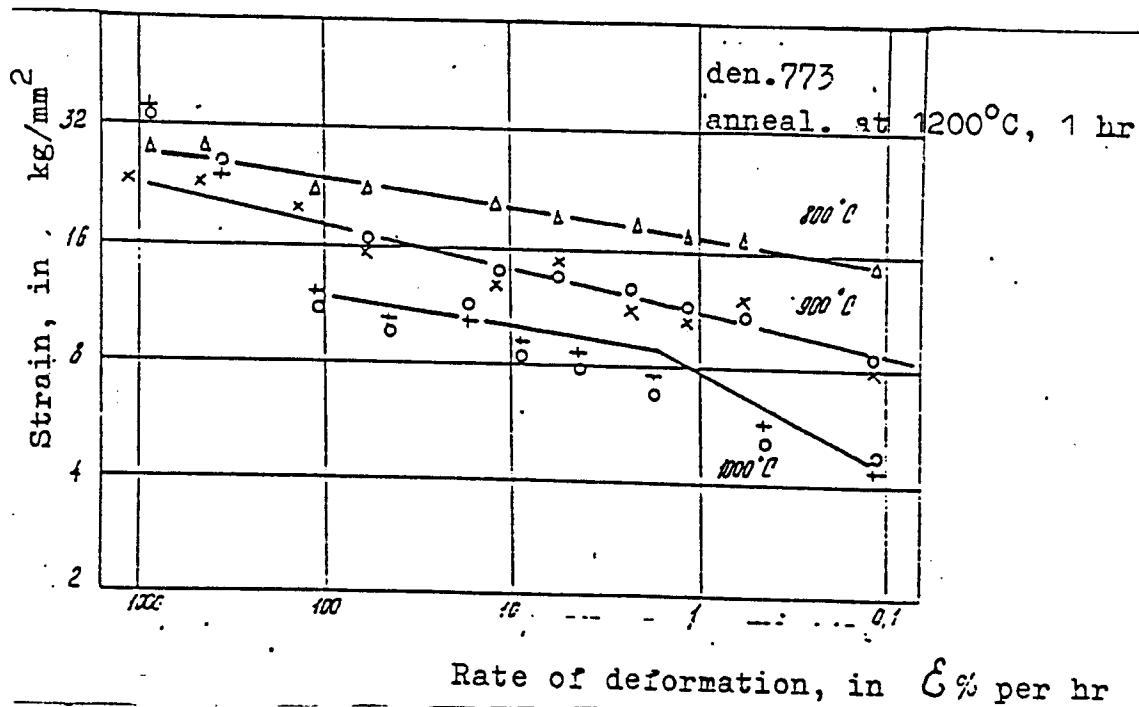


Fig.2. High-temperature capacity of VZCM  
vanadium alloy, V- 10Mo-2,5Zr-0,3C

## PRICE OF ALLOY SEMIFINISHED PRODUCTS

Semifinished products of Vanadium alloys are supplied against list and agreed prices. The maximum list price of 1 kg of semifinished products amounts to: for VZCN10-1 alloy (Vanadium, 10% of Niobium, 1.0% of Zirconium, 0.1% of Carbon) expressed in Rubles:

ingots - 200, rods 440-1200, sheets and strips - 770-1100.

An agreed price of semifinished products may be higher or lower than a list price.

---

(\*)Weldability was investigated by E.A.Gouseva, L.G.Strizhevskaya, S.P.Syomkin.

## LIST OF ASSOCIATED LITERATURE

1. Druzhinina I.P., Yelutin A.V., Perkova G.N., Lalayan M.S. Vanadium alloys of solid solution structure. The Giredmet Transactions, V.57, M., Metallurgy, 74.

2. Alyabyev V.B., Druzhinina I.F., Zentsova N.A. Perkova G.N. and others. Structure and mechanical properties of model vanadium alloys. The USSR Academy of Science, FMM, V.67, edition 4, 89.

3. Druzhinina I.P., Perkova G.N., Yelutin A.V., Lalayan M.S., Arakelov A.G. and others. Properties and phase composition of Vanadium alloys alloyed with Zirconium and Carbon. Ed. of the USSR AS. Metals No 4, 76

4. Kazakov V.A., Anisimov Yu.V., Druzhinina I.P., Perkova G.N., Zentsova N.A. and others. Evaluation of corrosion resistance of Niobium and Vanadium based bench tests. M., Central Research Institute of Information (TSNIIInform), 86. NIIAR. Preprint. Radiation Material Investigations.

# Problems of the development of low-activated vanadium alloys.

S.N.Votinov, A.I.Dediurin,  
A.A.Grigorian

One of the most important tasks under elaboration of the thermo-nucleare reactors is a problem of the development of the alloys having not only necessary complex of the physical and mechanical properties, but also the low activation and its quick falling in time [1]. It is especially important in regard to ecologically safe and reliable work of the fusion reactors and their capacity for competition in comparison with the fission power stations.

Vanadium is the most perspective metal as a base of low-activated alloys not only from the point of view of the nucleare and mechanical properties, but also because under the neutron irradiation the short-half-life nucleai-transmutantors are formed in it [2,3]. As the main alloying elements of vanadium alloys may be used Ti,Cr,Si and some others elements when certain limitation of their contents [3]. However, the development of the low-activated alloys only on the basis of the activation characteristics of the alloying elements ensures necessary complex of the material properties not in all cases.

Vanadium alloys have been attained suffuciently long-time strength when alloying with Ti,Cr and Si by different relations between them. In the contents limitations, which ensures to vanadium alloys necessary workability, weldability and others technological properties, its long-time strength changes inessentially when such alloying. As an example in this respect the data on the mechanical properties of some vanadium alloys with different contents of Ti and Cr are shown in Table 1 in comparison with a stainless steel and VZY-alloy. It can be seen, that the strength properties of vanadium alloys are closed with each other, but excels essentially the properties of the stainless steel and VZY-alloy.

Table 1.

Material	20°C		600°C		800°C	
	UTS	Elong	UTS	Elong	UTS	Elong
Stainless steel	580	60	350	42	160	57
V-2,5Zr-0,06Y-0,35C (VZY)	650	3,2	320	10	190	14
V-15Cr-5Ti	700	28	550	16	500	15
V-9,4Ti-6,1Cr-0,09Zr- -0,06Si (VTU-16)	580	59	590	18	560	16

UTS-kg/mm<sup>2</sup>, elong.-%

However, such alloying results in considerable change of the radiation properties of vanadium. So, a neutron irradiation of vanadium and its alloys in the reactor BOR-60 up to fluence  $1,25 \times 10^{23} \text{ cm}^{-2} (E > 0)$  in variable temperature regime -  $740-830^\circ\text{C}$ , 358 eff. days and  $350-460^\circ\text{C}$ , 890 eff. days, causes the low-temperature irradiation embrittlement (Fig.1a,b), while alloying of vanadium by Ti up to 10,6 at% suppress the low-temperature irradiation embrittlement, and an alloy ductility is remained on 7-10% level (Fig.1c).

Alloying of vanadium by Ti and Cr exerts different influence on the corrosion resistance of vanadium alloys under exposure in Li with different content of  $\text{N}_2$  (0,03-0,25%) at  $700^\circ\text{C}$  and 1500h duration. Corrosion resistance of 1-2mm thick flat samples previously annealed at  $1100^\circ\text{C}$  during one hour tests were performed under static conditions with compulsed lithium circulation in niobium containers.

Vanadium and chromium alloyed samples were saturated with nitrogen practically over the whole depth of the samples, and this effect increased with the rising of nitrogen content in lithium (Fig.2a,b). Saturation of vanadium with titanium and chromium localized nitrogen saturation in the surface layers of the alloys and the depth of the saturation zone decreased when the titanium content increased in the alloy (Fig.2b). The values of initial microhardness of the alloys in Fig.2a,b are given after the exposition of the alloys in argon at  $700^\circ\text{C}$  during 1050 hours.

Thermonuclear reactor construction materials must stand high thermal and heat stresses caused by pulsed ignition conditions of plasma. Such parameters of the materials as thermal conductivity, elasticity module, thermal expansion factor are also significant. Definite limits on the level of alloying are put on by the drop of thermal conductivity of vanadium alloyed by titanium and chromium because of large linear distortion [4].

The obtained experimental data concerning thermal variation of thermal conductivity of vanadium and its alloy (V-9,4%Ti-6,1%Cr-0,09%Zr-0,06%Si) are compared in Fig3. with the same parameters of the stainless steel and the well known alloy V-15Cr-5Ti. The value of thermal conductivity of the vanadium alloys is larger than that of the stainless steel, but smaller than that of pure vanadium. It is necessary to decrease the alloying level of the solid solution to obtain the increase of thermal conductivity [4].

Accumulation of hydrogen is also observed together with transmutation elements during the irradiation of the thermonuclear reactor (TNR) materials. 0,01at% hydrogen output [5] may be observed in the first wall material (vanadium) of TNR at heat loads about  $1 \text{ MW/m}^2$  per year. Moreover, plasma itself may be one of the dominant sources of hydrogen accumulation in the first wall materials. Its content (equilibrium concentration) is thought to be determined by plasma temperature and density in the TNR discharge chamber, the latter parameters determining hydrogen solubility in vanadium and its alloys [6]. The definite influence on hydrogen accumulation in the first

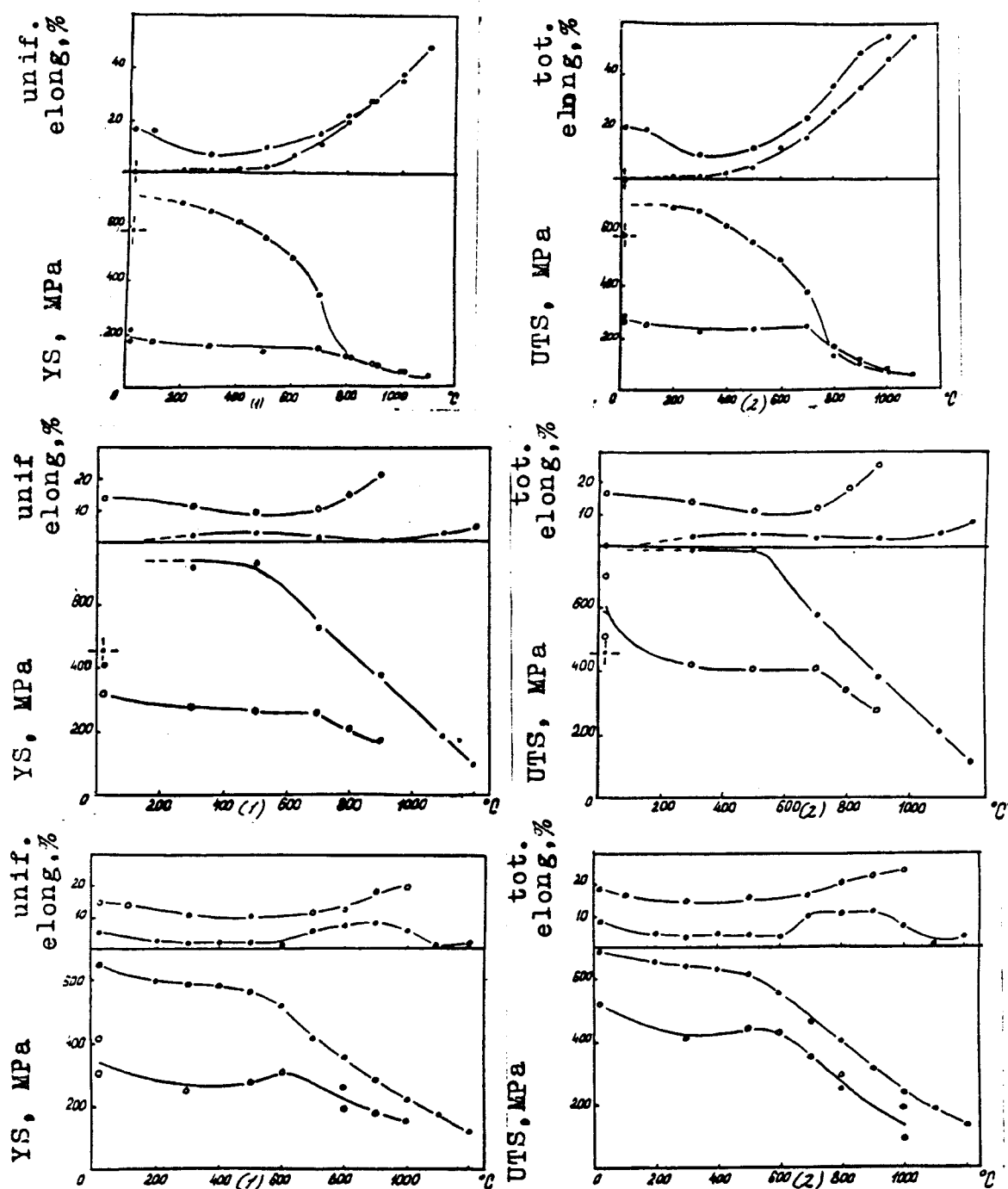


Fig.1. Temperature dependence of the mechanical properties change of vanadium and its alloys before (o) (heat treatment under 1000°C, 1 h) and after (●) irradiation.  
a - V; b- V - 10 at.% Cr - 3 at.% Ti - 1 at.% Zr - 0,3 at.% C; c - V - 10,6 at.% Ti.  
1- uniform elongation and yield strength  
2- total elongation and ultimate tensile strength.

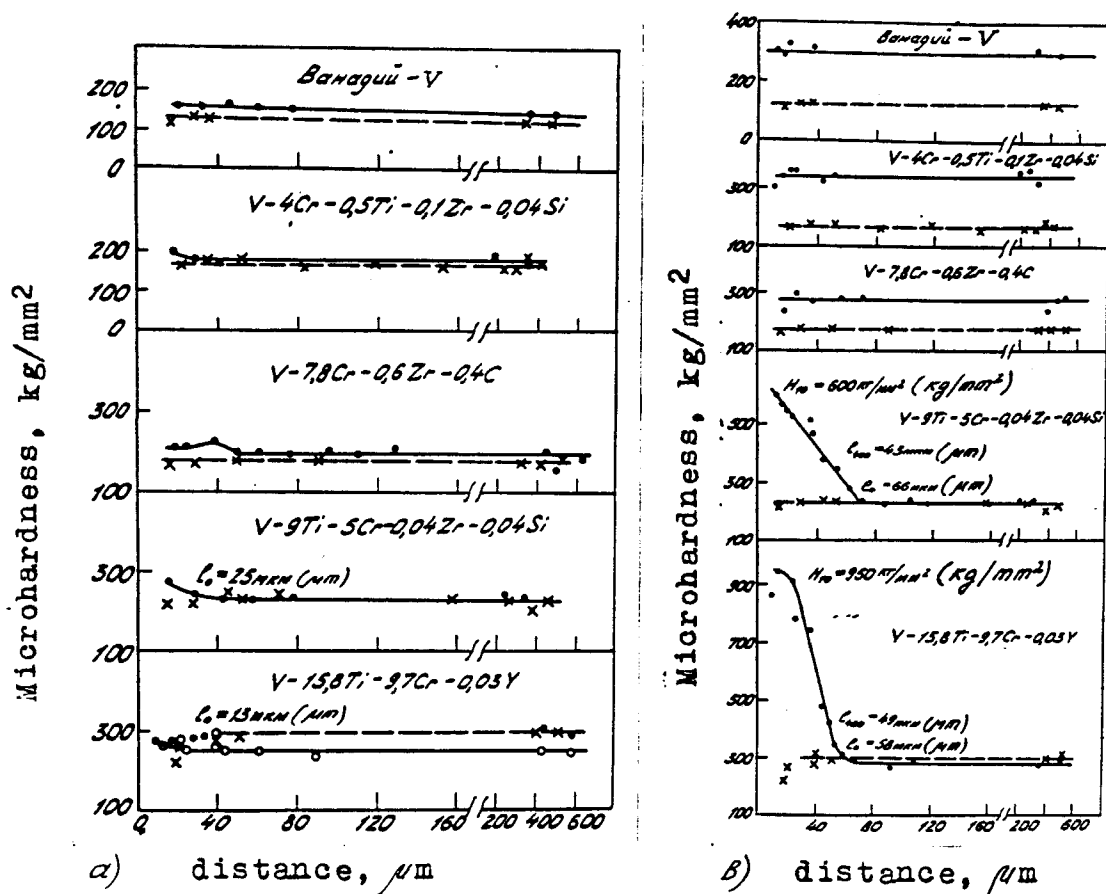


Fig.2. Profiles of the microhardness on the across section of the samples of vanadium and its alloys in Li with different content of  $N_2$  (0,03 -a; 0,25 -b).

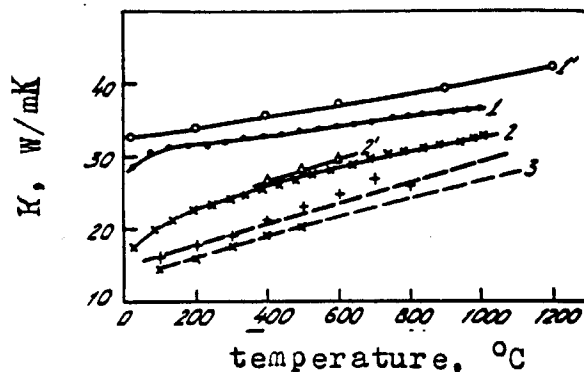


Fig.3. Temperature dependence of the heat conduction of vanadium (1) and alloy V - 9,4 Ti - 6,1 Cr - 0,09 Zr - 0,06 Si (2), annealed at 1000°C, 1 h, alloy V - 15 Cr - 5 Ti (2), stainless steel (3).

wall materials have alloying elements relative to their hydrides enthalpies compared with the enthalpies of vanadium hydrides ( $\Delta H$ , kJ/g-atom),  $\gamma\text{-TiH}_2$  (-66,95),  $\gamma\text{-VH}$  (-41,54),  $\text{CrH}$  (-6,26) [7] and thus determining the stability of hydrides.

Hydrogen content in vanadium is given in Table 2 [2] at pressures close to the values typical for TNR discharge chamber ( $10^{-3}$  Pa) and 250-550°C temperatures. According to [8], equilibrium hydrogen concentration in V-15Cr-5Ti alloy is approximately twice as large as this value in unalloyed vanadium at 600°C.

Table 2.

Solubility of Hydrogen in Vanadium

Temperature, °C	Dimension	H <sub>2</sub> pressure, torr.		
		10 <sup>-3</sup>	10 <sup>-2</sup>	10 <sup>-1</sup>
250	at%	0,08	0,27	0,84
550	at%	0,008	0,03	0,08

The temperature of brittle - ductile transition of vanadium depends on hydrogen content [6]. The temperature of brittle-ductile transition of vanadium exceeds room temperature when hydrogen content in vanadium is over 0,04 weight%. This temperature may notably rise at higher concentrations of hydrogen in vanadium alloys. Thus the alloys behaviour needs further specific studies in the region of TNR hydrogen pressures and temperatures.

TNR operation conditions will be determined on the base of possessive data, especially cooling regimes and possible variants of the first wall outgassing.

One of the main items is hydrogen penetration of vanadium alloys. The high rate of hydrogen diffusion in vanadium ( $1 \times 10^{-4}$  cm<sup>2</sup>/s at 300°C) [9] and its definite drop of its alloyings [2] cannot suppress hydrogen penetration into the coolant. Barrier films are needed to decrease hydrogen penetrability. Their natural formation from the side of lithium coolant is mostly perspective - the phenomenon of formation of nitridooxide films. Titanium alloying is mostly preferable in the discussed case.

The mentioned above data concerning the influence of radiation, corrosion and mechanical properties, the influence of hydrogen on the alloying elements show that further production of the optimized alloys is not yet finished and needs further studies.

A number of problems may be solved, especially corrosion resistance of the alloys in lithium, providing for low nitrogen impurity content of lithium.

#### References.

1. English C.A., Mazey D.I. Materials development for fusion reactor. Nucl. Energy, 1990, 29, No1, Feb, 67-80.

2. Votinov S.N., Gomofov L.I., Dedjurin A.I., Zavialsky L.P. Peculiarities of vanadium alloys as low-activated materials for the thermonuclear reactors. Voprosi atomnoi nauki i tehniki, vip.3, 1989, 49-54.
3. Masatoshi Okada, Tetsuji Noda, Fujio Abe. On the development of low-activation materials for fusion reactors. J.Nucl.Mat., 169, (1989), 249-256.
4. Livshic B.G., Kraposhina V.S., Linezkii Ja.L. Physical properties of the metals and alloys. M., Metallurgija, 1980, s.320.
5. Rovherad L., Hopkins G. Nucl. Technol., 1976, v.29, No3, p.274.
6. From E., Gebhardt E. Gases and carbon in the metals. M., Metallurgija, 1980, s.428-430.
7. Burchanov G.S., Efimov Ju.V. Refractory metals and alloys. M., Metallurgija, 1986, s.120.
8. Smith D.L., Loomis B.A., Dierecs D.R. Vanadium-base for fusion reactor application - a review. J.Nucl.Mat., 1985, t.135, No.2-3.
9. Galaktionova N.A. Hydrogen in the metals. M., G.I.Ch.M., 1959, s.100.



## **Reduced Activation Stainless Steels for Fusion Reactors**

G.L. Kulcinski, M.E. Sawan and H.Y. Khater

Fusion Technology Institute  
University of Wisconsin-Madison  
1500 Johnson Drive  
Madison, Wisconsin 53706

Presented at the US-USSR Workshop on D-<sup>3</sup>He Reactor Studies, 25 September - 2 October 1991, Moscow.

## **I. Introduction**

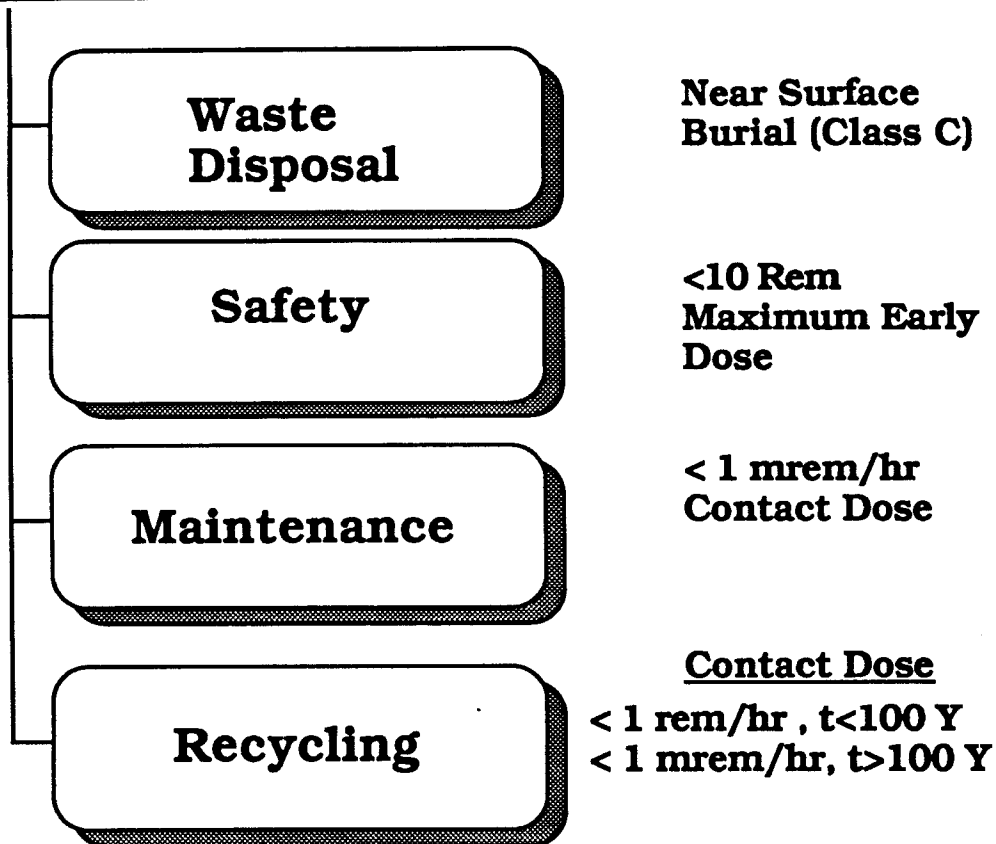
One of the major reasons for developing the fusion option over that of fission is the widely held belief that the level and impact of radioactivity produced per kWh is considerably less than that in fusion. However, because there are 4 times as many neutrons released per kWh from a DT fusion plasma compared to a fission reactor, and because those 14 MeV neutrons can induce different, and sometimes longer lived, radioisotopes, the fact is that the levels of radioactivity in fusion plants are sometimes actually the same order of magnitude as in fission plants at shutdown!<sup>(1,2)</sup> While the radioactivity level at shutdown is at least as important for afterheat and safety, most of the attention in the literature has been focused on the long lived radioactivity and waste disposal problems. It has been shown that fusion reactor structural materials, such as stainless steels, can have long lived radioactivity levels of 10 to 100 times less than those generated in fission reactors on an equivalent energy output basis.<sup>(1-3)</sup> There have been recent attempts to increase that margin by substituting alloying elements that produce less long lived radioactivity<sup>(4-6)</sup> and this paper summarizes some of the benefits and problems which result from that activity.

## **II. Reasons For Developing Low Activation Stainless Steels**

There have been at least 4 motivations for the research in this area and they have not always been consistent (see Figure 1). The most prominent has been the desire to allow near surface burial, followed by the improvement in safety of the reactor, increased maintainability, and most recently, to allow recycling of irradiated components. A detailed discussion of each one of these reasons is beyond the scope of this short review but the main arguments for each will emerge in the following sections.

Figure 1

## **The Reasons for Developing Low Activation Stainless Steels Have Not Always Been the Same**



The arguments for and against developing low activation steels still need to be debated and a list of pros and cons is given in Table 1. For example, while it would certainly be beneficial, from both a cost as well as a public relations standpoint, to dispose of spent reactor components in a near surface waste burial facility, the replacement of the alloying elements which generate the long lived isotopes usually aggravates the short term radioactivity. If the short term activity increases, then the afterheat increases as does the activity that could be released in the event of an accident.

**Table 1**

**Why Develop Low Activation Stainless Steels?**

<b><u>For</u></b>	<b><u>Against</u></b>
Reduce long term radiation level to allow near surface burial	Usually aggravates the short term afterheat problem
Reduce long term waste disposal costs	Cost of developing and qualifying new low activation alloy can be substantial
Reduce exposure to workers if alloy is recycled	May increase short term radiation levels and increase radiation levels during maintenance
Makes fusion more attractive to environmentalists and politicians	Time involved in developing and qualifying low activation materials may delay the implementation of fusion

Similarly, the reduction of long lived isotopes may result in lower waste disposal costs, but the cost of developing, testing and qualifying a new alloy system in a nuclear environment will be substantial. Such a materials development program may take 10 to 20 years, extending the duration and cost of the R & D phase.

The reduction of exposure to workers in recycling plants by reducing long lived isotopes is desirable but is the corresponding increase in short term activity worth the increased risk to both workers and the public in the event of an accident? The higher short term activity also will increase the radiation levels in the maintenance areas and one could be trading lower exposure to one segment of the working population for increased exposure to workers of another segment.

The question of public relations is hard to quantify but it is clear that the benefits of lower long lived radioactivity (as perceived by the public) are presently being enjoyed by the fusion community. However, if the need to develop entirely new alloys, including all the testing and quality assurance that is necessary for nuclear grade systems, requires too much time (and money), then the public might just opt for a quicker solution to our future problems.

In any case, further debate on these topics, and others, will certainly be necessary before we commit to multi-billion dollar materials development programs.

### III. How Are the Waste Limits Presently Defined?

Table 2 shows how the U.S. waste burial classes are defined. The key parameters include: the time period to decay to acceptable level, whether or not the radioactive material meets the minimum waste form and stability requirements, whether an "intruder barrier" has to be provided, and the burial depth of the waste material. Class A waste is the most benign in the U.S. system and is clearly the most desirable from cost and the time of surveillance required. Class C is also a big improvement over the deep geological systems that we now are trying (without much success) to build for fission wastes. Unmodified stainless steels in use today would probably have to be treated as deep geologic waste if they were used in DT systems (the use of the D<sup>3</sup>He fuel cycle would change that conclusion). The cost of deep burial for fission materials is now estimated at  $\approx$  \$440/kg, roughly 10 times the initial fabricated cost of the component itself.

**Table 2**

**Current Definitions of U.S. Waste Burial Classes**

<u>Radwaste Class</u>	<u>Period From Decay to Acceptable Level</u>	<u>Meets Minimum Waste Form Requirement</u>	<u>Meets - Stability Requirement</u>	<u>Provides an Intruder Barrier</u>	<u>Depth of Burial</u>
A	<<100 y	Yes	No	No	<<5 m
B	<100 y	Yes	Yes	No	<5 m
C	<500 y	Yes	Yes	Yes	>5 m
Deep Burial	>500 y	Yes	Yes	Yes	Deep Geologic Burial Site

### IV. Representative Reduced Activation Steels

Table 3 lists the major alloying and important impurities in 4 steels considered for fusion applications. Included are 2 austenitic steels (PCA, a slightly modified form of 316 SS and Tenelon, a high manganese steel) and 2 ferritic steels (HT-9 and modified HT-9). The main difference in the austenitic steels is the increase in the Mn content and a reduction in the Ni, Mo and Nb. The ferritic steels were modified by reducing the Ni, Nb and Mo and adding W.

**Table 3.****Elemental Composition of Normal and Reduced Activation Steels**

<u>Element</u>	<u>PCA</u>	<u>Concentration in Wt. %</u>		
		<u>Tenelon</u>	<u>HT-9</u>	<u>MHT-9</u>
B	0.005	0.001	0.01	0.001
C	0.005	0.15	0.2	0.15
N	0.01	0.005	0.05	0.001
O		0.007	0.01	0.007
Al	0.03	0.008	0.01	0.008
Si	0.5	0.2	0.35	0.2
P	0.01	0.13	0.02	0.013
S	0.005	0.004	0.02	0.004
Ti	0.3	0.003	0.09	0.1
V	0.1	0.002	0.3	0.3
Cr	14.0	15.0	12.0	11.0
Mn	2.0	15.0	0.55	0.53
Fe	64.88	69.4	85.0	85.2
Co	0.03	0.005	0.02	0.005
Ni	16.0	0.006	0.5	0.006
Cu	0.02	0.003	0.09	0.003
Zr	0.005	0.001	0.001	0.001
Nb	0.03	0.00011	0.0011	0.00011
Mo	2.0	0.00027	1.0	0.00027
Ag	0.0001	0.00009	0.0001	0.00009
Sn	0.005	0.003	0.003	0.003
Ta	0.01	0.0004	0.001	0.0004
W	0.05	0.01	0.5	2.50
Pb	0.001	0.0005	0.001	0.0005
Bi	0.001	0.0002	0.001	0.0002

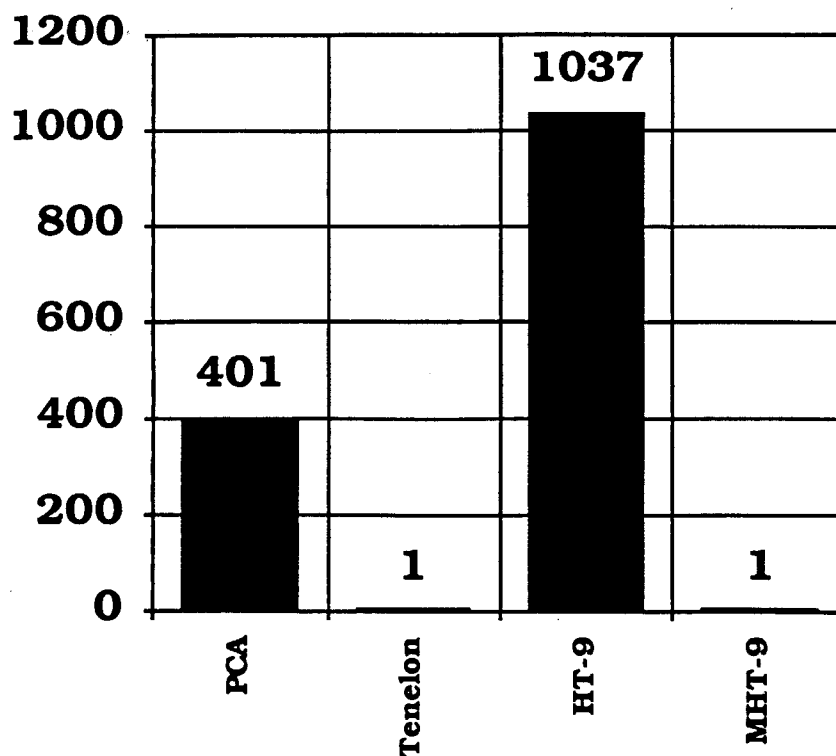


Figure 2. The relative waste disposal rating can be greatly reduced in stainless steels by elemental substitution.

## V. Effect of Alloying Modifications on Long Lived Radioactivity

The effect of alloying elements on the relative Waste Disposal Ratings (WDR) of steels is given in Figure 2. The first thing one notices is that the reduction in Ni, Mo, and Nb (shown in Table 3) drops the relative WDR by a factor of 400 in austenitic steels and by over 1000 in ferritic steels.

The specific effect of each major element in PCA is shown in Figure 3. For example, even though Mo is only 2% of the composition of PCA, it contributes over 55% of the long lived activity for Class C burial. An even more dramatic effect can be seen with respect to Nb. The Nb impurity amounts to only 100 ppm by weight and yet this small amount of Nb contributes over 40% to the Class C waste limit in PCA. When the alloying changes are made, the Nb then becomes the dominating element even though it would be present at  $\approx 1$  ppm by weight. A similar effect in HT-9 is shown in Figure 4 where reducing the Mo content to 0.00027% drops its contribution to a few percent and even at  $\approx 1$  ppm by weight, Nb contributes over 95% to the Class C rating.

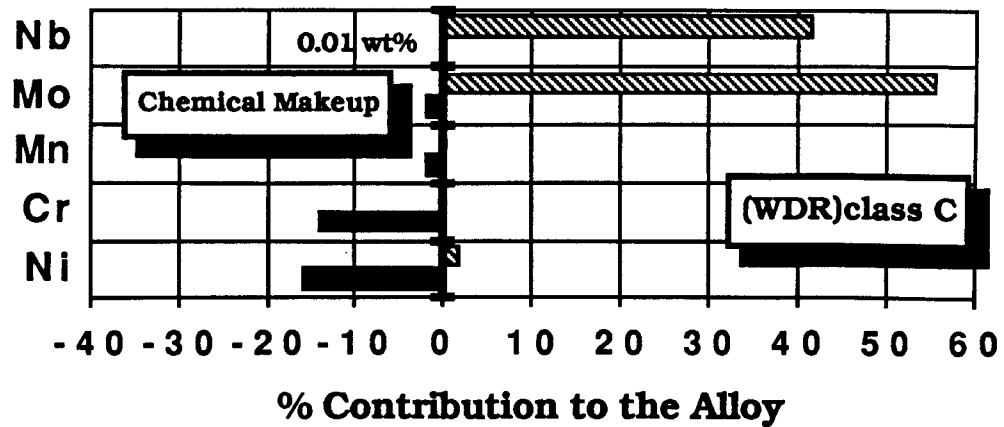


Figure 3. The Mo alloying element and the Nb impurity produce essentially all the long lived radioactivity in PCA austenitic steel.

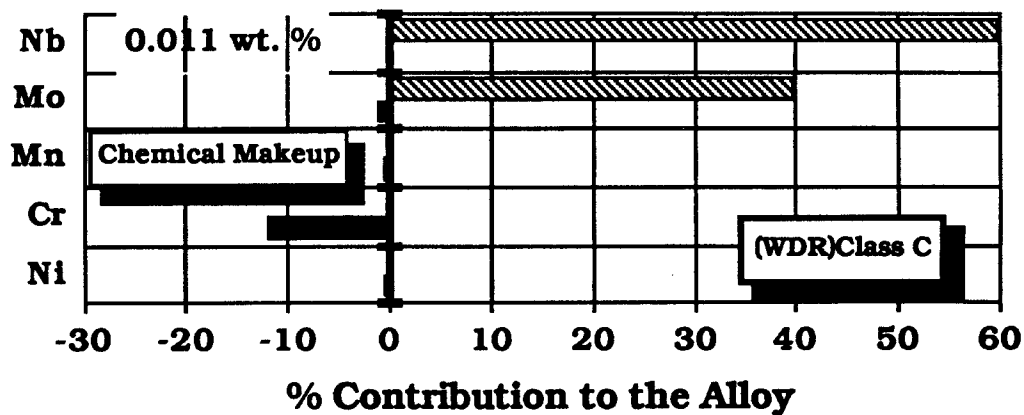


Figure 4. Mo and Nb produce essentially all the long lived radioactivity in HT-9 ferritic steel.

## VI. Effect of Alloying Modifications on Afterheat

Another important feature of the alloy modifications is the increased short term radioactivity in high Mn austenitic steels. The relative levels of afterheat are compared in Figure 5 normalized to the afterheat in HT-9. It is obvious that the alloying changes in the ferritic systems have essentially no effect but that the addition of Mn in austenitic alloys more than doubles the afterheat level in a system which was already higher than ferritic alloys.



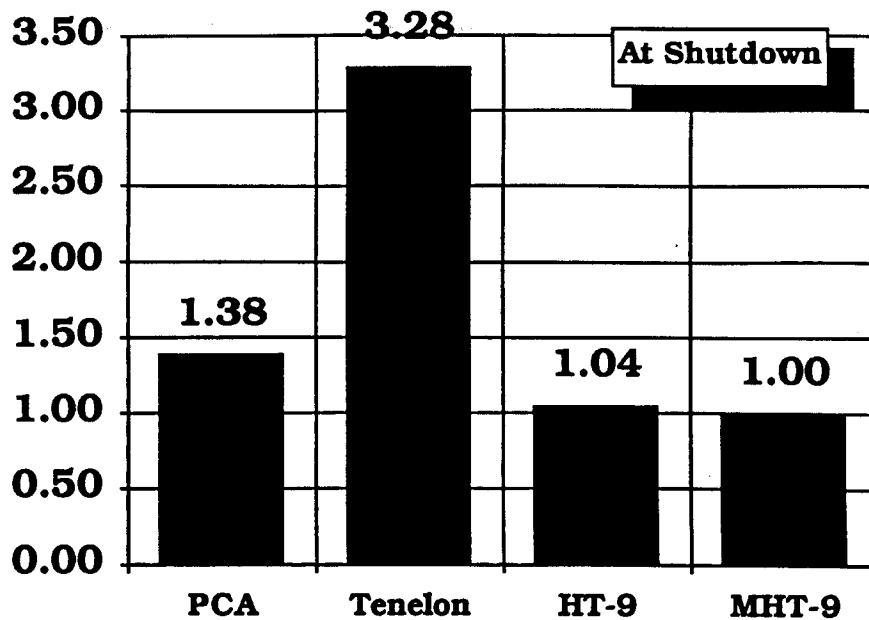


Figure 5. The relative afterheat in low activation alloys is increased in austenitic but unchanged in ferritic steels.

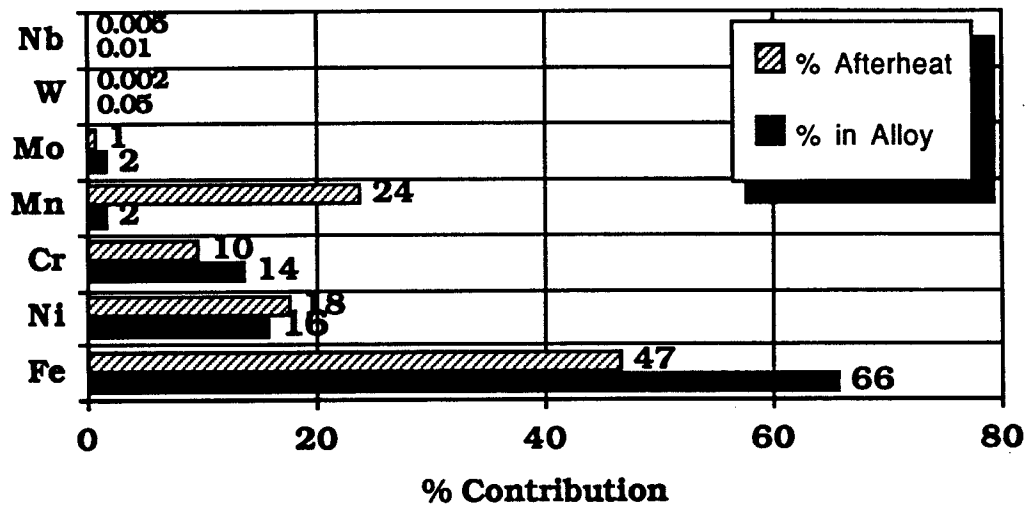


Figure 6. The manganese in PCA contributes more than 10 times to the afterheat than it does to the overall composition.

The specific reason for the change in afterheat in Tenelon is given in Figure 6. Here the percent contribution to the afterheat is compared to the percent contribution to the chemical composition for the 4 alloys. It is clear that even with only 2% Mn in PCA, that element contributes  $\approx 10$  times more to the afterheat than its composition level would indicate. In the reduced activation alloy, Tenelon, the Mn contributes 75% to the afterheat even though it is present in only 15% (Figure 7).

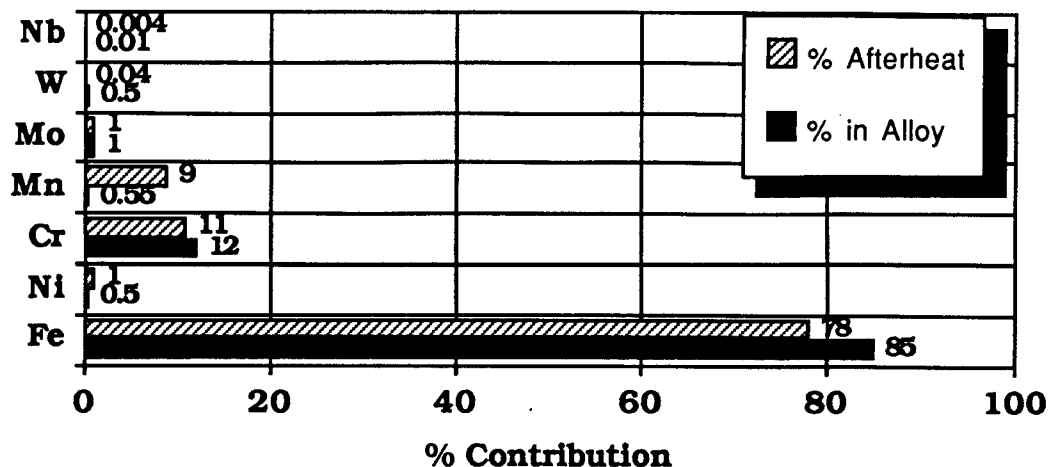


Figure 7. The manganese in HT-9 contributes more than 16 times to the afterheat than it does to the overall composition.

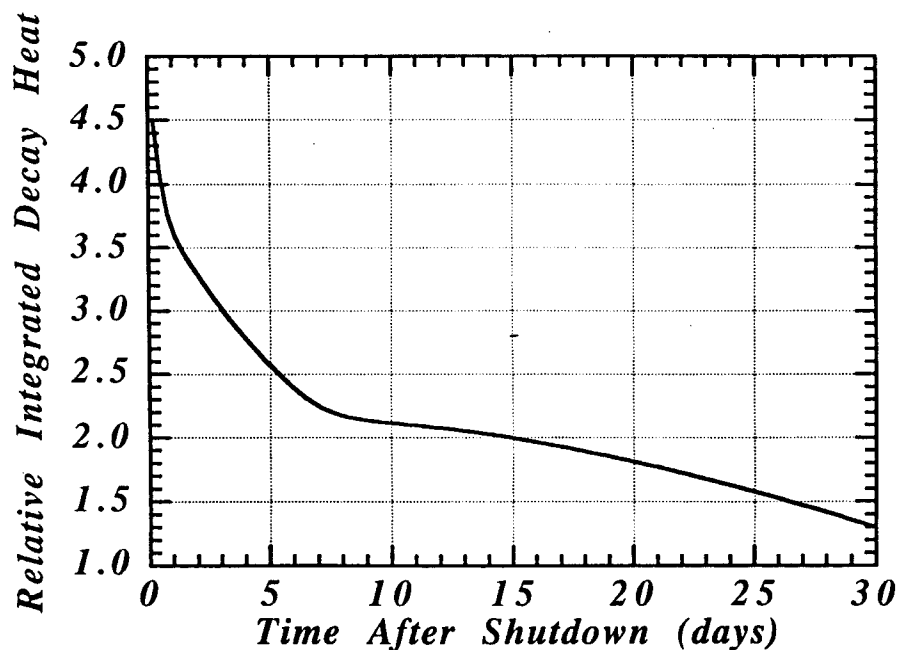


Figure 8. In spite of the short term afterheat released from high Mn steels, the total integrated energy released from Tenelon (high Mn) and 'normal' 316 stainless steels is about the same.

Even though the integrated afterheat from Tenelon is more than twice that of PCA, the actual afterheat within a few days of an accident might be as high as 4.5 times that of PCA (Figure 8).

Disposing of such afterheat in this short period is a problem as well as the fact that the radioactive elements responsible for this afterheat, Mn, have a particularly high vapor pressure

compared to the rest of the steel components (Figure 9). Such a high vapor pressure could be a safety hazard for the public in the event that primary containment were to fail. Obviously, the specific effect on the safety and general operation of a DT power plant must be examined in more detail before one could determine the degree of benefit obtained by using a high Mn, reduced activation alloy.

## VII. The "Everything Goes Deep" Philosophy

At the recent IEA Workshop on Low Activation Material held in Culham, England<sup>(2)</sup>, the following philosophy was proposed:

"Shallow land burial is impractical and politically unsound. This is true in many European countries at present and will probably be true in the U.S. soon. It should be dropped from consideration in the definition of criteria for low activation materials."

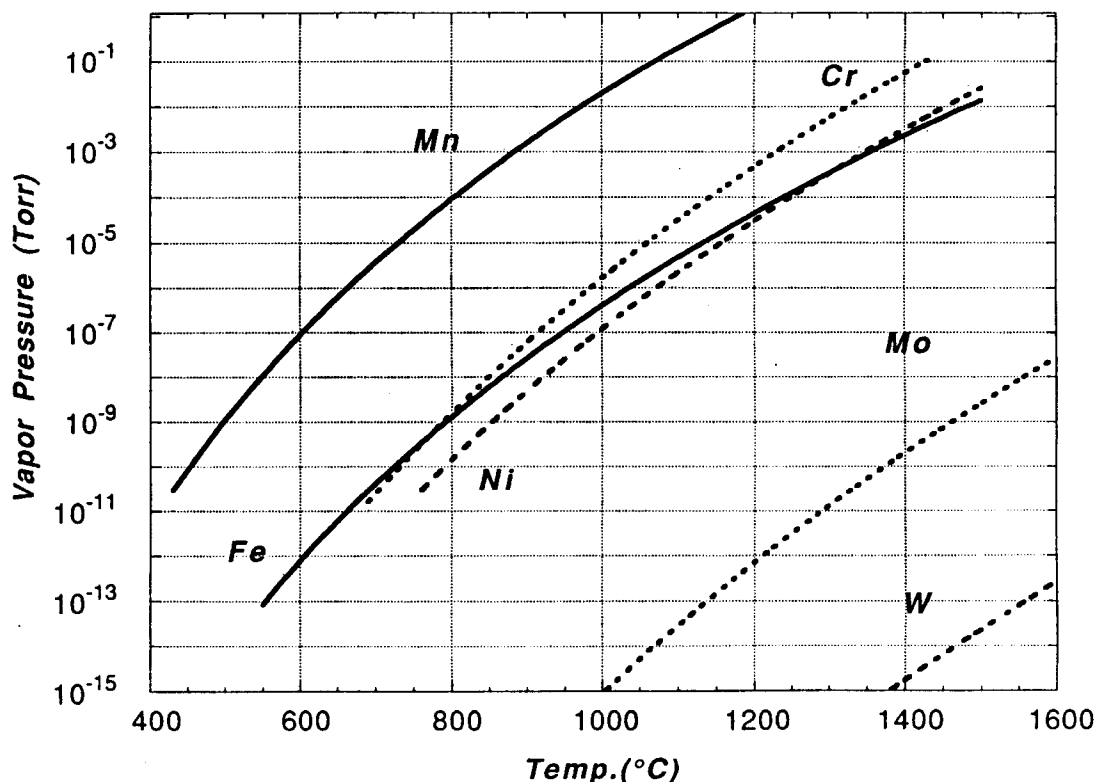


Figure 9. Manganese is the most volatile radioactive alloying element in stainless steel.

The implication of this philosophy is that if deep geological disposal replaces shallow land burial, then there is a greatly reduced benefit of low activation materials over conventional materials. If this philosophy were to be adopted, that is, even if the alloys are slightly radioactive, they must be buried in deep geological waste burial facilities, then one must ask why develop reduced (in the long term sense) activation alloys at all?

## **VIII. Effect of Advanced Fusion Fuels**

One way to alleviate the waste disposal problems while at the same time reduce the radiation damage to the structural alloys is to use an advanced fuel cycle like  $D^3He$ . Only the side DD reactions contribute to the neutron flux and that can be kept to as low as 1-5% depending on the  $^3He/D$  ratio and the magnetic configuration. The reduction in WDR possible with this fuel is shown in Figure 10. For the same net electrical power output, we can see that the relative WDR in HT-9 is reduced by a factor of over 10. Very often this level of reduction can make the difference between deep geologic or Class C burial, or even Class A vs. Class C.

## **IX. Conclusions**

It is clear that all else being equal, one should strive to use materials in fusion power plants that have the least amount of long lived radioactivity. However, when the solution to long lived radioactivity requires elements that aggravate the short term afterheat problem, then the advantages of low activation steels become less clear. Furthermore, the use of elements with short half lives may increase the short and medium term risk to maintenance workers, or those involved in recycling. One solution to this problem is to use a fuel cycle that greatly reduces the total number of neutrons released per  $kWh_e$  of net electricity produced. Such a fuel cycle exists in the  $D^3He$  system and this may allow the materials community to use "off the shelf" alloys while still retaining low afterheat and low levels of long lived radiation.

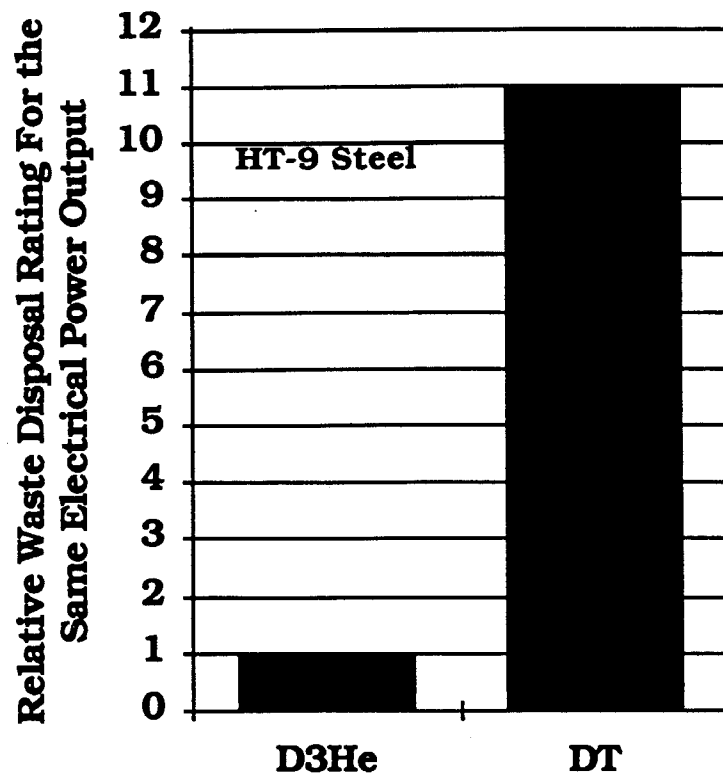


Figure 10. The use of the  $D^3He$  fuel cycle can reduce the WDR of HT-9 by more than an order of magnitude for the same electrical energy output.

## Acknowledgements

The author wishes to acknowledge helpful discussions with Dr. Frank Garner, Dr. Everette Bloom, and Dr. F. W. Wiffen. Several members of the Wisconsin Fusion Technology Institute provided helpful data in the area of radioactive inventories and safety implications. Financial support for this work was provided by the Grainger Foundation.

## References

1. W. Haefele, J.P. Holdren, G. Kessler, and G.L. Kulcinski, "Fusion and Fast Breeder Reactors," Intern. Inst. Appl. Syst. Analysis, A-2361 Laxenberg, Austria (1977).
2. Proceedings of the IEA Workshop on Low Activation Materials, Culham, England, April 8-12, 1991.
3. R.W. Conn et al., "Lower Activation Materials and Magnetic Fusion Reactors," Nucl. Technol./Fusion, **5**, 291 (1984).
4. J.P. Holdren and Steve Fetter, "Contribution of Activation Products to Fusion Accident Risk: Part II. Effects of Alternate Materials and Designs," Fusion Technology, **4**, 599 (1983).
5. R.C. Maninger and D.W. Doren, "Issues in Radioactive Waste Management," IEEE Trans., Nucl. Sci., NS-30, 571 (1983).
6. N.M. Ghoniem, et al., p. 201 in "Development of a Low Activation V Steel for Fusion Applications," Proc. Conf. on Ferritic Alloys for Use in Nuclear Energy Technologies," Published by AIME, Warrendale, PA (1983).

# THE POSSIBILITY OF MANUFACTURING LOW-ACTIVATION SUPERCONDUCTORS

A.D. Nikulin, A.K. Shikov, E.A. Dergunova, A.E. Vorobjova,  
A.G. Silaev (Bochvar All-Union Scientific and Research  
Institute of inorganic materials)  
E.Yu. Klimenko, V.S. Kruglov, N.A. Chernopliokov (Kurchatov  
Atomic Energy Institute)

The creation of magnetic systems for the fusion reactors is impossible without usage of superconducting materials. Nowadays complexes for large-scale production of the  $Nb_3Sn$  and  $Nb-Ti$  superconductors have already been developed throughout the whole world (the USSR including). However, Nb-based superconductors during irradiation form long-lived period isotopes, therefore from the point of view of creation safe low-activating materials, the search of V-based superconductors is inevitable. Moreover, copper acts as a stabilizing materials for all superconductors commercially produced in large-scale. The usage of aluminium as a stabilizer complicates considerably the process due to poor adhesion and low temperature of melting Al  $660^\circ C$  (lower than the temperature of diffusion annealing).

The  $V_3Ga$  superconductors are manufactured in a smaller quantity than the  $Nb_3Sn$  and  $NbTi$  superconductors, but they are promising materials for work in the fields up to 20 T. These superconductors are mainly used for the fabricating of the high-field magnetic system inner sections /1/.

In our institute the technology of production of the  $V_3Ga$  multifilamentary superconductors having high critical performances, is developed /2/. The industrial technology for production of the special grade of vanadium with increased purity was developed for such materials fabrication. As a result of this work the possibility of vanadium deep purification from gases, non-metallic and metallic impurities was shown.

The grade of vanadium named VNM-00 chemical composition is given in table 1:

Table 1

V	Al	Fe	Si	C	N	H	O	
basis	0,1	0,06	0,1	0,009	0,01	0,001	0,010	wt%

Vanadium of this grade produced had the Hardness of 46-48 HB, high plasticity ( $\delta = 20-25\%$ ), low strength ( $\sigma_b = 180 \text{ MPa}$ ), that made it possible to use it for the  $V_3Ga$  and  $V_3Si$  multifilamentary superconductors production. The cross-section of such a conductor is presented in fig.1.

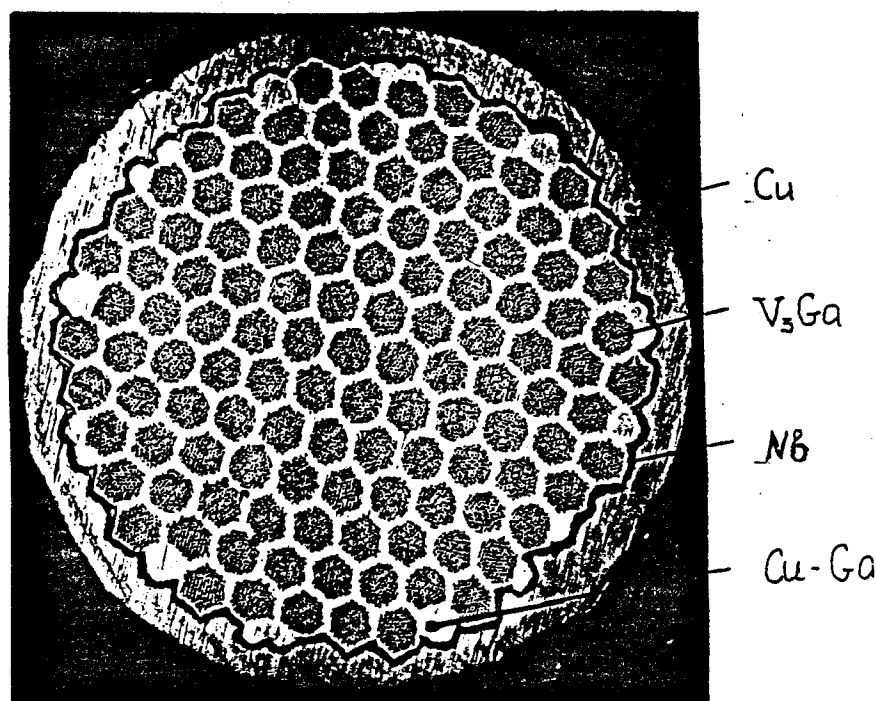


Fig.1.  $V_3Ga$  superconductor.

The wire diameter is up to 1,5-0,5 mm, the number of filaments reaches 15000, the filament diameter varies from 5 to 1,7  $\mu\text{m}$ . Jointly with AEI we have fabricated the  $V_3Ga$  conductor inner section for the high field magnet. The magnetic field induction in the 40 mm dia inner hole reaches 15,3 T at 4.2 K. And the reduction of operational temperature to 2 K increases the ultimate magnetic field by 2-4 T. To get the highest properties we have investigated in details the effect of parameters of diffusion annealing at which the  $V_3Ga$  layers formation takes place, on the  $V_3Ga$  conductors critical characteristics.

The decrease of annealing temperature to 600°C (below melt temperature of aluminium) is shown to cause the increase of  $V_3Ga$  superconductors current-carrying capacity throughout the whole field range investigated (8-20 T). The force of pinning



characterizing the strength of magnetic current fluxoids fixing on the  $V_3Ga$  layers structural defects is also increased with the annealing temperature reduction (fig.2).

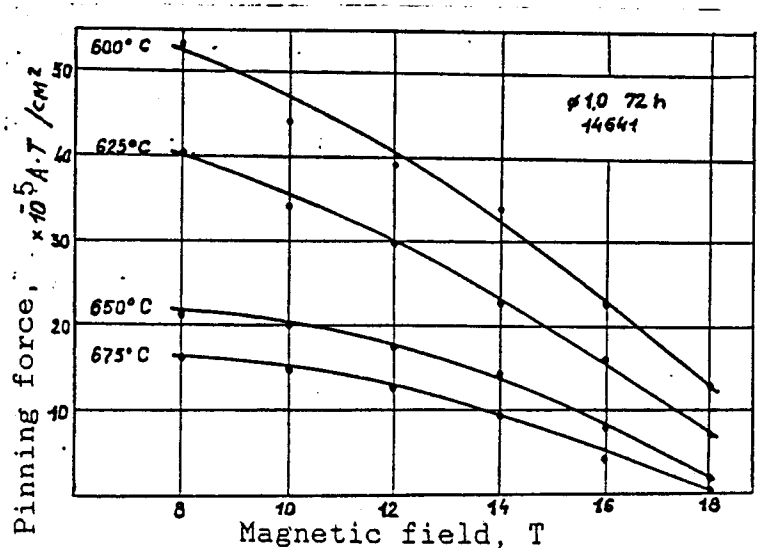


Fig.2. Magnetic field dependence of pinning force for  $V_3Ga$  superconductors

The comparison of current-carrying capacity of  $V_3Ga$  and  $Nb_3Sn$  superconductors of the same designs (fig.3) has shown that with the magnetic field increase the difference between  $V_3Ga$  and  $Nb_3Sn$  conductors is increased. Thus in the field of 14 T the  $V_3Ga$  conductors characteristics are twice as large, in that of 16 T - by a factor of 3 and in the field of 18 T - almost by a factor of 5. The optimum annealing temperature for  $V_3Ga$  formation made up 600 C at holding for 24 hours.

Fig.4 shows the effect of the annealing temperature on upper critical magnet field for  $V_3Ga$  and  $Nb_3Sn$  conductors. The increase of  $B_{c2}$  for  $V_3Ga$  conductors is seen with the annealing temperature falling down, unlike  $Nb_3Sn$  conductors. Thus, the  $V_3Ga$  compound was established to have high critical characteristics and could be of interest for use as a winding material for fusion reactor magnetic systems.

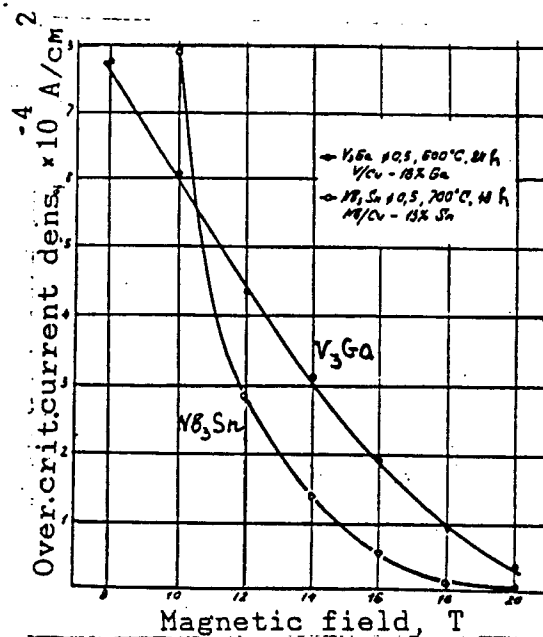


Fig.3. Magnetic field dependence of the  $V_3Ga$ ,  $Nb_3Sn$  superconductors on overall critical current density

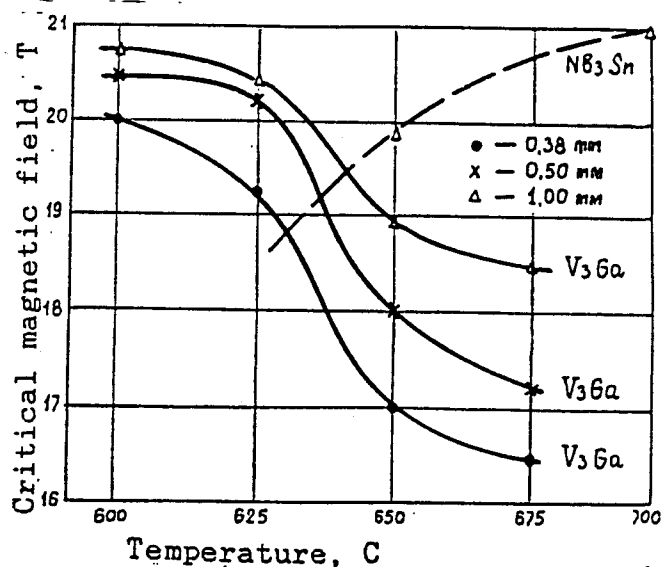


Fig.4. Dependence of  $B_{c2}$  at 4.2 K on the diffusion anneal temperature with 72 h holding for  $V_3Ga$  and  $Nb_3Sn$  superconductors.

However, the compositional materials at issue are manufactured by the bronze method and contain in their composition a considerable amount of copper that presents disadvantage of just such superconductors usage in fusion reactors with a low activity. The possibility of  $V_3Ga$  compound

formation in Al-matrix is considered. But, without copper the temperature of this compound formation is increased and that makes problem for the formation in the presence of Al.

The coating method of vanadium tapes with liquid gallium and subsequent copper cladding is also known /3/. That includes conduction of diffusion annealing in the presence of copper, its subsequent stripping and aluminium stabilization and could be one of the given method variety.

We have performed the first experiments by the given process pattern, but it's too early to speak about the results.

So, it's interesting to consider  $V_3Si$  superconductor in view of manufacturing of superconductors with low activity as it's not only vanadium but silicon as well that forms no long-lived isotopes. Multifilamentary  $V_3Si$ -superconductors with high temperature of transition into superconducting state (17 K) are obtained in our institute and the diffusion process of the compound formation has been studied /4/. This process is complicated by the fact that the ballast brittle phases are formed on vanadium filament. The investigation conducted by us have shown that only  $V_3Si$  compound layers could be formed at a specific wire design (fig.5 a,b).

The critical current density in such multifilamentary conductors makes up  $1,2 \times 10^5 A/cm^2$  in the field of 7 T. However, like in the case of  $V_3Ga$ , the presence of copper is necessary here, because it has an influence on the  $V_3Si$  formation temperature reduction.

The change of copper matrix by an aluminium one is possible only after the diffusion annealing but it's difficult due to intermetallic layers natural embrittlement. Works in this direction is in process.

Thus, the level of critical properties of V-superconducting phases mentioned above is enough for engineering usage. Successful test of  $V_3Ga$  superconductors allow to consider them as promising ones for low-active current-carrying element creation.

The main trends of our further developments on creation of technology for manufacturing superconductors with low activity:

1. The solid phase manufacturing of long-length  $V_3Ga$  wires with non-copper matrix.

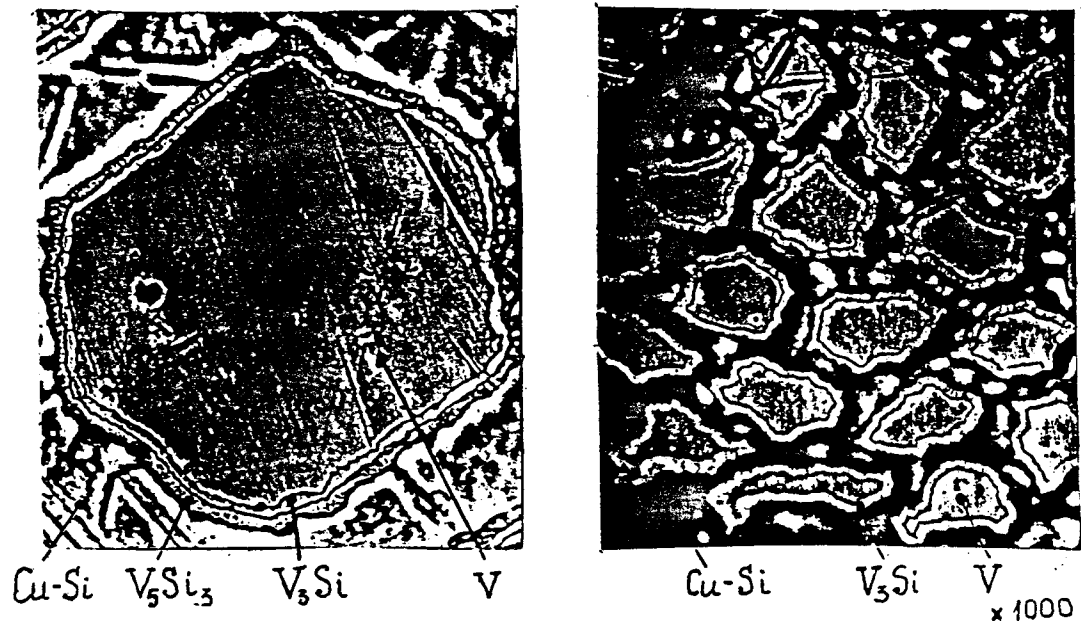


Fig.5. Fragments of 19 (a) and 361 (b) filamentary  $V_3Si$  conductors cross sections

2. The long-length  $V_3Ga$  tapes manufacturing the diffusion method with the subsequent coating by Al-stabilizing layers.
3. Development of the solid phase technology for  $V_3Si$  wires manufacturing.

It's apperently difficult to consider other superconducting compounds based on vanadium as promising ones due to the upper critical field low values.

#### References

1. A.D.Nikylin, E.A.Dergynova "Sverhprovodniki na osnove soediniy  $V_3Ga$ ". Obzor. Vip.8(87) Moscov-AUSRIIM-1983, 43 p.
2. E.A.Dergunova, A.K.Shikov, A.D.Nikylin e.a. Tokonesyschia spocobnost mnogovolokonniakh sverchprovodnikov na osnove  $V_3Ga$  i  $Nb_3Sn$  v visokich magnitnich poliach. Visokotemperatyrnia sverhprovodimost. VIMI. N 4, 1989, p.93-97.
3. Tachikawa K., Tanaka Y., Rinderer L. Preparation and properties  $V_3Ga$  superconductors. J.Mater.Sci.1972, vol.7, N 10, p.1154-1160.
4. A.D.Nikulin, V.A.Kovaleva, A.K.Schikov, I.I.Davidov, V.V.Schestakov e.a. VANT, ser. Atomic metallovedenia, vip. 1(21), 1986, p.32-36.

Permanent lunar bases.

Stages of creation and technological possibilities.

Academician V.P.Barmin, Prof. I.V.Barmin,  
Dip.Eng. A.S.Borisov

DBGM

For using the lunar resources with the purpose of solving the Earth power problems, it is necessary, first in the practice of space explorations, to greatly expand the human activity in space, which will require perfectly new methods and approaches, when developing the technical policy of creating industrial centers of the future.

As is known, many technical achievements, when realizing such programs as the landing of the man on the Moon surface according to the Apollo Project, a cycle of explorations of the lunar soil by the Soviet automatic apparatus, at the present time are lost to a considerable extent because solving concrete problems was their final aim.

In this connection it is necessary to develop a system approach, when for each stage of the Moon development prospects of its further development must be determined.

If to take the years 2010-2020 as an initial period of realizing the power program as a whole, the Moon development, conceptually must include the following stages:

- to 2005 - a stage of explorations with the help of lunar surface automatic apparatus of the second generation with the purpose of sounding areas, with good prospects for producing  $^3\text{He}$  and delivering lunar soil samples to the Earth.

- 2000-2010 - the deployment and operation of a lunar base, as a center of broad explorations of the lunar industrial resources and the development of equipment for producing  $^3\text{He}$ .

- 2010-2020 - a stage of creating lunar settlements and industrial complexes.

Considering time and technological factors, the realization of the programs of the automatic apparatus and the lunar base will be determined, to a considerable extent, by the possibilities of the active launch vehicles of the Proton and Energya type.

It is necessary to note that we consider the automatic

apparatus stage as the most reasonable way to return to explorations on the Moon. In addition, it is supposed to widely use the experience of creating the apparatus for delivering lunar soil to the Earth and the methods of remote probing the element composition of the rocks on the Venus surface.

The key stage of the successful realization of the power program is creating a permanent lunar base on the Moon.

The main volume of the research on the problem in the USSR was fulfilled in the period of the seventies and at the beginning of the eighties.

Since the design development was based on the principle of delivering loads to the Moon by separate lots by the launch vehicle of the Energya type, we believe, that the main conclusions of that period are vital at the present time as well.

The cycle of the works, fulfilled by the DBGM together with 150 main centers of USSR Academy of Sciences and branch organizations, has made it possible to solve the problems on determining the character of the main PLB, technical characteristics and requirements for the lunar surface objects and the lunar bases equipment.

The technical-economic analysis has shown, that the PLB can be created within 10-15 years on the basis of the present technological possibilities of rocket and space technology.

The lunar base, designed for permanent living of a crew of 12 persons, includes:

- main structure of a modular type;
- power center;
- complex of portable units;
- oxygen-producing unit;
- scientific equipment;
- lunar spacedrome.

At all stages of deploying and functioning the PLB it is envisaged to use a heavy lunokhod. The lunokhod power supply system envisages a combination of a radioisotope generator and a solar battery.

The lunokhod is equipped with a manipulator. The inner space of the pressurized cabin is divided into two sections: an air lock and a laboratory-living module. The latter is divided by non-sealed partitions into a control cabin, a saloon-

laboratory, a sanitary unit, a galley and a room for full-pressure suits storage.

The outer dimensions of the heavy lunokhod frame are: a length - 7m, a diameter - 2,8m. The vehicle mass is up to 6000kg.

During the base building the heavy lunokhod is used as a temporary dwelling for the cosmonauts, for unloading and delivery of modules from the landing site of the transport spacecraft to the modules assembly and excavation.

At the first stage of the base functioning all members of the crew are mainly busy with building and assembly works and with putting the base systems into operation.

At the second stage, in addition to three members of the crew, three cosmonaut-researchers are delivered to the base for carrying out scientific programs and technological experiments. The number of modules of the base main structure can reach five in this period. This stage is main, and a further deployment of the PLB is connected with increasing a volume of scientific and technical research and, accordingly, the crew size.

It was decided to use a concept of building the PLB from modules with a high degree of technological readiness, which greatly decreases the volume of building and assembly works on the Moon; ensures program "flexibility" on the launch rate and the composition of the equipment to be delivered.

The analysis of various structural arrangements of the main base structure has shown the advantages of the arrangement, according to which the structure consist of separate modules. This makes it possible, from one side, to devide the structure into transportation lots, and, from the other side, to devide all the structure into separate sealed cells. For convenience of the structure assembly in all planes and with any combinations of types, the modules diameter and length are unified according to the module net, selting their dimensions multiplicity. Besides, a horizontal arrangement of the modules at the lunar surface is most favourable, since it ensures the greatest coefficient of using the rooms floor. The weight and dimension characteristics of the main structure modules are:

- mass - from 2500kg to 6300kg;
- diameter - 4.15m;
- length - from 5.95m to 8.3m.

The main structure of the PLB, designed for constant living of 12 persons, consist of 9 modules, equipped with living cabins, rest rooms, laboratory compartments, a medical station etc. and ensures 600-700m<sup>3</sup> of a free volume of the inner space, with a floor area, equal to 195m<sup>2</sup>.

The technological possibilities of the lunar base are mainly determined by the power capacity of the base, the characteristics of its machine fleet and also by the effectiveness of a man's operation under the lunar conditions. A nuclear thermoemission power plant with output electric power of 60kW and a service life of up to 20000 hours was taken as the main part of the PLB power supply system.

The power supply system, built on the basis of such a NPP, envisages to use two independent plants, placed in craters, located at a distance of 0.5-2.0km from the main structure of the PLB. The plant mass (without the radiation protection system) with the voltage converter will be no more than 2.5t.

The PLB machine fleet includes three types of mechanisms:

- transportation facilities;
- soil-digging mounting equipment;
- hoisting apparatus.

The transportation facilities include:

- a movable shelter-laboratory with a mass of 7000kg, 4 seats and self-sufficiency of 60 earth days;
- a prime mover with a mass of 4000kg;
- a movable power unit with a mass of 2000kg and a power of the power plant, equal to 10kW;
- a trailer-platform with a load-carrying capacity of 1000kg.

The coupling of the transportation facilities makes it possible to form a road train with a distance endurance of up to 1500km and a speed of 5-10km/h.

The soil-digging mounting equipment consists of:

- a mounting bullgrader with a blade width of 3m;
- a mounting excavating machine with a bucket volume of 1.0-1.5m<sup>3</sup>;
- a mounting drill with a drilling depth of 3-10m;
- a soil-throwing machine with a capacity of 3m<sup>3</sup>/min.

The hoisting apparatus fleet includes:

- a coupled crane with a load-carrying capacity of 1000kg;



- a mounting manipulator with a load-carrying capacity of 200kg;

- a three-support telescopic crane with a load-carrying capacity of 1000kg.

And, at last, the third factor, determining the level of the technological possibilities of the lunar base, is a possibility to create a man's living medium on the base, preventing the decrease of the effectiveness of the crew operation at its long stay under the extreme lunar conditions. In this connection the DBGGM has conducted a research cycle on evaluating the quality level of the man's living medium in the main structure of the PLB. Besides, we proceeded from fact, that, unlike the scientific and technological equipment, which has relatively short obsolescence periods, the main needs and possibility of the man will not considerably change in the near future.

The experiments have been conducted on a full-scale mock-up of a PLB living module, models of various zones of the crew operation and rest, and also, together with the Gagarin cosmonauts training center, under the conditions of a complex effect of hypogravitation and a limited space.

The study has shown, that the proposed concept of the lunar base ensures rather comfort operation conditions of its crew and solves the problem of permanent stay of the man on the Moon surface.

The technical possibilities of the lunar base are rather great and, on a level with solving problems on modifying the lunar-surface equipment for producing  $^3\text{He}$ , it can also solve traditional space problems, including the study of great geological formations on the lunar surface, creation of unique astronomical instruments for various radiation bands, etc. As the lunar-surface technological infrastructure develops, the lunar base will become its component. At the present time it is difficult to analyze in detail the appearance of lunar-surface industrial complexes. Many still little-known problems are to be analyzed, such as preventing the effect of the lunar industry on the Moon ecology. We consider, that the technical possibilities of world astronautics make it possible to solve the problem of the Moon industrial development. It is necessary to note, that this process will lead without fail to the

appearance a powerful power complex on the Moon surface.

Taking into account, that the Moon is not far from the Earth and that programs may appear, influencing the proceeding, for example, natural phenomena in near space, we consider that it is reasonable, from the stage of creating lunar-surface automatic devices, to carry out all the works in co-operation with other countries, which is specially important for preserving and strengthening the confidence climate between countries, and we have a possibility to take part in it.

## **A Resource Assessment and Extraction of Lunar $^3\text{He}$**

Gerald L. Kulcinski

Wisconsin Center For Space Automation and Robotics  
and  
Fusion Technology Institute  
University of Wisconsin-Madison  
Madison, Wisconsin 53706  
U.S.A.

Presented at the US-USSR Workshop on D- $^3\text{He}$  Reactor Studies, 25 September - 2 October 1991,  
Moscow.

## 1. Introduction

The attractiveness of a  $D^3He$  fusion reactor economy has been shown in previous papers.<sup>1-6</sup> The main advantages of such an energy source stem from the low fraction of fusion energy released in neutrons (a few %) compared to 80% from the more "traditional" DT fuel cycle. This low neutron fraction has several important consequences:

- Greatly reduced radioactivity.
- Greatly reduced radiation damage to reactor components.
- Inherently safe reactor operation.
- Much higher overall efficiency of operation.
- Potentially lower cost of electricity.
- Shorter time to commercial electrical power plants.

There are two reasons that such a fuel cycle has not been pursued in the past:

1. the physics requirements of the  $D^3He$  cycle are more demanding than those for the DT cycle,<sup>3</sup> and
2. there was no known large  $^3He$  resource available prior to 1985.<sup>7</sup>

The situation with the  $D^3He$  physics has greatly improved in the past 5 years with a world record 140 kW of  $D^3He$  fusion power being produced in JET<sup>8</sup> and plasma ion temperature of 35 keV (roughly half of what is required for a  $D^3He$  reactor plasma) produced in TFTR.<sup>9</sup> There has been even greater progress in the  $^3He$  resource picture in the last 5 years. Prior to that, the only known  $^3He$  resource accessible to us on the earth was the primordial  $^3He$  collected in underground natural gas reserves ( $\approx 200$  kg) and the  $^3He$  from decaying tritium in thermonuclear weapons and heavy water CANDU fission plants ( $\approx 300$  kg). With an energy content of  $\approx 10$  MWe-y/kg of  $^3He$  burned this would only provide  $\approx 5$  GWe-y of fusion energy, hardly enough around which to develop an energy industry.

In 1985, scientists at the University of Wisconsin postulated that there should be a large amount of  $^3He$  implanted in the lunar surface from the solar wind. This was confirmed by data originally collected by the U.S. Apollo and U.S.S.R. Lunakhod program.<sup>7</sup>

The purpose of this paper is to examine the extent of that resource and discuss methods by which it could be extracted.

## 2. $^3\text{He}$ Resource Estimates on the Lunar Surface

Several studies of the extent and distribution of the lunar  $^3\text{He}$  resources have been made in the past few years, principally by Cameron,<sup>10-12</sup> Gibson,<sup>13</sup> and corroborated by Jordan.<sup>14</sup> The source of the  $^3\text{He}$  comes from the solar wind which has been incident on the lunar surface for  $\approx 4$  billion years and has showered the moon with  $\approx 500$  million tonnes of  $^3\text{He}$ . The low energy hydrogen and helium atoms have been implanted 100's of angstroms into the material covering the lunar surface. However, the  $^3\text{He}$  has been detected to a depth of several meters because the surface has been "gardened" (i.e., the surface has been turned over and over) by the action of meteorites over the billions of years the moon has been exposed to the solar wind and debris from space.

A summary of the He content measured in lunar samples is given in Fig. 1. It can be seen that the He content is generally higher in the lunar maria (i.e., the "Seas of the Moon") than it is in the highlands and basin ejecta (mountains of the moon). The reasons for this higher retention of the helium in lunar regolith (the name given to the very fine grained material making up the maria) is unknown at this time. In any case, it is very fortunate that the helium is preferentially retained in the regolith because it has the consistency of "dust" which makes it easier to handle.

By knowing the  $^3\text{He}/^4\text{He}$  ratio (it was essentially the same as in the solar wind,  $\approx 480$  ppm) and the relative area in maria of the moon, one can calculate the approximate amount of  $^3\text{He}$  present on the lunar surface. Table 1 shows that this is in the neighborhood of 1,000,000 tonnes divided roughly equally between the maria and the highlands.

Just how much energy is there in the lunar  $^3\text{He}$ ? Some perspective on the number can be obtained by noting that it would take only 25 tonnes of  $^3\text{He}$ , combined with deuterium, to provide

the  $\approx 250 \text{ GW}_e\text{-y}$  of electrical energy consumed in the U.S. in 1991. Furthermore, that 25 tonnes when liquified, would fit in the cargo bay of just one present U.S. shuttle craft. Another comparison is that the  $6 \times 10^{23}$  joules of potential thermal energy in the  $^3\text{He}$  atoms is  $\approx 10$  times the energy in all the economical fossil fuels left on the earth.

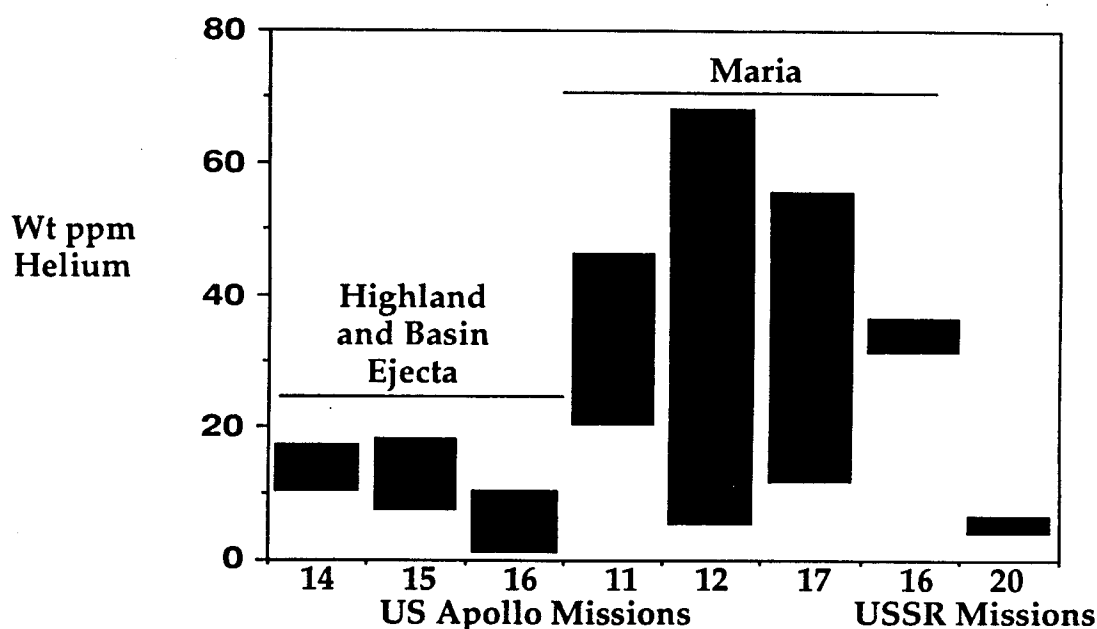


Fig. 1. All the samples returned from the moon that were tested for helium revealed  $^3\text{He}$  and  $^4\text{He}$  at approximately the solar wind ratio.

Table 1

**Lunar  $^3\text{He}$  Reserves Calculated From U.S. Apollo and Soviet LUNA Missions**

<u>Location</u>	<u>% Lunar Surface</u>	<u>Average He Conc. wtppm</u>	<u>Tonnes <math>^3\text{He}</math></u>
Maria	20	30	600,000
Highlands and Basin Ejecta	80	7	500,000
Total			1,100,000

### 3. Distribution of the $^3\text{He}$ on the Moon

Cameron<sup>10</sup> noticed that there was an important relationship between the amount of He in lunar material and the  $\text{TiO}_2$  content (Fig. 2). If that relationship is consistent around the lunar surface, then it should be easier to know where the first mining sites should be located. Such an analysis reveals that we should concentrate on the maria of the moon. As an example, Cameron<sup>13</sup> has examined the Mare Tranquillitatis from UV/IR spectral photographs. Such diagnostics reveal the  $\text{TiO}_2$  distribution and by using the correlation in Fig. 2, he was able to estimate that there is over 15,000 tonnes of  $^3\text{He}$  in Mare Tranquillitatis alone. At the present U.S. electrical consumption rate, this Mare alone would provide over 600 years of our needs.

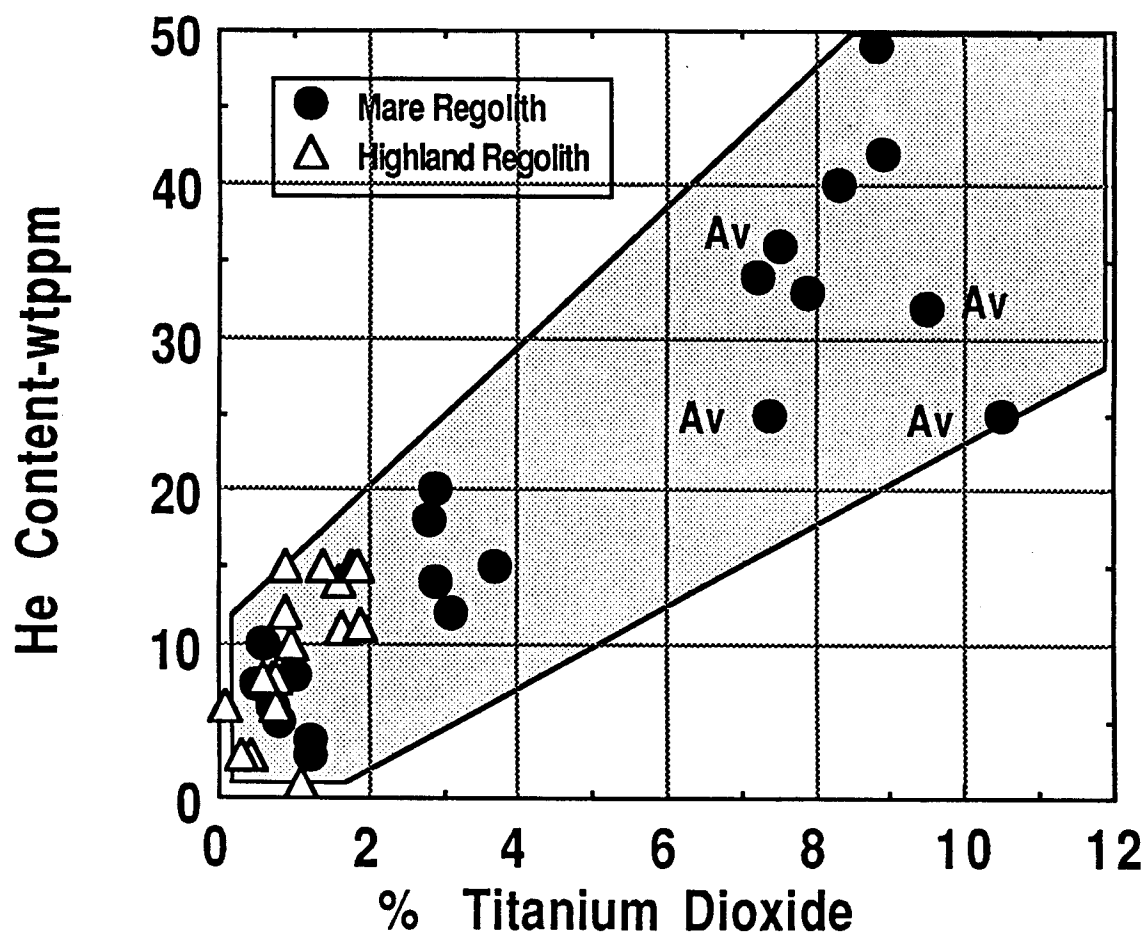


Fig. 2. There is a reasonable correlation between  $\text{TiO}_2$  and He content in lunar samples.<sup>10</sup>

#### 4. Extraction of the Lunar $^3\text{He}$

The basis for the extraction of  $^3\text{He}$  from lunar regolith was discovered over 20 years ago by Pepin.<sup>15</sup> In the process of studying the samples from Apollo 11, he found that heating the lunar regolith to temperatures of  $\approx 700^\circ\text{C}$  would cause  $\approx 85\%$  of the  $^3\text{He}$  to be evolved (Fig. 3). In an interesting side note, Pepin was studying the Apollo samples in a purely scientific manner and had no idea of the value associated with  $^3\text{He}$  in fusion. This information was in the scientific literature for more than 15 years before fusion scientists at the University of Wisconsin "rediscovered" it.

Knowing that the  $^3\text{He}$  could be extracted by heating the regolith allowed other scientists at Wisconsin to design equipment capable of operating in the lunar environment. Sviatoslavsky and co-workers<sup>16-18</sup> designed lunar mining equipment (see Fig. 4) that is capable of collecting the loose regolith, separating the material to grains less than 50 microns in diameter, and heating the regolith to  $\approx 700^\circ\text{C}$  using the indigenous energy source, the sun. Once the solar wind volatiles have been evolved and collected in gas tanks, the warm spent regolith is passed through a

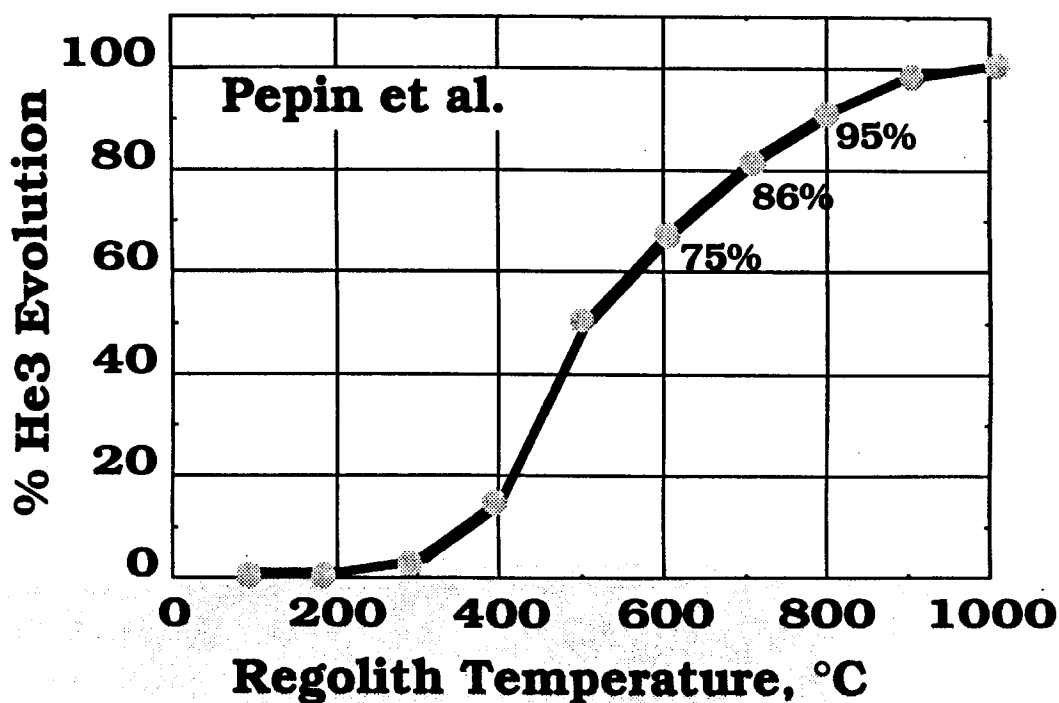


Fig. 3. Early experiments by Pepin<sup>(15)</sup> revealed the temperatures required to evolve  $^3\text{He}$ .



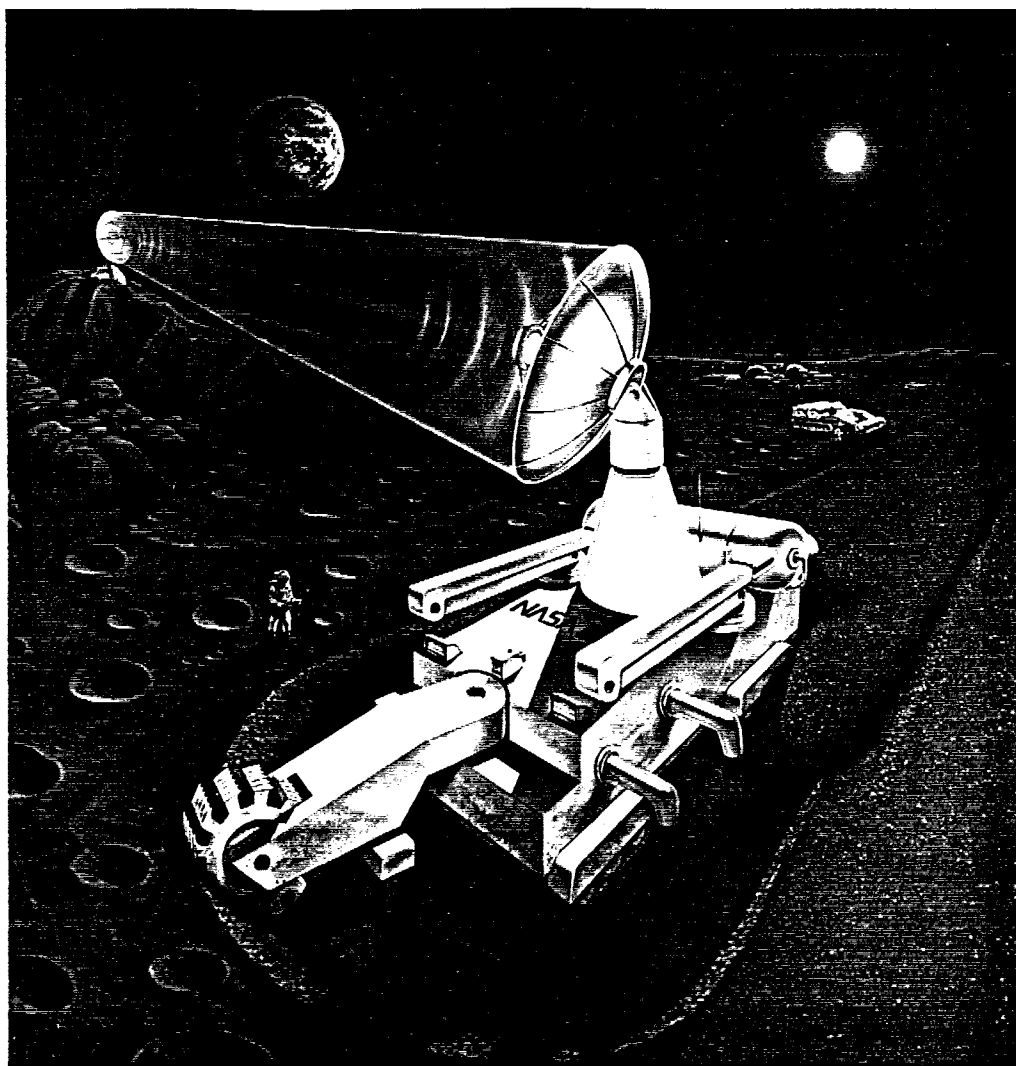


Fig. 4. The Lunar Volatiles Miner designed at the University of Wisconsin makes use of the "local" energy supply.<sup>18</sup>

regenerative heat exchanger to heat the incoming, colder regolith. The spent regolith is then returned to the lunar surface thus avoiding the transport of large amounts of lunar material around the lunar surface.

## 5. Important By-Products from Lunar $^3\text{He}$ Mining

In addition to the important  $^3\text{He}$  isotope, several other elements and compounds are released from the lunar regolith during the heating process. For every tonne of  $^3\text{He}$  collected large amounts of valuable gases will also be produced<sup>19</sup> (see Fig. 5). The water comes from the reaction of the implanted hydrogen and the oxygen in the lunar regolith ( $\approx 50\%$  by weight).

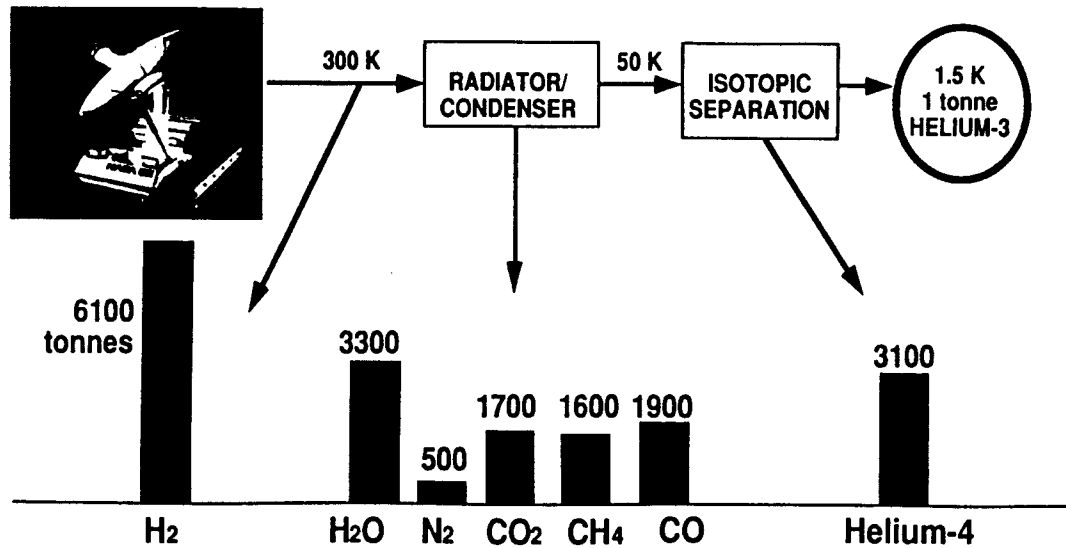


Fig. 5. The volatiles associated with  $^3\text{He}$  extraction can have an enormous effect on the ability of society to support a human occupied base on the moon.

The  $\text{H}_2$  is removed first through a heated permeable Pd membrane. Next, the mixture of gases is allowed to cool during the (14 earth day) lunar night by radiation to outer space. This will bring the temperature down to  $\approx 50^\circ\text{K}$  where all the gases except the He will be either liquified or solidified. The separation of  $^3\text{He}$  from  $^4\text{He}$  takes place using "superleak"<sup>7</sup> techniques at very low temperatures ( $< 4^\circ\text{K}$ ). The low temperatures are provided by cryogenerators run by batteries charged by solar energy during the 14 earth day lunar day. The important feature of this process is that most of the energy required to extract and separate the  $^3\text{He}$  is provided by the sun and the "coldness" of outer space. Hence the energy payback from this scheme will be very favorable.

It should be obvious that the lunar volatile by-products will be extremely valuable to the development of bases on the moon and even Mars. The 18,200 tonnes of gases generated per tonne of  $^3\text{He}$  can be used for propellant, growing of food, life support, atmosphere control, pressurization, etc. To transport that much mass to the Moon, even at one tenth the launch costs of today ( $\approx \$10,000/\text{kg}$ ), would cost 18 \$B! And that is only if one tonne of  $^3\text{He}$  is produced. Clearly, the benefits of the other lunar volatiles will be of equal or higher value than the  $^3\text{He}$  itself.

## 6. Energy Payback For Lunar $^3\text{He}$ Mining

An estimate of the energy payback ratio for mining  $^3\text{He}$  can be made by knowing the mass of mining, processing, and associated personnel related equipment required to produce a kg of  $^3\text{He}$ .<sup>20,21</sup> Figure 6 shows the mass required and coupling this with the energy involved in transportation,<sup>20</sup> results in 2085 GJ per kg of  $^3\text{He}$  delivered to the earth. Since the fusion of 1 kg of  $^3\text{He}$  with D produces  $\approx 600,000$  GJ of energy, we conclude that the energy payback is  $\approx 300$  to 1. When the construction of the power plant is included, this ratio drops to  $\approx 80$  to 1.<sup>21</sup>

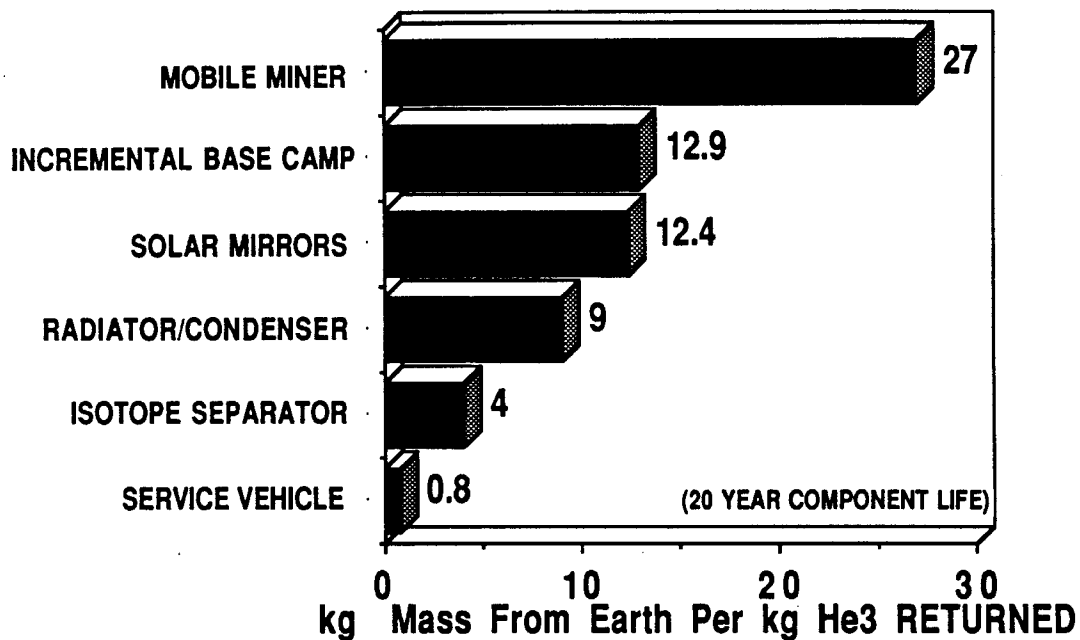


Fig. 6. The mass required to mine  $^3\text{He}$  on the moon is dominated by the mass of the miner.<sup>20,21</sup>

## 7. Economic Value of $^3\text{He}$

The value of an energy resource is not always based on a straight substitution for other forms of energy. Factors such as waste disposal, safety, dependability, etc., can also have a major impact. However, at this point in time we can make some rough estimates of the economic value of  $^3\text{He}$  based on historical energy prices. For example, the U.S. spent  $\approx 50$  \$B for fuels alone to make electricity in 1990. If 25 tonnes of  $^3\text{He}$  will produce the same amount of electricity, then one

might conclude that  $^3\text{He}$  was worth  $\approx 2$  \$B/tonne. This assumes that the cost of the facilities to make the electricity from either fuel is the same.

Another estimate could be made by considering the allowable contribution to the cost of electricity, or mills/kWh for the fuel. If we assume that the fusion fuel can contribute  $\approx 10$  mills/kWh, then the  $^3\text{He}$  is worth  $\approx 1$  \$B/tonne. Note that coal contributes  $\approx 18$  mills/kWh in the U.S. and the fission fuel cycle contributes  $\approx 10$  mills/kWh.

One might also compare the energy in  $^3\text{He}$  to oil. At 1 \$B/tonne for  $^3\text{He}$ , this would make  $^3\text{He}$  equivalent to oil at 7 \$/barrel or coal at 15 \$/tonne. Both of these values are far below the current cost of oil (20 \$/barrel) and coal (20 \$/tonne), indicating that  $^3\text{He}$  is worth more than 1 billion dollars/tonne.

A recent NASA sponsored study<sup>22</sup> showed that even at 1 billion dollars/tonne, the rate of return on investment for the research, development, collection, and delivery of  $^3\text{He}$  is  $>20\%$  even without use of the valuable by-products. Work by Ott<sup>23</sup> shows that government investment in this technology would justify the 15 to 20% rate of return.

The conclusion is that the value of  $^3\text{He}$  is at least 1 billion dollars/tonne on the earth and that such a value should be sufficient to stimulate investment if 10's of tonnes were to be needed per year.

## 8. Other Considerations

The legal regimes for mining  $^3\text{He}$  have been investigated by Bilder et al.<sup>24</sup> and the conclusion of that study was that the present international treaty structure is sufficient to insure that  $^3\text{He}$  could be commercialized. A proposal for an international company called INTERLUNE was made and possible internationalization mechanisms outlined.<sup>25</sup> The problem is not one of politics as much as one of technology.

The question of the net environmental impact to the moon and the earth has been examined by Cameron et al.<sup>22</sup> The conclusion from that study was that the detrimental effects to the moon would be very small and that the beneficial effects to the earth would be large. The main concern

on the moon was the potential for spoiling the vacuum around the moon and for changing the reflectance of the area mined. Both problems seem to be easily solved or of little consequence in the long run.

## 9. Timing

There are two technologies to consider in this case: the commercialization of  $D^3He$  fusion reactors, and the establishment of lunar bases for the mining equipment. Figure 7 presents one possible scenario for the simultaneous development of both technologies. The present world fusion program is on the verge of achieving the first breakeven experiments with DT and getting ready for the construction of a 1000 MW reactor called ITER.<sup>26</sup> It is expected that ITER will operate shortly after the turn of the century. With minor modifications of ITER, it is possible that we could approach the ignition point in  $D^3He$  early in its operating sequence.<sup>27</sup> Assuming that a successful reactor grade plasma can be produced in ITER, it could then be shut down, refitted with power reactor components, and restarted as a demonstration power plant by 2010. Meanwhile, the design of a commercial power plant could be conducted so that as soon as successful operation of the demo plant was achieved, construction could begin on the commercial unit. In this case, one might have commercial electricity by the year 2015. All of this development could be accomplished with the  $^3He$  presently on the earth.

The timetable for the return to the moon is probably a bit more certain than the fusion schedule. After robotic missions in the 1990's, it is anticipated that humans will again be on the moon by the first decade of the 21st century. It will probably take 5 years or so to establish a permanent base and thereafter small, mobile miners can be utilized to demonstrate the volatile collection process. By the year 2015, 100 kg quantities of  $^3He$  could be returned to the earth and industrial sized miners could be in place to increase the output to the tonne/y level. The generation of valuable by-products could be used to finance the operation.

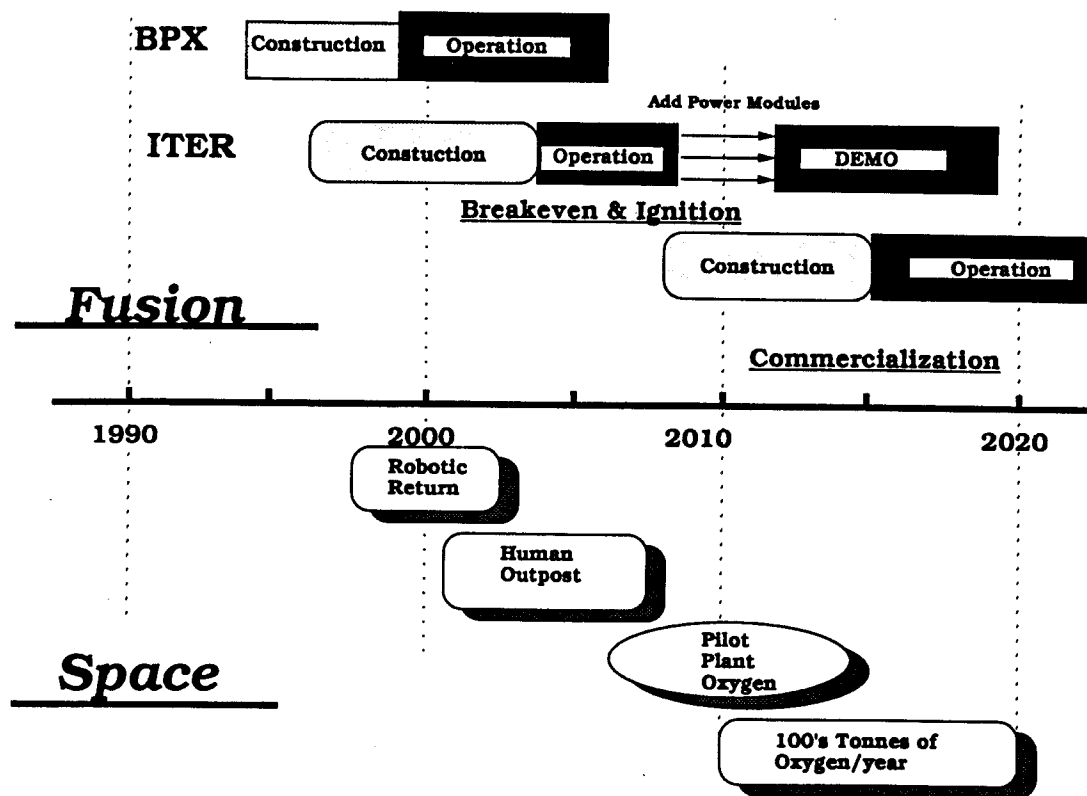


Fig. 7. The schedules for the commercialization of fusion and the return to the moon are compatible with the use of lunar  $^3\text{He}$ .

## 10. Conclusion

For the first time in human history, we have found a portable energy source in space that could satisfy the energy needs of the earth for 100's of years to come. It could do this while greatly improving our environment and in a manner which is both safe and efficient. The problem that lies before use is to, on the one hand, demonstrate that a  $\text{D}^3\text{He}$  plasma can be produced and controlled in an economical manner, while at the same time, demonstrate that  $^3\text{He}$  can be obtained in a dependable, and economical fashion. This will require the efforts of both the energy and space communities in parallel. The successful use of lunar resources may open a whole new era of international collaboration and could replace the intense military competition which has prevailed for the past 4 decades.

## Acknowledgements

The author is grateful to NASA, Office of Commercialization and the Grainger Foundation for support of this work.

## References

1. *Ra: A High Efficiency, D-<sup>3</sup>He, Tandem Mirror Fusion Reactor*; J.F. Santarius, H.M. Attaya, M.L. Corradini, L.A. El-Guebaly, G.A. Emmert, G.L. Kulcinski, E.M. Larsen, C.W. Maynard, Z. Musicki, M.E. Sawan, I.N. Sviatoslavsky, W.F. Vogelsang, P.L. Walstrom and L.J. Wittenberg, October 1987, 12th Symposium on Fusion Engineering, Monterey, CA, Proceedings, Vol. 1, p. 752.
2. *The Commercial Potential of D-He<sup>3</sup> Fusion Reactors*; G.L. Kulcinski, I.N. Sviatoslavsky, G.A. Emmert, H.M. Attaya, J.F. Santarius, M.E. Sawan and Z. Musicki, October 1987, 12th Symposium on Fusion Engineering, Monterey, CA, Proceedings, Vol. 1, p. 772.
3. *Apollo - An Advanced Fuel Fusion Power Reactor for the 21st Century*; G.L. Kulcinski, G.A. Emmert, J.P. Blanchard, L. El-Guebaly, H.Y. Khater, J.F. Santarius, M.E. Sawan, I.N. Sviatoslavsky, L.J. Wittenberg, R.J. Witt, Fusion Technology, 15, 1233 (1989).
4. *Apollo-L2, An Advanced Fuel Tokamak Reactor Utilizing Direct Conversion*; G.A. Emmert, G.L. Kulcinski, J.P. Blanchard, L.A. El-Guebaly, H.Y. Khater, J.F. Santarius, M.E. Sawan, I.N. Sviatoslavsky, L.J. Wittenberg, R.J. Witt, Proc. of 13th Symposium on Fusion Engineering, Knoxville, TN, 1989 (IEEE, 1990), p. 1043.
5. *Apollo-L3, An Advanced Fuel Fusion Power Reactor Utilizing Direct and Thermal Energy Conversion*, G.L. Kulcinski, G.A. Emmert, J.P. Blanchard, L.A. El-Guebaly, H.Y. Khater, C.W. Maynard, E.A. Mogahed, J.F. Santarius, M.E. Sawan, I.N. Sviatoslavsky, L.J. Wittenberg, Ninth Topical Meeting on the Technology of Fusion Energy, Oak Brook, IL, October 7-11, 1990, Fusion Technology, 19, 791 (1991).

6. *An Improved First Stability Advanced Fuel Tokamak, Apollo-L3*; G.A. Emmert, G.L. Kulcinski, J.P. Blanchard, L.A. El-Guebaly, H.Y. Khater, C.W. Maynard, E.A. Mogahed, J.F. Santarius, M.E. Sawan, I.N. Sviatoslavsky, L.J. Wittenberg, 14<sup>th</sup> IEEE/NPSS Symposium on Fusion Engineering, 30 September - 3 October 1991, San Diego CA, (submitted to Fusion Technology).
7. *Lunar Source of He-3 for Commercial Fusion Power*; L.J. Wittenberg, J.F. Santarius and G.L. Kulcinski, *Fusion Technology*, 10, 167 (1986).
8. *D<sup>3</sup>He Fusion in the JET Tokamak: Recent Experimental Results*, J. Jacquinot and G. Sadler, to be published, Fusion Technology.
9. *Recent TFTR Results*, D. M. Meade et al., Paper IAEA-CN-53/A-I-1 in Plasma Physics and Controlled Nuclear Fusion Research 1990, IAEA Vienna, 9 (1991).
10. *Titanium in Lunar Regolith and Its Use in Mining Site Selection*; E.N. Cameron, WCSAR-TR-AR3-8708 (1987).
11. *Helium Mining on the Moon: Site Selection and Evaluation*; E.N. Cameron, April 1988, Lunar Bases and Space Activities of the 21st Century Second Symposium (Lunar and Planetary Institute, Houston, 1989).
12. *Helium-3 From the Moon - An Alternative Source of Energy*, E.N. Cameron and G.L. Kulcinski, International Conference on Environmental Issues and Management of Waste in Energy and Mineral Production, Battelle Memorial Institute (1992), pp. 319-357.
13. *Thermal Analysis and Inorganic Gas Release Studies of Lunar Samples*, E.K. Gibson, Jr. and S.M. Johnson, Proc. 2nd Lunar Sci. Conf., Vol. 2, 1351 (1971).
14. *Predictions of He Distributions at the Lunar Surface*, M.L. Jordan, Symp. Space, Mining, and Manufacturing, University of Arizona, p. VII-38 (1989).
15. R.O. Pepin et al., Proc. First Apollo 11 Scientific Conference, Vol. 2, 1435 (1970).



16. *Mobile Helium-3 Mining System and Its Benefits Toward Lunar Base Self-Sufficiency*; I.N. Sviatoslavsky and M. Jacobs, August 1988, Engineering, Construction and Operations in Space, Proc. of Space 88 (ASCE, 1988), p. 310.
17. *Lunar Surface Mining for Automated Acquisition of Helium-3: Methods, Processes and Equipment*; Y.T. Li and L.J. Wittenberg, April 1988, Lunar Bases and Space Activities of the 21st Century Second Symposium (Lunar and Planetary Institute, Houston, 1989).
18. *Lunar He-3 Mining: Improvements on the Design of the UW Mark II Miner*, I.N. Sviatoslavsky, Space '92 Conference on Engineering, Construction and Operations in Space, May 31 - June 4, 1992, Denver, CO.
19. *Potential of Derived Lunar Volatiles for Life Support*; R.J. Bula, L.J. Wittenberg, T.W. Tibbits, and G.L. Kulcinski, April 1988, Lunar Bases and Space Activities of the 21st Century Second Symposium (Lunar and Planetary Institute, Houston, 1989).
20. *Energy Requirements for Helium-3 Mining Operations on the Moon*; G.L. Kulcinski, I.N. Sviatoslavsky, J.F. Santarius, L.J. Wittenberg, E.N. Cameron, T.N. Crabb and M.K. Jacobs, Space Nuclear Power Systems 1988 (Orbit, 1989), pp. 77-82.
21. *Processes and Energy Cost for Mining Lunar Helium-3*; I.N. Sviatoslavsky, Lunar Helium-3 and Fusion Power NASA Conference Publication 10018, held at NASA-Lewis, April 25-26, 1988.
22. *Analysis of the Financial Factors Governing the Profitability of Lunar Helium-3*; G.L. Kulcinski, H. Thompson and S. Ott, Report of the Lunar Energy Enterprise Case Study Task Force, NASA Technical Memorandum 101652 (July 1989), pp. 40-55.
23. *Economic Analysis of the Use of Lunar Helium-3 as a Fuel in the U.S. Energy Policy*, Howard Thompson, Steve Ott and Gerald Kulcinski, submitted to Energy Economics, 1991.
24. *Legal Regimes for the Mining of Helium-3 from the Moon*; R.B. Bilder, E.N. Cameron, G.L. Kulcinski, H.H. Schmitt, WCSAR-TR-AR3-8901-1 (1989).

25. *INTERLUNE Concept for Helium-3 Fusion Development*, H.H. Schmitt, Space '92 Conference on Engineering, Construction and Operations in Space, May 31 - June 4, 1992, Denver, CO.
26. *ITER Conceptual Design Report*, ITER Documentation Series, No. 18, IAEA, Vienna.
27. *Breakeven and Ignition Conditions for D-<sup>3</sup>He Fusion*; G.A. Emmert, L.A. El-Guebaly, R. Klingelhöfer, G.L. Kulcinski, J.F. Santarius, J.E. Scharer, I.N. Sviatoslavsky, P.L. Walstrom, L.J. Wittenberg, Proceedings of the Fifth International Conference on Emerging Nuclear Energy Systems (Karlsruhe, FRG, 3-6 July 1989), pp. 188-191.

Lunar-surface automatic units:  
Present possibilities and development prospects

Academician V.P.Barmin, Prof. I.V.Barmin,  
Dip.Eng. A.S.Borisov

DBGM

The success of the program on creating a power system on the basis of using lunar  $^3\text{He}$  in the nearest decade will be determined by two factors. The first one, obvious and decisive, is progress in the field of thermonuclear power. The other important factor is the resumption of operations on the lunar surface.

Almost a 15-years interval in lunar exploration, and this is noted by Soviet and foreign specialists, has resulted in essential losses of the technological experience of the lunar programs realization, obtained by the end of the seventies. At the same time the transfer to a stage of creating lunar bases, an industrial infrastructure on the Moon surface is impossible without essential modification of such traditionally earth disciplines, as vehicles, mining machinery, building etc., for operation in space.

The resumption of the Moon exploration is also important for search of areas with a higher concentration of  $^3\text{He}$  in lunar regolith, since a detailed clarification of this question is also important for selecting sites for lunar bases and for determining detailed requirements for a lunar-surface technological complex at the earliest stages of its development. For example, in case of discovering local zones with industrial stores of regolith on the Moon, its mining may be optimal with using equipment of an open-cut type.

We considered that the first experiments on the Moon on the power program must include:

- experiments on discovering areas, where mineralogical composition of regolith contributes to accumulating  $^3\text{He}$ . For solving this problem it is reasonable to use a method of taking cores from a depth up to several meters without disturbing soil stratification, with its subsequent delivery to the Earth;

- experiments on discovering zones with industrial stores of regolith of deep bedding.

The experiment, in this case, must consist of a complex of studies, including geophysical probing (seismic and electric prospecting etc.), to control the interface "continent base-regolith", drilling to a depth of over 10 meters without disturbing the granulometric composition of the soil with the subsequent analysis of its physical-chemical properties. Such studies can be carried out by an automated station. The experimental gear of this station includes: a seismic unit with equipment for scattering detonating charges to a distance from several tens to hundreds of meters, a drilling unit of depth drilling for taking cores for the subsequent analysis, a complex of devices for determining element, granulometric composition and other parameters of the lunar soil.

The realization of the above-mentioned experiments in the nearest years is possible only by using the rocket system Proton, functioning at the present time.

With the help of this system lunokhods were delivered to the Moon surface, and in 1976 operations were ensured on taking a core of the lunar soil with its subsequent delivery to the Earth.

The soil-taking drilling unit ГЗУ/Б09, developed by the DBGM for this experiment, carried out the following tasks:

- drilling lunar soil to a depth of 2.5m;
- taking the selected soil column to a taking drum without disturbing the sample stratification;
- delivery of the drum with a soil-carrier into the re-entry vehicle of the Luna 24 station.

The technical data of the ГЗУ/Б09 unit are:

- mass of the soil-taking unit with a control block, kg - 54.5;
- mass of the soil taken, g - 130-250;
- drilling speed, cm/min - 15.

The ГЗУ/Б09 unit construction is designed for drilling various soils: from hard rocks to soft dust rocks, including separate stones of various dimensions.

The main problem of the ГЗУ/Б09 unit was taking a long ( up to 2.5m ) soil column with undisturbed soil stratification.

According to our estimations, the ГЗУ/Б09 unit after the corresponding modernization can be used for exploring lunar areas with good prospects, from the mineralogical-composition

point of view, for <sup>3</sup>He extraction.

As it is known, the scientific possibilities of the lunokhods were extremely limited. It was mainly caused by an extremely small weight of its payload. The version of delivering a stationary station on the the basis of the landing rocket and space lunokhod stage, the mass of the experimental gear increases to several hundreds of kilograms.

The design estimations, carried out by our organization, show that with these weight possibilities it is quite practicable to create a multipurpose automated research laboratory on the Moon with a possibility of carrying out depth drilling with taking soil samples and carrying out well logging.

The experiment program is based, as it was already noted, on the means of the launch vehicle Proton, being in operation.

However, its realization will certainly depend not only on the estimation of its significance for the power program, but also on a degree of support, including financial one, of the world association.

# ANALYSIS OF CRYOGENIC TECHNOLOGY OF PURIFICATION OF THE LUNAR HELIUM AND SEPARATION OF ITS ISOTOPS

J.S.Zhitomirsky, V.A.Mikheev, E.Ya.Rudavsky

Institute for Low Temperature Physics and Engineering, Kharkov

A new promising source of energy is being discussed lately, which is based on the thermonuclear fusion of  $D - {}^3\text{He}$  <sup>1,2</sup>. This method of energy production however requires large amounts of pure  ${}^3\text{He}$ . Since the Earth sources of  ${}^3\text{He}$  are strictly limited, the idea of using the lunar supplies of the element, which is available in the lunar dust - regolithe, seems to be quite attractive.

To produce 1 kg  ${}^3\text{He}$ , about  $10^5$  tons of regolithe must be processed. On heating this amount of regolithe, 6.1 t hydrogen, 3.6 t carbon oxides, 3.3 t water, 3.1 t  ${}^4\text{He}$ , 1.6 t methane and 0.5 t nitrogen are released in addition to  ${}^3\text{He}$  <sup>1</sup>. It is then necessary to extract  ${}^3\text{He}$  from the gas mixture, in which its volume concentration is not more than  $10^{-4}$ .

Here we propose and analyse a commercial setup for a 1 kg/day production of the lunar  ${}^3\text{He}$ . According to <sup>1</sup>, the lunar dust is annealed at 900 K under the pressure 0.02 MPa. Regolithe is fed to furnace 1 from quarry 2 by conveyor 3 (Fig.1). The raw regolithe is preliminary heated by the reverse flow of annealed regolithe 4 directed to waste 5, as well as by gas flow 6 from the furnace.

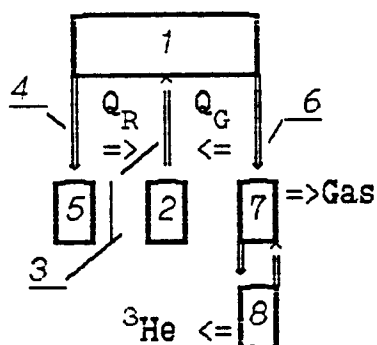


Fig.1

On cooling to 400 K, the gas transmits the heat flux  $Q_G = 60 \text{ GJ/kg } {}^3\text{He}$  to regolithe, which corresponds to about 700 kW power. The gas mixture at 400 K is supplied to block 7, where helium is freed from impurities, cooled to 2 K and liquefied. Finally, in block 8 the  ${}^3\text{He}$  isotope is separated, and  ${}^4\text{He}$  is fed to the reverse flow of block 7, where it is used to cool the direct flow.

Block of helium purification and cooling. The purification process begins in a palladium diffusion filter, after which the content in the mixture of the hydrogen diffusible outwards drops down to negligible values.

In addition to the filter, there is an eight-stage cascade of cooling and purification; each of them consists of a recuperative heat exchanger, a cold source for additional cooling of the direct flow compensating the heat exchanger imperfection.

A radiator with the surface temperature  $\approx 270$  K releasing heat to space is used as a cold source at the first stage. As the direct flow passes through this stage, about 80 % water vapors are condensed and discharged to a special storage, which gives about 2.7 t water per day. The radiator discharges the heat flow of about 85 kW, which requires that the radiator area should be  $\approx 300$  m<sup>2</sup>.

Each subsequent stage (Fig.2) of the block incorporates refrigerator 3 as a cold source. The thermomechanical compressor in these refrigerators appears to be more energy-advantageous than the conventional mechanical one, since it needs no additional energy transformations which usually results in considerable losses.

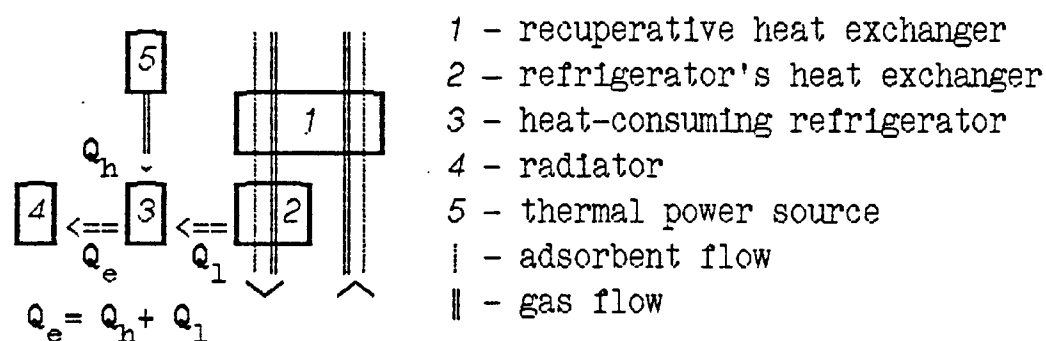


Fig.2

The thermal power for the thermomechanical compressors is gained during the Moon day using solar radiation concentrators. To provide for a 24-hour operation, a thermal accumulator should be used during the Moon nights, which last for about 7.5 Earth days. The best known thermal accumulators using lithium salts as a working body have energy capacity of about 4.5 GJ/m<sup>3</sup>. In the situation considered, it is reasonable to use a thermal accumulator common for the whole system and connected by heat pipes with self-contained Taconis-Vuilleumier type refrigerators at each stage.

Each refrigerator consuming the thermal power  $Q_h$  at a high temperature level  $T_h \approx 900$  K and taking its thermal payload  $Q_1$

at the corresponding level  $T_l$  should discharge the heat flow  $Q_e = Q_h + Q_l$  from the radiator at a certain intermediate level  $T_e$  ( $T_l < T_e < T_h$ ). The lower is  $T_e$ , the smaller is the Carnot factor  $\tau_c = (T_e / T_l - 1) / (1 - T_e / T_h)$  relating the possible minimum heat consumptions  $Q_h^0$  to the net refrigerating capacity  $Q_l$ :  $Q_h^0 = \tau_c Q_l$ . The real heat consumption  $Q_h$  is found from the relation  $Q_h = Q_h^0 / \eta_e$ , where  $\eta_e$  is exergetic efficiency of the refrigerator. On the other hand, a decrease in  $T_e$  would require a greater radiator area  $A$  to discharge the heat  $Q_e$ :  $A = Q_e / (\sigma T_e^4)$ , where  $\sigma$  is the Stefan-Boltzmann constant.

According to literature data <sup>4-6</sup>, the exergetic efficiency for the refrigerators considered decreases from  $\eta_e = 0.15$  to  $\eta_e = 0.05$  as the temperature level drops from 135 K to 2 K. It is possible that by the end of the century, the refrigerator efficiency would be improved at the 2 to 5 K levels using the combined refrigerating effect of gas expansion and the magnetocaloric effect.

Helium may be freed from impurities using both adsorption and condensation processes. Although adsorption has greater latent heat than condensation, it is more advantageous, since no condensed impurity precipitations remain in the heat exchanger channels after adsorption, which permits the use of more advanced heat exchangers with efficiency up to 0.97. Besides, adsorption occurs at higher temperature than condensation, hence the refrigerator withdrawing the adsorption heat operates at the lower Carnot factor.

The adsorbent is expected to be placed into containers mounted on the conveyor belt, which moves the adsorbent towards lower temperatures in the channels of direct flow and towards higher temperatures in the reverse flow. The container with the adsorbent moves from the reverse flow channel to the direct one at  $T \approx 270$  K and backwards at  $T \approx 2$  K through special seals. The adsorption heat discharge in the direct flow and its absorption in the reverse flow produce an additional thermal load both on the heat exchangers and on the refrigerators.

The parameters of individual stages of the block calculated taking into account the above factors are given in Table 1 and the integral block parameters in Table 2.



Table 1

Stage No	2	3	4	5	6	7	8
$T_l$ , K	135	75	30	11	5	2.4	2
$Q_l$ , W	2200	1500	350	104	35	15	18
$Q_h$ , kW	$T_e=300$ K	27	56	47	45.5	44	46.5
	$T_e=200$ K	9	27	25.5	25.5	25	26.5
							80.5
							46

Table 2

	$\Sigma Q_h$ , GJ/kg $^3\text{He}$	$V$ , m <sup>3</sup>	$A_\Sigma$ , m <sup>2</sup>
$T_e=300$ K	30	50	800
$T_e=200$ K	16	30	2100

As seen in Table 2, the decrease in the heat discharge temperature from 300 K to 200 K only slightly influences the necessary supply  $\Sigma Q_h$  and the thermal accumulator volume  $V$  but requires an essentially larger radiator area  $A_\Sigma$ . One may expect that a more detailed study and allowance for all the attending factors would give the optimum  $T_e$  close to 300 K. Note that  $\Sigma Q_h$  in Table 2 significantly exceeds that in <sup>1</sup>. The difference results from the choice of a more realistic coefficient  $\eta_e$  and higher temperature of heat discharge.

**Block of helium isotope separation.** The liquid helium from the foregoing block at 2 K is a mixture of  $^4\text{He}$ - $^3\text{He}$  isotopes with  $^3\text{He}$  concentration of  $\approx 0.03$  %. To separate this isotope, the specific superfluid features should be exploited. The combination of thermosmosis and rectification were shown <sup>7-10</sup> to be the most effective method of helium isotope separation. In practice <sup>9-10</sup> the use of the thermomechanical effect can give the solution with not more than 5 or 6 %  $^3\text{He}$ , the further separation requires rectification <sup>11-13</sup>.

The scheme for separation of  $^3\text{He}$ - $^4\text{He}$  solutions is presented in fig.3. The solution with initial concentration enters duct 1 and the first enrichment occurs due to the thermomechanical effect through superleak 2. The heat power  $Q_1$  which is needed for realization of the thermomechanical effect is supplied from the warmer parts of the installation. The outlet flow of  $^4\text{He}$  is carried out by the duct 3.

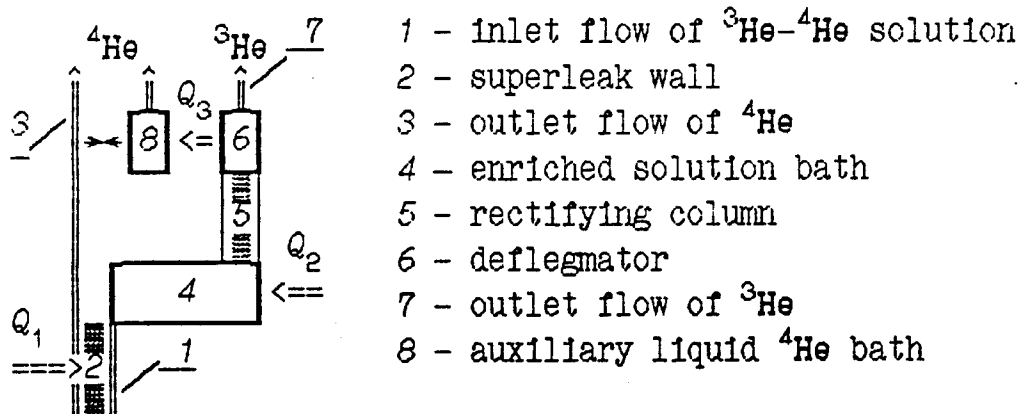


Fig.3

After the first stage of enrichment the solution with concentration a few per cent  ${}^3\text{He}$  enters bath 4 of rectifying column 5. The heat power  $Q_2$  to the bath is provided from the warmer parts of the device too. The rectification is the second stage of enrichment of the solution.

The cold level of  $\approx 1.8$  K required for operation of deflegmator 6 is provided by auxiliary liquid  ${}^4\text{He}$  bath 8 pumped off into space. After the rectification the pure  ${}^3\text{He}$  is removed through duct 7.

If the rectifying column capacity is  $5 \cdot 10^{-5}$  mole/s, about 80 columns must be employed to obtain 1 kg  ${}^3\text{He}$  per day. In this case it is necessary to withdraw about 3.1 t  ${}^4\text{He}$ . If conventional thermomechanical pumps, e.g. those used in dilution refrigerators with  ${}^4\text{He}$  circulation and providing  $2 \cdot 10^{-3}$  mole/s circulation<sup>14</sup>, are used, this would require 9000 pumps of this kind.

The system may be simplified using a porous wall as a "distributed pump" to substitute individual thermomechanical pumps. The heat from the direct flow in the final stage of the purification and cooling block acts as a thermal source providing the thermomechanical effect.

### References

1. Wittenberg L.W., Santaris J.F., Kulcinski G.L. Lunar source of  ${}^3\text{He}$  for commercial fusion power// *Fus.Techn.*, 1986, 10.- P.165-178.
2. Головин И.Н. Малорадиоактивный управляемый термоядерный синтез (реакторы с D- ${}^3\text{He}$ ). Препринт ИАЭБ 4885/8.- 1989.- 48 с.
3. Ридер Г., Хупер Ч. Двигатели Стирлинга. - М.: Мир.- 1986.- 464 с.
4. Автономные криорефрижераторы малой мощности/ М.Ю.Боярс-

кий, А.Б.Грачев, Н.В.Калинин и др.: под ред. В.М.Бродянского.- М.: Энергоатомиздат.- 1984.-208 с.

5. Криогенные системы/ А.М.Архаров, В.П.Беляков, Е.И.Микулин и др.- М.: Машиностроение.-1987.-536 с.

6. Баррон Р.Ф. Криогенные системы.-М.:Энергоатомиздат.-1989.-408 с.

7. Растворы квантовых жидкостей/ Б.Н.Есельсон, В.Н.Григорьев, В.Г.Иванцов и др.- М.: Наука. - 1973.- 424 с.

8. Есельсон Б.Н., Лазарев Б.Г. Некоторые свойства растворов  $^3\text{He}$  в  $^4\text{He}$ . I.Разделение изотопов гелия/ ЖЭТФ.-1950.-20.-С. 742-751.

9. Пешков В.П. Опыты по обогащению гелия изотопом  $^3\text{He}$  // ЖЭТФ.-1956.-30.-в.5.-С. 850-854.

10. Кузнецов В.М. Разделение изотопов гелия ректификацией и термоосмосом // ЖЭТФ.-1957.-32.-в.5.- С. 1001-1011.

11. Gifford R.P., Harrison R.B., Hatton J., Truscott W.S. Rectification column for purifying  $^3\text{He}$  // Cryogenics.-1967.-7.-No.3.-P. 179-180.

12. Sherman R.H. The separation of  $^3\text{He}$  from  $^3\text{He}$ - $^4\text{He}$  mixtures // Proc. LT-10.- М.: ВИНТИ.-1967.- С. 188-191.

13. Григорьев В.Н., Есельсон Б.Н., Михеев В.А., Толкачева О.Ф. Исследование ректификации смесей изотопов гелия в безнасадочных колонках // ЖЭТФ.-1967.-527.-в.4.-С. 871-879.

14. Pennings N.H., de Bruyn Ouboter, Taconis K.W. Leiden dilution refrigerator // Physica.-1976.-81B.-No.1.-P.101-106.

# D-<sup>3</sup>He Magnetic Fusion for Space Propulsion

John F. Santarius

*University of Wisconsin, Madison, WI 53706*

## Abstract

*This paper gives a brief overview of the reasons why magnetic fusion energy using the D-<sup>3</sup>He fuel cycle appears attractive for space applications—particularly space propulsion. The paper also surveys some fusion reactor configurations, examines the capabilities of these reactors, and explores the implications for space development. Based on several conceptual designs of fusion reactors for space propulsion, such systems could enable the efficient, large-scale exploration and development of the Solar System.*

## 1 Overview

Modern developments in fusion reactor science and technology now make possible the realization of a thirty-year old idea: that D-<sup>3</sup>He fusion reactors can provide very attractive space propulsion systems [1]. The key reason for this attractiveness is that high exhaust velocity (specific impulse) can be achieved at sufficient thrust-to-weight ratios for both fast, human transport and large-payload, cargo transport throughout the Solar System.

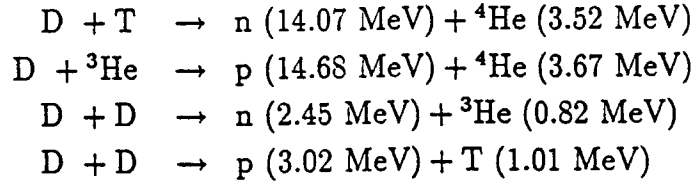
Advantages for D-<sup>3</sup>He fusion over chemical or nuclear fission reactors in space include:

- No radioactive materials are present at launch, and only low-level radioactivity is present after operation;
- Conceptual designs project higher specific power values (1–10 kW<sub>thrust</sub>/kg) for fusion than for nuclear-electric or solar-electric propulsion.
- Fusion gives high, flexible specific impulses (average exhaust velocity), enabling efficient long-range transportation.
- D-<sup>3</sup>He produces net energy and is available throughout the Solar System.
- D-<sup>3</sup>He fuel provides an extremely high energy density.

The fusion power density in a D-<sup>3</sup>He plasma is smaller than that of a D-T plasma, and, for this reason, the D-T fuel cycle is more commonly investigated for terrestrial fusion reactors. These two main fusion reactions, plus the important 'side' D-D reactions are shown in Table 1.

The charged fusion products from D-<sup>3</sup>He reactions can be guided to provide direct

Table 1: *Key fusion fuels, including main secondary reactions.*



thrust or electricity, whereas 80% of the energy from D-T reactions is produced as neutrons and requires more massive shielding, thermal cycle energy conversion at relatively low efficiency with larger radiator mass for waste heat rejection, and an intermediate system to convert the resulting electricity into thrust. The D-T fuel cycle also requires a tritium breeding blanket, adding a great deal of complexity to the system.

Depending on the configuration, the plasma exhausted from the core and used to provide thrust can range from  $\sim 10$  eV to  $\sim 1$  MeV. For hydrogen, this corresponds to  $\sim 4 \times 10^4$  m/s to  $\sim 10^7$  m/s. The high end of that range is not useful within the Solar System, so matter must be added to the exhausted plasma to decrease velocity and increase thrust. Traditionally, the average exhaust velocity is normalized to Earth's surface gravity and termed the *specific impulse*,  $I_{sp} = v_{ex}/g_0$ . A detailed discussion of rocket dynamics and so-called "low-thrust" trajectories may be found, for example, in Ref. [2].

In comparing D- ${}^3\text{He}$  fusion to other options, the specific impulse and the thrust-to-weight ratio (T/W) for the propulsion system are useful indicators of performance. These are plotted in Fig. 1 [3]. Fusion's capabilities lie in a niche important for propulsion throughout the Solar System:  $I_{sp} \sim 10^4$ – $10^5$  s and  $T/W \sim 10^{-3}$ .

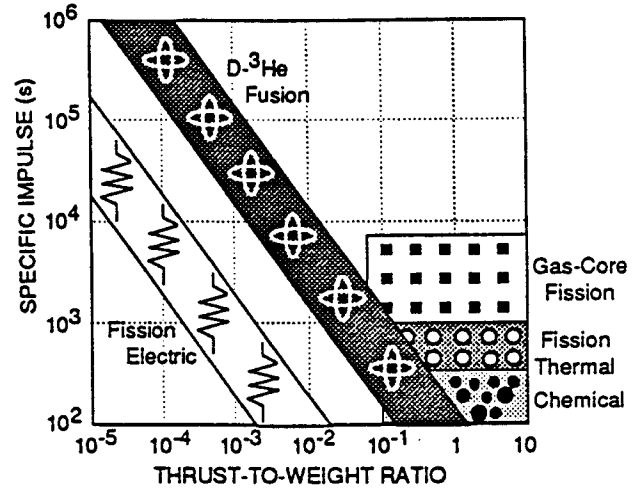
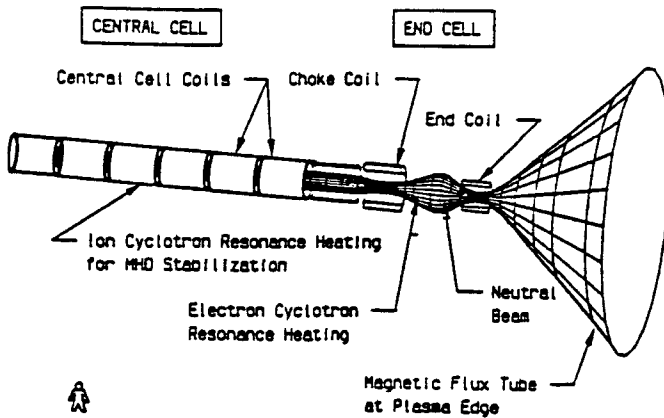


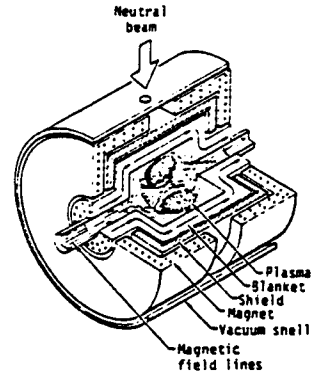
Figure 1: *Comparison of D- ${}^3\text{He}$  fusion with chemical, nuclear thermal, and nuclear electric propulsion systems.*

In addition to the technical advances in fusion energy research, two factors increase the timeliness of studying space fusion propulsion: (1) U.S. President Bush's Space Exploration Initiative [4] provides a framework and incentive for long-range space development, and (2) the identification of major resources of  ${}^3\text{He}$  on the Moon [5] solves, in principle, the problem of the scarcity of  ${}^3\text{He}$  on Earth. A review of research on terrestrial and lunar  ${}^3\text{He}$  resources is contained in Ref. [6].

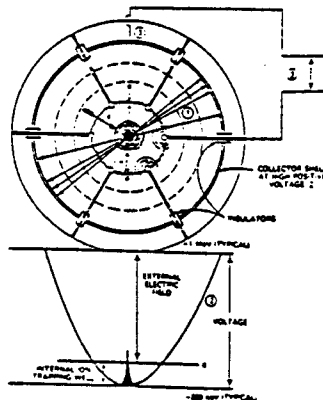
## Tandem Mirror



## FRC



## SCIF



## Dipole

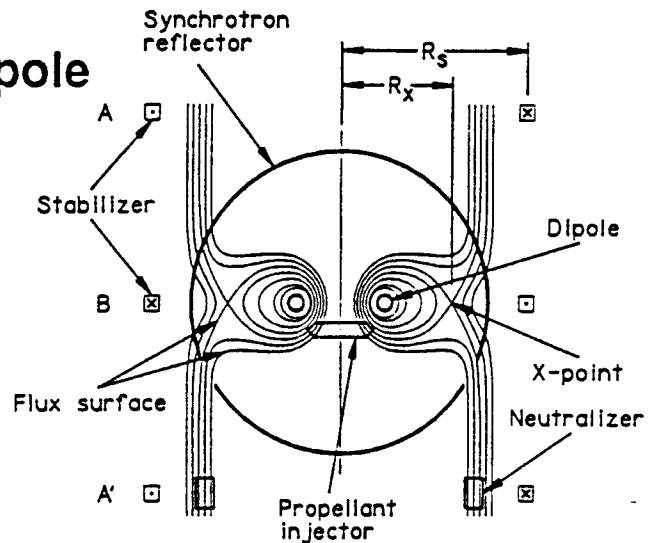


Figure 2: Some potential  $D^3He$  magnetic fusion propulsion configuration options [7, 16, 14, 3].

## 2 Potential Configurations

Several studies of space fusion propulsion have been performed, although all have been small in scope. They have included reactors of many configurations, such as:

- Simple mirror [1],
- Tandem mirror [7],
- Dipole [3],
- Field-reversed configuration (FRC) [8, 9, 10],

- Colliding compact toroids [11],
- Spheromak [12],
- Spherical torus (ST) [12],
- Bumpy torus [13], and
- Spherically convergent ion flow (SCIF) [14].

A discussion of some of these concepts, including a brief historical overview may be found in Ref. [15]. Figure 2 shows some configuration examples, and illustrates the diversity of fusion propulsion options.

### 3 Mission Capabilities

Magnetic fusion propulsion gains greatly in comparison to other options by the ability to optimize the thrust parameters as a function of time along the trajectory. The advantages of tunable systems have been known for some time [2], but a typical nuclear electric system, for example, is limited in its range of exhaust velocities. Figure 3 shows optimized  $I_{sp}$  and  $T/W$  over a three-month trajectory from Earth to Mars [2]. Note, from Fig. 1, that these parameters fall within the projected range for  $D-^3He$  magnetic fusion propulsion systems.

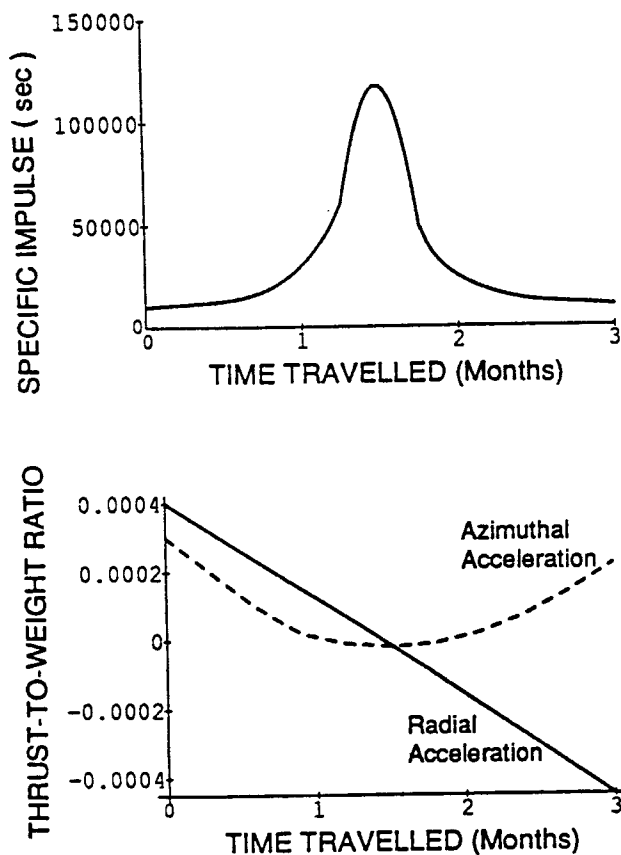


Figure 3: Specific impulse and thrust-to-weight values during an optimized, three-month trajectory from Earth to Mars.

Such performance leads to a continuum of capabilities from fast, human transport to large-payload, cargo transport. For these alternatives,  $D-^3He$  fusion propulsion is compared to chemical propulsion for one-way missions from Earth to Mars and to Jupiter in Figs. 4 and 5.

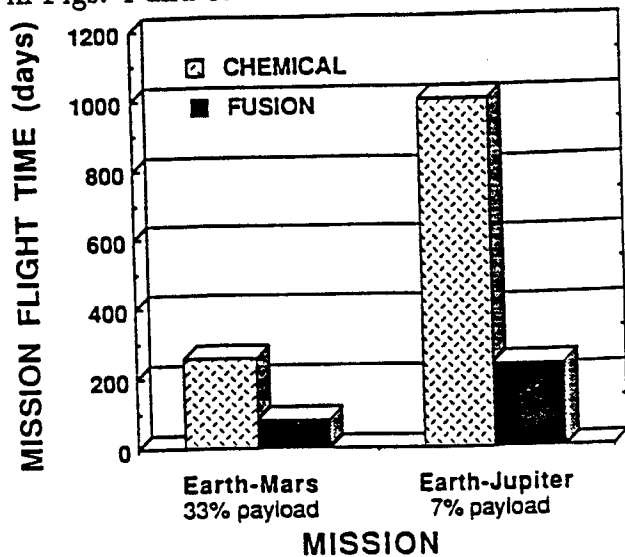


Figure 4: One-way flight time at the same payload fractions for chemical and  $D-^3He$  fusion missions from Earth to Mars and to Jupiter.

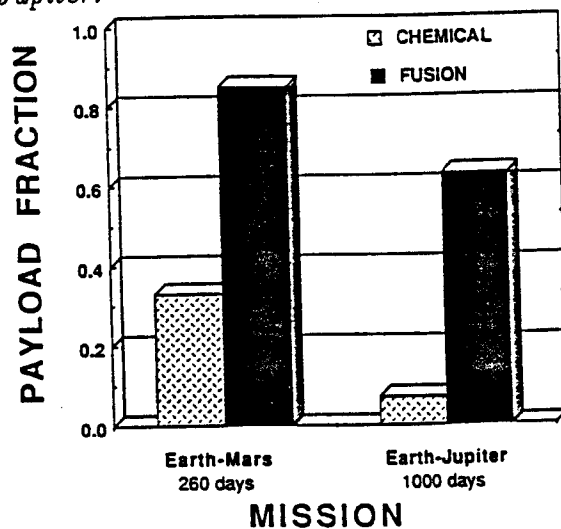


Figure 5: Payload fractions for same flight time for chemical and  $D-^3He$  fusion missions from Earth to Mars and to Jupiter.

These capabilities will enable large-scale development of the Solar System. Furthermore, D-<sup>3</sup>He fusion systems will enable scientific outposts analogous to Antarctic bases—with groups of scientists and technicians in orbit around the gas giant planets, for example. Fusion will be able to provide propulsion, space power, beamed power to surface bases, and materials processing. In particular, there presently appear to be no alternatives to D-<sup>3</sup>He fusion for the attractive ranges at very high specific impulse and modest thrust-to-weight ratios.

## 4 Conclusions

Magnetic fusion for space applications, particularly propulsion, appears attractive from both generic arguments and from pre-conceptual design studies. The key performance parameters are specific power  $\sim 1$ – $10$  kW/kg, specific impulse  $\sim 10^3$ – $10^6$  s, and thrust-to-weight ratio  $\sim 10^{-1}$ – $10^{-5}$ . Thus, D-<sup>3</sup>He magnetic fusion power can provide safe, efficient transport of humans and cargo, and can enable large-scale settlement and exploration of the Solar System.

## Acknowledgement

This research was funded by the Grainger Foundation and the University of Wisconsin.

## References

[1] G.W. Englert, "Towards Thermonuclear Rocket Propulsion," *New Scientist* 16:16, 307 (1962).

- [2] Ernst Stuhlinger, *Ion Propulsion for Space Flight* (McGraw-Hill, NY 1964).
- [3] E. Teller, A.J. Glass, T.K. Fowler, A. Hasegawa, and J.F. Santarius, "Space Propulsion by Fusion in a Magnetic Dipole," Lawrence Livermore National Laboratory Report UCRL-JC-106807, to be published in *Fusion Technology* (1992).
- [4] T.P. Stafford, et al., *America at the Threshold* (U.S. Government Printing Office, Washington, D.C., 1991).
- [5] L.J. Wittenberg, J.F. Santarius, and G.L. Kulcinski, "Lunar Source of <sup>3</sup>He for Commercial Fusion Power," *Fusion Technology* 10, 167 (1986).
- [6] L.J. Wittenberg, E.N. Cameron, G.L. Kulcinski, J.F. Santarius, G. Sviatoslavsky, I.N. Sviatoslavsky, et al., "A Review of Helium-3 Resources and Acquisition for Use as Fusion Fuel," to be published in *Fusion Technology* (1992).
- [7] J.F. Santarius, "Lunar <sup>3</sup>He, Fusion Propulsion, and Space Development," in *Lunar Bases and Space Activities of the 21st Century-II* (Lunar and Planetary Institute, Houston, held 1988, to be published in 1992).
- [8] R. Chapman, G.H. Miley, and W. Kernbichler, "Fusion Space Propulsion with a Field Reversed Configuration," *Fusion Technology* 15, 1154 (1989).
- [9] N.R. Schulze, G.H. Miley, and J.F. Santarius, "Space Fusion Energy Conversion Using a Field-Reversed Configuration Reactor," *Proc. NASA Space Transportation Propulsion Technology Symposium* (1991).



- [10] H. Momota, et al., "Conceptual Design of D-<sup>3</sup>He FRC Reactor 'Artemis,'" these proceedings (1991).
- [11] V.E. Haloulakos and R.F. Bourque, "Fusion Propulsion Systems," *25th Joint Propulsion Conference*, paper AIAA 89-2629 (1989).
- [12] S.K. Borowski, "A Comparison of Fusion/Antiproton Propulsion Systems for Interplanetary Travel," *23rd Joint Propulsion Conference*, paper AIAA-87-1814 (1987).
- [13] J.R. Roth, W.D. Rayle, and J.J. Reinmann, "Fusion Power for Space Propulsion," *New Scientist*, p. 125 (April 20, 1972).
- [14] R.W. Bussard, "Some Physics Considerations of Magnetic Inertial-Electrostatic Confinement: A New Concept for Spherical Converging-Flow Fusion," *Fusion Technology* 19, 273 (1991).
- [15] J.F. Santarius, "Magnetic Fusion Energy and Space Development," *24th Intersociety Energy Conversion Engineering Conference*, Vol. 5, p. 2525 (IEEE, NY, 1989).
- [16] W.C. Condit, et al, "Preliminary Design Calculations for a Field-Reversed Mirror Reactor," Lawrence Livermore National Laboratory Report UCRL-52170 (1976).

## NPS OPTIONS FOR LUNAR BASES POWER SUPPLY

Nikolay N. Ponomarev-Stepnoi, Vladimir A. Pavshook,  
and Veniamin A. Usov

Kurchatov Institute of Atomic Energy

## INTRODUCTION

The studies and exploration of Moon and Solar System planets side by side with the solution of fundamental scientific tasks will allow to realize the practical assimilation of technologies of extrapure matters, new materials, biological, and medical preparations. In prospect, outposts for the extraction and utilization of space mineral resources (including He-3 for nuclear fusion) and for the penetration in the far space may be created. The power necessities for space exploration greatly depend on specific purposes, mission durations, crew staff and used instrumentation and may vary from several kW to tens of MW. Nevertheless, the power necessities may be estimated conformably to Moon exploration (and then, to Mars exploration) in the following values [1,2]:

- less than 100 kW - the power supply of communications with Earth and observations of the lunar surface from the lunar orbit, as well as the lunar rover;
- 100 kW - 1 MW - the power supply of piloted space platforms of observation and communication, providing the initial stage of the lunar base creation;
- more than 1 MW - the creation of the permanent lunar base.

The analysis of the mentioned above needs shows that the power sources using nuclear reactors practically don't have backups with the operation duration more than a month and the electric power more than several tens of kW (Fig.1).

## NPS POSSIBLE CONCEPTS

In the USSR, scientific researches in the field of space electric power systems have been performed since the beginning of the 1960s, including the systems on the base of thermoelectric and thermionic conversion of a nuclear reactor thermal power into electric one. In 1964, the facility "Romashka" on the base of the hightemperature reactor-converter with thermoelectric generators. The similar facility was also considered in the USSR for the purposes of Moon exploration. During nuclear power tests the facility "Romashka" successfully operated for 15,000 hours. Space NPS of low power (several kW) with the thermoelectric converter was used in the series of space satellite of "Cosmos" type. The system supplied electric power to the radiolocation instrumentation of the space vehicle for the observation of the ocean surface.

The further works were concentrated in general, on the creation of reactor-converters with thermionic fuel elements installed in the core. The benefits of such reactors are as follows [3,4]:

- High (in comparison with thermoelectric and turbomachine energy conversion) temperature level of heat removal. This important circumstance provides the minimum size of a radiator and, consequently, its mass which contributes to the total NPS mass, and according to the power increase becomes more and more great, and may exceed the total mass of all other components.
- The possibility to generate maximum electric power with the given system dimensions.
- The high level of the upper temperature of the thermodynamic cycle localized in the emitter nod of thermionic fuel elements and compatible with the technologically acceptable temperature level in the other NPS elements.
- The existed possibilities to force power, increase the

efficiency and achieve protracted resources.

Studies of thermionic NPS conducted in the USSR in terms of Program "TOPAZ" were led to flight tests in 1987-1988 during two flights of space satellites of "Cosmos" type. For Moon conditions, at the initial stage of its exploration, an option of a static thermionic NPS of "Romashka" type with the electric power of 5-10 kW with plate thermionic elements located between the core and reflector and anodic heat pipes was also developed. The similar facility option considered in the USA has got the name STAR-C.

Thermionic and thermoelectric NPS may be used with the required power up to 1 MWe but with the further power increase, NPS with the turbomachine energy conversion and hightemperature gas-cooled reactor becomes more perspective as a prototype of which a nuclear thermal reactor or HTGR may be considered for the ground based purposes (power or energy-technological). The following benefits of NPS of such type may be pointed out [5]:

- Increased safety due to the impossibility of melting of refractory ceramic core materials and to the negative temperature coefficient of reactivity.
- NPS good economic indices determined by high efficiency of a thermodynamic cycle (up to 50%) and by the possibility to achieve the protracted resource.

Helium may be used as a coolant in the NPS with turbomachine energy conversion during its location on Moon because it is not subjected to phase transition, neutron activation, and has good thermal physical properties. In a series of designs a mixture of xenon and helium (up to 4% according to mass) is also considered which possesses better thermal hydraulic characteristics than pure helium.

Side by side with SNPS on the base of solid-fuelled nuclear reactors the systems are studied in the USSR which use nuclear fuel in gas phase (plasma) state, among which the systems with

the great operational protraction are of the greatest interest. The nuclear fuel is circulated  $UF_6$  which is suggested to be used as a coolant of the primary loop with the power less than 100 kWe. In more powerful NPS, it is suggested to remove heat by another gas. Such NPS concept is quite attractive due to the following reasons [6]:

- The possibility to launch NPS without fissiles in the reactor core.
- The possibility to replace the fissile during the operation or to purify it from fission products to reduce the accumulated activity level.
- The presence of the negative temperature coefficient of reactivity according to  $UF$  density and the simplicity of the fission material burnup compensation.
- The reduction of a fuel cycle and the possibility to locate all the operations of this cycle directly near NPS.

#### NPS POSSIBLE SCHEMES

As far as concerned thermionic reactors of TOPAZ type, the studies of which are jointly conducted by the Soviet and American scientists there is a specific suggestion for the utilization of such systems on Moon.

TOPAZ is a reactor-converter critical dimensions of which are close to minimum possible ones; core volume is 20 l, uranium-235 loading is 12 kg, the mean portion of moderator in the core is 0.7, a total emitting area is about  $0.8 \text{ m}^2$ , electric power is up to 10 kW.

Maximum temperature of a thermodynamic cycle or emitter temperature of a thermionic fuel element is 1800 K, temperature of heat removal through the radiator is 900 K.

Fig.2 [4] shows NPS mass and specific mass change depending on electric power output. One can see that the power increase from 5

to 500 kW leads to the mass increase only 6 times as much.

The idea to use the systems of such type on Moon is determined by the intention to compensate not high efficiency of a thermionic cycle by the additional use of removed heat [7]. This may be realized by introducing of the second conversion system operating in the range of 900-500 K in Stirling cycle.

The analyses show that total power of thermionic conversion will be 5 kWe and 25 kWe for Stirling machine with NPS thermal power 100 kW for such an option, that is, it is possible to achieve 30 kWe with a total NPS mass equal to 1500-2000 kg. In future, it is possible to achieve 130 kWe 30 kWe of which will be achieved in the thermionic system. It should be noted that these assessments have been done suggesting that a radiator specific mass is  $5-6 \text{ kg/m}^2$  and temperature is 450-500 K.

Fig.3 shows the principal scheme of one of the possible turbomachine conversion options which fits to any gas-cooled hightemperature reactor (NRE, HTGR with a gas core and so on). It is a simple closed gas turbine Brayton cycle with regeneration where a heat source is a nuclear reactor (1) and heat is removed through a radiator (7). Besides the reactor and radiator, the system includes a turbocompression unit (4) located on one and the same shaft with an electric generator (5), a recuperative heat exchanger (6), and an intermediate heat exchanger (2). Calculated characteristics of a turbomachine loop are given in Table 1.

Table 1

Parameters	Options	
	1	2
Electric power, kW	75	
Coolant	Xe + He (1.75%)	

Table 1 (continued)

Maximum pressure in the loop, MPa	1	
Inlet turbine temperature, K	970	1200
Outlet radiator temperature, K	370	
Cycle efficiency	0.20	0.29
Radiator area, m <sup>2</sup>	265	132
Radiator mass, kg	2550	1270
Total equipment mass, kg	3600	1810

The first of the given in Table 1 options allows to use relatively low-temperature materials (ZrH neutron moderator, chromium-nickel steels as construction materials) and provides the possibility of protracted operation. However, the primary loop equipment becomes too cumbersome, 60% of a total mass fall on the radiator. While increasing gas temperature up to 1200 K, the equipment mass will reduce almost two times but in this case, the application of more refractory materials is necessary.

For reactors with circulating gas fuel, the technology of flow control has been developed and experimentally validated which allows to perform the necessary velocity profile in channels [6]. For example, the use of honeycomb arrangements with pipes of variable length allows to solve the problems of turns, expansion and other flow transformations. It allows to provide the redistribution of coolant rates and heating both with the monocomponent flow (with NPS power of about 100 kW and lower) and with the bicomponent flow when the flow of buffer gas appears along the walls (Fig.4) removing heat from the reactor. The bicomponent scheme of flow removes  $UF_6$  temperature limits which allows to reduce its rate to the necessary level according to

thermal-hydraulic characteristics. However, it should be noted that for NPS with gaseous fission matter, a series of principal problems connected with plasma-chemistry of uranium hexafluoride and other materials, the realization of the system of uranium hexafluoride and buffer coolant separation, experimental validation of technical solutions during the in-pile and out-of-pile studies and so on has to be solved. Thus, only the performance of multilateral future works may show if the enthusiasts of this trend development are right or not.

### CONCLUSIONS

For practical realization of considered NPS options for lunar bases, scientific researches have to be conducted in the following trends:

- The improvement of heat power conversion, in particular, the search of new non-traditional ways of waste heat removal (a droplet radiator and so on), the development of combined NPS on the base of thermionic reactor-converters and machine conversion schemes (including Stirling engine).
- Studies and development of advanced fuel compositions.
- Development of refractory materials including cermet, composite, carbon-carbon, and other ones.

The problem of radiation and nuclear safety providing should be pointed out because the possibility to use NPS in space greatly depends on the solution of this problem.

The above mentioned trends don't cover the whole list of necessary studies but give the notion about the coming works. For the successful development of such complex knowledge-capacious objects, it is desirable to join scientific-technical and intellectual potentials of different countries, in the first place, the USSR and USA possessing the largest theoretical and practical experience in the field of space nuclear power engineering.



## References

1. America at the Threshold. America's Space Exploration Initiative. Report of the Synthesis Group. 1991.
2. Space Power 1991 and Beyond. Allied-Signal Aerospace Company. 1990.
3. Ponomarev-Stepnoi, N.N. "Nuclear Power in Space". Presentation to the 6-th Symposium on Space Nuclear Power Systems. 1989, Albuquerque, NM, USA. Atomnaja Energia, v.66, 1989.
4. Griaznov, G.M., Zhabotinsky, E.E., "Thermionic reactor-converters for space NPS". Presentation to the 6-th Symposium on Space Nuclear Power Systems. 1989, Albuquerque, NM, USA. Atomnaja Energia, v.66, 1989.
5. Carre, F., Proust, E., et al. "Current trends in the Erato Study Program on Space Nuclear Brayton System". Anniversary Specialist Conference on Nuclear Power Engineering in Space. Selected Papers. Obninsk, USSR. May 15-19, 1990.
6. Pavel'ev, A.A., Volkov, A.B., et al. "Nuclear Power Systems with Circulating  $UF_6$ ". Summary reports of Soviet specialists at the Anniversary Specialist Conference on Nuclear Power Engineering in Space. Obninsk, USSR. May 15-19, 1990.
7. Wetch, J., Ponomarev-Stepnoi, N., et al. "TOPAZ Based Nuclear Power Systems for Early Lunar Outposts". Presentation to the Anniversary Specialist Conference on Nuclear Power Engineering in Space. Obninsk, USSR. May 15-19, 1990.
8. Beljakov, M.S., Pavshoock, V.A., et al. "The Problem of Brayton Cycle Application in Bimodal Nuclear Power System". Presentation to the 7-th Symposium on Space Nuclear Power Systems, Albuquerque, NM, USA. 1990.

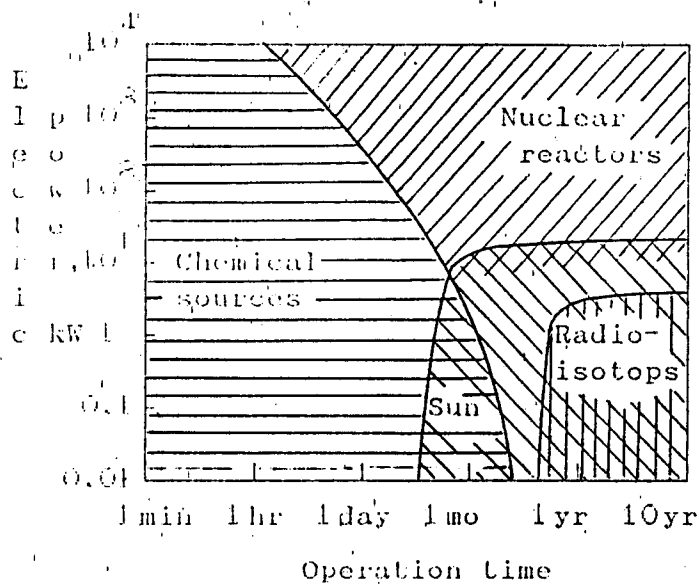


Fig.1 Fields of application of different SNPS types.

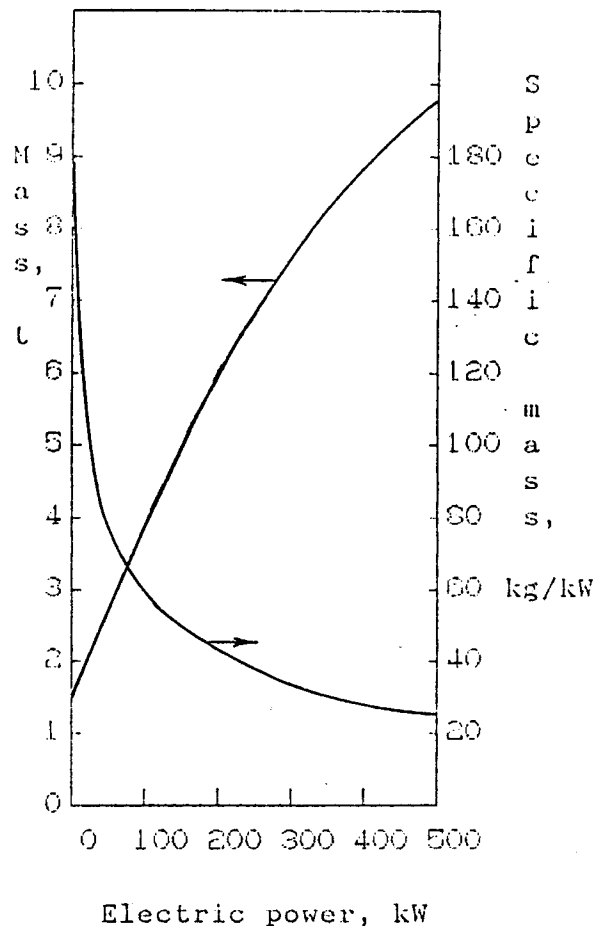


Fig.2 Thermionic systems characteristics.

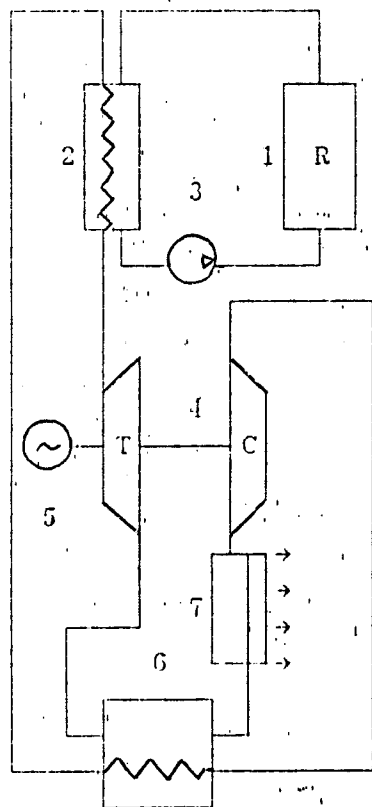


Fig.3 NPS Scheme with Turbomachine Conversion

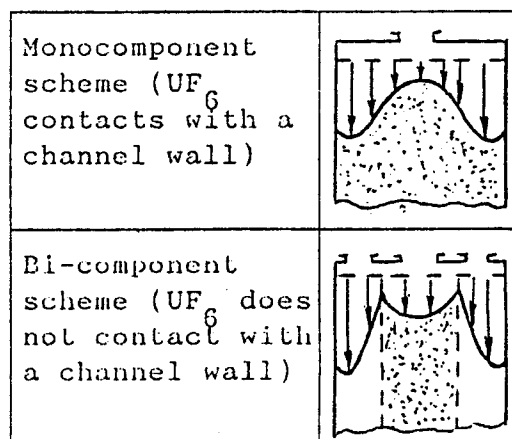


Fig.4 Flow in a Channel with Circulating Uranium Fluoride